Aus der Klinik für Innere Medizin II

Universitätsklinikum des Saarlandes, Homburg/Saar

Alterations of liver dendritic cell subsets during NAFLD and the influence of the batf3-dependend population on disease progression

Dissertation zur Erlangung des Grades eines Doktors der Medizin

der Medizinischen Fakultät

der UNIVERSITÄT DES SAARLANDES

2018

Vorgelegt von: Eva-Carina Heier

geb. am 17.03.1992 in München

Meinen Eltern

Table of contents

List of Tables

List of Figures

Abstract

The metabolic syndrome has increased considerably worldwide and so have its associated conditions including non-alcoholic fatty liver disease (NAFLD). In most cases NAFLD manifests as relatively benign hepatic steatosis, but around 10% of the patients develop the more severe non-alcoholic steatohepatitis (NASH), which is associated with a higher risk for end stage liver disease and hepatocellular carcinoma. The exact pathomechanism that leads to progression of hepatic steatosis towards NASH is incompletely understood. Dendritic cells (DC) have been implicated to play a protective role in the progression of NASH. DCs are specialized antigen-presenting cells that play an important role in the regulation of immune responses. They are a heterogenous group of cells and consist of several subtypes, such as plasmacytoid DCs (pDC), $CD103^+$ classical DCs type 1 (cDC 1) and $CD11b^+$ classical DCs type 2 (cDC 2) as well as a monocyte derived DCs. This study aims to characterize the changes of individual DC subtypes during development and progression of NAFLD and focuses on the specific role of the $CD103^+$ cDC 1 population using the batf3-knockout model (batf3-KO). Steatosis and steatohepatitis was induced in wildtype (WT) and batf3-KO mice through feeding of high sucrose diet (HSD) and methionine-choline-deficient diet (MCD) respectively and changes of hepatic immune cells were mapped using multicolor flow cytometric analysis. Together with HE-staining, cytokine arrays and serum analysis, flow cytometry was further used to investigate the effect of $CD103^+$ cDCs 1 on the composition of hepatic immune cells and disease progression.

All DC subtypes increase in the steatohepatitis model, suggesting their involvement in the pathogenesis of NASH. Lack of $CD103^+$ cDCs 1 during HSD feeding results in progression towards steatohepatitis with increased presence of inflammatory cells types including inflammatory monocytes, monocyte derived DCs and other myeloid cells as well as elevated production of pro-inflammatory cytokines. Importantly disease progression in batf3-KO animals is not associated with aggravated adipose tissue inflammation or increased insulin resistance, indicating a local mechanism rather than a systemic effect of batf3-KO cells

This study shows, that murine $CD103^+$ cDCs 1 hold an important protective role in the progression of steatosis towards steatohepatitis, by regulating the composition of hepatic immune cells, the influx of inflammatory cells and the intrahepatic production of cytokines. Furthermore, it implies a role of the remaining DC subsets in the pathogenesis of NASH, which is less specified and will need further clarification in future studies.

Zusammenfassung

Die nicht-alkoholische Fettlebererkrankung (NAFLD), welche als hepatische Konsequenz des metabolischen Syndroms betrachtet wird, trat in den letzten Jahrzehnten weltweit vermehrt auf. In den meisten Fällen der NAFLD handelt es sich um die relativ benigne *Steatosis Hepatis* (Fettleber), allerdings kommt es bei etwa 10% der Fälle zu der Genese einer nicht-alkoholischer Steatohepatitis (NASH), die durch entzündliche Infiltrate und Hepatozytenschäden charakterisiert ist und mit einem erhöhten Risiko für die Entwicklung von terminaler Leberinsuffizienz oder eines hepatozellulären Karzinoms einhergeht. Der genaue Pathomechanismus für die Progression der *Steatosis Hepatis* zur Steatohepatitis ist noch nicht vollständig geklärt. Den dendritischen Zellen (DC) wird eine protektive Funktion im Rahmen der Pathogenese einer NASH zugeschrieben. DCs sind spezialisierte, antigen-präsentierende Zellen, welche eine wichtige Rolle bei der Regulation von Immunantworten spielen. Sie werden meist als $CD11c^+MHC\text{-}II^+$ Zellen identifiziert. Allerdings handelt es sich bei DCs um eine sehr heterogene Gruppe, welche unter anderem aus plasmazytoiden DCs (pDCs), $CD103^+$ klassischen DCs Typ 1 (cDCs 1), $CD11b^+$ klassischen DCs Typ 2 (cDCs 2) sowie DCs der monozytären Linie (moDCs) besteht. Um ein besseres Verständnis der Funktion dieser Zellen zu erhalten wurden in der vorliegenden Studie die Veränderungen dieser individuellen Subtypen während der Genese und Progression der NAFLD untersucht.

Zudem wurde an batf3-*knockout* (batf3-KO) Mäusen, welchen der $CD103^+$ cDCs 1 Subtyp fehlt, die Rolle dieses Zelltyps in der Entwicklung einer NASH genauer betrachtet. Hierzu wurden anhand unterschiedlicher Ernährungsregime 3 Gruppen gebildet. Um eine *Steatosis Hepatis* beziehungsweise Steatohepatitis zu induzieren erhielt je eine Gruppe eine saccharosereiche (*high sucrose diet*, HSD), respektive eine methionin- und cholindefiziente Diät (*methionin-choline-deficient diet*, MCD). Die dritte Gruppe erhielt ein normales Ernährungsregime. Als Kontrolle dienten Wildtyp (WT) Mäuse mit jeweils identischen Diäten. Veränderungen der hepatischen Immunzellen wurden mit Hilfe der *Multicolor* Durchflusszytometrie untersucht. Diese wurde zudem in Verbindung mit HE-Färbungen der Leberproben, Zytokin *Arrays* und Serum Analysen genutzt, um den Effekt von cDCs 1 auf die anteilige Zusammensetzung der hepatischen Immunzellen und den Progress der *Steatosis Hepatis* zur Steatohepatitis zu untersuchen.

In dieser Studie wird gezeigt, dass alle DC Subtypen im Rahmen einer NASH vermehrt in der Leber auftreten, was auf ihre mögliche Involvierung in der Pathogenese der NASH hinweist. Eine HSD führt bei WT Mäusen zu einer benignen *Steatosis Hepatis*, während sie bei cDCs 1-defizienten batf3-KO Mäusen zur Entwicklung einer NASH führt. Bei Letzteren

kommt es hierbei zu einer Zunahme von inflammatorischen Monozyten, monozytären DCs und anderer Zellen der myeloiden Reihe in der Leber sowie zu einer Verschiebung der intrahepatischen Zytokinproduktion in Richtung eines pro-inflammatorischen Milieus. Dabei führt die HSD trotz Fortschreiten der Erkrankung in batf3-KO Tieren allerdings nicht zu einer verstärkten Entzündung im Fettgewebe oder der Verschlechterung der Insulinresistenz, was darauf schließen lässt, dass die Progression der Erkrankung ein lokal begrenzter Effekt von cDCs 1 ist und nicht in Folge einer systemischen Verschlechterung beim Fehlen von cDCs 1 auftritt.

Zusammenfassend kann in dieser Studie gezeigt werden, dass cDCs 1 eine wichtige protektive Rolle in der Entwicklung der Steatohepatitis aus der *Steatosis Hepatis* innehaben indem sie die Zusammensetzung hepatischer Immunzellen, die Einwanderung inflammatorischer Zellen und die intrahepatische Zytokinproduktion regulieren. Außerdem deuten die Ergebnisse dieser Studie daraufhin, dass die übrigen DC Subtypen ebenfalls eine Rolle in der Pathogenese der NASH einnehmen. Diese müssen in weiteren Studien noch genauer spezifiziert werden.

Abbreviations

ACK lysis	Ammonium-chloride-potassium lysis
APC	Antigen-presenting cell
Batf3	Basic leucine zipper transcription factor ATF-like 3
CCL	Chemokine (C-C motif) ligand
CCl4	Carbon tetrachloride
CD	Cluster of differentiation
CD11c-DTR	CD11c-diptheria toxin receptor
cDC 1	Classical dendritic cell type 1
cDC 2	Classical dendritic cell type 2
CDP	Common dendritic cell precursor
CXCL	Chemokine (C-X-C motif) ligand
DC	Dendritic cell
DM-II	Diabetes mellitus type II
DNA	Deoxyribonucleic acid
EDTA	Ethylendiaminetetraacetic acid
FBS	Fetal bovine serum
FFA	Free fatty acid
Flt3L	FMS-like tyrosine kinase 3 ligand
FMO	Fluorescence minus one
FSC	Forward scatter
HBSS	Hank’s balanced salt solution
HE	Hematoxylin eosin
HFD	Hight fat diet
HSC	Hepatic stellate cell
HSD	High sucrose diet
Id2	Inhibitor of DNA binding 2
IL	Interleukin
IPGTT	Intraperitoneal glucose tolerance test
IR	Insulin resistance
IRF4	Interferon regulatory factor 4
IRF8	Interferon regulatory factor 8
KC	Kupffer cell
KO	Knock-out
LPS	lipopolysaccharides

MCD	Methionine-choline deficient diet
MHC	Major histocompatibility complex
moDC	Monocyte-derived dendritic cell
MPS	Mononuclear phagocyte system
NAFL	Non-alcoholic fatty liver
NAFLD	Non-alcoholic fatty liver disease
NASH	Non-alcoholic steatohepatitis
NC	Normal chow
NFIL3	Nuclear factor interleukin 3
NK cell	Natural killer cell
NKT cells	Natural killer T cell
NPC	Non-parenchymal cell
OPN	Osteopontin
PBS	Phosphate Buffered Saline
pDC	Plasmacytoid dendritic cell
PDCA-1	Plasmacytoid dendritic cell antigen 1
PFA	paraformaldehyde
PI	Proprium iodide
PMN cells	Polymorphonuclear cells
pre-DC	Precursor dendritic cell
qPCR	quantitative Polymerase Chain Reaction
RNA	Ribonucleic acid
SSC	Sideward scatter
TAA	Thioacetamide
TCR	T cell receptor
TG	Triglyceride
TGF-β	Transforming growth factor beta
T_H1	$CD4^+$ T-helper cell type 1
T_H17	IL-17 producing $CD4^+$T-helper cell
T_H2	$CD4^+$T-helper cell type 2
TLR	Toll-like receptor
TNFα	Tumor necrosis factor alpha
T_{reg}	regulatory T cell
wks	Weeks
WT	Wildtype

1 Introduction

1.1 Non-alcoholic fatty liver disease

1.1.1 Definition

In 1980 Ludwig *et. Al* described a hepatic disease of unknown origin characterized by a histology similar to alcoholic hepatitis, while the patients' history lacked typical increased alcoholic intake (1). They established the term non-alcoholic steatohepatitis (NASH). NASH has since emerged as one of the most common causes for liver disease in developed countries (2). It belongs to a group of liver pathologies comprised in the term non-alcoholic fatty liver disease (NAFLD) which are characterized by increased lipid accumulation in the absence of any other cause of secondary steatosis, such as ethanol consumption >20g ethanol/day, drugs, viral hepatitis or genetic conditions (3). According to the Sk2 Guidelines of the German Society for Digestive and Metabolic Diseases the spectrum of NAFLD ranges from simple steatosis hepatis, also referred to as non-alcoholic fatty liver (NAFL), to more severe NASH with inflammatory infiltrate and hepatocellular damage and can ultimately result in end-stage liver diseases such as cirrhosis or hepatocellular carcinoma (4,5). NAFL is defined as steatosis in >5% of hepatocytes, with a further division in mild (<33%), moderate (33-66%) and severe steatosis (>66%), while NASH is characterized by an additional necroinflammatory component with or without fibrosis (5). Histologically this corresponds to the presence of inflammatory infiltrates, hepatocellular ballooning and necrosis (3,6). Since until now no reliable biomarker has been identified to distinguish between NAFL and NASH liver biopsies remain gold standard for the diagnosis of NASH (7–9)

1.1.2 Epidemiology

The number of patients with NAFLD has increased dramatically within the last few decades affecting both adults and children worldwide (2,10). The prevalence of NAFL in the western population is 20-30%, but increases further in obese patients and patients with diabetes mellitus or hyperlipidemia (2,3). The more severe NASH affects 2-3% of the general population, up to 20% of the obese and 50% of the morbidly obese (2,11,12). While bland, uncomplicated steatosis does not affect long-term prognosis, the presence of inflammation and fibrosis is associated with a higher risk of progression towards end stage liver disease

(13,14). In fact NASH has been identified as a major cause of cryptogenic cirrhosis and it has been suggested to be the first cause for liver transplant during the next years (2,15,16). Therefore, it is crucial to understand the mechanisms that promote the progression of NAFL towards NASH.

1.1.3 Pathophysiology

NAFLD is considered the hepatic consequence of the metabolic syndrome (17). It is closely correlated with obesity, dyslipidemia, insulin resistance (IR) and type-II diabetes mellitus (DM-II) (1,18–20). The exact mechanisms involved in the development of NAFLD and the progression towards NASH are not yet fully understood. The “two-hit” hypothesis has for a long time been widely accepted as a model for the pathogenesis of NASH (21). First published in 1998 by Day *et al.* it suggests that insulin resistance causes steatosis and leads to increased hepatic lipid accumulation, considered the “first hit”, which leaves the liver more susceptible to injury (21). In consequence mitochondrial dysfunction and oxidative stress in lipid-loaded hepatocytes would, as a “second hit”, be more likely to trigger inflammatory reactions that result in steatohepatitis (21,22). The extensive research that has been conducted since challenges this hypothesis and suggests a pathogenesis of “multiple parallel hits”. It becomes evident that the relationship between steatosis and inflammation is not as straight forward as suggested in the “two-hit” hypothesis (22). In some cases of NASH hepatic inflammation actually precedes steatosis and there is some evidence suggesting that increased intrahepatic triglyceride content could actually serve as a protective mechanism to eliminate free fatty acids (FFA) from the liver (23–25). FFAs are believed to play a key role in the pathogenesis of NASH through a mechanism called lipotoxicity, which describes a variety of toxic effects caused by the accumulation of FFA and their metabolites in the liver. Such effects include the formation of reactive oxygen species, endoplasmatic reticulum stress, activation of inflammatory pathways and cell death (22,26–28). Obesity and the associated IR contribute to this, by enhancing the influx of FFA to the liver through inappropriate lipolysis of the large amounts of adipose tissue (22). Increased amounts of adipose tissue further contribute to disease progression by promoting innate immune responses through the production of inflammatory cytoadipokines (29). Besides such alterations of the lipid metabolism, changes of the gut microbiome and increased intestinal permeability resulting in endotoxinemia with toll-like receptor (TLR) activation have also been described as an additional factor for disease development (30,31). Furthermore, several genes have been identified that predispose individuals to NAFLD and NASH (29,32).

So it becomes evident that the pathogenesis of NASH is more complex than originally thought and includes a combination of genetic variances, dysregulation of lipid metabolism, changes in the gut microbiome and local inflammatory responses (12). It remains to be determined how these mechanisms interact with each other, how they influence innate and adaptive immunity and what triggers disease progression.

1.1.4 Mouse models to investigate NAFLD

Several models are available to study NAFLD in mice. However, none of the available models completely replicates the human phenotype (33).

Methionine-choline deficient diet

Methionine-choline deficient diet (MCD) is a popular model to investigate NASH in mice. Feeding MCD results in mild steatosis and minimal focal inflammation after as early as 1 week into the diet. A 4 week MCD treatment increases steatosis and causes prominent inflammation within the liver, while after 8-10 weeks fibrosis development can be observed (34,35). The MCD treatment differs from human NAFLD in several important aspects: animals fed MCD diet experience severe weight loss, have low plasma triglyceride (TG) levels and a reduced liver weight/body weight ratio. Further they generally do not develop IR or DM-II during MCD treatment. Although this stands in contrast to the human NAFLD, the MCD model is still the best-established model to study inflammatory and fibrotic elements of the NAFLD spectrum (33).

High sucrose diet

Feeding of a high sucrose (a disaccharide of glucose and fructose) or high fructose diet is another model to investigate NAFLD in mice. Increased consumption of fructose is reported to be a risk-factor for NAFLD development in humans (36). Feeding of a diet containing 65% sucrose for 8 weeks to C57BL/6 mice causes obesity, IR and macrovesicular steatosis, but does not result in histopathological evidence of NASH or fibrosis NASH (37,38). Treatment with high sucrose diet (HSD) mimics the human disease better than the MCD model and is a useful model to investigate bland liver steatosis in mice.

1.2 Basics of Immunology

The immune system is a complex system with the key role to protect the organism from exogenous or endogenous damage while simultaneously controlling its own response (39). It

consists of a group of specialized, closely connected cells which constantly communicate with each other and their surroundings. Cells and functions of the immune system are attributed to either innate or adaptive immunity. Innate immunity is characterized by an immediate availability of specialized cells or defense mechanisms against a wide range of pathogens, regardless of a prior exposure (39). Adaptive immunity on the other hand requires a first-time exposure, before being able to initiate an immune response towards an individual pathogen. On a second encounter with this antigen it then acts highly specific and with a great efficiency (39). Importantly innate and adaptive immunity are not two isolated systems, but are closely connected with many regulatory overlaps and feedback mechanisms. For a better understanding of dendritic cells (DCs) and their role in immunity the following chapter will briefly recapitulate the basics of innate and adaptive immune responses. Described surface markers and transcription factors refer to the murine immune system, since this study is based on murine models.

1.2.1 Innate immune responses

Cells of the innate immune system can recognize molecules that are expressed by microbes or released during tissue damage and cell death as danger signals through specialized, highly conserved receptors (40). When recognizing such danger signals, cells of the innate immune system are activated within seconds and start to initiate and amplify the inflammatory response. This includes recruiting more inflammatory cells to the site of danger, setting the whole organism in a state of alertness and initiating a systemic response (39).

One group of innate immune cells are so called polymorphonuclear cells (PMN cells), which include neutrophils, basophils, eosinophils and mast cells. PMN cells are in line of first defense against intruding microorganisms and are recruited to sites of inflammation within the first hour of an immune response (40). Another type of innate immune cells are natural killer cells (NK cells). These cells represent the major lymphocyte populations of the innate immune response and are crucial for controlling infection and immune surveillance (41). NK cell surface receptors (NKR) recognize changes in major histocompatibility complex I (MHC-I) expression patterns on cells, which occur for example after infection or tumor transformation, and then kill the transformed cells through cell lysis (39). NK cells are also potent producers of cytokines (42). A third part of the innate immune system is the mononuclear phagocyte system (MPS), which includes macrophages, DCs and monocytes (43). Macrophages and DCs are tissue resident phagocytic cells, which ingest exogenous proteins and cellular debris. As professional antigen-presenting cells (APCs) they process ingested proteins and present them on MHC-II molecules on their cell surface, which helps to initiate an adaptive immune response. They

also produce antimicrobial peptides as well as chemokines and cytokines with messenger function to mediate inflammatory responses (39). Functionally macrophages specialize in the clearance of cellular debris, pathogens and foreign material, whereas DCs are markedly more potent in antigen presentation and initiating T cell response (43). Monocytes represent a very dynamic cell population within the MPS. Classical monocytes, which are characterized by a high expression of Ly6C, circulate the blood from where they migrate into tissues and differentiate to replenish the macrophage and DC populations (44,45). This is a process which happens mostly during inflammation, whereas in steady state tissue resident macrophages are mainly maintained through self-renewal and DCs evolve from circulating precursor DCs (pre-DCs) from the bone marrow (43,46,47).

1.2.2 Adaptive immune responses

Adaptive immunity is mostly mediated through T- and B lymphocytes, also referred to as T- and B cells. B cells are producers of immunoglobulins and play an important part in humoral adaptive immune defense. B cell activation is facilitated through cytokine production of activated T helper cells (40). T cells are the main cell type of cellular adaptive immune responses and they interact closely with DCs. They express a specialized, unique T cell receptor (TCR) which recognizes antigens presented on MHC molecules. Due to genetic rearrangement the individual TCRs are extremely diverse, with up to 10^{16} specificities (39). Until they are presented with “their” antigen, naïve T cells circulate between blood and peripheral lymphoid tissue. When activated, T cells proliferate and differentiate into different effector cells (48). Activation of T cells happens mainly in lymph nodes and is accomplished through professional APCs especially DCs (39). The two main subsets of T cells are $CD8^+$ cells, also called cytotoxic T cells, and $CD4^+$ cells, so called T helper cells (T_H cells), which are further divided into individual subsets. $CD8^+$ T cells recognize alternated MHC-I molecules on virus infected or tumor cells and subsequently kill the target cell (48). The major effector function of $CD4^+$ T cells is the production of cytokines, which then influence multiple other cell types. The four major subsets of $CD4^+$ cells are T_H1, T_H2, T_H17 and regulatory T cells (T_{reg}): T_H1 cells produce cytokines which act on macrophages, NK cells and $CD8^+$ T cells and induce cell-mediated immunity. T_H2 cells promote humoral immunity (49). T_H17 cells produce cytokines that promote pro-inflammatory responses and seem to be involved in processes of autoimmunity (50). T_{regs} ($CD25^+FoxP3^+$) secrete the anti-inflammatory cytokines IL-10 and TGF-β and suppress immune responses directed towards both foreign and self-molecules (48).

As mentioned above naïve lymphocytes are only activated through antigen presentation on MHC molecules. $CD8^+$ T cells recognize antigens on MHC-I molecules and $CD4^+$ T cells recognize antigens on MHC-II molecules (51). Full activation requires the binding of corresponding co-stimulatory molecules such as CD80/CD86 and CD28, as isolated recognition of the TCR with MHC-complexes results in T cell inactivation, a process called anergy, which prevents unwanted immune responses against harmless or self-antigens (52). In contrast to the innate immune system, which reacts immediately, activation and differentiation of lymphocytes is a four to five day process (39). After the first encounter with the antigen most effector T cells die, except for a few long-lived memory cells, which continue to circulate the organism. Upon a second encounter with the antigen, memory T cells lead to a direct proliferation and differentiation of T cells and thus a more rapid and effective response (48).

Lastly a third subpopulation of T cells exists, the so called NKT cells. These are characterized by the expression of both an invariant TCR and the NK cell marker NK1.1 (53). Importantly, unlike regular T cells, NKT cells recognize antigens through interaction with CD1d, a MHC-I like molecule that presents mostly glycolipid antigens (54). This means that NKT cells are important for the recognition of lipid antigens as opposite to the other T cells, which are primarily presented with peptide fragments of protein antigens (54,55). Moreover NKT cells have a potent capacity of producing both pro- and anti-inflammatory cytokines involved in T_H1- and T_H2-regulation (55). NKT cells are especially abundant in the liver. Here they inhabit a regulatory role by patrolling the hepatic sinusoids, interacting with other cell types and modulating T cell response (56).

1.3 Dendritic cells and their role in immunity

DCs were first described by Steinman *et al.* in 1973 and have since been in the focus of intensive immunological research (57). They were identified as the cellular subset which is mainly responsible for T cell activation. This function is reflected in their potent capabilities of antigen-presentation, migration and cytokine-production (58). Ubiquitous in the organism, DCs especially reside at locations targeted by disease-relevant stimuli such as the skin, mucosal surfaces or the respiratory and gastrointestinal system (59). They constantly scan their environment for antigens and recognize pathogens and other danger signals (60). Once they have sampled an antigen they migrate from their position in the periphery to lymph nodes, where they present it to naïve T cells and regulate their response (61). This capability to migrate into lymphoid organs is one of the primary functional properties of DCs, since it allows them to initiate adaptive cellular immune responses in lymphoid organs (62). Importantly they

are not only responsible for initiating adaptive immune responses, but are also important for maintaining homeostasis in the immune system. Through presenting self-antigens to T cells, deleting autoreactive T cells and inducing regulatory T cells, DCs also play a crucial role in developing immune tolerance (63).

Until recently it was thought that DCs exist in two distinct functional states: immature and mature DCs (58). Immature DCs appear under non-inflammatory conditions and show a tolerogenic phenotype, i.e. expressing low levels of co-stimulatory molecules and producing low amounts of pro-inflammatory cytokines (64). Mature, immunogenic DCs express high levels of co-stimulatory molecules (e.g. CD80/86 and CD40) and produce pro-inflammatory cytokines like IL-12 or IL-6 to induce an immunologic response (65). Today a more accurate thesis is believed, that when activated, DCs evolve into different effector DCs with distinct functional capabilities. Depending on the effector type they will then initiate T helper cell differentiation, start cytotoxic T cell responses, or induce T cell tolerance (60,66).

Generally, when presenting antigens, all cells express MHC-I molecules to present endogenous, intracellular produced antigens and specialized antigen-presenting cells also use MHC-II molecules to present exogenous antigens (67). In addition to this DCs have developed a third mechanism called cross-presentation: they take up antigens from an exogenous source and present them on MHC-I molecules (68). Cross-presentation enables DCs to activate naïve $CD8^+$ T cells towards an antigen which is not directly expressed by DCs themselves. This is especially important for initiating cytotoxic T cell responses against viruses or intracellular pathogens (69).

In addition to their strong role in adaptive immunity several studies in both mice and humans have presented evidence for crosstalk between NK cells and DCs. DCs seem to promote NK cell survival and proliferation, cytokine production, activation and cytotoxicity (41,70–73). Reciprocal, NK cells can on the one hand induce DC activation and enhance their ability to stimulate naïve allogeneic $CD4^+$ T cells, but may on the other hand also lyse autologous DCs in vitro depending on the NK:DC ratio (41,72,74). This links DCs to innate immune responses and further underlines their importance as mediators of immune responses.

1.4 Murine dendritic cell subtypes

Although often simply defined as $CD11c^+MHC\text{-}II^+$ cells, DCs are in fact a heterogeneous group of different cell subtypes. Since their discovery several nomenclature systems have been introduced to distinguish between DC subtypes. The most recent and currently used system classifies DCs and other cells of the MPS primarily based on their ontogeny and

secondarily accordingly to their function and phenotype (43). This classification categorizes DCs into three subsets, which all stem from a common DC precursor (CDP) in the bone-marrow, and one subset, which develops from circulatory monocytes particularly during inflammatory conditions (43). Cells that develop from the CDP are named classical DCs Type 1 (cDC 1), classical DCs Type 2 (cDC 2) and plasmacytoid DCs (pDC), while the fourth subset is called monocyte derived DC (moDC) (43). The CDP develops in a FMS-like tyrosine kinase 3 ligand (Flt3L) dependent fashion from a common macrophage-DC-progenitor cell and from this stage on is restricted to producing cDCs and pDCs (47,75). Distinct sets of transcription factors determine the further differentiation of the CDP into the DC subsets (46). Pre-DCs enter the peripheral circulation from the bone marrow, traveling to lymphoid and non-lymphoid organs where they differentiate into the different cDC or pDC subtypes (75,76). Pre-DCs express CD11c on their surface, but are not yet MHC-II positive (47).

The development of cDCs 1 is dependent on several transcription factors such as basic leucine zipper transcription factor ATF-like 3 (batf3), inhibitor of DNA binding 2 (Id2), interferon regulatory factor 8 (IRF8) and nuclear factor interleukin 3 (NFIL3) (43,77–80). Phenotypically cDCs 1 are characterized by the expression of CD11 and MHC-II as well as CD8α in lymphoid tissues or CD103 in non-lymphoid tissues (81). This subset is specialized in the cross-presentation of cell-associated and soluble antigens on MHC-I molecules as well as initiation of a cytotoxic $CD8^+$ T cell response (60,69,73). Furthermore, cDCs 1 of the gut and airways have shown the ability to induce $CD4^+$ $CD25^+$ $FoxP3^+$ T_{regs} indicating that these cells also hold an important role in the induction of tolerance and regulation of immune responses (60,82–84).

cDCs 2 are DCs whose development is regulated through IRF4 and which express CD11b (43). In this context it is important to mention that the classification system based upon ontogeny is fairly new and until recently cDCs were classified into the $CD8\alpha^-/CD103^-$ $CD11b^+$ DC subtype and $CD103^+/CD8\alpha^+$ $CD11b^-$ DC subtype merely based on their surface expression pattern (61,85). Here the $CD103^+/CD8\alpha^+$ $CD11b^-$ DC subtype corresponds to the above described batf3-dependent cDC 1 subtype, whereas the $CD8\alpha^-/CD103^-$ $CD11b^+$ population is heterogeneous with different origins and functions (61). In fact the IRF-4 dependent cDCs 2 share their expression pattern of $CD11c^+$ $MHC\text{-}II^+$ and $CD11b^+$ with moDCs, which means that the simple categorization into CD11b expressing DCs is not sufficient to investigate the individual cell populations (86). It is possible to distinguish the cDC 2 and moDC subset through the surface marker CD64, which is expressed by moDCs but not cDCs 2 (87–89). Because of these overlaps in surface markers and the only recent discrimination of cDCs 2 and moDCs it is not surprising that functions of cDCs 2 are less characterized. Nevertheless, cDCs 2 have

been identified as a critical cell type for type 3 immune responses against extracellular bacteria and fungi through IL-23 production and also seem to play a role in the induction of T_H2 cells, but the exact mechanism involved remains unclear (73,90,91). Additionally, CD11b expressing DCs have been described to be more efficient in the induction of a type 2 immune response, $CD4^+$ T cell activation and seem to have a potent role in presenting MHC-II molecules (73,92).

pDCs build the third big subtype of DCs. Although they differ from cDCs in morphology and function they share their origin in the bone marrow (47). Their differentiation from the CDP is facilitated through the transcription factor E2-2 (93). pDCs express PDCA-1 and are specialized in the fast secretion of large amounts of type I interferons during viral infections (61,94,95).

1.5 The liver as a lymphoid organ

The liver is considered the biggest metabolic organ the body. It is responsible for the extraction and storage of nutrients, elimination of toxins and production of vital protein (56). Everyday arterial and venous blood mixes within the liver sinusoids, which creates a unique microenvironment unseen anywhere else in the organism. Here, circulatory leukocytes from the arterial flow encounter gut derived macromolecules like toxins, food antigens and microbial products arriving through the portal vein. This renders the liver a central “meeting point” for immune cells and antigens, which explains its important role in the induction of immunity, the setup of immune memory and maintaining immune tolerance (96). Due to the constant exposure towards pro-inflammatory agents, the risk of immune activation in the liver appears to be higher than anywhere else in the organism. Still, hepatic immune cells usually do not elicit an immune response during steady state. Despite the continuous antigenic challenge they are able to maintain immune homeostasis (97).

Several different cell populations with immunologic function exist within the liver. Hepatocytes can present endogenous antigens to naïve $CD8^+$ T cells, which results in apoptotic death of the stimulated cells and contributes to the tolerizing phenotype of the liver (98). Furthermore, all liver sinusoidal cells, such as Kupffer Cells (KCs), hepatic stellate cells (HSC), endothelial cells as well as DCs, are capable of antigen presentation to $CD4^+$ and $CD8^+$ T cells. They cross-present hepatocyte-derived antigens as well as present circulating antigens. Thus sinusoidal cells influence adaptive immunity towards both local and systemic antigens (96). During steady state, this is strongly biased towards the prevention of inflammatory responses: Liver APCs inhibit antigen-specific T cell activation and induce tolerance in naïve $CD8^+$ T cells (56). Further, $CD4^+$ T cell differentiation is skewed towards the

differentiation into non-T_H1 and non-T_H17 effector cells, such as a T_H2 cells that secrete low levels of IL-4 and IL-10 (49,99).

1.6 DCs in NAFLD – What do we know?

During NASH the tolerogenic environment of the liver, which normally withstands constant immunologic stimuli without an overreactive immune response, switches into an inflammatory state. Immune cell activation then causes hepatocellular damage and promotes hepatic fibrosis (29). To elucidate the cellular and molecular mechanisms which promote this switch will be a major step in understanding the pathogenesis of NASH and thereby identifying potential therapeutic targets.

The liver hosts more DCs than other parenchymal organs, probably as a consequence of the high occurrence of antigens in portal blood (100). All previously described DC subsets can be found within the liver (101). Several studies have been conducted about liver DCs and their role in NAFLD and liver fibrosis, however, most of these studies focused on the role of all CD11c expressing cells, which are not exclusively DCs (101,102).

$CD11c^+$ cells of the healthy liver exhibit a tolerogenic phenotype in accordance to the unique microenvironment they inhabit (100,101). They have a lower capability to endocytose antigens or stimulate T cells, express low levels of MHC-II and costimulatory molecules and have a low intracellular lipid content (i.e. triglycerides, phospholipids), a feature which has also been attributed to a tolerogenic phenotype (103–105). Furthermore, they show a higher production of the anti-inflammatory cytokines IL-10 and IL-27 (106).

The role of $CD11c^+$ cells in during liver injury and fibrosis development has been described in various disease models: Generally, during fibrosis the level of $CD11c^+$ cells is elevated and the majority of these cells display a pro-inflammatory phenotype, which includes the upregulation of MHC-II and costimulatory molecules, production of pro-inflammatory cytokines and high intracellular lipid content (62,101,105,107–109). In mice with biliary fibrosis monocyte-derived $CD11c^+$ cells show a higher capacity to acquire antigens and stimulate T cells (108). During thioacetamide (TAA) and recombinant leptin induced fibrosis $CD11c^+$ cells produce an increased amount of pro-inflammatory TNFα and IL-6 and show a high capability to activate HSC, the key fibrogenic cells in the liver (107). Further, depletion of $CD11c^+$ cells reduces the expression of pro-inflammatory cytokines in other non-parenchymal cells (NPCs) (107). As opposite to this, other data suggests that $CD11c^+$ cells protect liver integrity. $CD11c^+$ cell depletion worsens liver pathology in acetaminophen-induced acute liver injury (110). Furthermore, they seem to promote fibrolysis during fibrosis regression as shown in a model

of carbon tetrachloride (CCl4) induced liver fibrosis, where $CD11c^+$ cell depletion delays fibrosis regression and clearance of activated HSC (111).

Thus the role of DCs in hepatic injury is considered to be of a dichotomous character: on the one hand liver DCs have been accredited a pro-inflammatory function as they showed higher lipid content, elevated cytokine production and increased capacity for T cell stimulation (101,105,107,108). On the other hand depletion of DCs exacerbates liver pathology and slows fibrosis regression, suggesting a protective role (110,111).

Concerning the potential role of DCs in the pathogenesis of NASH Hennig *et al.* published a well conducted study in 2012 using the MCD model in mice. They used a combination of phenotypical and functional analyses both *in vivo* and *in vitro* to clarify the role of DCs during disease progression (109): After 6 weeks of MCD treatment the $CD11c^+$ MHC-II^+ population expands 3-4 fold and displays an activated, pro-inflammatory phenotype as measured by upregulation of the co-stimulatory molecules CD54, CD80 and CD86. At the same time other leukocyte cell populations like KCs, neutrophils, monocytes and $CD8^+$ T cells also increase, whereas NKT cells, B cells and $CD4^+$ T cells diminish. $CD11c^+$ MHC-II^+ cells isolated from a NASH liver produce increased levels of TNFα, IL-6, MCP-1 and IL-10 and show an increased cytokine response to TLR9 ligation. *In vitro* they also show an increased ability to activate $CD4^+$ T cells, but not $CD8^+$ T cells compared to cells from healthy liver. Furthermore, $CD4^+$ T cells produce higher levels of T_H1, T_H2 and T_H17 cytokines, while the expression of the T_{reg} phenotype is downregulated. Since these results implicate that DCs contribute to disease progression, a the authors continued their study under the hypothesis that DC depletion in CD11c-DTR mice mitigates hepatic insult (109). Interestingly, contrary to this hypothesis, the absence of $CD11c^+$ cells causes an exacerbation of the NASH phenotype. CD11c depleted animals experience higher weight loss, develop a higher intrahepatic inflammatory infiltrate, show accelerated hepatic fibrosis and increased production of pro-inflammatory cytokines by other liver NPCs. The frequency of KCs, neutrophils and inflammatory monocytes increases and KCs exhibit an elevated TLR9 and TLR4 expression, which has been linked to the pathogenesis and severity of NASH (112,113). The $CD8^+$ T cell population also increases, whereas the number of $CD4^+$ T cells and T_{regs} decreases compared to the control (109). Moreover, an increased presence of apoptotic bodies can be observed in CD11c depleted animals and expression of apoptotic markers increases. DC depletion also leads to the accentuation of sterile inflammation within the liver which has been connected to the pathogenesis of NASH (112–114). Additionally, DCs isolated from NASH-liver show a greater capacity to clear necrotic debris compared to those from healthy animals. This lead the authors to the conclusion that DCs limit sterile inflammation in NASH via the clearance of necrotic

cellular debris (109). In a final experiment, the role of DCs in the recovery phase of NASH was investigated by switching the diet back to normal chow. Here DC depletion delays the resolution of NASH. In summary, this study shows that DCs play a role both during progression and regression of NASH: On the one hand DCs expand in NASH and assume an activated phenotype, on the other hand depletion of $CD11c^+$ cells worsens the disease and delays its resolution. The authors conclude from their study that DCs limit fibroinflammatory injury in NASH through limiting sterile inflammation by clearance of cellular debris and by regulating the expansion of innate and adaptive immune cell subsets (109).

When looking at this data it is important to consider two major limitations. First, most of our current understanding of liver DCs is based on the study of MHC-II^+ or $CD11c^+$ cells. This marker combination is not sufficient, however, to distinguish DCs from other cell types, since CD11c expressing cells also include macrophages, monocytes or NK cells and MHC-II is present on all professional APCs (101,102,115). In addition, investigating $CD11c^+$ MHC-II^+ cells does not take into account the different functions of previously described individual DC subsets. Second, the most widely used animals model for investigating DCs is the CD11c-DTR model, which is depleted of all $CD11c^+$ cells (116). Observations made in these animals might not mimic the effect of DCs in vivo but are the result of the animal being depleted from all $CD11c^+$ cells (101)

In conclusion, current data suggests a potential role of DCs in both NASH and more severe liver injuries with established fibrosis. However, studies conducted so far do not permit a differentiation of liver DCs from other cells or between individual DC subsets. Various novel animal models have been developed in order to characterize specific cellular subtypes, such as the batf3-KO mouse for $CD103^+/CD8^+$ DCs or the IRF4-KO mouse for cDCs 2 (73,77). Only few of those have been investigated during NASH and fibrosis, they will present a powerful tool to gain better understanding of the role of immunologic cells in NASH (117).

1.7 Relevant surface markers of murine liver immune cells

The various subsets of immune cells found in the liver can be distinguished through their expression of surface molecules. Table 1 details the surface markers used in this study to identify various immune cells.

Antigen	Description
CD45	also known as *common leukocyte marker*, is a tyrosine kinase expressed on all nucleated cells of the hematopoietic lineage. It is often used as a general marker for all immune cells (118).
Antigens to distinguish DC subsets	
CD11b	also known as *integrin αM,* is expressed on a variety of cells such as granulocytes, monocytes, macrophages, various DC subsets and NK-cells (61,119).
CD11c	also known as *integrin αX,* is expressed on DCs, but also macrophages, monocytes and NK cells. A high expression of CD11c is especially attributed to DCs (101).
MHC-II	The major histocompatibility complex type II is present on APCs such as macrophages, DCs and B-cells (115).
CD103	This glycoprotein is expressed on the cDC 1 subtype in non-lymphoid tissue and can be used to distinguish this subsets from other DCs (76).
PDCA-1	also known as CD317 is typically used as a marker for pDCs, but can also be upregulated in other cells activated by IFN (94,115).
CD64	is a cellular receptor for immunoglobulins (Fc-Receptor). It can be used to distinguish monocyte-derived DCs from classical DC subtypes (87)
Antigens to distinguish monocyte, macrophage and granulocyte populations	
F4-80	F4-80 is typically highly expressed in all macrophages including KCs and on lower levels on monocytes (120).
Ly6C	a high expression of Ly6C is typical for classical monocytes, while low expression can be observed on the non-classical monocyte subset, KCs and restorative macrophages (45,117).
Ly6G	is a marker used for neutrophils (121).
Antigens to distinguish lymphocyte subsets	
CD19	is a costimulatory receptor and typically used as the hallmark antigen to identify the B cell lineage (122).
CD3ε	is a subunit of the CD3 surface molecule on T cells, which is necessary for TCR-mediated signal transduction. It is typically used as the hallmark antigen to identify the T cell lineage (39,123).
NK1.1	is a stimulatory receptor expressed on NK cells and NKT cells (39).

CD4	is a T cell co-receptor for signal transduction through MHC-II molecules. It is also present on monocytes, macrophages and some DC subtypes (39,60) .
CD8	is a T cell co-receptor for signal transduction through MHC-I molecules, but also present on some NK cells and the lymphoid cDC 1 subset (39,65).

Table 1 Surface markers used for flow cytometry to distinguish of various immune cells in the liver

1.8 Aims of this project

The aim of this project was to characterize changes of liver DC subtypes during developing and established steatohepatitis and to investigate the influence of batf3-dependent cDCs 1 on inflammation and the cellular infiltrate during disease progression.

As the hepatic consequence of the metabolic syndrome the incidence of NAFLD has increased dramatically in the past decade and is now the number one cause of liver disease in developed countries. The mechanisms which promote the progression from steatosis to steatohepatitis are not yet completely understood. DCs have been described to play a protective role in the development of NASH by limiting fibro-inflammation, however the role of individual DC subsets remains to be determined.

In this study, we used different dietary models to investigate animals with various severities of NAFLD, that is bland steatosis, initiating NASH and established NASH. The first aim of this study was to map changes of individual DC subsets based on their surface markers using multicolored flow cytometric analysis during disease development. As a second step, we wanted to investigate if and how batf3-dependent cDCs 1 have an impact on disease progression and in this context how they influence the composition of the hematopoietic infiltrate in the liver. As part of this we also wanted to determine whether the lack of batf3-dependent cDCs 1 affects the systemic metabolism of the animals.

2 Material and Methods

2.1 Animals

2.1.1 Housing and maintenance

All experiments have been approved by the ethics and animal care committees of Saarland University Medical Center, Homburg, Germany (Animal protocol number 46/2012). Wildtype (WT) or batf3$^{-/-}$ C57Bl/6 mice were purchased at Charles River (Sulzfeld, Germany) or Jackson Laboratories (Bar Harbor, USA). They were kept at the Helmholtz Centre for Infectious Research in Braunschweig, Germany and were transported at 8-10 weeks of age to our institute at University of Saarland, Innere Medizin II (Homburg, Germany). During maintenance in an assigned mouse cabinet (Bioscape, Castrop-Rauxel, Germany) the animals were kept in special pathogen free conditions and had access to food and water *ad libitum*. No more than 4 mice were kept in a cage. Food, water levels and general condition of the animals was controlled daily. Cages and water bottles were changed weekly, weight was monitored weekly or every second week. Individual animals were distinguished using the ear punch system depicted in Figure 1.

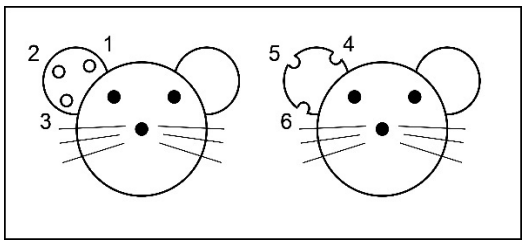

Figure 1 Ear punch system to distinguish individual animals (124)

2.1.2 Mouse strains

Batf3 knockout mice

Batf3-KO mice (Jackson Laboratories, Bar Harbor, USA, JAX stock number: 013755) were used to study the function of cDCs 1 *in vivo*. This knockout-strain lacks the exons 1 and 2 of the batf3 gene, abolishing gene function. The knock-out of batf3 results in the depletion of CD8α^{+} cDCs 1 in lymphoid organs and the corresponding CD103^{+} cDCs 1 in non-lymphoid organs (77).

Wild-type mice

C57Bl/6J mice were used as a wild-type control (WT). This is a widely used inbred strain and suggested by Jackson Laboratories as control strain for batf3-KO mice.

2.1.3 Dietary models

Normal chow diet

As an untreated control, C57BL/6J and batf3-KO mice matched in age and gender were fed cereal based chow (NC) for 5 weeks. The diet was purchased from Altromin (Lage, Germany; diet number 1324).

Methionine-choline-deficient diet

For experiments on NASH, mice were fed MCD purchased from Research Diet (New Brunswick, NJ, USA; diet number A02082002B). Its detailed composition is depicted in Table 2. MCD is a well-established model to investigate NASH as it induces severe liver inflammation, hepatic steatosis and hepatocellular damage in a short timeframe. For experiments to investigate established NASH the MCD treatment was continued over 5 weeks. For the pilot experiments investigating the onset of NASH the MCD treatment was continued over 2 weeks.

High sucrose diet

For experiments on hepatic steatosis mice were fed a HSD over the course of 5 weeks. The HSD was purchased from Research Diet (New Brunswick, NJ, USA; diet number A02082003B). Its detailed composition is depicted in Table 2.

	MCD		**HSD**	
Energy source	**g %**	**kcal %**	**g %**	**kcal %**
Protein	17	16	17	16
Carbohydrate	66	63	65	62
Fat	10	21	10	21
Ingredient	**g**	**kcal**	**g**	**kcal**
L-Alanine	3.5	14	3.5	14
L-Arginine	12.	48.4	12.	48.4
L-Asparagine-H2O	16	24	16	24
L-Aspartate	3.5	14	3.5	14
L-Cystine	3.5	14	3.5	14
L-Glutamine	40	160	40	160

Glycine	23.3	93.2	23.3	93.2
L-Histidine-HCl-H2O	4.5	18	4.5	18
L-Isoleucine	8.2	32.8	8.2	32.8
L-Leucine	11.1	44.4	11.1	44.4
L-Lysine-HCl	18	72	18	72
L-Phenylalanine	7.5	30	7.5	30
L-Proline	3.5	14	3.5	14
L-Serine	3.5	14	3.5	14
L-Threonine	8.2	32.8	8.2	32.8
L-Tryptophan	1.8	7.2	1.8	7.2
L-Tyrosine	5	20	5	20
L-Valine	8.2	32.8	8.2	32.8
Total L-Amino Acids	171.4	685.6	171.4	685.6
Sucrose	455.3	1821.2	452.3	1809.2
Corn Starch	150	600	150	600
Maltodextrin	50	200	50	200
Cellulose	30	0	30	0
Corn Oil	100	900	100	900
Mineral Mix S10001	35	0	35	0
Sodium Bicarbonate	7.5	0	7.5	0
Vitamin Mix V10001	10	40	10	40
L-Methionine	0	0	3	12
Choline Bitartrate	0	0	2	0
Total	**1009.2**	**4246.8**	**1011.2**	**4246.8**

Table 2 composition of methionine-choline-deficient and high sucrose diet: Mice were fed MCD for 5 weeks to induce steatohepatitis and HSD 5 weeks to induce steatosis. For pilot experiments on onset steatohepatitis mice were fed with MCD for 2 weeks. The composition is shown as indicated by the supplier, Research Diets (Brunswick, NJ, USA).

2.2 Organ harvest and collection of bodily fluids

For the organ harvest mice were anesthetised with isopropyl alcohol and killed through cervical dislocation. They were then placed on their back on a dissecting board and the belly fur was wetted with 70% ethanol. The skin was carefully cut along the midline and removed by blunt dissection to expose thorax and abdomen.

A thoracotomy was performed using scissors and 2-3ml blood were drawn from the heart's right ventricle using a 26G needle. The blood was left to clot in a 1.5ml tube for a minimum of 30 minutes at room temperature. It was then centrifuged at 1500g for 15 minutes to separate the serum and corpuscular parts. The serum was stored at -80°C until further usage.

For the organ harvest and fat collection the peritoneum was carefully cut open. To harvest the liver large and small intestines were mobilised and moved to the left to expose the liver. Liver lobes were cut at the base and carefully removed using a cotton swab. The tissue samples were either used to prepare a single cell suspension, further processed for histology, or flash frozen in liquid nitrogen and stored at -80°C for future analyzes. For fat tissue analyses all intraperitoneal organs were mobilized and all retroperitoneal fat was carefully cut off using scissors. The fat tissue was either used to prepare a single cell suspension or flash frozen in liquid nitrogen and stored at -80°C for future analyzes.

2.3 Preparation of a liver single cell suspension

Fig. 2 shows the liver digest protocol I to create a single cell suspension. This protocol was used during the early experiments of this study. Most dot-blots depicted in the results section were made with data obtained using the digest protocol II. In case data from earlier experiments with this protocol I is shown, it will be marked in the figure legend. Table 3 details the exact composition of used buffers.

Liver digest protocol I

To prepare a single cell suspension the median liver lobe or retroperitoneal fat was collected as described above and briefly stored in Hanks' Balanced Salt Solution (HBSS; Life technologies™, Carlsbad, USA) on ice until the organ harvest was completed. The tissue samples were cut into small pieces using a scalpel, transferred into a 15ml falcon tube and suspended in digestion buffer (3x800ml). All further mechanical and enzymatic digestion of the tissue was made in a 37°C water bath. At 5 and 15 minutes, the tubes were slightly tapped to mix the suspension and allow the buffer to thoroughly cover the tissue. After allowing the tissue to settle down the supernatant was collected and transferred through a 10µm mesh into a second 15ml falcon on ice containing 800ml collection buffer, which contains EDTA and stops the enzymatic digestion. The digestion buffer in the falcon was replaced and the tissue incubated further to continue the digest. After 15 minutes, the liver pieces were passed through a 1000 µl pipetting tip every 7 minutes. This helped to disperse loose cells and created a larger surface area for the enzymes. After each mixing step, the tissue was allowed to settle down

and the supernatant containing dissociated cells was collected into the second falcon as described above. After 50 minutes, the mixing interval was reduced to 5 minutes. In the beginning the pipetting tip was cut to allow bigger pieces to pass through, after 3 to 4 mixing steps all liver pieces were expected to be small enough to fit through an uncut tip.

In the second falcon collection buffer was added to the collected supernatant. Every second cycle the collected supernatant was centrifuged at 1400rpm for 4 minutes. The supernatant was discarded, and the pellet was then resuspended in 1600µl collection buffer and transferred for storage into a third falcon on ice until the digest was complete. After a maximum of 90 minutes the digest was terminated to avoid damage to already collected cells.

After the digest was completed the total amount of collected cell suspension was spun down and the supernatant discarded. To eliminate red blood cells an ammonium chloride potassium lysis (ACK-lysis) was performed: the cell pellet was resuspended in 2ml ACK-lysing buffer (Life technologies, Darmstadt, Germany), which was neutralized after one minute using 5ml collection buffer. It was then spun down as before, the pellet was resuspended in collection buffer to have total volume of 2 or 3ml, depending on pellet size, and kept on ice until further usage.

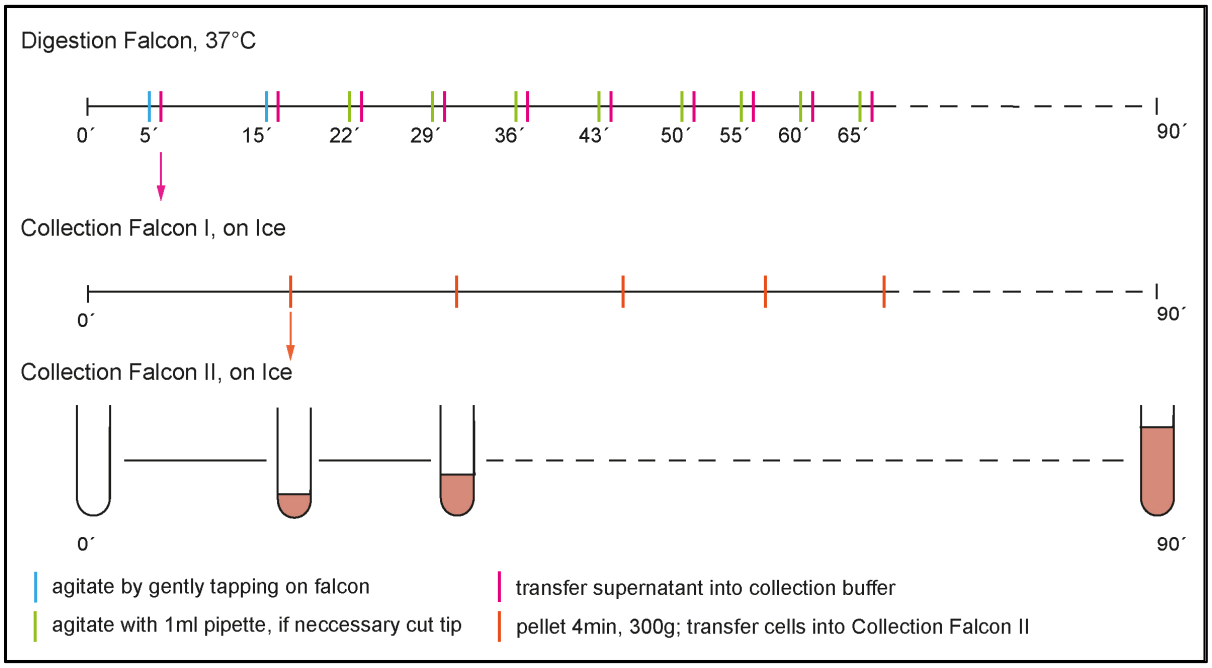

Figure 2 Flow chart of the digest protocol I: In this protocol the collected supernatant containing dispersed cells was centrifuged every 2 digestion cycles and then transferred into another falcon on ice. In the digest protocol II these centrifugation steps were abolished to reduce mechanical stress on cells.

Liver digest protocol II

During the course of the study the digest protocol was adjusted. The digest was performed as described above in digest protocol I, but the centrifugation steps during the digest

were abolished to reduce mechanical stress on cells. Further the collection buffer was prepared without EDTA as shown in Table 3. The disruption of enzymatic digestion was solely achieved by dilution of enzymes with collection buffer and storing it on ice. At the end of the digest all collected supernatant was centrifuged (180g, 8min, acc.4, decc. 2, 4°C) to pellet the cells and then ACK lysis was performed as described above. These modifications create less debris in the single cell suspension by reducing mechanical stress to the cells. All fat digests were made using this protocol as well as most of the liver digest for the representative data shown in this thesis.

Reagent	**Supplier**	**Concentration**
Digestion Buffer		
RPMI medium	Life technologies, Darmstadt, Germany	
Collagenase P	Roche, Mannheim, Germany	0.2 mg/ml
DNase	Life technologies, Darmstadt, Germany	0.1 mg/ml
Dispase	Roche, Mannheim, Germany	0.8 mg/ml
Heat inactivated FBS	Life technologies, Darmstadt, Germany	1 %
Collection Buffer (digest protocol I)		
RPMI medium	Life technologies, Darmstadt, Germany	
EDTA	Life technologies, Darmstadt Germany	2 mM
Heat inactivated FBS	Life technologies, Darmstadt, Germany	1 %
Collection Buffer (digest protocol II)		
RPMI medium	Life technologies, Darmstadt, Germany	
Heat inactivated FBS	Life technologies, Darmstadt, Germany	1%

Table 3 Composition of buffers used in the preparation of a liver or fat single cell suspension

2.3.1 Living cell count

To stain the cells for flow cytometric analysis (FACS-analysis) or to culture them it is important to determine the exact concentration of the cell suspension. This was done using the MACSQuant Flow Cytometer (Miltenyi, Bergisch-Gladbach, Germany). For this 10µl of cell suspension were stained with proprium iodide (PI) as shown in Table 4. PI is a fast and reliable method in flowcytometry to identify dead or dying cells. It permeates membranes of dead cells, while living cells are not affected, and binds to double stranded DNA (125). To avoid falsification of the results it is important to ensure a thorough mixing of the cell suspension prior to taking out the sample of the cell suspension. A volume of 15µl was measured on “high” setting and after debris exclusion (Figure 3.A) and cell doublets exclusion (Figure 3.B) the number of single PI negative cells (Figure 3.C) was used to calculate the living cell

concentration within the cell suspension. As the number of cells collected in the fat tissue digest is very low, the living cell concentration was not determined, but all cells were used for fluorescent staining.

Cell Count		
Reagent	**Supplier**	**Volume**
MACSQuant® Running Buffer	Miltenyi Biotec, Bergisch Gladbach, Germany	187 µl
Proprium Iodide	Miltenyi Biotec, Bergisch Gladbach, Germany	0.6 µg
Cell suspension		10 µl

Table 4 Composition of reagents to count the amount of living cells in the single cell suspension

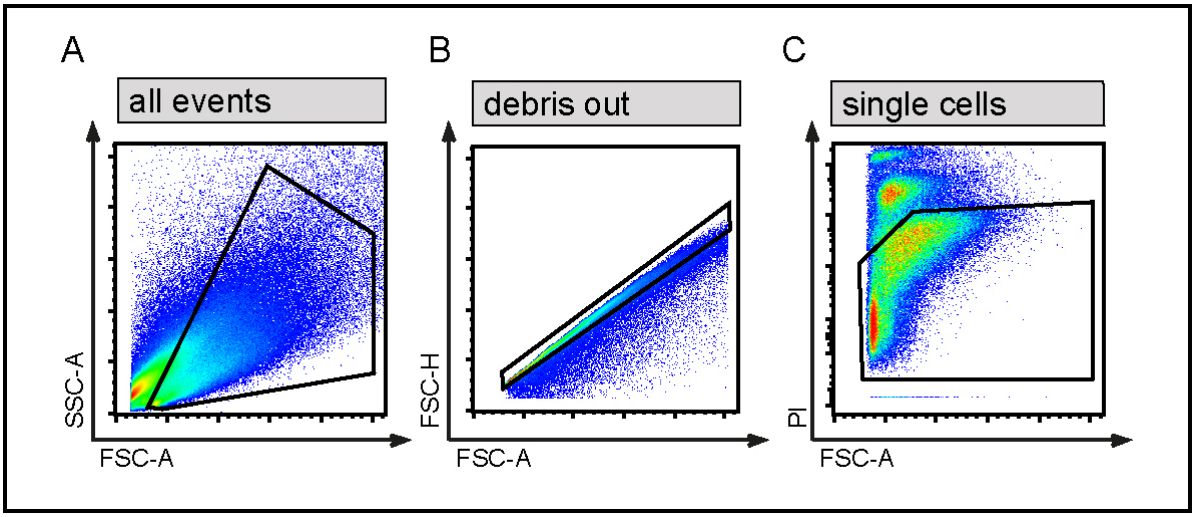

Figure 3 Gating strategy for living cell count: **A)** events with low values for size (FSC-A) and internal complexity (SSC-A) were excluded to get rid of cell debris **B)** cell area (FSC-A) was plotted against cell height (FSC-H) to exclude cell doublets **C)** events negative for PI signal were selected to measure only living cells

2.4 Flow-cytometric analysis

2.4.1 Basics of flow cytometry

Flow cytometry is a laser based technique used in immunology to analyze various qualitative and quantitative parameters of a cell suspension. Although a quite complicated system the flow cytometer can be broken down to 3 major parts: fluidics, optics and electronics. Fluidics guide the cells in a single cell stream through a path of light. Optics generate this light and can detect small changes caused by passing cells. Electronics convert these optical signals to electronic signals and depict them as an “event” on a histogram or dot plot. The information we gather is based on the manner how the passing cells scatter the light and if and how they emit fluorescence (126).

As a cell passes the light it reveals several information on its structural parameters without any prior handling: An increase of forward scatter (FSC) signifies a bigger cell size or surface area, while changes of sideward scatter (SSC) are proportional to the cells granularity (126).

To gather additional information on the cells such as surface receptors, intracellular proteins or viability fluorescent reagents can be used. When using a mixture of different fluorochromes-conjugated monoclonal antibodies these will bind to their respective antigen on the cell. The flow-cytometric analysis will then show a fluorescent signal proportional to the number of antibodies on the cell. The usage of different lasers and optical filters in a flow cytometer then enables the analysis of signals from various fluorochromes of different spectra, which allows the analysis of cell multiple parameters during a single measurement (126).

A problem in flow-cytometric analyzes can be unspecific background signals. These can be caused by binding of the antibodies to Fc-Receptors (FcR) on the target cell, nonspecific antibody interaction and cellular autofluorescence. To minimize background signals, it is therefore advisable to block unspecific binding prior to staining the cells using anti-FcR antibodies. Furthermore, a negative control staining should be performed for each fluorochrome. This can be done either by replacing the primary antibody of interest with an isotype control or simply not adding the antibody, which is called fluorescent minus one (FMO). The Isotype controls in class and type, but lack the specificity of the target, thus showing the level of unspecific binding (127).

In this study, we used the MACSQuant Analyzer 10 (Miltenyi Biotech, Bergisch Gladbach, Germany) for all flow-cytometric measurements. It is equipped with three lasers and eight optical filters which enables it to analyze probes with up to eight different fluorochromes as well as number, size and granularity of the cells. The optical configuration of the MACSQuant® Analyzer is detailed in Table 5.

Optical specification of MACSQuant Analyzer			
Laser + Excitation	**Channel**	**Filter**	**Dye**
Violet diode laser (405nm)	V1	450/50	VioBlue, AlexaFluor405, Pacific Blue BD, Horizon V450
	V2	525/50	VioGreen, AlexaFluor430
Blue argon laser (488nm)	B1	525/50	FITC, AlexaFluor488
	B2	585/40	PE
	B3	655 (LP)	PE-Cy5
	B4	750 (LP)	PE-Cy7

Red diode laser (635 nm)	R1	655 (LP)	APC, AlexaFluor647
	R2	759 (LP)	APC-Cy7
Blue argon laser	FSC	488/10	Size
	SSC	488/10	Granularity

Table 5 Optical configuration of a MACSQuant ®10 Analyzer

2.4.2 Monoclonal antibodies

Various combinations of fluorochromes-conjugated monoclonal antibodies were used in this study. A full list of the antibodies with their fluorochromes and isotype controls is depicted in Table 6. If no Isotype Control was available FMO was used as a negative control instead. Antibodies highlighted by *italic* print require a secondary antibody conjugated to a fluorochrome.

Antigen	**Conjugate**	**Dilution**	**Clone**	**Supplier**	**Host/ Isotype Control**	**Stock concentration**
CD 45	APC-Cy7	1:400	30F11	BioLegend	Rat IgG2α,κ	0.2 mg/ml
CD 11b	PE-Cy7	1:2000	M1/70	BioLegend	Rat IgG2b, κ	0.2 mg/ml
CD 11c	APC	1:400	N418	BioLegend	Armenian Hamster IgG	0.2 mg/ml
CD 11c	VioBlue	1:20	N418	Miltenyi Biotech	Hamster IgG	30 µg/ml
PDCA-1	FITC	1:400	927	BioLegend	Rat IgG2b, κ	0.5 mg/ml
PDCA-1	PE	1:200	129.C1	BioLegend	Rat IgG2b, κ	0.2 mg/ml
MHC-II	Alexa Fluor® 488	1:4000	M5/114.15.2	BioLegend	Rat IgG2b, κ	0.5 mg/ml
CD 103	PE	1:200	2.00E+07	BioLegend	Hamster IgG	0.2 mg/ml
Ly6G	FITC	1:200	1A8	BioLegend	Rat IgG2α, κ	0.5 mg/ml
CD 19	PE-Cy7	1:100	6D5	BioLegend	Rat IgG2α, κ	0.2 mg/ml
CD 3e	Alexa Fluor® 488	1:100	145-2C11	BioLegend	Armenian Hamster IgG	0.5 mg/ml
NK 1.1	*Biotin*	1:100	PK136	BioLegend	Mouse IgG2α, κ	0.5 mg/ml
CD 4	APC	1:100	GK 1.5	BioLegend	Rat IgG2b, κ	0.2 mg/ml
CD 8α	PE	1:200	53-6.7	Biolegend	Rat IgG2α, κ	0.2 mg/ml
F4/80	Alexa Fluor® 488	1:200	BM8	Biolegend	Rat IgG2α, κ	0.5 mg/ml
F4/80	PE	1:200	BM8	BioLegend	Rat IgG2α, κ	0.2 mg/ml
F4/80	*Biotin*	1:20	REA126	Miltenyi Biotech	Recombinant human IgG	30 µg/ml
Ly6C	APC	1:1000	HK1.4	BioLegend	Rat IgG2c, κ	0.2 mg/ml
TNFα	Alexa Fluor® A647	1:200	MP6-XT22	BioLegend	Rat IgG1, κ	0.5 mg/ml
CXCL 1	*unconjugated goat IgG*	1:500	polyclonal	Biotechne		1 mg/ml

Antigen	Conjugate	Dilution	Clone	Supplier	Host/ Isotype Control	Stock concentration
CCL 5	*unconjugated goat IgG*	1:500	polyclonal	Biotechne		1 mg/ml
Streptavidin (anti biotin)	Alexa Fluor® 405	1:400		Life Technology		1 mg/ml
Secondary AB Anti-Goat IgG	Alexa Fluor® 647	1:800*	polyclonal	Life Technology	Donkey IgG	2mg/ml

Table 6 Antibodies: Overview of all antibodies used in this study, including supplier, dilution, host and isotype control. Suppliers were Miltenyi Biotech (Bergisch Gladbach, Germany), BioLegend (San Diego, CA, USA), Life Technologies (Darmstadt, Germany). Antibodies highlighted by *italic* print are unlabled and required staining with a secondary antibody conjugated to a fluorochrome.

2.4.3 Multicolored fluorescent staining of surface antigens

Figure 4 shows the staining protocol for the staining of surface antigens. Cells and reagents were kept on ice during at all time. $1.25*10^5$ living, single cells were suspended in 400µl FACS-Buffer and pelleted at 300g for 4 minutes. To block nonspecific binding of fluorochromes-conjugated antibodies, cells were incubated for 5-10 minutes with 50µl FACS-Buffer containing murine Fc-Block and CD64 as detailed in Table 8. Then 50 µl staining mix containing various combinations of fluorochromes-conjugated primary antibodies was added and cells were incubated for further 20 minutes. To wash the cells 400 µl FACS-Buffer was added and the cells were spun down at 300g for 4min. For the analysis, the pellet was resuspended in 200 µl FACS-Buffer with 0.6 µg PI and measured using the MACSQuant Analyzer (Miltenyi Biotech, Bergisch Gladbach, Germany). Some markers were not available directly conjugated to a fluorochrome, which requires an additional staining step. The staining was performed as described above with the staining mix containing also the non-fluorescent primary antibody. Afterwards cells were incubated for another 20 minutes in 100 µl FACS-Buffer containing a secondary, fluorescent antibody to bind to the primary antibody. They were then washed and analyzed as described above. If the digest was done using digest protocol I the number of stained cells was $2.5*10^5$ living, single cells. The number of cells collected from a fat tissue digest is very low. Therefore, it was only possible to use one staining mix per animal when investigating fat tissue and all recovered cells were used for that stain. When staining for CD64 expression the Fc-Block was prepared without purified anti-CD64.

Table 7 details 5 basic marker combinations that were used in this study to look at individual cell populations. Antibodies highlighted by *italic* print were not used in all experiments.

Staining Mix	Antibodies
classical DCs	CD45, CD11b, CD11c, CD103, *CD64, MHC-II, F4-80*
plasmacytoid DCs	CD45, CD11b, CD11c, PDCA-1, MHC-II
lymphoid cells	CD45, CD19, CD3e, NK1.1, *F4-80, CD4*
myeloid cells	CD45, F4-80, CD11b, Ly6C
neutrophils	CD45, CD11b, *PDCA-1, F4-80*, Ly6G, *Ly6C*

Table 7 surface marker combinations used to identify different cell populations

Reagent	Supplier	Volume
Fc-Block I		
Fc-Block (anti-mouse CD16/32)	BioLegend, San Diego, USA	2 µl (stock 0.5 mg/ml)
CD64 purified	BioLegend, San Diego, USA	1 µl (stock 0.5 mg/ml)
MACS-Quant® Running Buffer	Miltenyi Biotech, Bergisch Gladbach, Germany	50 µl
Fc-Block II		
FcR-Blocking reagent	Miltenyi Biotech, Bergisch Gladbach, Germany	10 µl
CD64 purified	BioLegend, San Diego, USA	1 µl (stock 0.5 mg/ml)
MACS-Quant® Running Buffer	Miltenyi Biotech, Bergisch Gladbach, Germany	50 µl

Table 8 Composition of Fc-Blocking reagents used in multicolored fluorescent staining of surface antigens. The CD64 antibody was left out when analyzing CD64 expression.

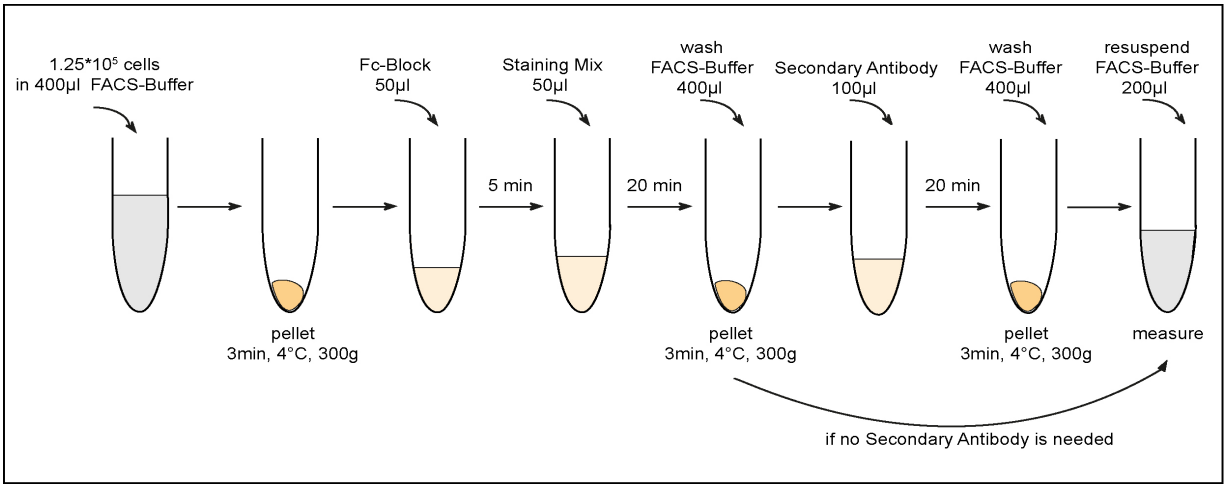

Figure 4 flow-chart of antigen staining protocol

2.4.4 Staining of intracellular cytokines

Staining of intracellular cytokines was performed using the BD Cytofix/Cytoperm™ Fixation/Permeabilization Kit (BD Biosciences, Heidelberg, Germany) according to the

manufacturers instructions. $2.5*10^5$ living, single cells were planted for 4h at 37°C in a U-Bottom 96-well plate as shown in Table 6. BD GolgiStop is a protein transport inhibitor that blocks intracellular transport processes which will result in the accumulation of most cytokine proteins in the Golgi complex. The cells were either left unstimulated or stimulated using LPS. After the incubation period cells were pelleted at 300g, 4°C for 3 minutes and kept on ice during all further steps. Staining of surface molecules was performed as described in chapter 1.3.4. After washing with 200 µl FACS-Buffer and pelleting the cells as described before, they were fixed and permeabilized by incubating them in 200 µl BD Fixation/Permeabilization solution for 20 min. They were then washed two times using 200 µl BD Perm/Wash™ buffer per well. To maintain cells in a permeabilized state mixes for intracellular staining were prepared using the BD Perm/Wash™ buffer rather than the standard FACS-Buffer. Cells were incubated for 20 minutes in 50 µl of staining mix containing the anti-cytokine antibody of interest. They then were washed two times using 200 µl BD Perm/Wash™ buffer and ultimately resuspended in 200 µl FACS-Buffer for flow cytometric analyses. Since the cells die during fixation it was not necessary to ad PI prior to measurement. If the digest was done using the original protocol the number of cells was $5*10^5$ living, single cells. Table 10 details the combination of antibodies used for surface stain and the antibodies used for intracellular staining.

Cell Culture		
Reagent	**Supplier**	**Volume or Concentration**
living, single cells		$5*10^5$ / well
RPMI	Life technologies, Darmstadt, Germany	200 µl / well
GolgiStop	BD Biosciences, Heidelberg, Germany	4 µl / 6ml culture medium
+/- LPS (*E. coli* O127:B8)	Sigma, Taufkirchen, Germany	250 ng / ml

Table 9: Composition of reagents for planting cell culture for intracellular staining.

Staining Mix	**Antibodies**
Surface staining	CD45, CD11b, CD11c, CD103, *PDCA-1, F4-80*
Intracellular staining	TNF or CXCL-1 or CXCL-2 or CCL-5

Table 10: Staining mix for surface stain during intracellular cytokine staining and the analyzed cytokines.

2.4.5 Data-analysis

Data was analysed using FlowJo 10.0.8 software (FlowJo LLC, Ashland USA). Statistical analyses were performed with Prism 5 software (Graphad Software). Performed tests were unpaired two-tailed T test, T test with Welch's correction or one-way ANOVA using Bonferroni post-test. *p<0.05, ** p<0.005, ***p<0.0001

2.5 Cytokine-array analysis

Cell culture supernatant was created by planting $5*10^5$ living, single cells in a total volume of 100 µl. Cells were incubated at 37°C for 18h either unstimulated or stimulated using LPS. The detailed composition of reagents is depicted in Table 11. Subsequently cells were spun down at 300g, 4°C for 3 minutes and a maximum of 90 µl supernatant was collected to avoid taking up any cells or debris. Supernatants of each group were pooled and stored at -80°C until further usage. The Cytokine Array was performed using the Proteome Profiler Mouse Cytokine XL protein array (Biotechne, Minneapolis, USA). This is a nitrocellulose membrane spotted with various capture and control antibodies to detect differences in cytokines, chemokines and growth factors between samples. The assay was performed according to the manufacturers' guidelines. For each membrane 200 µl supernatant was used. Prior to adding it to the membrane it was defrosted at room temperature and subsequently spun down (300g, 3min) to eliminate any particles. The membranes were imaged using Chemidoc^{MP} Imaging System (Biorad, Munich, Germany) and mean grey values were calculated using ImageJ 1.50i Software (Wayne Rasband, National Institutes of Health, USA).

Cell Culture		
Reagent	**Supplier**	**Volume or Concentration**
Living, single cells		$5*10^5$ / well
RPMI	Life technologies, Darmstadt, Germany	100 µl / well
+/- LPS (*E. coli* O127:B8)	Sigma, Taufkirchen, Germany	250 ng / ml

Table 11 Composition of reagents for cell culture to perform cytokine production array

2.6 Liver triglyceride quantification

Liver triglyceride content was determined using the abcam Triglyceride Quantification Kit (Cambridge, UK) following the manufacturer's guidelines. Liver tissue samples were harvested and stored at -80°C as described in chapter 2.2. 100mg of liver tissue was thawed on ice and then homogenized in a 5% NP-40/dH_2O solution using a Potter-Elvehjem tissue homogenizer (VWR, Darmstadt, Germany). Triglycerides were solubilized at 80-100°C and insoluble material was eliminated through centrifugation. In the assay triglycerides a lipase converts triglycerides to free fatty acids and glycerol. The latter is then oxidized to a product, which reacts with the probe to generate a colorimetric reaction. The resulting signal was measured using Tecan Sunrise^{TM} Microplate Reader (Tecan Group Ltd., Männedorf, Switzerland) at a wavelength of 570nm.

2.7 qPCR of retroperitoneal fat tissue

Real-time quantitative polymerase chain reaction (qPCR) is a widely used method to determine the expression levels of specific genes in a biological sample. PCR is a method to exponentially amplify highly specific DNA sections through repeating cycles of denaturation of template DNA to produce single stranded molecules, annealing of specific primers to the target sequence and the synthesis of the complementary sequence by a DNA polymerase. qPCR allows a real-time analysis of the DNA amplification and the starting amount of template DNA by using fluorescent dye that binds to double stranded DNA. The expression of specific genes in biological samples can be measured by isolating RNA from the samples and producing a complementary DNA (cDNA) through reverse transcription, which can then be used for qPCR with primers specific for the gene of interest. A housekeeping gene is used as a reference, which is a gene that does not vary in expression level in the sample type of interest.

Retroperitoneal fat tissue was collected as described in chapter 2.2. RNA extraction was performed using RNeasy Lipid tissue mini kit (Quiagen, Hilden, Germany) according to the manufacturer's guidelines. Following cDNA was synthesized through reverse transcription using the Quantinova RT system (Qiagen, Hilden Germany). qPCR was carried out with validated primers detailed in Table 12 using Qantinova SYBR Green qPCR reagen (Quiagen, Hilden, Germany) mix as a fluorescent dye. The plates were measured with the Applied Biosystems 7500 Fast (Darmstadt, Germany) using the following program: one cycle of DNA polymerase activation at 95°C for 2 min and 40 cycles of amplification with denaturation at 95°C for 5s and annealing and extension at 60°C for 30s. As a housekeeping gene beta-actin was used.

Gene	Catalog number	Supplier
CCL-2	QT00167832	Qiagen, Hilden, Germany
TNF	QT00104006	
CXCL-10	QT00093436	
IL-6	QT00098875	
Actb	QT00095242	

Table 12 Primers used for real-time quantitative PCR analysis of retroperitoneal fat tissue: target gene, catalog number and supplier are indicated for each primer used in this study

2.8 Serum analysis

Serum was prepared as described in chapter 2.2. ALT-Values were determined at the diagnostic laboratory center of Saarland University Hospital in Homburg, Germany. Serum

samples were diluted 1:2 or 1:5 with Sodium Chloride 0,9% (B. Braun, Melsungen, Germany) and the values calculated according to the dilution. Leptin levels were measured using leptin DuoSet® ELISA (Biotechne, Minneapolis, USA) according to the manufacturer's guidelines with the serum being diluted 1:10 or 1:5 in Reagent Diluent (0.5% Tween®20 in PBS). Serum insulin levels were measured using the murine insulin ELISA kit (Thermo Fischer Scientific, Germany) according to the manufacturer's guidelines. ELISA plates were measured using Tecan Sunrise Microplate Reader (Tecan Group Ltd., Männedorf, Switzerland) and values were calculated using the software www.elisanalysis.com (www.elisakit.com, Scoresby (Melbourne), Australia).

2.9 Intraperitoneal glucose tolerance test

For the intraperitoneal glucose tolerance test (IPGTT) animals were fasted for 6 hours. The blood for glucose testing was drawn from the tail vein. The mice were briefly warmed up under infrared light to dilate the blood vessels and then put in a restraining device. The vein was incised using a sterile scalpel and a small blood drop was put on the testing strip for blood glucose measurement using the Accu-check Aviva measuring system (Roche Diabetes Care GmbH, Mannheim, Germany). After measuring fasting glucose, the animals were injected intraperitoneal with 2 mg glucose/g body weight in a total volume of 200µl PBS. Blood glucose measurement was repeated at 30, 60, 120 and 180 minutes after the glucose injection.

2.10 HbA1c measurement

For HbA1c measurement blood was collected from the mice' tails as described in chapter 2.7. To prevent it from clotting blood was kept in PBS (Life technologies, Darmstadt Germany) containing 10mM EDTA (Life technologies, Darmstadt Germany). HbA1c was directly analyzed at the diagnostic laboratory center of Saarland University Hospital, Homburg, Germany.

2.11 Histology

2.11.1 Preparation of paraffin sections

For paraffin sections one liver lobe was carefully cut at the base and stored in 4% paraformaldehyde solution (VWR International GmbH, Darmstadt, Germany). The tissue samples were transferred to the Institute of Anatomy and Cell Biology, University of Saarland,

where it was embedded in paraffin, cut into 5 µm slices and either stained with hematoxylin-eosin (HE) or left native for later connective tissue staining.

2.11.2 Necroinflammatory score

The HE sections were assessed based on the presence of inflammation, necrosis and hepatocyte ballooning graded on a scale from 0 to 4 (Table 13). This was done using the Leica DM500B microscope (Leica Microsystems, Wetzlar, Germany). Of each liver lobe two different regions were blindly assessed with 200x magnification.

Necroinflammatory Score	
0	absent
1	mild or focal
2	noticeable
3	severe

Table 13: Score to assess necroinflammation in liver sections: scoring was based on presence of inflammatory infiltrate, hepatocellular balooning and necrosis

2.11.3 Connective tissue staining

Connective tissue staining of paraffin embedded liver sections was performed using the Picro Sirius Red Stain Kit (Abcam, Cambridge, UK) and evaluated using the Leica DM500B microscope (Leica Microsystems, Wetzlar, Germany). Sirius Red Stain is a technique for the histological visualization of collagen I and III fibers. Staining was performed according to the manufacturer's guidelines. Since paraffin sections were used, deparaffinization by submerging the slides in alcohol as following:

2 x 3min	Xylol
3 min	1:1 Xylol: 100% ethanol
2 x 3 min	100% ethanol
3 min	95% ethanol
3 min	70% ethanol
3 min	50% ethanol

Rinse of ethanol with tap water

3 Results

3.1 Effects of dietary treatment on WT mice

Figure 5.A shows representative pictures of HE-stained liver of WT mice treated with either 5 weeks NC, HSD or MCD. Animals treated with NC show a regular histologic liver structure without any signs of inflammation or steatosis. In HSD livers a mild, mostly microvesicular steatosis can be observed with occasional signs of necroinflammation such as inflammatory infiltrates or hepatocellular ballooning, but an overall low scoring for NASH at either 0 or 1 points. In the 5 weeks MCD treated WT animals the histological assessment shows established steatosis, both micro- and macrovesicular and severe signs of necroinflammation with frequent inflammatory infiltrates, necrosis and hepatocellular ballooning. The histological observations for steatosis are paralleled by the values for quantitative liver triglyceride measurement: in WT animals NC livers have a low level of triglyceride content (*mean NC WT 13.6 µg/mg liver*), which increases significantly to an average of *59.1 µg/mg liver* in HSD treated animals and even further to *117.8 µg/mg liver* in 5 weeks MCD treated animals (Figure 5.E). The inflammatory infiltrate can also be detected in flow cytometric analysis based on the influx of $CD45^+$ cells. These have an average percentage of *33.5%* $CD45^+$ cells within all living cells in the NC treated healthy WT animals. Parallel to the histological scoring in WT animals, this ratio does not change significantly in HSD treated animals (*mean WT HSD 29.2%*), but significantly doubles to an average of *68.7%* in the 5 weeks WT MCD treated group (Figure 5.B). Serum ALT values, as a further parameter for liver damage, also mirror these tendencies: in NC treated animals the mean ALT values are at *32.4 U/L* and slightly, albeit not significantly, increased to *81.1 U/L* in HSD. After MCD feeding the values more than triple to an average of *277.7 U/L* after 5 weeks (Figure 5.D).

Summary Chapter 3.1:

- 5 weeks HSD feeding results in bland liver steatosis with increased liver triglyceride content, but without histological signs of inflammation, increased $CD45^+$ cell infiltrate or elevated ALT serum values.
- 5 weeks of MCD feeding results in NASH, which is presented as severe histological signs of inflammation, increased $CD45^+$ cell infiltrate, increased liver triglyceride content and elevated ALT serum values.

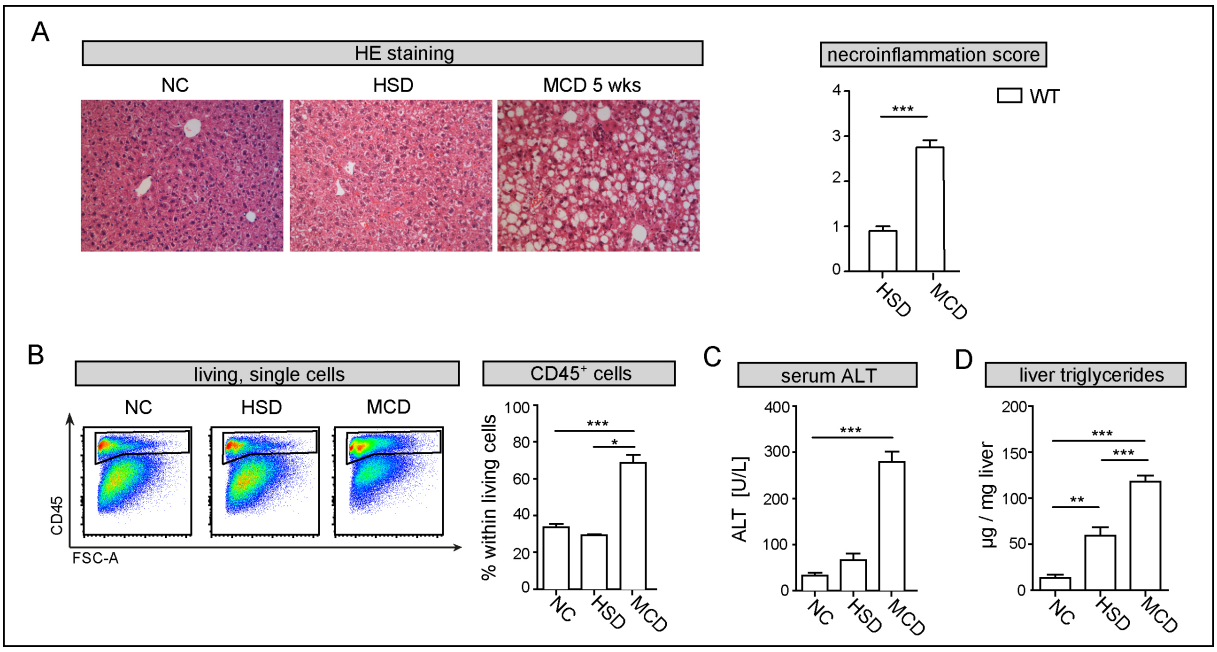

Figure 5 parameters of disease progression in WT C57Bl/6 mice after 5 weeks of HSD or MCD treatment or feeding of NC **A)** histological assessment of HE-stained liver sections imaged at 20x objectives. The bar graph shows the necroinflammatory scoring based on the presence hepatocellular ballooning, necrosis and inflammation: n_{HSD} = 10, n_{MCD} = 8. Data includes samples from 2-4 independently conducted experiments **B)** infiltrate of CD45$^+$ hematopoietic cells in the liver. Left figure shows representative dot-blots gated on living, single cells with signal for CD45 (*APC-Cy7 1:400*) plotted against forwards scatter and selecting leukocytes by gating on CD45$^+$ cells. Right figure shows bar-graph with percentage ratio of CD45$^+$ cells within living, single cells of WT mice after NC, HSD or MCD treatment: n_{NC}= 5, n_{HSD} = 5, n_{MCD} = 5. Data is representative of multiple, independent experiments for NC, HSD and MCD: repetitions$_{NC}$ = 3 (n=4-5/group), repetitions$_{HSD}$ = 6 (n=3-5/group), repetitions$_{MCD}$ = 4 (n=4-5/group). Bar-graphs depict mean + SEM. C) bar graph shows comparison of serum ALT values: n_{NC} = 12, n_{HSD}= 13, n_{MCD} = 18. Data includes samples from 2-4 independently conducted experiments per treatment group D) bar graph shows comparison of liver triglyceride levels. Data for liver triglyceride measurement was provided by Anna Maier. Bar-graphs depict mean + SEM. Data includes samples from 3-4 independently conducted experiments per treatment group. Significance is indicated through *p<0.05, ** p<0.005, ***p<0.0001. Underlined asterisks show statistical significance compared to the respective NC group of WT animals.

3.2 Identifying cDC subtypes in the murine liver

Since the characterization of CD11c$^+$MHC-II$^+$ cells as DCs is not sufficient to map cDC subtypes in the murine liver it is necessary to develop a gating strategy, that employs a more accurate marker combination. This is depicted in Figure 6*:* A basic gating strategy is used for all flow-cytometric analyses in this study (Section A). It includes gating on living, single cells as described in chapter 2.3.1 and subsequently selecting all CD45$^+$ to gate on all immune cells. When looking at the CD11c expression of CD45$^+$ leukocytes it is possible to distinguish between CD11c negative and positive cells (Figure 6.B). Since cDCs are characterized by a high expression of CD11c a gate was drawn that included only events with a high CD11c signal, but left out all events with an intermediate or negative signal. As the two cDC subtypes are characterized by their expression of either CD11b or CD103 these markers are then plotted against each other as depicted (Figure 6.C). This separates the CD11c^{hi} cells into three different populations: One population shows a positive signal for CD11b (yellow gate), one is

positive for CD103 (dark blue gate) and the remaining cells are negative for both markers. A CD11b CD103 double positive population is not present. This expression pattern marks the $CD11c^{hi}CD103^{+}CD11b^{-}$ events as cDCs 1 and the $CD11c^{hi}CD103^{-}CD11b^{+}$ events as both cDCs 2 and monocyte derived DCs, while the $CD11c^{hi}CD11b^{-}CD103^{-}$ events are a mixture of other CD11c expressing cells. To verify that cells of the yellow and dark blue gate are indeed DCs the MHC-II expression can be checked (Figure 6.D, Figure 6.E). Indeed, both cell populations show a positive signal for MHC-II (pink gate, light blue gate) and do not contain MHC-II negative cells. Consequently, all cells in the yellow and dark blue gate of Figure 6.C are DCs and adding MHC-II to the staining mix does not further separate the cell populations, thus does not provide further information. Therefore, to differentiate between the cDC subtypes, it is sufficient to gate on $CD11c^{hi}$ cells and subsequently $CD103^{+}$ or $CD11b^{+}$ cells without the need for MHC-II as an additional marker.

An alternative gating method for $CD11b^{+}$ DCs is depicted in Figure 6.G and Figure 6.H, with the respective isotype controls in Figure 6.J. Here the CD11c and MHC-II signal of $CD45^{+}$ leukocytes is first plotted against each other and only $CD11c^{hi}MHC\text{-}II^{hi}$ expressing cells are gated on (red gate). Subsequently $CD11b^{+}$ expressing cells (orange gate) are selected. This is valid, as in Figure 6.C $CD11c^{hi}$ cells do not contain a CD11b CD103 double positive cell population, therefore all CD11b expressing cells are CD103 negative and vice versa. This is a gating strategy that can be useful during the inflammatory state, in which some non-DC cells upregulate their CD11c expression and possibly shift into the $CD11c^{hi}$ gate. Adding the criterion of a high MHC-II expression to the gating strategy preempts that non-DCs are included in the analysis.

Since the $CD11b^{+}$ DCs can either origin from the monocyte cell-line or develop from preDCs. CD64, which is expressed by moDCs, but not cDCs, can be used to separate these two cell types. As depicted in Figure 6.I when plotting $CD11b^{+}$ DCs accordingly to their $CD64^{+}$ expression, they separate into a $CD64^{+}$ population (red gate), which represent moDCs, and a $CD64^{-}$ population (dark green gate) which represent cDCs 2.

Concluding a reliable way to identify the cDC 1 and $CD11b^{+}$ DC subpopulation is to use a marker combination that includes CD11c and CD11b or CD103 respectively, with the crucial step being the selection of only $CD11c^{hi}$ signals. As additional markers MHC-II can be used, which is especially useful in the inflamed liver, and CD64 to separate the $CD11b^{+}$ DC population accordingly to its origin.

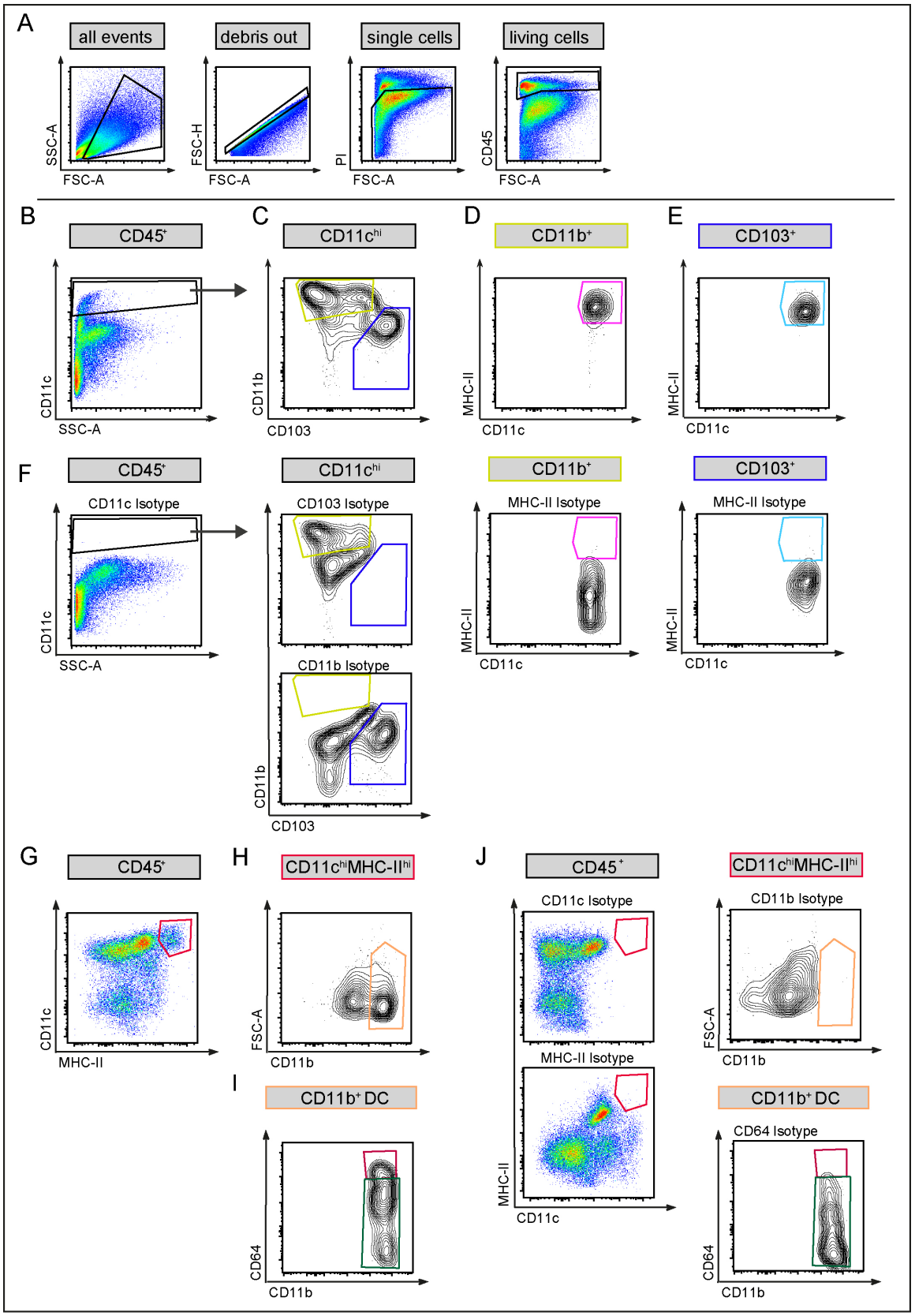

Figure 6 Gating strategy for cDC subtypes in the murine liver **A)** basic gating strategy: debris, doublet and dead cell exclusion. Gating on leukocytes by selecting all CD45$^+$cells. **B)** representative dot blots of CD45$^+$ cells showing CD11c signal (*APC 1:400*) plotted against sideward scatter: gating on CD11c^{hi} cells **C)** representative contour blots of CD11c^{hi} cells showing CD11b signal (*PE-Cy7 1:2000*) plotted against CD103 signal (*PE 1:200*) to gate on

$CD103^+CD11b^-$ cells (dark blue gate) and $CD103^-CD11b^+$ cells (yellow gate) **D)** representative contour blots of $CD103^-CD11b^+$ cells showing MHC-II signal (*FITC 1:4000*) plotted against CD11c signal (*APC 1:400*) to gate on $MHC\text{-}II^+$ cells (pink gate) **E)** representative contour blots of $CD103^+CD11b^-$ cells showing MHC-II signal (*FITC 1:4000*) plotted against CD11c signal (*APC 1:400*) to gate on $MHC\text{-}II^+$ cells (light blue gate) **F)** isotype controls for gating strategy of figures B-F **G)** representative dot blots of $CD45^+$ cells showing CD11c signal (*APC 1:400*) plotted against MHC-II signal (*FITC 1:4000*) to gate on $CD11c^{hi}$ $MHC\text{-}II^{hi}$ cells (red gate) **H)** representative contour plot of $CD11c^{hi}MHC\text{-}II^{hi}$ cells showing CD11b signal (*PE-Cy7 1:2000*) plotted against forwards scatter to gate on $CD11b^+$ cells (orange gate) **I)** representative contour plot of $CD11c^{hi}MHC\text{-}II^{hi}CD11b^{hi}$ cells showing CD64 signal *(Brilliant Violet 421 1:200)* plotted against CD11b (*PE-Cy7 1:2000)* to gate on $CD64^+$ (dark red gate) and $CD64^-$ (dark green gate) **J)** isotype controls for gating strategy of figures G-I

3.3 Mapping DC subtypes during disease progression

Liver DCs have been suggested to be involved in the pathogenesis of NASH. The first aim of this study was to determine how DC subtypes change during disease progression in WT animals. For this purpose, WT animals were fed either HSD or MCD for five weeks to induce steatosis or steatohepatitis respectively. NC fed animals served as a control group. The DC subtypes were then tracked based on their expression of DC surface antigens using flow cytometry.

3.3.1 cDCs 1

To track changes of the $CD103^+$ cDC 1 population in different treatment groups the flow cytometric data can be analyzed as described in chapter 3.1. Figure 7.B shows an influx of $CD11c^{hi}$ cells in the MCD diet group, whereas the dot blot of the HSD experiment does not change compared to the control NC fed group. When looking at the $CD103^+$ cells among this population they show similar changes (Figure 7.C and E). The percentage ratio of $CD11c^{hi}CD103^+$ cells does not change significantly in the HSD treated animals (*means WT: NC 1.8%, HSD 2.2%*) nor does the total cell amount per gram liver (*means WT: NC 36x10^3 cells/g liver, HSD 27x10^3 cells/g liver*). After 5 weeks of MCD diet the percentage ratio of cDCs 1 increases about 2.4-fold to *mean 4,4%*. These changes are even more distinct in the absolute cell count per gram liver, where the numbers increase 8.2-fold to *mean 300x10^3 cells/g liver*. Thus 5 weeks feeding of HSD does not cause any significant change in the cDC 1 subpopulation, whereas MCD treatment leads to an influx of cDCs 1.

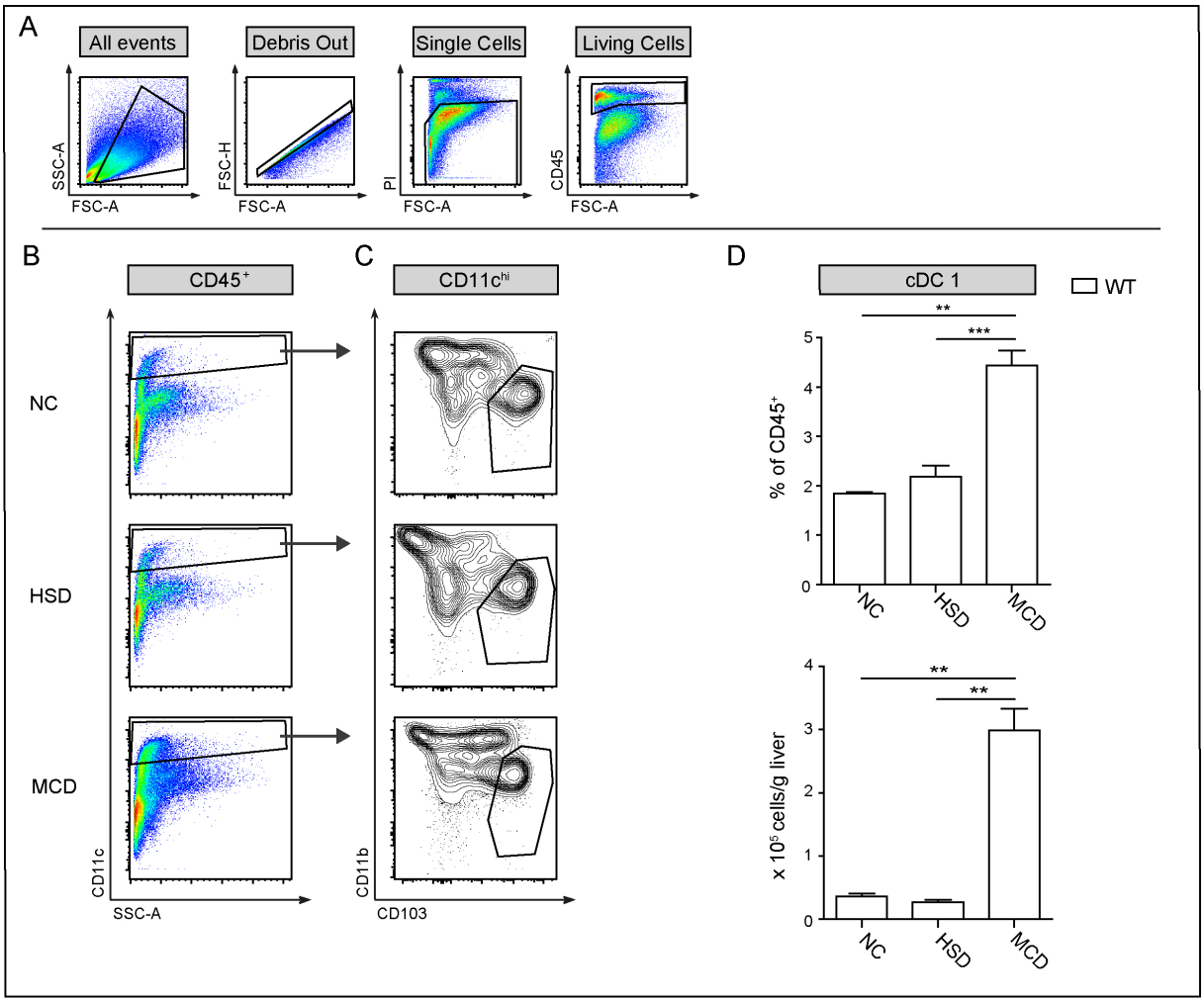

Figure 7 changes of cDCs 1 in WT C57Bl/6 after 5 weeks of HSD or MCD compared to NC fed animals **A)** basic gating strategy: debris, doublet and dead cell exclusion. Gating on leukocytes by selecting all CD45$^+$cells. **B)** representative dot blots of CD45$^+$ cells showing CD11c signal (*APC 1:400*) plotted against sideward scatter: gating on CD11c^{hi} cells **C)** representative contour blots of CD11c^{hi} cells showing CD11b signal (*PE-Cy7 1:2000*) plotted against CD103 signal (NC: *PE 1:200*; HSD, MCD: *A488 1:200*) to gate on CD103$^+$ DCs **D)** bar-graphs show comparison of percentage ratio within CD45$^+$ cells (upper graph) and total cell amount per gram digested liver (lower graph) of cDCs 1 in different dietary models. n_{NC}= 5, n_{HSD} = 5, n_{MCD}= 5.
Data (A-D) for NC, HSD and MCD is representative of multiple independent experiments: repetitions$_{NC}$= 3 (n= 4-5), repetitions$_{HSD}$= 5 (n=4-5), repetitions$_{MCD}$= 4 (n=4-5). Bar-graphs depict mean + SEM. Significance is indicated through *p<0.05, ** p<0.005, ***p<0.0001. Underlined asterisks show statistical significance compared to the respective NC group of WT animals.

3.3.2 CD11b$^+$ DCs

Changes in the CD11b$^+$ DC population are investigated using a gating strategy as described in chapter 3.1: a gate is drawn around cells that show a high expression of CD11c and MHC-II and then CD11b positive events are selected. Similar as described for CD11c^{hi} cells in Figure 7 it is possible to detect an influx of CD11c^{hi}MHC-II^{hi} cells in the MCD treated group, whereas the dot blot for HSD animals does not show distinct changes compared to the control group (Figure 8.B). And same as cDCs 1, changes of CD11b$^+$ DCs mirror those of the CD11c^{hi} population: the average percentage ratio in the HSD group does not change

significantly compared to the control group (*means WT: NC 2.2%, HSD 2.7%*), nor are there any significant changes in total cell count per gram liver (*means WT: NC 34x10^3 cells/g liver, HSD 27x10^3 cells/g liver*). On the other hand, MCD treatment amplifies the percentage ratio 3.6-fold to an average of *7.8%* after 5 weeks feeding. This observation is mirrored in the total cell count with a 13-fold increase after 5 weeks MCD treatment *(mean WT: MCD 448x10^3 cells/g liver*).

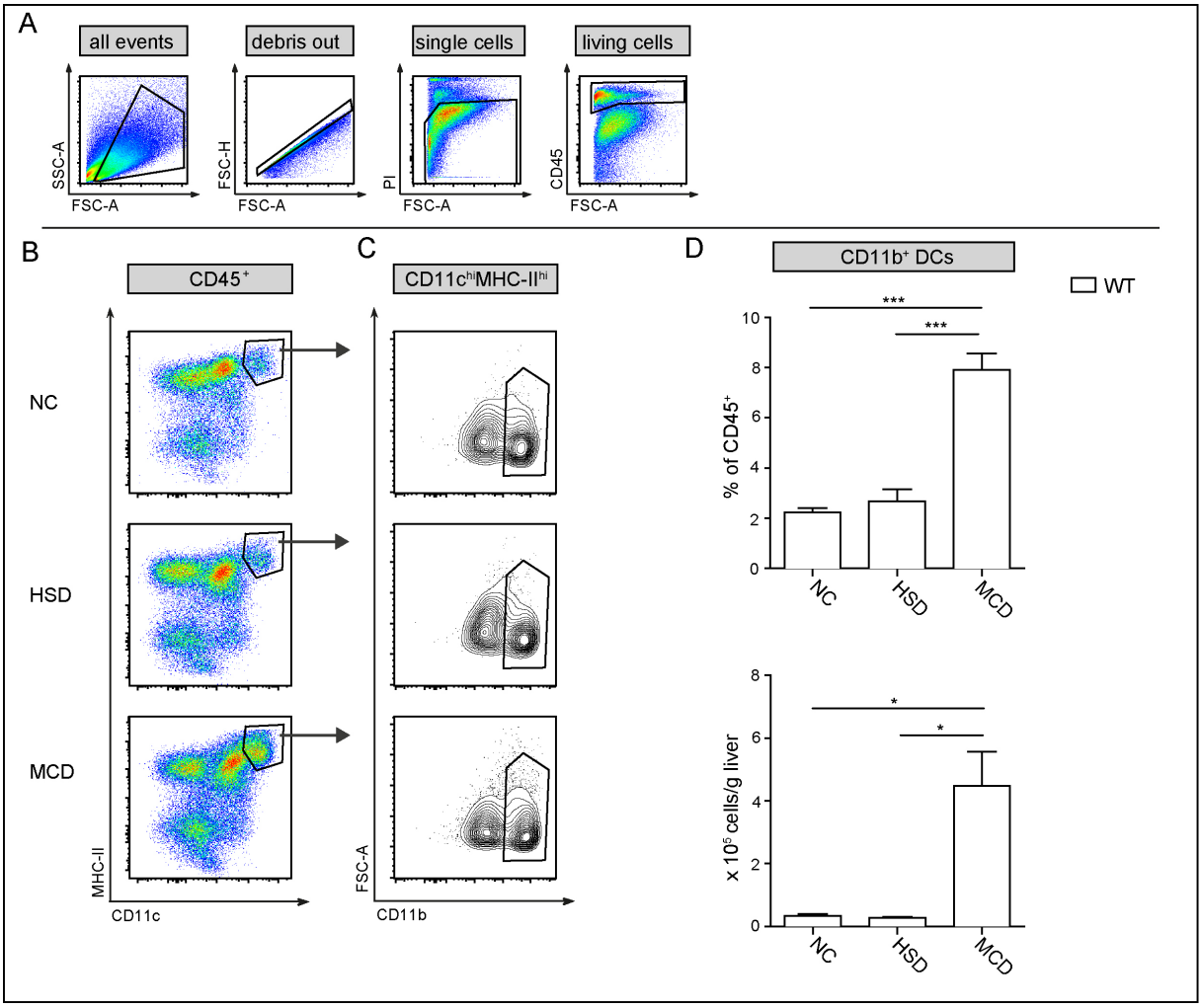

Figure 8 changes of CD11b$^+$ DCs in WT C57Bl/6 mice after 5 weeks of HSD or MCD compared to NC fed animals. **A)** basic gating strategy: debris, doublet and dead cell exclusion. Gating on leukocytes by selecting all CD45$^+$cells. **B)** representative dot blots of CD45$^+$ cells showing CD11c signal (*APC 1:400*) plotted against MHC-II signal *(FITC 1:4000):* gating on only high expression of CD11c and high MHC-II **C)** representative contour blots of CD11c^{hi}MHC-II^{hi} cells showing CD11b signal (*PE-Cy7 1:2000*) plotted against forwards scatter to gate on CD11b$^+$ DCs **D)** bar-graphs show comparison of percentage ratio within CD45$^+$ cells (upper graph) and total cell amount per gram liver (lower graph) of CD11b$^+$DCs in different dietary models. n_{NC}= 5, n_{HSD}= 5, n_{MCD}= 5.
Data (A-D) for NC, HSD and MCD is representative of multiple independent experiments: $repetitions_{NC}$= 2 (n=3-5), $repetitions_{HSD}$= 5 (n=4-5), $repetitions_{MCD}$= 3 (n=4-5). Bar-graphs depict mean + SEM. Significance is indicated through *p<0.05, ** p<0.005, ***p<0.0001. Underlined asterisks show statistical significance compared to the respective NC group of WT animals.

3.3.3 pDCs

The pDC population can be identified using a staining mix that contains CD11c, CD11b and PDCA-1. After gating on living, single cells that express CD45 (Figure 9.A) a gate is drawn based on the expression of CD11c. Unlike cDCs, pDCs express intermediate levels of CD11c therefore all CD11c positive cells are selected (Figure 9.B). When subsequently plotting the CD11b signal against the PDCA-1 signal the pDC population, which is negative for CD11b expression and positive for PDCA-1 expression, distinctly separates from remaining events (Figure 9.C). Tracking this population in different treatment models reveals that the percentage ratio of pDCs is significantly altered only after 5 weeks of MCD diet in the steatohepatitis model (*means WT: NC 3.0%*, *MCD 5.2%*), but does not change in the HSD treated animals (*mean WT: HSD 3.3%*). The total cell count per 10^6 living cells mirrors this increase in the MCD group (*means WT: NC 9x10^3 cells/10^6 living cells, MCD 28x10^3 cells/10^6 living cells*). In the HSD model, the total cell count per 10^6 living cells does not alter significantly (*mean WT: HSD 10x10^3 cells/10^6 living cells*).

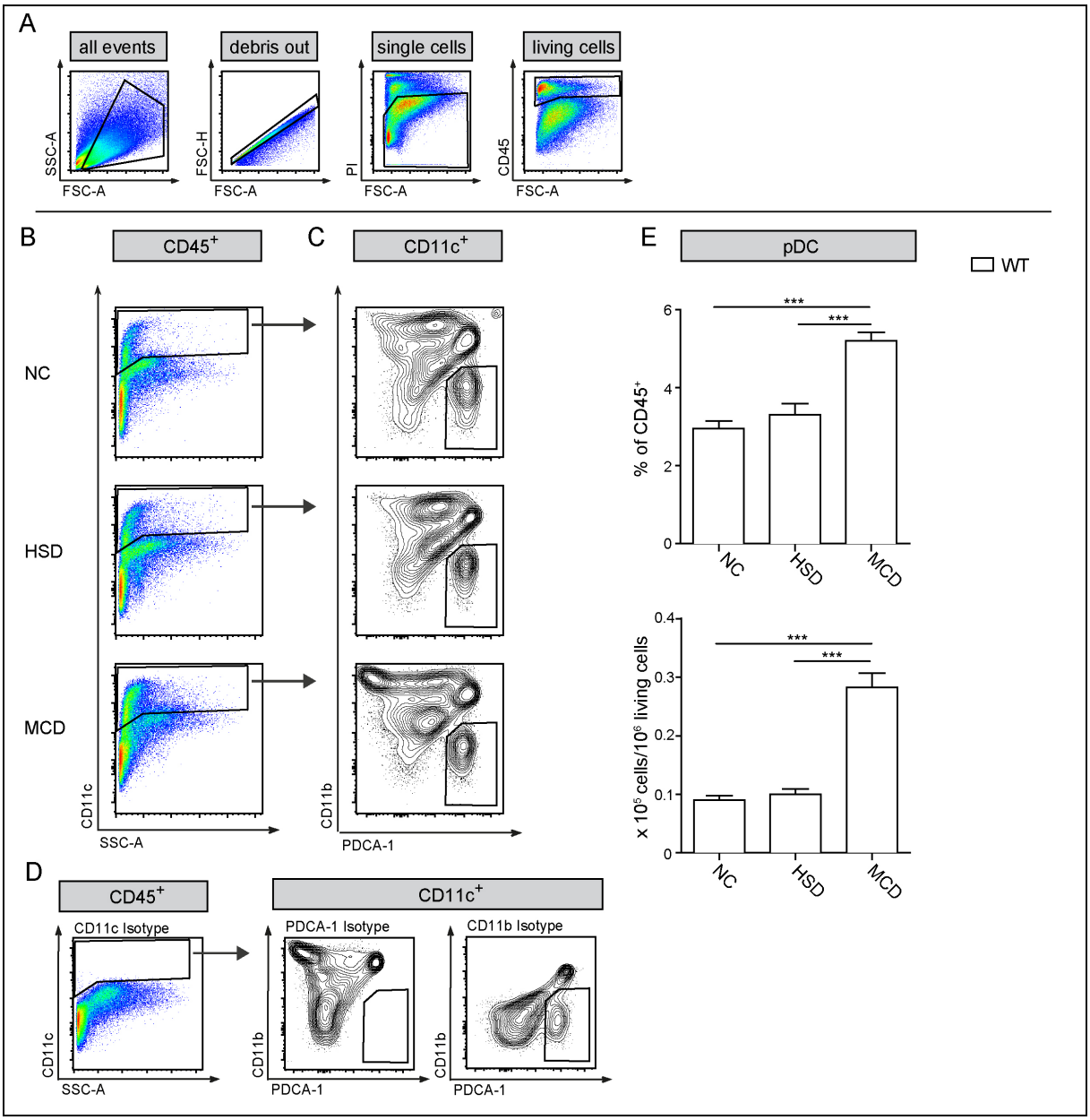

Figure 9 changes of pDCs in WT C57Bl/6 mice after 5 weeks of HSD or MCD compared to NC fed animals. **A)** basic gating strategy: debris, doublet and dead cell exclusion. Gating on leukocytes by selecting all CD45$^+$cells. **B)** representative dot blots of CD45$^+$ cells showing CD11c signal (*APC 1:400*) plotted against sideward scatter to gate on all CD11c$^+$ cells **C)** representative contour blots of CD11c$^+$ cells showing CD11b signal (*PE-Cy7 1:2000*) plotted against PDCA-1 signal (*PE 1:200*) to gate on PDCA-1$^+$ CD11b$^-$ cells **D)** Isotype controls for CD11c (*APC 1:400*), PDCA-1 (*PE 1:200*) and CD11b (*PE-Cy7 1:2000*) **E)** bar-graphs show comparison of percentage ratio within CD45$^+$ cells (upper graph) and total cell amount per 10^6 living cells (lower graph) of pDCs in different dietary models. n_{NC}= 5, n_{HSD}= 5, n_{MCD}= 5.
Data (A-E) for HSD and MCD is representative of multiple independent experiments: $repetitions_{HSD}$ = 4 (n=4-5), $repetitions_{MCD}$ = 3 (n=4-5). NC experiment was performed one time. Data shown for MCD was created using the digest protocol I. Bar-graphs depict mean +SEM. Significance is indicated through *p<0.05, ** p<0.005, ***p<0.0001. Underlined asterisks show statistical significance compared to the respective NC group of WT animals.

3.3.4 TNFα production by DC subtypes

To further characterize the role DCs play in the pathogenesis of NASH the subtypes can also be analyzed on a functional level. This can be done through intracellular cytokine staining with TNFα-antibodies and a surface staining with a combination of cDC markers.

Since the cells die during the permeabilization step of the cell membrane during the staining procedure, gating on PI positive, living cells is not necessary. The basic gating strategy is limited to debris exclusion, single cell selection and gating on $CD45^+$ cells (Figure 10.A). DC subtypes are gated on as described in chapter 3.2 by selecting $CD11c^{hi}$ expressing cells and then either $CD103^+$ cells or $CD11b^+$ cells (Figure 10.B middle). Additional gates are drawn to analyze the total CD11c expressing population as well as all $F4\text{-}80^+$ cells (Figure 10.B right and left). When subsequently plotting the TNFα signal against forward scatter the populations are split into positive and negative events, where the positive population corresponds to the intracellular produced TNFα (Figure 10.C). $CD11c^+$ cells show an average TNFα production of *5.0%* in WT NC fed mice, which does not change significantly in HSD treated WT animals (*mean WT: HSD 5.6%*). In WT MCD treated animals TNFα production of $CD11c^+$ cells increases significantly to an average of *12.6%*. In the $CD11b^+$ DC population the overall ratio of TNFα positive cells is higher at an average of *12.9%* in the NC fed group, but it is not affected significantly neither in HSD treated animals nor in MCD treated animals (*mean WT: HSD 14.4%, MCD 10.6%*). cDCs 1 neither show any significant increase in TNFα positive cells in HSD or MCD compared to NC (*mean WT: NC 2.9%, HSD 3.1%, MCD 2.4%*). Also, the overall percentage ratio of TNFα producing cells is markedly lower than that of $CD11b^+$ DCs. The average ratio of TNFα producing cells in $F4\text{-}80^+$ cells of NC fed mice is at *4.3%*. This does not change in HSD treated animals, where the average percentage ratio is at *3.6%*. Parallel to the TNFα production of the $CD11c^+$ population the ratio of TNFα positive cells increases significantly to *21.5%* in the MCD treated group. Taken together neither cDC subtype significantly increases its TNFα production in HSD induced steatosis or MCD diet induced NASH, whereas the total of CD11c and F4-80 expressing cells show a significant upregulation of TNFα-production in MCD induced NASH. This points towards the fact that the upregulated TNFα-production in the $CD11c^+$ population stems from upregulated production of $F4\text{-}80^+$ cells rather than the DC populations.

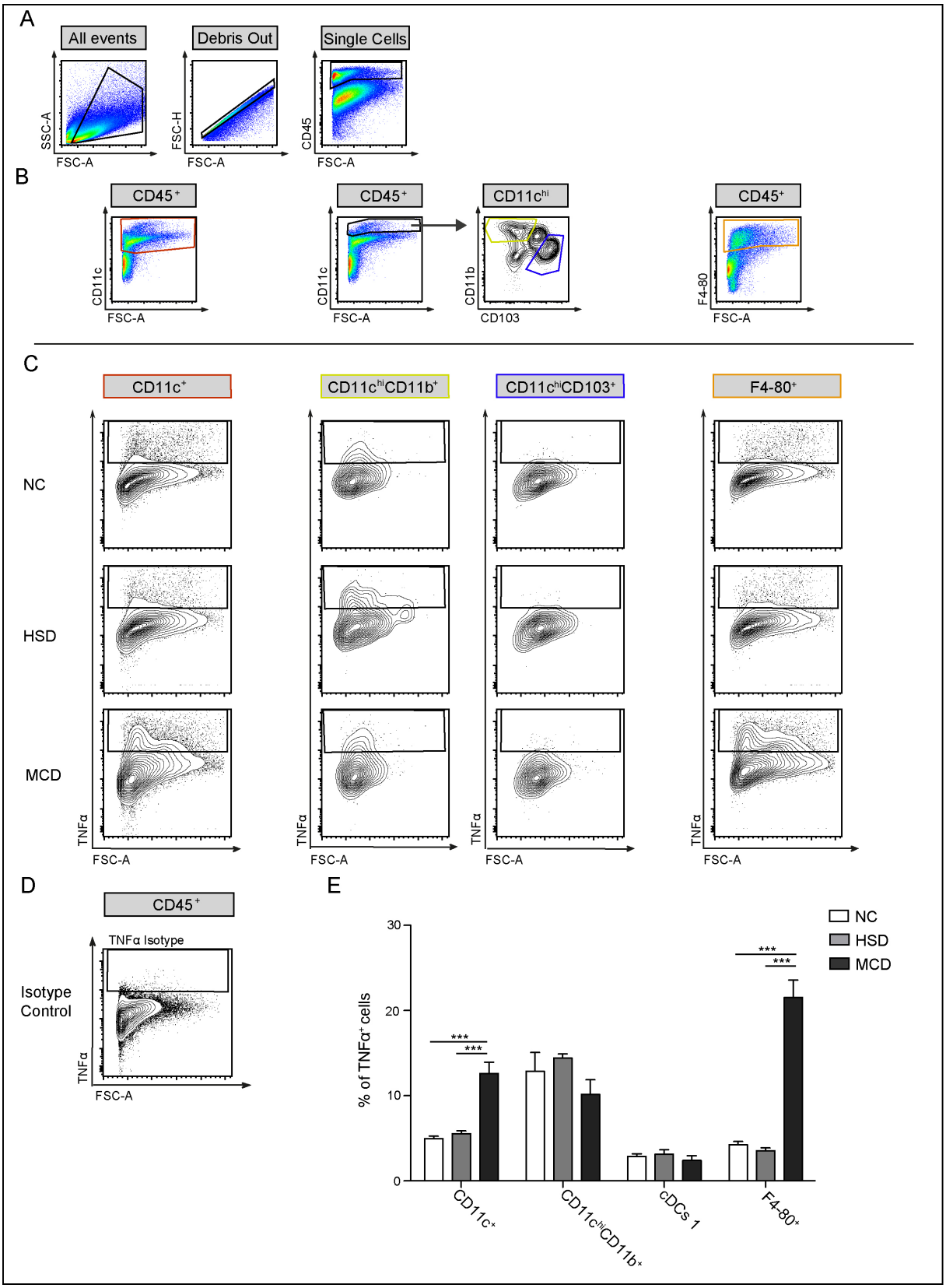

Figure 10 TNFα production of different cell populations stimulated with 250ng/ml LPS for 5 hours in WT C57Bl/6 mice after 5 weeks of HSD or MCD treatment compared to NC fed animals. **A)** basic gating strategy with debris and doublet cell exclusion. Gating on leukocytes by selecting all CD45$^+$cells. **B)** representative dot-blots for pre-gating on different cell populations within CD45$^+$ cells to be analyzed for TNFα-production. Plotting CD11c signal (*VioBlue 1:20*) against forward scatter: left dot-blot is gating on all CD11c$^+$ cells (red gate); middle dot-blots are

gating on CD11c^{hi} cells (black gate) and then plotting CD11b signals *(PE-Cy7 1:2000*) against CD103 signals (*PE 1:200*) to gate on CD11b^{+} DCs (lime green gate) or *c*DCs 1 (dark blue gate). Plotting F4-80 signal (*A488 1:200*) against forward scatter to gate on all F4-80^{+} cells (orange gate) **C)** representative contour-blots of the TNFα signal (*APC 1:200*) plotted against forward scatter within the cell populations of interest (red, lime green, blue and orange). Gated on TNFα^{+} cells **D)** Isotype control for TNFα (*APC 1:200*) **E)** bar-graph shows comparison of percentage ratio of TNFα^{+} cells within CD11c^{+} cells, CD11b^{+} DCs, cDCs 1 or F4-80^{+} cells. n_{NC}=4, n_{HSD}=4, n_{MCD}=4.
Data (A-E) shown for CD11c^{+}, CD11b^{+} DCs, cDCs 1 is representative of multiple independent experiments for HSD and MCD: $repetitions_{HSD}$= 4 (n=4), $repetitions_{MCD}$ = 3 (n=4). Experiment for NC was performed one time. Data (A-E) shown for F4-80^{+} cells are representative multiple independent experiments of HSD: $repetitions_{HSD}$ = 3 (n=4). Experiments for MCD and NC were performed one time. Bar-graphs depict mean + SEM. Significance is indicated through *p<0.05, ** p<0.005, ***p<0.0001. Underlined asterisks show statistical significance compared to the NC group of WT animals.

Summary chapter 3.3:

- All DC subtypes show an elevated abundance in the NASH model, but not the steatosis model
- CD11b^{+} DCs show the overall highest fold change, followed by cDCs 1 and pDCs
- CD11c^{+} cells show an increased production of TNFα in NASH, which does not stem from increased TNFα production by the DC subpopulation, but from F4-80^{+} cells.
- Bland steatosis does not lead to increased production of TNFα by either investigated cell population

3.4 The effect of batf3-dependent cDCs 1 on disease progression

Figure 11 depicts changes of disease progression parameters in WT animals compared to batf3-KO animals. After 5 weeks NC diet, batf3-KO animals show no difference to WT animals: the histological assessment of HE stained liver section shows no evidence of inflammation or steatosis. The CD45^{+} cell infiltrate of batf3-KO animals is similar to WT animals (*means NC: WT 33.5%, batf3-KO 34.8%*). ALT-values also show no significant difference with average *32.4 U/L* in WT and *37.3 U/L* in the batf3-KO neither does the mean liver triglyceride content with a mean *13.6 µg/mg liver* in WT and *17.6 µg/mg liver* in batf3-KO animals.

The HSD treated groups on the other hand show distinct differences between WT and batf3-KO animals. The histological assessment of liver sections shows an increase in NASH scoring in batf3-KO animals with higher prevalence of inflammatory infiltrates, hepatocellular ballooning and necrosis. Also, the liver sections show more prominent macrovesicular and microvesicular steatosis compared to the WT (Figure 11.A). This is paralleled by a significantly higher influx of CD45^{+} cells in batf3-KO mice, with an average percentage ratio of *45.5%* within living single cells compared to *29.2%* in the WT (Figure 11.B). The microscopically observed increased steatosis can also be measured as triglyceride content in the liver. In HSD treated batf3-KO animals this almost 2.4-fold increased (Figure 11.E*, means HSD: WT 59.1 µg/mg liver, batf3-KO 140.6 µg/mg live*r). Serum ALT-values do not mirror these changes. Similar as

in the WT a slight increase of Serum-ALT values compared to the NC group can be detected in batf3-KO animals, albeit this remains non-significant. Also, serum ALT-values do not differ significantly between HSD treated WT animals and HSD KO animals (Figure 11.D, *means HSD: WT 81.1 U/l, batf3-KO 108.4 U/l*). Connective tissue staining of the liver in HSD treated animals does not show any significant fibrosis development, neither in WT nor in batf3-KO animals (Figure 11.C).

In batf3-KO animals treated with MCD for 5 weeks disease progression parameters are worse compared to the NC and HSD treated batf3-KO animals. However, differences between WT and batf3-KO animals as observed in the HSD treated groups are not present here. In NASH scoring of liver sections WT and batf3-KO animals show no significant difference (Figure 11.A). This is also true for the $CD45^+$ cell infiltrate, where the percentage ratio of both, WT and batf3-KO, doubles to *mean 68.7%* and *mean 70.9%* respectively (Figure 11.B). The tendency of batf3-KO animals towards higher liver triglyceride content as observed in HSD treated animals is also present in the MCD treated groups: batf3-KO animals show a significant increase of liver triglycerides compared to the NC group. Moreover, this is significantly higher than the liver triglyceride content of WT MCD treated animals (*means MCD: WT 117.8 µg/mg liver, batf3-KO 142.0 µg/mg liver*). Interestingly the liver triglyceride content does not change significantly between the batf3-KO HSD group and MCD group (Figure 11.E). Serum ALT-values of MCD treated batf3-KO animals are almost ten times increased compared to the NC group (*means batf3-KO: NC 37.3 U/l, MCD 33.9 U/l*). Like the HSD groups, MCD treated batf3-KO mice also show a slight tendency towards higher ALT values compared to the WT (*mean WT: MCD 277.7 U/L*), however this remains non-significant (Figure 11.D). In the connective tissue stain MCD treated animals show some slight increase of collagenous fibers in the parenchyma compared to the HSD group, but there is no evidence of established fibrosis and no differences can be observed in WT compared to batf3-KO animals (Figure 11.C).

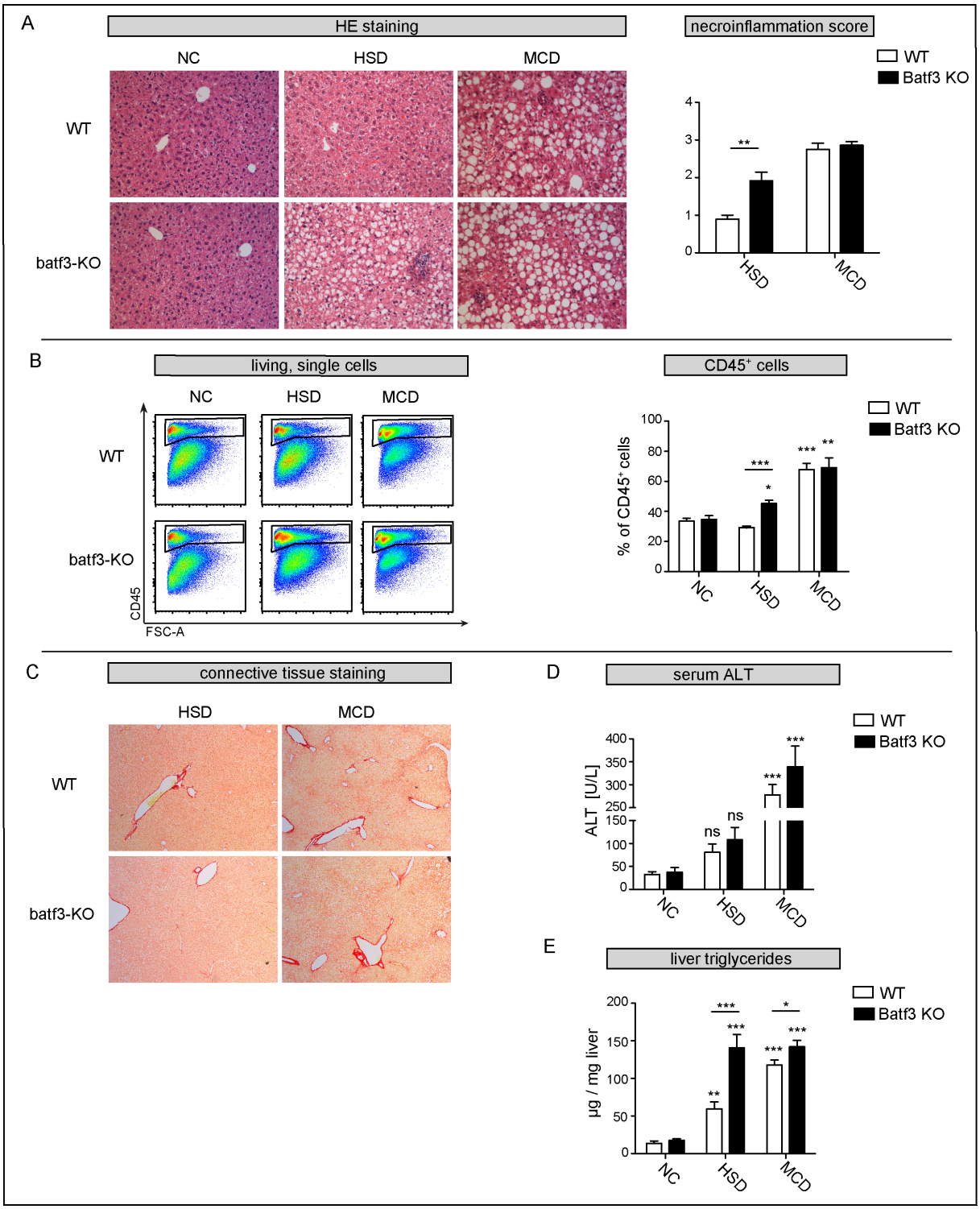

Figure 11 parameters of disease progression in WT C57Bl/6 mice compared to batf3-KO mice after 5 weeks of NC, HSD or MCD treatment **A)** histological assessment of HE-stained liver sections imaged at 20x objectives. Bar graph shows the necroinflammatory scoring based on the presence hepatocellular ballooning, necrosis and inflammation: $n_{WT\ HSD}$ = 10, $n_{KO\ HSD}$ = 13, $n_{WT\ MCD}$ = 8, $n_{KO\ MCD}$ = 15. Data (A) includes samples from 2-4 independently conducted experiments **B)** infiltrate of CD45$^+$ hematopoietic cells in the liver. Left figure shows representative dot-blots of living, single cells with signal for CD45 (*APC-Cy7 1:400*) plotted against forward scatter. Selecting leukocytes by gating on CD45$^+$ cells. Right figure shows bar-graph with comparison of percentage ratio of CD45$^+$ cells within living, single cells of C57Bl/6 WT (white) and batf3-KO (black) mice after NC, HSD and MCD treatment: n_{NC}= 5/group, n_{HSD} = 5/group, n_{MCD} = 5/group. Data (B) is representative of multiple, independent experiments for NC, HSD and MCD: $repetitions_{NC}$ = 3 (n=4-5/group), $repetitions_{HSD}$ = 6 (n=3-5/group), $repetitions_{MCD}$ = 4 (n=4-5/group). Bar-graphs depict mean + SEM. **C)** Representative pictures of connective tissue stained paraffin-embedded liver slides. Slides

were stained with Sirius Red stain and imaged at 5x objectives. n = 3/group **D)** bar graph shows comparison of serum ALT values: $n_{NC\ WT}$ = 12, $n_{NC\ KO}$= 7, $n_{HSD\ WT}$= 13, $n_{HSD\ KO}$= 16, $n_{MCD\ WT}$= 18, $n_{MCD\ KO}$= 26. **E)** bar graph shows comparison of liver triglyceride levels. Data for liver triglyceride measurement was provided by Anna Maier. n_{NC}=6, n_{HSD}=9, n_{MCD}=9 Bar-graphs depict mean + SEM. Data (C-E) includes samples from 3-4 independently conducted experiments per treatment group.
Bar-graphs depict mean + SEM. Significance is indicated through *p<0.05, ** p<0.005, ***p<0.0001. Asterisks on top of the bar show statistical significance compared to the respective NC group of WT or batf3-KO mice, underlined asterisks show statistical significance of WT compared to batf3-KO.

Summary chapter 3.4:

- The lack of cDCs 1 results in the aggravation of several NASH related parameters in HSD treated animals, such as a higher NASH scoring in the histological analysis, higher liver triglyceride content in the liver and a higher $CD45^+$ cell infiltrate. It does not affect serum ALT levels or liver fibrosis.
- The lack of cDCs 1 does not affect the liver on a baseline level in NC treated animals concerning histological analysis, $CD45^+$ cells influx or liver triglycerides.
- The lack of cDCs 1 does not aggravate established NASH in MCD treated animals regarding NASH scoring, $CD45^+$ cell infiltrate, ALT values or fibrosis progression, but increases liver triglyceride content.

3.5 The effect of batf3-dependent cDCs 1 on the hematopoietic infiltrate in the liver

With the above described differences detected in batf3-KO animals, especially concerning the HSD group, the next aim of this study was to investigate how the lack of cDCs 1 causes the observed progression of bland steatosis towards steatohepatitis. Considering the influx of $CD45^+$ cells during NASH and the increase in the batf3-KO HSD group compared to the WT, changes of the hematopoietic cell infiltrate were analyzed with regards to different cellular subtypes such as DC populations, lymphocyte subsets and myeloid cells.

3.5.1 DC-Populations

To investigate how the lack of batf3-dependent cDCs 1 influences the remaining DC subtypes, flow cytometric analysis was done on $CD11b^+$ DCs as well as pDCs in the control group as well as HSD or MCD treated animals.

3.5.1.1 *$CD11b^+$ DCs*

Figure 12 shows the analysis of the $CD11b^+$ DC subtype in WT and batf3-KO animals treated for 5 weeks with NC, HSD or MCD. $CD11b^+$ DCs were gated on as described in chapter

3.2, by first gating on CD11c^{hi}MHC-II^{hi} expressing cells and then on the CD11b^{+} population. The CD11b^{+} DC population in batf3-KO animals follows similar changes as in WT animals (Figure 12.D). Compared to the NC treated control group the percentage ratio of CD11b^{+} DCs is not altered significantly in the HSD group (*means batf3-KO: NC 3.9%, HSD 4.9%*), but increases significantly in MCD treated animals (*mean batf3-KO: MCD 11.0%*). The average cell count in HSD animals is also significantly higher in NC treated animals and increases further in the MCD group (*means batf3-KO: NC 59x10^3 cells/g liver, HSD 165x10^3 cells/g liver, MCD 589x10^3 cells/g liver*). Comparison of WT and batf3-KO animals shows a significant baseline difference in percentage ratio: While in WT animals it is at *2.2%* in NC treated animals, it is increased to *3.9%* in batf3-KOs. This difference can also be observed in the HSD treated animals. With an average of *4.9%* percentage values in batf3-KO animals are significantly higher than the average 2.7% in the WT. In MCD treated groups the difference is slightly lessened, although there is still a tendency towards higher values in batf3-KO mice (*means MCD: WT 7.9%*, *batf3-KO 11.0%*). When looking at percental ratio it is important to consider that these are relative values and not absolute numbers. Since batf3-KO animals are missing the cDC 1 population it is important to confirm whether differences detected in the CD11b^{+} subtype are true changes or merely a shift of proportions due to the missing population. For this purpose, the absolute cell count per gram liver can be calculated. Batf3-KO animals show a significant higher cell count in the HSD group (*means HSD: WT 27x10^3 cells/g liver, batf3-KO 165x10^3 cells/g liver*), whereas differences on a baseline level in the control group or in MCD treated animals cannot be confirmed (*means NC: WT 34x10^3 cells/g liver, batf3-KO 59x10^3 cells/g liver; means MCD: WT 448x10^3 cells/g liver, batf3-KO 589x10^3 cells/g liver*).

Figure 13 shows further characterization of CD11b^{+} DCs in NC and HSD treated animals using CD64 as an additional marker. The gating is performed as described in chapter 3.2. The percentage ratio for CD64^{-} cDCs 2 does not change significantly in the HSD treated WT group compared to the NC control (*means WT: NC 1.4%, HSD 2.3%*). Likewise, batf3-KO animals show no significant difference in percentage ratio between NC and HSD (*means batf3-KO: NC 3.0%, HSD 3.8%*). Calculated in absolute numbers per gram liver the cDC 2 population shows no significant difference between WT and batf3-KO, neither on a baseline level (*means NC: WT 28x10^3 cells/g liver, batf3-KO 46x10^3 cells/g liver*) nor after HSD treatment (*means HSD: WT 30x10^3 cells/g liver, batf3-KO 68x10^3 cells/g liver*). This indicates that the difference in percentage ratio is mostly due to a shift in proportions because of the missing DC population in the batf3-KO animals (Figure 13.C). Values for CD64^{+} moDCs are notably lower than those of cDC 2s, which indicates that the majority of the CD11b^{+} DCs are cDCs 2 (Figure 13.D). The percentage ratio of moDCs does not change significantly between NC and HSD groups, neither

in WT nor in batf3-KO mice (*means WT: NC 0.3%, HSD 0.4%*; *means batf3-KO: NC 0.3%, HSD 1.1%*). However, comparing values of WT and batf3-KO, there is a significant difference in HSD treated animals. The increase in percentage ratio of HSD treated batf3-KO animals compared to the WT also manifests in cell count per gram liver *(means HSD: WT 5x10^3 cells/ g liver, batf3-KO 20x10^3 cell/g liver)*, thus explaining the increase of CD11b$^+$ DCs in batf3-KO mice.

Concluding, in batf3-KO animals the CD11b$^+$ DC population increases significantly both after HSD and MCD diet. The majority of CD11b$^+$ DCs consists of CD64$^-$ cDCs 2, but it also includes some CD64$^+$ moDCs. On baseline level batf3-KO mice show a higher frequency of CD11b$^+$ DCs, which is mostly due to a shift of proportions because of the missing cell population. This can also be observed in the MCD treated animals, which show a significant difference in percentage ratio between WT and batf3-KO that cannot be confirmed in absolute numbers. Under HSD an increase of CD11b$^+$ DCs can be observed in the batf3-KO animals compared to their WT counterparts. This can be attributed to a higher influx of moDCs in batf3-KO animals.

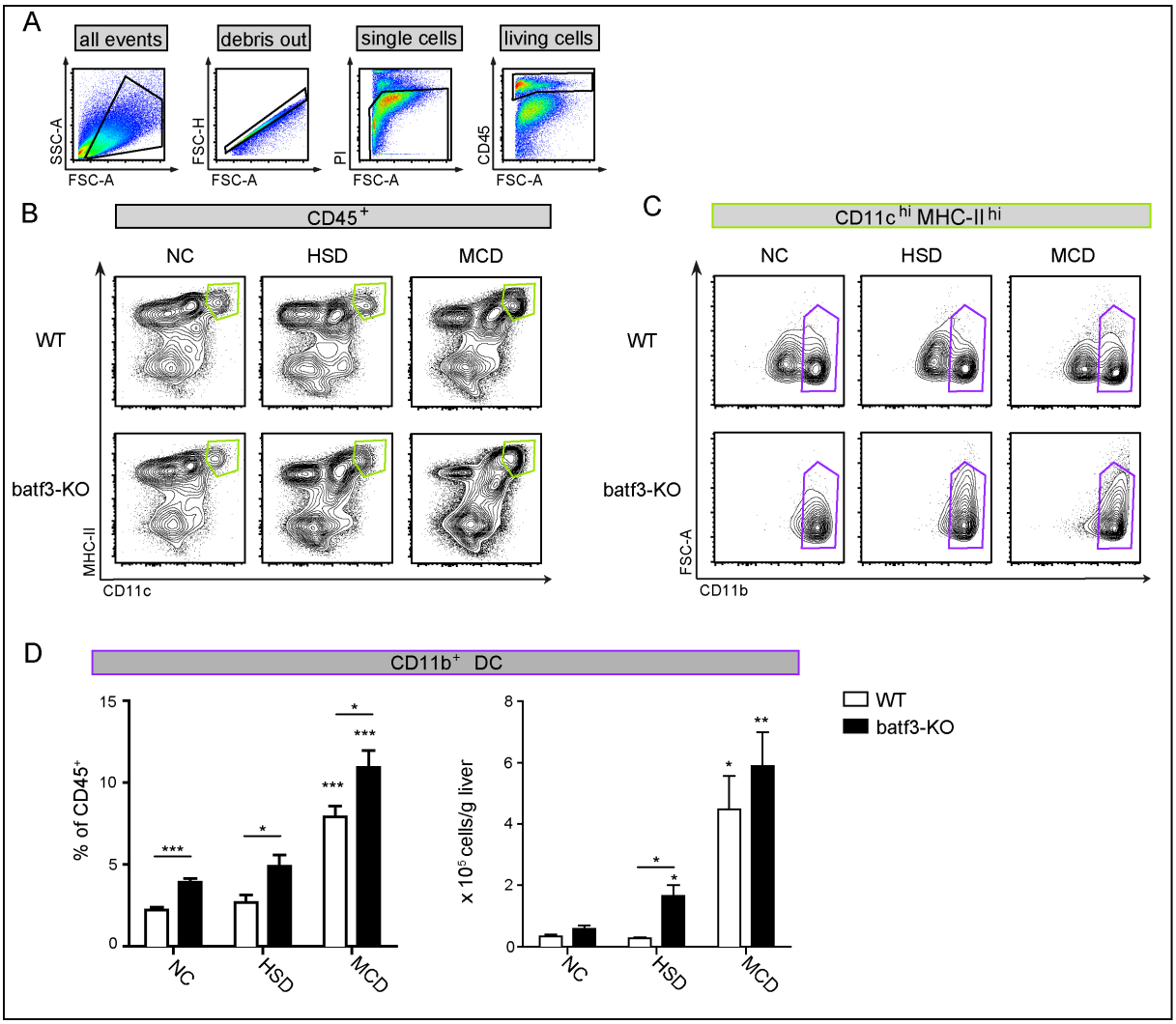

Figure 12 changes of CD11b$^+$ DCs in WT C57Bl/6 mice compared to batf3-KO mice after 5 weeks of HSD, MCD or NC treatment **A)** basic gating strategy: debris, doublet and dead cell exclusion. Gating on leukocytes by selecting all CD45$^+$cells. **B)** representative dot blots of CD45$^+$ cells showing CD11c signal (*APC 1:400*) plotted against MHC-II signal (*FITC 1:4000)* to gate on cells with high expression of CD11c and MHC-II (green gate) **C)** representative contour blots of CD11c^{hi}MHC-II^{hi} cells showing CD11b signal (*PE-Cy7 1:2000*) plotted against forward scatter to gate on CD11b$^+$ DCs (purple gate) **D)** bar-graphs show comparison of percentage ratio within CD45$^+$ cells (left graph) and total cell amount per gram digested liver (right graph) of CD11c^{hi} MHC-II^{hi} CD11b$^+$ DCs. n_{NC}= 5/group, n_{HSD}= 5/group, n_{MCD}= 5/group.
Data (A-D) for NC, HSD and MCD is representative of multiple independent experiments: repetitions$_{NC}$= 2 (n=3-5/group), repetitions$_{HSD}$= 5 (n=4-5/group), repetitions$_{MCD}$= 3 (n=4-5/group). Data shown for MCD was created using digest protocol I. Bar-graphs depict mean + SEM. Significance is indicated through *p<0.05, ** p<0.005, ***p<0.0001. Asterisks on top of the bar show statistical significance compared to the respective NC group of WT or batf3-KO, underlined asterisks show statistical significance of WT compared to batf3-KO.

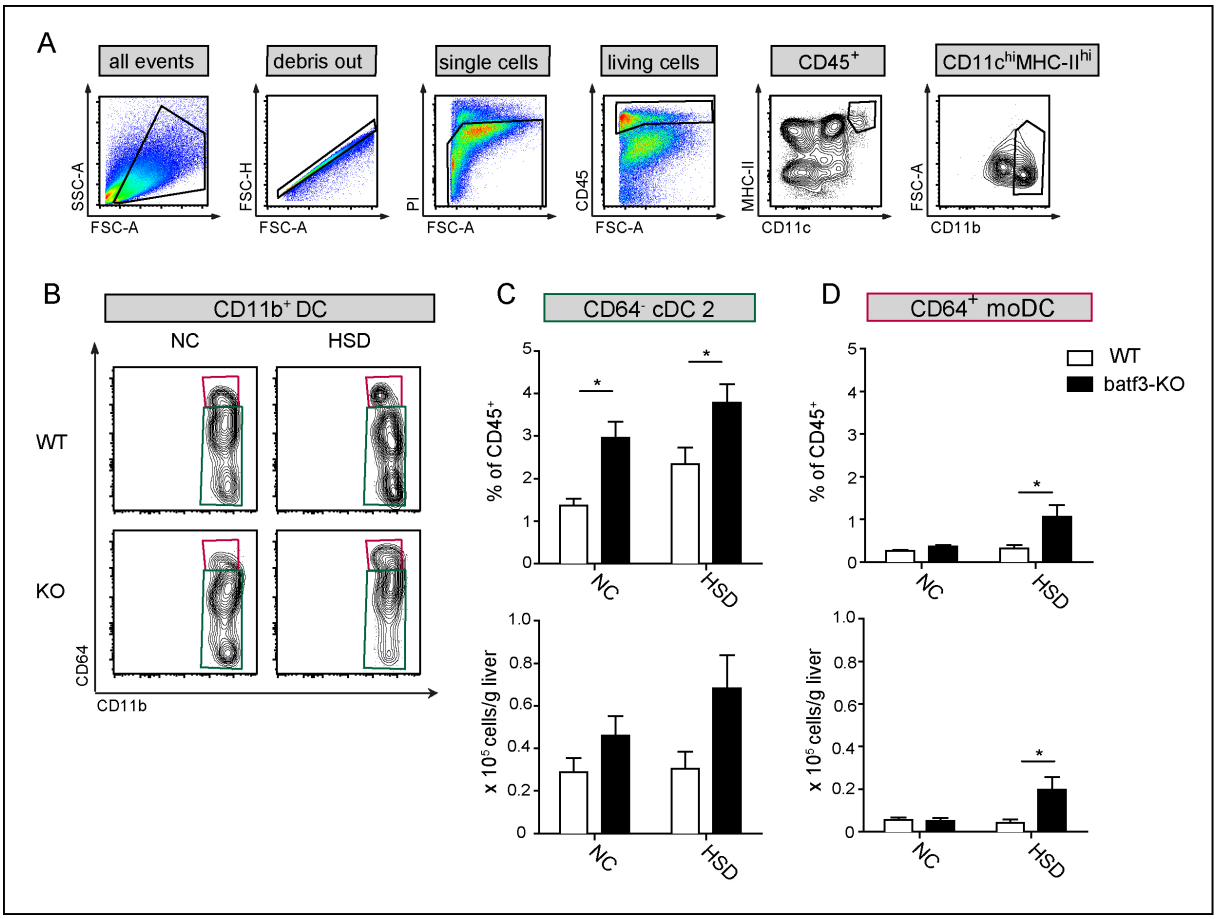

Figure 13 changes of CD11b⁺ DCs based on CD64⁺ expression in WT C57Bl/6 mice compared to batf3-KO mice after 5 weeks of HSD or NC feeding **A)** basic gating strategy: debris, doublet and dead cell exclusion. Gating on leukocytes by selecting all CD45⁺ cells. Selecting CD11c^{hi} MHC-II^{hi} cells, then CD11b⁺ cells. **B)** representative contour-blots of CD11c^{hi}MHC-II^{hi}CD11b⁺ cells showing CD64 signal (*Brilliant Violet 421 1:200*) plotted against CD11b signal (*PE-Cy7 1:2000)* to gate on CD64⁺ cells (red gate) or CD64⁻ cells (green gate) **C)** bar-graphs show comparison of percentage ratio within CD45⁺ cells (upper graph) and total cell amount per gram digested liver (lower graph) of CD11c^{hi} MHC-II^{hi} CD11b⁺ CD64⁻ DCs. n_{NC}= 3/group, n_{HSD}= 5/group **D)** bar-graphs show comparison of percentage ratio within CD45⁺ cells (upper graph) and total cell amount per gram digested liver (lower graph) of CD11c^{hi} MHC-II^{hi} CD11b⁺ CD64⁺ DCs. n_{NC}= 3/group, n_{HSD}= 5/group.
Experiments were performed one time per group. Bar-graphs depict mean + SEM. Significance is indicated through *p<0.05, ** p<0.005, ***p<0.0001. Asterisks on top of the bar show statistical significance compared to the respective NC group of WT or batf3-KO, underlined asterisks show statistical significance of WT compared to batf3-KO.

3.5.1.2 *pDCs*

Changes of the pDC population as depicted in Figure 14 were analysed using the same gating strategy as described in chapter 3.3.3. Like in the WT experiments, significant changes of the pDC population can only be detected in the MCD treated batf3-KO animals (Figure 14.D). Here the percentage ratio increases from *2.8%* in the NC group to *5.3%* in the MCD group and the total cell count from an average *9x10^3 cells/10^6 living cells* to *35x10^3 cells/10^6 living cells*. Although there is a slight tendency towards higher values in HSD treated animals, changes in percentage ratio and total cell count are not significant (*means HSD batf3-KO 3.7%, 13x10^3 cells/10^6 living cells*).

Between WT and batf3-KO animals the treatment groups show no significant difference, neither in percentage ratio nor in total cell count per 10^6 living cells.

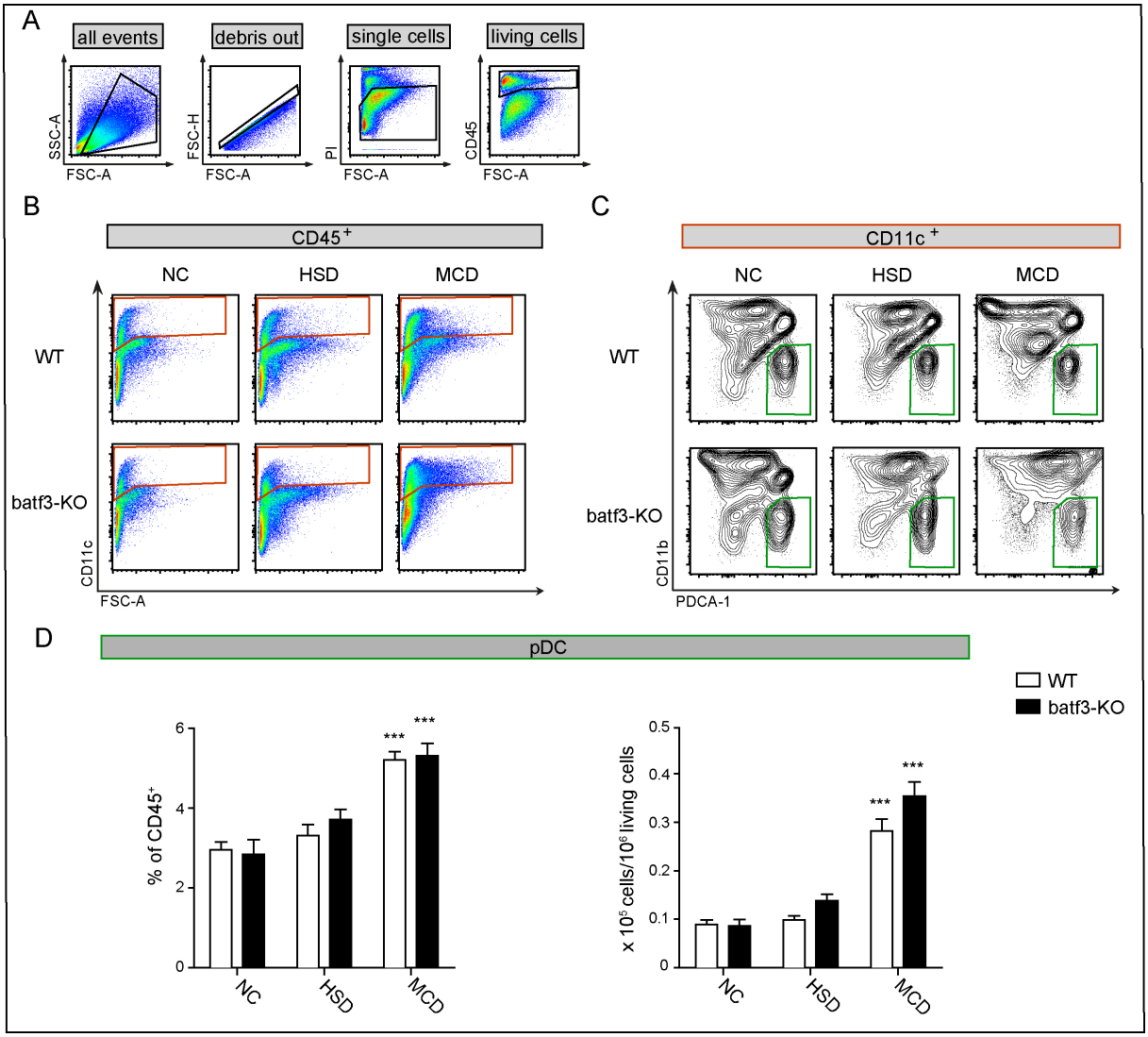

Figure 14 changes of pDCs in WT C57Bl/6 mice compared to batf3-KO mice after 5 weeks of HSD, MCD or NC feeding. **A)** basic gating strategy: debris, doublet and dead cell exclusion. Gating on leukocytes by selecting all CD45$^+$cells. **B)** representative dot blots of CD45$^+$ cells showing CD11c signal (*APC 1:400*) plotted against sideward scatter to gate on all CD11c$^+$ cells (red gate) **C)** representative contour blots of CD11c$^+$ cells showing CD11b signal (*PE-Cy7 1:2000*) plotted against PDCA-1 signal (*PE 1:200*) to gate on PDCA-1$^+$ CD11b$^-$ cells (green gate) **D)** bar-graphs show comparison of percentage ratio within CD45$^+$ cells (left graph) and total cell amount per 10^6 living cells (right graph) of pDCs. n_{NC}= 5/group, n_{HSD}= 5/group, n_{MCD}=5/group.
Data (A-D) for HSD and MCD is representative of multiple independent experiments: repetitions$_{HSD}$ = 4 (n=4-5/group), repetitions$_{MCD}$ = 3 (n=4-5/ group). NC experiments were performed one time. Data shown for MCD was created using digest protocol I. Bar-graphs depict mean + SEM. Significance is indicated through *p<0.05, ** p<0.005, ***p<0.0001. Asterisks on top of the bar show statistical significance compared to the respective NC group of WT or batf3-KO, underlined asterisks show statistical significance of WT compared to batf3-KO.

Summary chapter 3.5.1:

- The CD11b$^+$ DCs population consists mostly of CD64$^-$ cDCs 2 and to a smaller proportion of CD64$^+$ moDCs

- The lack of cDCs 1 results in a significant influx of $CD11b^+$ DCs in HSD treated animals, which can mainly be accounted to an increase of $CD64^+$ moDCs.
- The lack of cDCs 1 causes a shift of proportions of $CD11b^+$ DCs within $CD45^+$ cells in the NC and MCD treatment group.
- The lack of cDCs 1 does not affect the pDC population.

3.5.2 Myeloid cell populations

Figure 15 shows the flow-cytometric analysis of various myeloid cell subsets with a staining mix containing the surface markers CD45, F4-80 and Ly6C. After the basic gating strategy on $CD45^+$ cells with debris, doublets and dead cell exclusion (Figure 15.A) the signals for F4-80 and Ly6C are plotted against each other. As Figure 15.B shows, it is possible to separate four major populations that differ in their expression of these two surface markers. The light blue gate contains a population that has a positive signal for Ly6C, but is negative for F4-80. This gate, which contains both cells with high and intermediate Ly6C expression, represents a mixture of myeloid cells such as neutrophils, eosinophils or myeloid derived suppressor cells. Cells within the red gate show both a positive signal for Ly6C as well as for F4-80, a marker combination which characterizes inflammatory monocytes. Events in the green gate exhibit a positive signal for F4-80, but do not express Ly6C. F4-80 is highly expressed in macrophages and thus identifies this population as KCs. Respective isotype controls are depicted in Figure 15.C.

Figure 15.D depicts changes of percentage ratio and total cell count per gram liver of the KC population in 5 weeks NC, HSD or MCD treated mice. In both WT and batf3-KO animals the mean percentage ratio is not significantly altered between the NC and HSD treated mice, but decreases significantly after MCD treatment (*means WT: NC 18.2%, HSD 26.9%, MCD 10.7%; means batf3-KO: NC 16.7%, HSD 19.5%, 10.5%*). The total cell count equally shows no significant change between both WT and batf3-KO NC and HSD treated mice. Contrary to the percentage ratio however, in MCD treated animals KCs in fact increase significantly (*means WT: NC 517x10^3 cells/g liver, HSD 408x10^3 cells/g liver, MCD 949x10^3 cells/g liver; means batf3-KO: NC 482x10^3 cells/g liver, HSD 466x10^3 cells/g liver, MCD 848x10^3 cells/g liver*).

Figure 15.E depicts changes of percentage ratio and total cell count per gram liver of the $Ly6C^{hi/int}F4\text{-}80^-$ gate in NC, HSD and MCD treated mice. In WT animals fed with HSD the percentage ratio increases slightly from *16.9%* in NC to *19.2%* in the HSD group, while the total cell count shows no significant difference between NC and HSD (*means WT: NC 385x10^3 cells/g liver, HSD 286x10^3 cells/g liver*). In the MCD treated group the percentage ratio almost

doubles to an average of *32.5%*, which is reflected in a significant increase to *2.6x10^6 cells/g liver* in total cell count. Unlike the WT, HSD treatment in batf3-KO mice causes a clear increase of the percentage ratio of Ly6C$^{hi/int}$F4-80$^-$ cells from an average *17.2%* in NC to *26.5%* in HSD, which is mirrored by the change of total cell count from a mean of *356x10^3 cells/g liver* in NC to *674x10^3 cells/g liver* in HSD. MCD treated animals do not differ significantly from the WT and show a similar increase of percentage ratio and cell count per gram liver (*means batf3-KO: MCD 33,4%, 2.6x10^6 cells/g liver*).

Figure 15.F depicts changes of percentage ratio and total cell count per gram liver of cells in the Ly6C$^{hi/int}$F4-80^{low} gate in NC, HSD and MCD treated mice. In WT animals HSD feeding does not significantly alter the percentage ratio nor the absolute cell count per gram liver compared to the NC group (*means WT: NC 0,8%, 27x10^3 cells/g liver, HSD 1,1%, 16x10^3 cells/g liver*). 5-week treatment with MCD significantly increases the percentage ratio to an average of *8.4%*, which is also reflected in the massive increase of cell count to an average of *898x10^3 cells/g liver*. NC fed batf3-KO animals show no significant difference in percentage ratio or absolute cell count compared to the WT (*mean batf3-KO: NC 0,8%, 33x10^3 cells/g liver*). Meanwhile HSD treated batf3-KO mice show a significant increase in percentage and absolute cell count compared to the baseline NC treated batf3-KO animals as well as the HSD treated WT control (*means batf-KO: HSD 5.0%, 130x10^3 cells/g liver*). After MCD treatment percentage ratio and absolute cell count in batf3-KO mice increase significantly compared to the baseline batf3-KO control, but are not significantly altered compared to the MCD treated WT animals (*means batf3-KO: MCD 9.7%, 930x10^3 cells/g liver*).

Figure 16 depicts the analysis of the neutrophil cell population in NC, HSD and MCD treated WT and batf3-KO mice using a staining mix containing CD45, Ly6C and Ly6G. Figure 16.A show the basic gating strategy for leukocytes by gating on CD45$^+$ cells after debris, doublet and dead cell exclusion. In Figure 16.B signals for Ly6C and Ly6G are plotted against each other and the upper right cell population distinctly separates from the remaining cells (black gate). Cells in this population express both Ly6C and Ly6G surface markers (compare isotype control in Figure 16.C) and are thus identified as neutrophils. Figure 16.D depicts changes in percentage ratio and absolute cell count of neutrophils in WT and batf3-KO mice during NC, HSD and MCD treatment. In WT animals, HSD treatment causes a significant increase of percentage ratio to 3.2% from an average of *1.8%* in NC. The cell count per gram liver also is tendentially higher in HSD, although this remains insignificant (*means WT: NC 35x10^3 cells/g liver, HSD 40x10^3 cells/g liver*). After MCD treatment percentage ratio and cell count increases significantly to an average of *9.5%* and *781x10^3 cells/g liver*. Batf3-KO mice show no significant baseline difference in neutrophil percentage ratio or absolute cell count in

the NC group compared to the WT control (*means batf3-KO: NC 1.5%, 24x10^3 cells/g liver*). Changes in the HSD or MCD group compared to the NC fed control group match those of the WT and there are no significant differences between batf3-KO and WT (*means batf3-KO: HSD 2.5%, 45x10^3 cells/g liver, MCD 7.1%, 456x10^3 cells/g liver*).

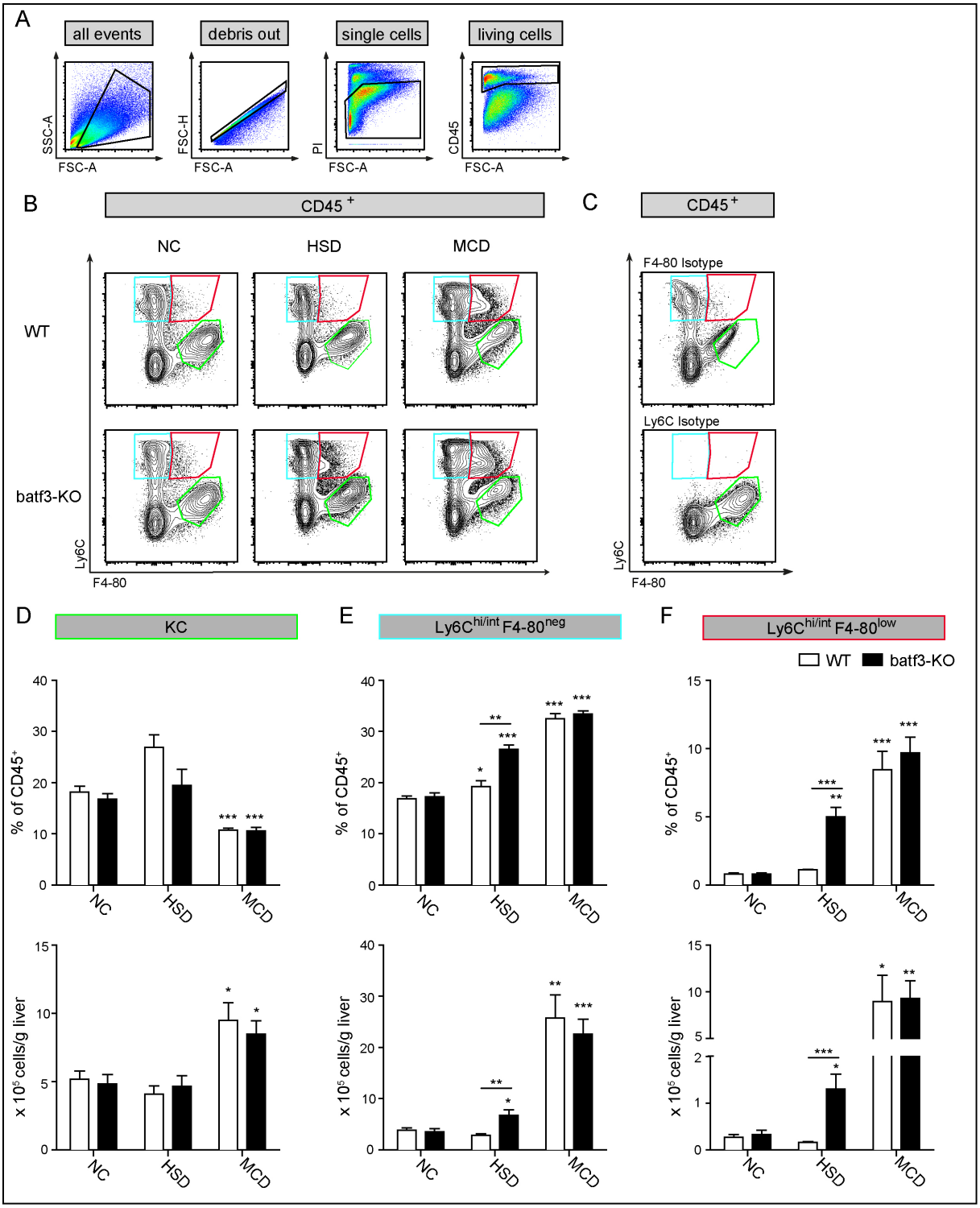

Figure 15 changes of monocyte and macrophage populations in WT C57Bl/6 mice compared to batf3-KO mice after 5 weeks of HSD, MCD or NC feeding A) basic gating strategy: debris, doublet and dead cell exclusion. Gating on

leukocytes by selecting all CD45⁺cells. B) representative contour blots of CD45⁺ cells showing Ly6C signal (*APC 1:1000*) plotted against F4-80 signal *(A488 1:200)* to gate on Ly6C$^{hi/int}$ F4-80^{-} cells (light blue gate), Ly6C$^{hi/int}$ F4-80^{low} cells (red gate) and Ly6C$^{low/neg}$ F4-80⁺ KCs (green gate) C) Isotype controls for Ly6C (*APC 1:1000*) and F4-80 (*A488 1:200*) D) bar-graphs show comparison of percentage ratio within CD45⁺ cells (upper graph) and total cell amount per gram digested liver (lower graph) of Ly6C$^{low/neg}$ F4-80⁺ KCs E) bar-graphs show comparison of percentage ratio within CD45⁺ cells (upper graph) and total cell amount per gram digested liver (lower graph) of Ly6C$^{hi/int}$ F4-80^{neg} cells F) bar-graphs show comparison of percentage ratio within CD45⁺ cells (upper graph) and total cell amount per gram digested liver (lower graph) of Ly6C$^{hi/int}$ F4-80^{low} cells (right graph). n_{NC}= 5/group, n_{HSD}= 5/group, n_{MCD}= 5/group.
Data (A-F) for HSD and MCD is representative of multiple independent experiments: repetitions$_{HSD}$ = 5 (n=4-5/group), repetitions$_{MCD}$ = 3 (n=4-5/group). NC experiment was performed one time. Significance is indicated through *p<0.05, ** p<0.005, ***p<0.0001. Asterisks on top of the bar show statistical significance compared to the respective NC group of WT or batf3-KO, underlined asterisks show statistical significance of WT compared to batf3-KO.

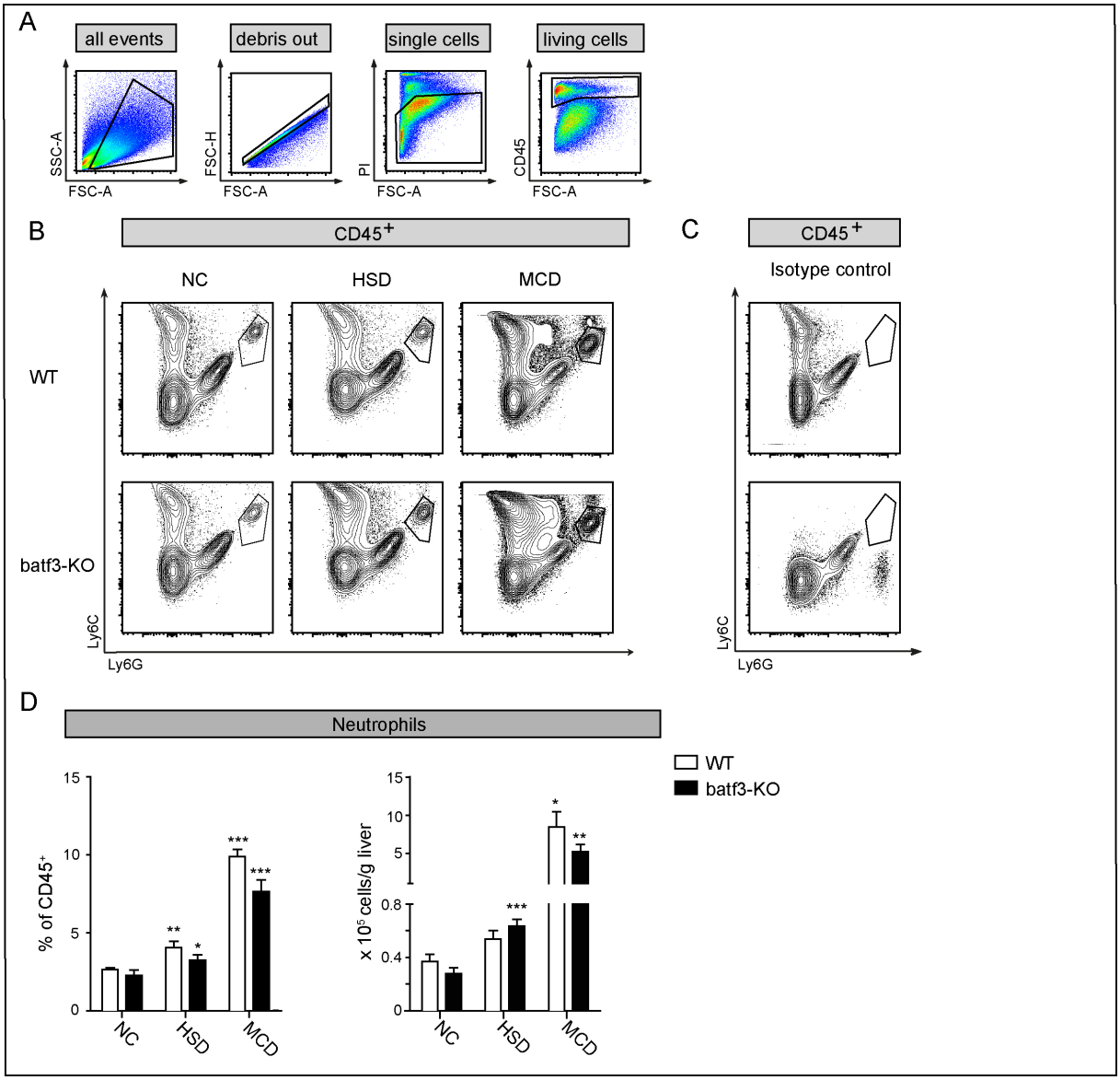

Figure 16 changes of neutrophils in WT C57Bl/6 mice compared to batf3-KO mice after 5 weeks of HSD, MCD or NC feeding A) basic gating strategy: debris, doublet and dead cell exclusion. Gating on leukocytes by selecting all CD45⁺cells. B) representative contour blots of CD45⁺ cells showing Ly6C signal (*APC 1:1000*) plotted against Ly6G signal *(FITC 1:200)* to gate on Ly6C⁺ Ly6G⁺ cells C) Isotype controls for Ly6C (*APC 1:1000*) and Ly6G (*FITC 1:200*) D) bar-graphs show comparison of percentage ratio within CD45⁺ cells (right graph) and total cell amount per gram digested liver (left graph) of Ly6C⁺ Ly6G⁺ cells. n_{NC}= 5/group, n_{HSD}= 5/group, n_{MCD}= 5/group.

Data (A-D) for HSD and MCD is representative of multiple independent experiments: $repetitions_{HSD}$ = 4 (n=4-5/group), $repetitions_{MCD}$ = 4 (n=4-5/group). NC experiment was performed one time. Bar-graphs depict mean + SEM. Significance is indicated through *p<0.05, ** p<0.005, ***p<0.0001. Asterisks on top of the bar show statistical significance compared to the respective NC group of WT or batf3-KO, underlined asterisks show statistical significance of WT compared to batf3-KO

Summary chapter 3.5.2:

- HSD induced steatosis in WT animals does not affect KCs, inflammatory monocytes, neutrophils or Ly6C$^{hi/int}$F4-80^{neg} cells.
- During MCD induced NASH it is possible to observe an influx of all these myeloid populations in the liver.
- The lack of cDCs 1 results in an elevated abundance of inflammatory monocytes and Ly6C$^{hi/int}$F4-80^{-} cells, but does not affect neutrophils or KCs during HSD treatment.
- The lack of cDCs 1 does not affect the myeloid cell populations of the liver during NC or MCD treatment.

3.5.3 Lymphoid cell populations

To determine whether cDCs 1 also have an impact on lymphoid cell infiltrate a FACS-analysis was performed using a staining mix containing the lymphoid markers CD3ε, CD19, NK1.1 as well as CD45 and F4-80 for pre-gating. The basic gating strategy for the analysis of lymphoid cell population includes an additional gating step on F4-80 negative cells. This is performed to facilitate the distinction of different lymphoid cell populations by excluding macrophages, which typically show a strong autofluorescence in FACS-analyses (Figure 17).

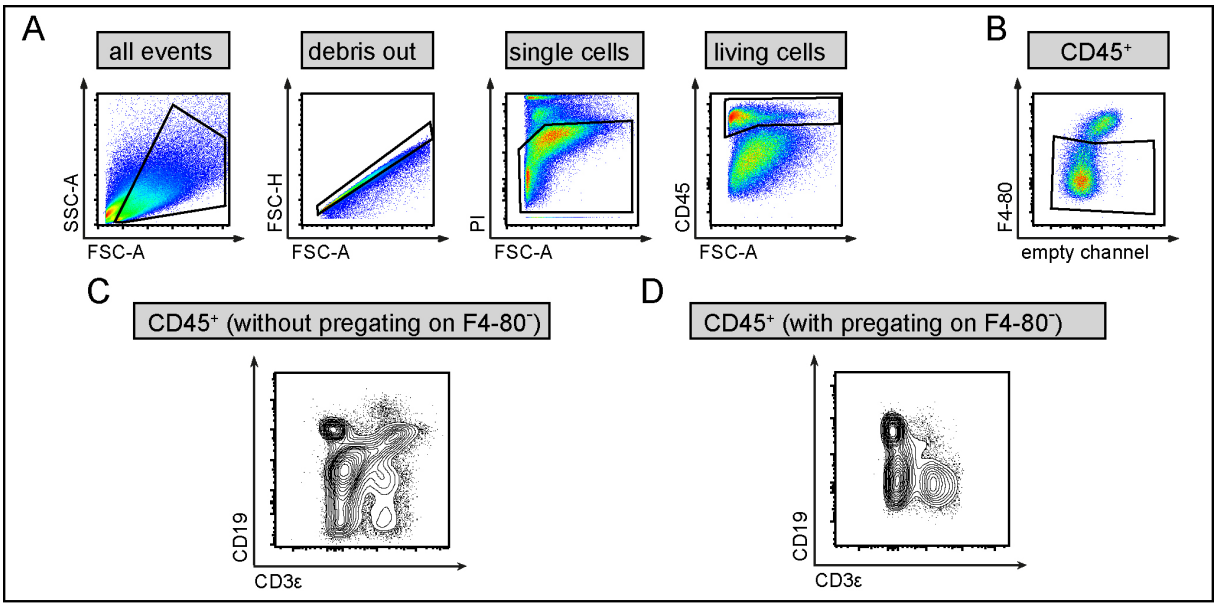

Figure 17 discriminating lymphoid cell populations with and without pre-gating on F4-80$^-$ cells **A)** basic gating strategy: debris, doublet and dead cell exclusion. Gating on leukocytes by selecting all CD45$^+$cells. **B)** pre-gating on F4-80$^-$ cells by plotting F4-80 signal of CD45$^+$ cells against an empty channel to gate on negative cells. **C)** representative contour blots of all CD45$^+$ cells showing CD19 signal (*PE-Cy7 1:100)* plotted against CD3ε (*A488 1:100)* to distinguish lymphoid cell populations **D)** representative contour blots of F4-80$^-$ CD45$^+$ cells showing CD19 signal (*PE-Cy7 1:100)* plotted against CD3ε (*A488 1:100)* to distinguish lymphoid cell populations

3.5.3.1 *B cells*

Figure 18 depicts the analysis of B cells in 5 weeks NC, HSD and MCD treated WT and batf3-KO animals. Figure 18.A shows the basic gating strategy with debris, doublet and dead cell exclusion and gating on CD45$^+$ cells. The CD45$^+$ F4-80$^-$ cells are then subsequently plotted accordingly to their expression of CD3ε and CD19. This separates the cells into three populations: CD19$^+$CD3ε$^-$, CD19$^-$CD3ε$^+$ and CD19$^-$CD3ε$^-$ (Figure 18.C). CD19 is a marker for B cells, therefore CD19$^+$CD3ε$^-$ cells (yellow gate) are identified as such. Figure 18.B shows the respective isotype control.

Figure 18.D depicts changes of percentage ratio and total cell count per gram liver in the B cell population of NC, HSD and MCD treated animals. HSD causes a slight, significant decrease of percentage ratio in WT animals (*means WT: NC 33%, HSD 26%*), which can also be observed in absolute cell count (*means WT: NC 670x10^3 cells/g liver, HSD 318x10^3 cells/g liver*). In MCD treated animals the decrease of B cells to an average *11%* seems to be a shift in percentage ratio due to influx of other cell populations as the count per gram liver slightly, but not significantly increases to *791x10^3 cells/g liver*. Batf3-KO animals show similar tendencies in their numbers with no significant difference to the WT control: HSD feeding causes a slight, albeit not significant decrease of percentage ratio (*means batf3-KO: NC 32%, HSD 24%*) as well as total cell count (*means batf3-KO: NC 651x10^3 cells/g liver, HSD 439x10^3 cells/g liver*). MCD treatment also shows a significant decrease of percentage ratio whereas

the total cell count contrarily shows a slight, but insignificant increase (*means batf3-KO: MCD 12%, 820x10³ cells/g liver*). Concluding B cells represent a large population within immune cells of the liver, but are not recruited during NASH or steatosis, which leads to a relative decrease of the population within CD45⁺ cells. cDCs1 do not influence the B cell population during steady state or NASH.

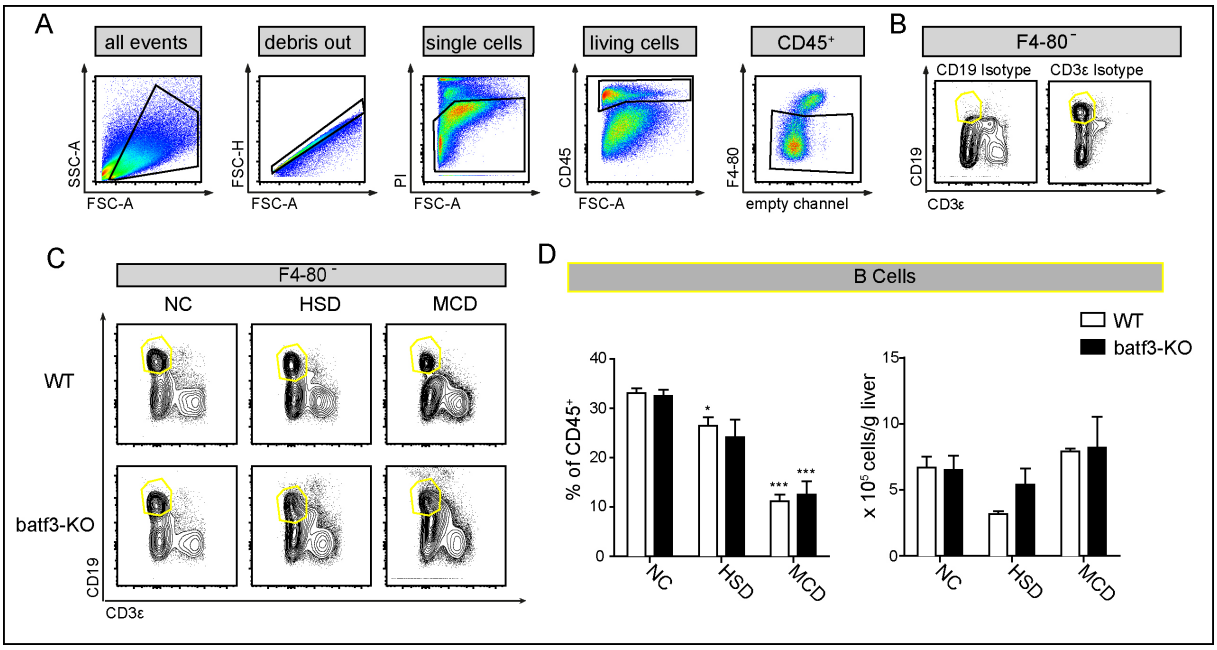

Figure 18 changes of B cells in WT C57Bl/6 mice compared to batf3-KO mice after 5 weeks of HSD, MCD or NC feeding **A)** basic gating strategy: debris, doublet and dead cell exclusion. Gating on leukocytes by selecting all CD45⁺cells. Plotting F4-80 signal of CD45⁺ cells against an empty channel and gating on all F4-80⁻ cells. **B)** Isotype control for CD19 (*PE Cy-7 1:100)* and CD3ε (*A488 1:100)* **C)** representative contour blots of F4-80⁻ cells showing CD19 signal (*PE-Cy7 1:100)* plotted against CD3ε (*A488 1:100)* to gate on CD19⁺ CD3ε⁻ cells (yellow gate) **D)** bar-graphs show comparison of percentage ratio within CD45⁺ cells (upper graph) and total cell amount per gram digested liver (lower graph) of CD19⁺ CD3ε⁻ cells. n_{NC}= 5/group, n_{HSD}= 5/group, n_{MCD}= 5/group.
Data (A-D) for HSD and MCD is representative of multiple independent experiments: $repetitions_{HSD}$ = 5 (n=4-5/group), repetition $_{MCD}$ = 3 (n=4-5/group). NC experiment was performed one time. Bar-graphs depict mean + SEM. Significance is indicated through *p<0.05, ** p<0.005, ***p<0.0001. Asterisks on top of the bar show statistical significance compared to the respective NC group of WT or batf3-KO, underlined asterisks show statistical significance of WT compared to batf3-KO.

3.5.3.2 *T cells*

Figure 19 depicts the analysis of T cells in WT and batf3-KO mice after 5 weeks feeding of NC, HSD or MCD. Figure 19.A shows the basic gating strategy as described in chapter 3.5.3.1 with gating on living, single CD45⁺F4-80⁻ cells and the subsequent plotting of CD3ε signal against CD19. To investigate T cells the CD19⁻CD3ε⁺ population (magenta gate, isotype control is depicted in Figure 18.C) is selected, as CD3ε is a universal T cell marker. In a following step, these cells are divided based on their expression of NK1.1. to exclude the NK1.1. positive T cells, which are analyzed separately (compare chapter 3.5.3.3). As Figure 19.C depicts, the majority of CD3ε⁺ are NK1.1⁻ (orange gate), a population which includes the

two major T cell subtypes $CD4^+$ T-cells and $CD8^+$ T-cells. The FMO-staining control for NK1.1 is shown in Figure 19.B.

Changes of percentage ratio and total cell count per gram liver is depicted in Figure 19.D: Interestingly a significant baseline difference in percentage ratio of T cells can be observed in batf3-KO animals compared to the WT (*means NC: WT 12.6%, batf3-KO 10.5%*). This discrepancy is even larger in HSD treated animals with *12.2%* in the WT and *8.2%* in batf3-KO. In batf3-KO animals the percentage ratio of T cells decreases significantly compared to the respective NC control whereas percentage ratio in WT animals remains unchanged. A slight gap in percentage ratio can still be observed in the MCD treated animals however this is not significant (*means MCD: WT 10.6%, batf3-KO 8.0%*). This can be explained by the fact, that the percentage ratio in WT animals slightly, but not significantly, decreases compared to the NC and HSD group. In MCD treated batf3-KO animals the percentage ratio does not further decrease compared to the HSD group, but is significantly lower compared to the NC group.

Subsequently absolute cell count per gram liver is determined to see whether these differences are real or merely due to shifts in percentage ratio as result of cell infiltrate or lack of the cDC 1 population. Interestingly the significant changes between NC and HSD treated WT and batf3-KO animals seem to be percentage shifts, as in absolute numbers there are no significant difference between the two groups *(means NC: WT 212x10^3 cells/g liver, batf3-KO 149x10^3 cells/g liver; means HSD: WT 151x10^3 cells/g liver, batf3-KO 173x10^3 cells/g liver*). Meanwhile in MCD treated animals both WT and batf3-KO show a significant influx of T cells, which interestingly is significantly higher in the WT than in the batf3-KO (*means MCD: WT 759x10^3 cells/g liver, batf3-KO 517x10^3 cells/g liver)*. In conclusion, the lack of batf3-dependent cDCs 1 does not affect the absolute count of T cells in NC or HSD, but reduces the amount of T cell infiltrate in MCD treatment. Nevertheless, it does cause a significant change in percentage ratio on a baseline level as well as in HSD treated animals, which might result in a relative mismatch of T cells towards other immune cells.

Since the investigated population includes both the $CD8^+$ and the $CD4^+$ subtype a pilot experiment was conducted to see whether the lack of cDCs 1 affects $CD4^+$ T cells in particular. Figure 20.A shows the basic gating strategy to gate on $CD3\varepsilon^+CD19^-NK1.1^-$ T cells by gating on single, living $CD45^+$ cells. Since CD4 was added to the staining mix, F4-80 could not be used in these experiments, as the number of antibodies per staining mix is restricted. Therefore $CD45^+$ cells are directly separated based on the CD3ε and CD19 expression and T cells are further gated on as described above. Figure 20.C shows the CD4 signal of T cells, where $CD4^+$ cells separate nicely from the remaining events (forest green gate). The corresponding isotype control is depicted in Figure 20.B. The percentage ratio of $CD4^+$ does not differ significantly

between WT and batf3-KO mice, neither in the HSD, nor the MCD group. However, in HSD treated animals a tendency towards lower numbers in batf3-KO animals can be observed (*means HSD: WT 6.4%, batf3-KO 3.9%*). Interestingly the percentage ratio of CD4$^+$ T cells decreases in MCD treated animals and the in the HSD group observed gap between WT and batf3-KO also diminishes after MCD feeding (*means MCD: WT 2.8%, batf3-KO 2.1%*). Absolute numbers were only calculated for the HSD group. Here the total cell count per gram liver is significantly lower in batf3-KO animals (*means HSD: WT 128x10^3 cells/g liver, batf3-KO 62x10^3 cell/g liver*), a phenomenon which cannot be observed when looking at the complete T cell population (compare Figure 19.D).

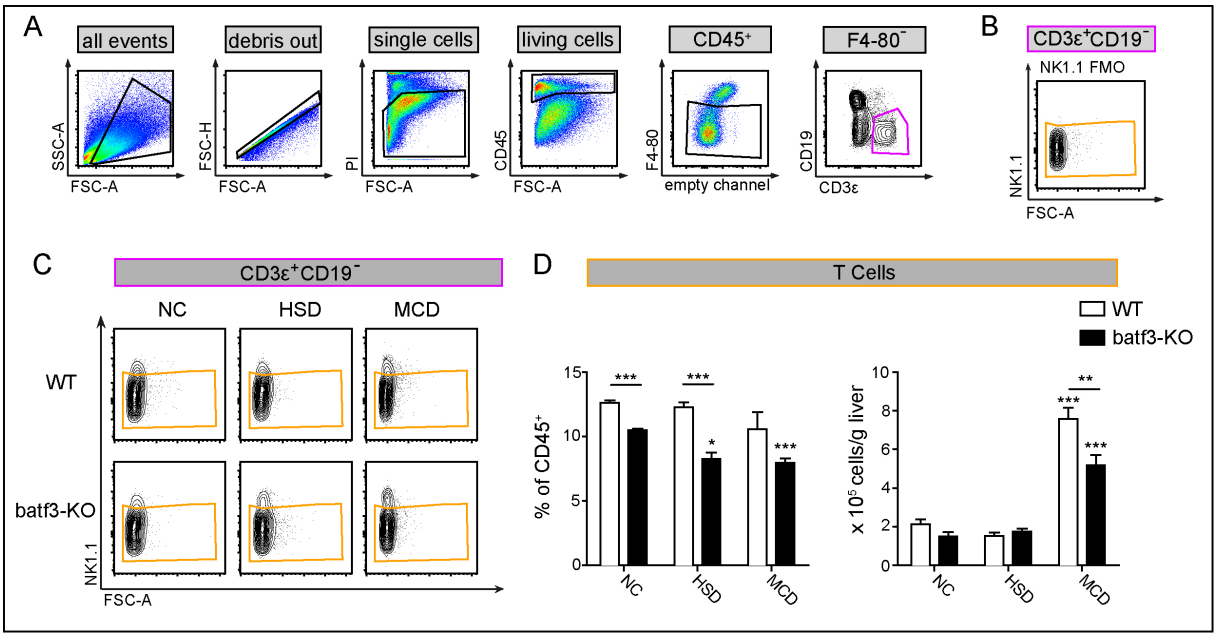

Figure 19 changes of all T cells in WT C57Bl/6 mice compared to batf3-KO mice after 5 weeks of HSD, MCD or NC feeding **A)** basic gating strategy: debris, doublet and dead cell exclusion. Gating on leukocytes by selecting all CD45$^+$cells. Plotting F4-80 signal of CD45$^+$ cells against an empty channel and gating on all F4-80$^-$ cells. Then plotting CD19 against CD3ε and gating on CD19$^-$ CD3ε$^+$ cells (magenta gate) **B)** representative contour blots of CD19$^-$ CD3ε$^+$ cells showing NK1.1 signal (*primary AB: biotin 1:100, secondary AB: A405 1:400)* plotted against forwards scatter to gate on NK1.1$^-$ cells (orange gate) **C)** FMO control for NK1.1 (*secondary AB: A405 1:400)* **D)** bar-graphs show comparison of percentage ratio within CD45$^+$ cells (left graph) and total cell amount per gram digested liver (right graph) of CD19$^-$ CD3ε$^+$ NK1.1$^-$ cells. n_{NC}= 5/group, n_{HSD}= 5/group, n_{MCD}= 5/group.
Data (A-D) for HSD and MCD is representative of multiple independent experiments: $repetitions_{HSD}$ = 5 (n=4-5/group), $repetitions_{MCD}$ = 3 (n=4-5/group). NC experiment was performed one time. Bar-graphs depict mean + SEM. Significance is indicated through *p<0.05, ** p<0.005, ***p<0.0001. Asterisks on top of the bar show statistical significance compared to the respective NC group of WT or batf3-KO, underlined asterisks show statistical significance of WT compared to batf3-KO

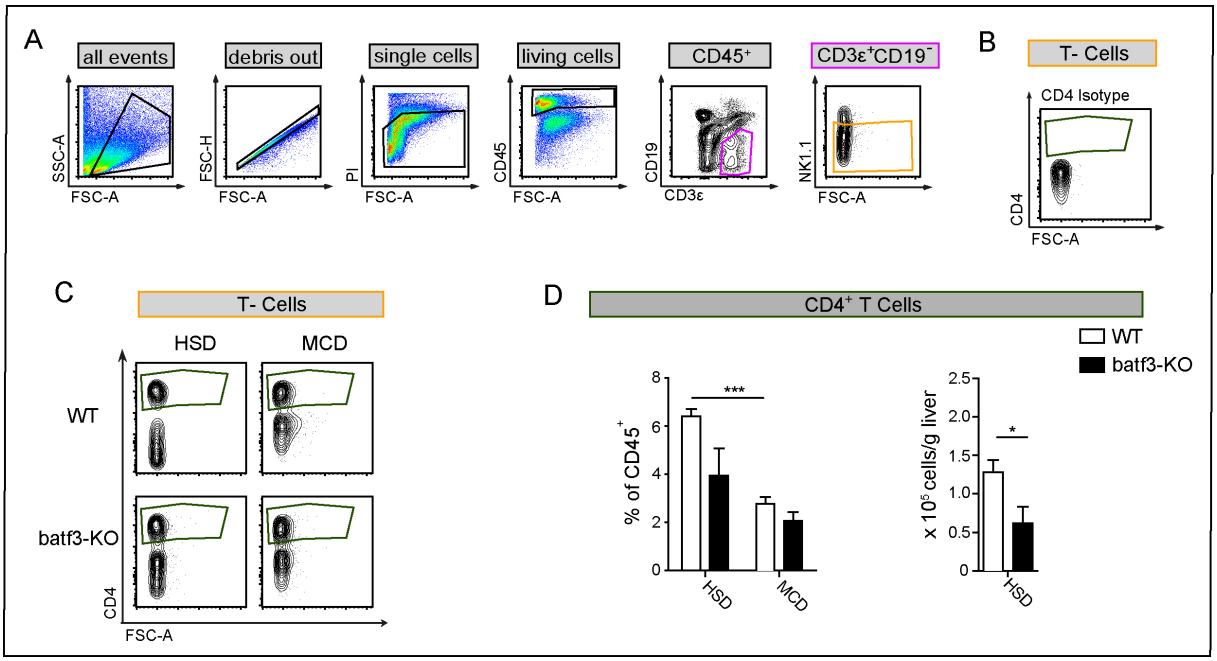

Figure 20 changes of CD4⁺ T cells in WT C57Bl/6 mice compared to batf3-KO mice after 5 weeks of HSD, MCD or NC feeding **A)** basic gating strategy: debris, doublet and dead cell exclusion. Gating on leukocytes by selecting all CD45⁺cells. Plotting CD19 against CD3ε and gating on CD19⁻ CD3ε⁺ cells (magenta gate). Then plotting NK1.1 signal against forwards scatter to gate on NK1.1⁻ cells (orange gate) **B)** isotype control for CD4 (*APC 1:100*) **C)** representative contour blots showing CD4 signal (*APC 1:100*) plotted against forwards scatter of CD19⁻ CD3ε⁺NK1.1⁻ cells to gate on CD4⁺ cells (forest green gate) **D)** bar-graphs show comparison of percentage ratio within CD45⁺ cells (left graph) and total cell amount per gram digested liver (right graph) of CD19⁻ CD3ε⁺ NK1.1⁻ CD4⁺ cells. $n_{HSD\ WT}$=4, $n_{HSD\ KO}$=3, $n_{MCD\ WT}$=5, $n_{MCD\ KO}$=4.
Data (A-D) for MCD is representative of two independent experiments (n=4-5/group). HSD experiment was performed one time. Bar-graphs depict mean + SEM. Significance is indicated through *p<0.05, ** p<0.005, ***p<0.0001. Asterisks on top of the bar show statistical significance compared to the respective NC group of WT or batf3-KO, underlined asterisks show statistical significance of WT compared to batf3-KO

3.5.3.3 *NKT cells*

A further lymphoid population investigated are NKT cells, as depicted in Figure 21. Basic gating strategy on T cells is performed as described in chapter 3.5.3.2. Subsequently the events are plotted accordingly to their NK1.1 expression and the NK1.1⁺ cells are selected accordingly to the isotype control (Figure 21.B and C). Figure 21.D depicts changes of the percentage ratio as well as the absolute cell count per gram liver. The NKT cell population represents a quite small fraction of liver immune cells with less than one percent during steady state (*means NC: WT 0.84%, batf3-KO 0.64%*). Neither HSD nor MCD treatment significantly changes the percentage ratio, although there is a slight tendency towards higher numbers after MCD treatment (*means WT: HSD 0.58%, MCD 1.15%; means batf3-KO: HSD 0.69%, MCD 1.42%*). Importantly there is no difference between WT and batf3-KO. Baseline absolute numbers in NC treated animals are an average *18x10³ cell/g liver* in WTs and *13x10³ cells/g liver* in batf3-KOs. HSD treatment does not change the cell count significantly compared to the NC control (*means HSD: WT 10x10³ cells/g liver, batf3-KO 19x10³ cells/g liver*). Interestingly MCD treatment causes an influx of NKT cells and numbers increase in WT to *89x10³ cells/g*

liver and in batf3-KO to *93x10³ cells/g liver*. Concluding NKT cells are a quite small population within the immune cells of the liver, but increase in numbers during NASH. cDCs1 do not influence the NKT cell population during steady state, bland steatosis or NASH.

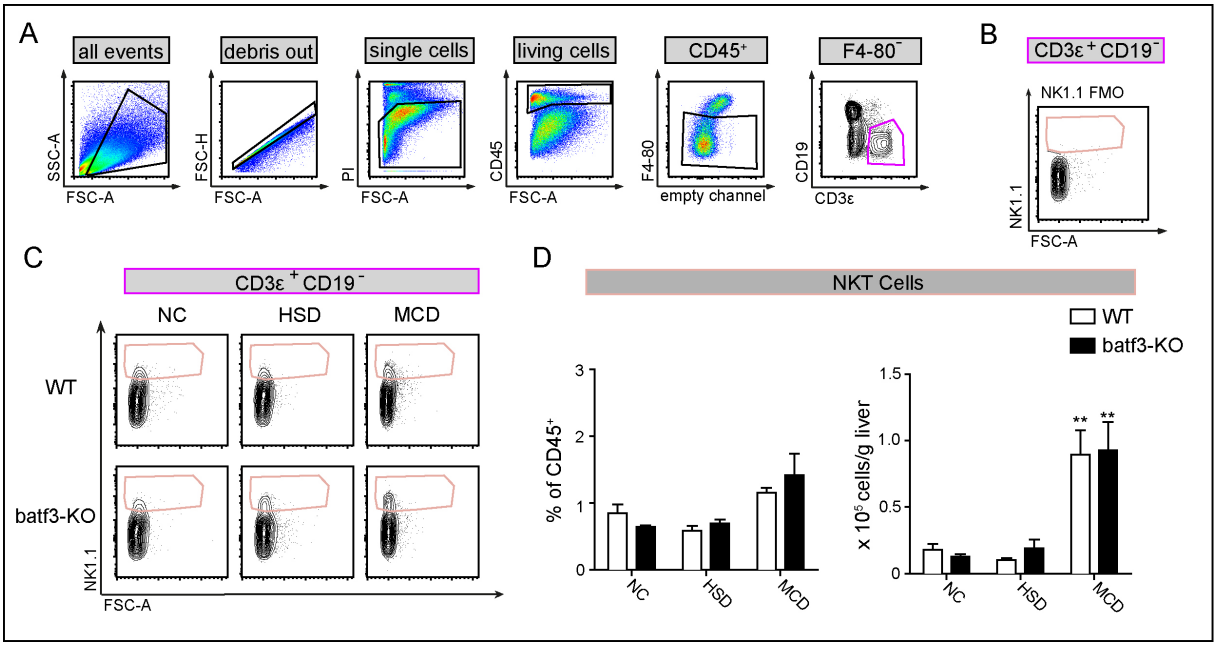

Figure 21 changes of NKT cells in WT C57Bl/6 mice compared to batf3-KO mice after 5 weeks of HSD, MCD or NC feeding **A)** basic gating strategy: debris, doublet and dead cell exclusion. Gating on leukocytes by selecting all CD45⁺cells. Plotting F4-80 signal of CD45⁺ cells against an empty channel and gating on all F4-80⁻ cells. Then plotting CD19 against CD3ε and gating on CD19⁻ CD3ε⁺ cells (magenta gate) **B)** representative contour blots of CD19⁻ CD3ε⁺ cells showing NK1.1 signal (*primary AB: biotin 1:100, secondary AB: A405 1:400)* plotted against forwards scatter to gate on NK1.1⁺ cells (rosé gate) **C)** FMO control for NK1.1 (*secondary AB: A405 1:400)* **D)** bar-graphs show comparison of percentage ratio within CD45⁺ cells (right graph) and total cell amount per gram digested liver (left graph) of CD19⁻ CD3ε⁺ NK1.1⁺ cells. n_{NC}= 5/group, n_{HSD}= 5/group, n_{MCD}= 5/group.
Data (A-D) for HSD and MCD is representative of multiple independent experiments: $repetitions_{HSD}$ = 5 (n=4-5/group), $repetitions_{MCD}$ = 3 (n=4-5/ group). NC experiment was performed one time. Bar-graphs depict mean + SEM. Significance is indicated through *p<0.05, ** p<0.005, ***p<0.0001. Asterisks on top of the bar show statistical significance compared to the respective NC group of WT or batf3-KO, underlined asterisks show statistical significance of WT compared to batf3-KO

3.5.3.4 *NK cells*

Figure 22 depicts dynamics of the NK cells in WT and batf3-KO mice after 5 weeks NC, HSD or MCD treatment. As described in chapter 3.5.3.1 living, single CD45⁺F4-80⁻ cells are plotted according to their CD19 and CD3ε expression. As NK-cells express neither of the latter surface markers the double negative population (dark blue gate) is selected (Figure 22.A). Subsequently the NK1.1 signal is plotted against forward scatter and the positive NK cells (light blue gate) separate nicely from the remaining NK1.1⁻ events (Figure 22.C , FMO control in Figure 22.B). Changes in percentage ratio as well as absolute cell count per gram liver are depicted in Figure 22.D: HSD treated animals show no significant difference in percentage ratio, neither compared to the respective healthy control nor between WT and batf3-KO within the different dietary groups (*means NC: WT 4.4%, batf3-KO 4.6%; means HSD: WT 5.0%,*

batf3-KO 5.3%). Parallel to this, no significant changes or tendencies in absolute cell count per gram liver can be observed in these groups (*means NC: WT 93x10^3 cells/g liver, batf3-KO 94x10^3 cells/g liver; means HSD: WT 55x10^3 cells/g liver, batf3-KO 136x10^3 cells/g liver*). In MCD treated animals, percentage ratio of NK cells does not increase significantly in the WT whereas the percental mean in batf3-KO animals shows a significant increase (*means MCD: WT 5.5%, batf3-KO 7.1%)*. When looking at the absolute cell count, however, this difference is relativized as the mean cell count is not significantly increased in the batf3-KO compared to the WT. Importantly both animal groups show a significant increase in cell count compared to the respective NC control group (*means MCD: WT 411x10^3 cells/g liver, batf3-KO 465x10^3 cells/g liver*). In conclusion steatosis does not cause an influx of NK cells in the liver, whereas established NASH is accompanied by increased abundance of these cells. Further a lack of cDCs 1 does not significantly alter the presence of NK cells in the liver or influence their recruitment.

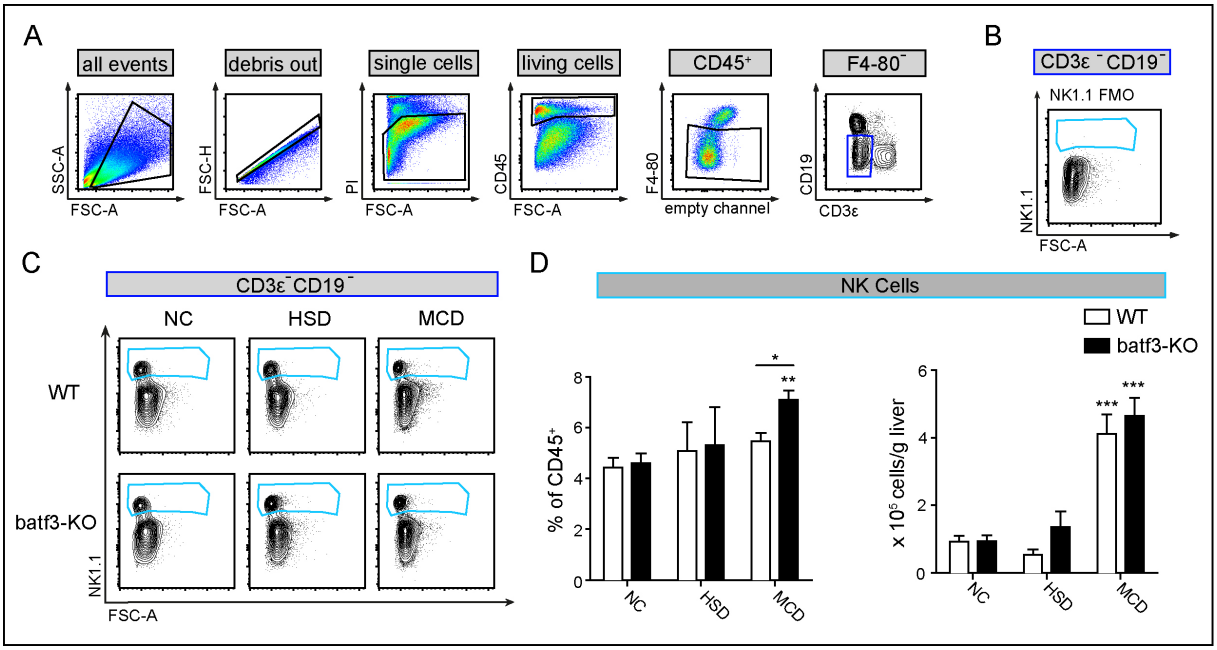

Figure 22 changes of NK cells in WT C57Bl/6 mice compared to batf3-KO mice after 5 weeks of HSD, MCD or NC feeding **A)** basic gating strategy: debris, doublet and dead cell exclusion. Gating on leukocytes by selecting all CD45$^+$cells. Plotting F4-80 signal of CD45$^+$ cells against an empty channel and gating on all F4-80$^-$ cells. Then plotting CD19 against CD3ε and gating on CD19$^-$ CD3ε$^-$ double negative cells (dark blue gate) **B)** representative contour blots of CD19$^-$ CD3ε$^-$ cells showing NK1.1 signal (*primary AB: biotin 1:100, secondary AB: A405 1:400)* plotted against forwards scatter to gate on NK1.1$^+$ cells (light blue gate) **C)** FMO control for NK1.1 (*secondary AB: A405 1:400)* **D)** bar-graphs show comparison of percentage ratio within CD45$^+$ cells (left graph) and total cell amount per gram digested liver (right graph) of CD19$^-$ CD3ε$^-$ NK1.1$^+$ cells. n_{NC}= 5/group, n_{HSD}= 4/group, n_{MCD}= 5/group.
Data (A-D) for HSD and MCD is representative of multiple independent experiments: repetitions$_{HSD}$ = 5 (n=4-5/group), repetitions$_{MCD}$ = 3 (n=4-5/group). NC experiment was performed one time. Bar-graphs depict mean + SEM. Significance is indicated through *p<0.05, ** p<0.005, ***p<0.0001. Asterisks on top of the bar show statistical significance compared to the respective NC group of WT or batf3-KO, underlined asterisks show statistical significance of WT compared to batf3-KO

Summary chapter 3.5.3:

- B cells do not increase in numbers during NASH, which leads to a relative diminution of the population within liver immune cells due to an influx of other $CD45^+$ cells. The lack of cDCs 1 does not affect the B cell population.
- The number of T cells is increased during MCD induced NASH, but not in bland steatosis. The lack of cDCs 1 does not affect absolute numbers in the healthy control or steatosis model, but causes a relative diminution of the T cell population within all $CD45^+$ cells and absolute reduction of T cells during MCD induced NASH.
- The relative amount of $CD4^+$ T cells is decreased after MCD treatment compared to the HSD group in WT animals. The lack of cDCs 1 does not affect the relative amount of $CD4^+$ cells in MCD, but causes a decrease of $CD4^+$ T cells during HSD.
- NKT cells increase in number during NASH but not during bland steatosis. No relevant differences can be observed in the batf3-KO compared to the WT.
- NK cells increase in number during NASH, but not during bland steatosis. No relevant differences can be observed in the batf3-KO compared to the WT.

3.5.4 Cytokine production of liver NPC

Compared to the WT control batf3-KO mice show a progression of steatosis towards steatohepatitis and exhibit alterations in the cellular infiltrate of the liver. Additional experiments were performed to investigate whether the lack of cDCs 1 also influences the hepatic cell infiltrate on a functional level, in particular concerning cytokine production of liver nonparenchymal cells. The analysis was performed using a cytokine array to have a general overview of cytokine production within the liver single cell suspension. Further individual cytokines were selected for intracellular staining to gather information on a cellular level.

3.5.4.1 *Cytokine array*

To get a broad overview of cytokines produced within the liver of HSD and MCD treated animals, a cytokine array was performed using cell culture supernatant of LPS stimulated liver homogenate. Figure 23.A depicts the assay membranes of the HSD groups together with the mean grey values of cytokines, that differ between batf3-KO and WT. The major differences can be found in Serpin E1, IL-1ra, CCL22, CCL2, CXCL1 and CCL5, which show higher signals in batf3-KO mice. Interestingly the production of resistin is higher in WT animals. In MCD treated animals, batf3-KOs also exhibit a higher cytokine production of Serpin E1, IL-1ra,

CXCL1 and CCL5 as depicted in Figure 23.B. Further they also show higher values of CXCL5, Osteopontin, CXCL1 and CXCL2.

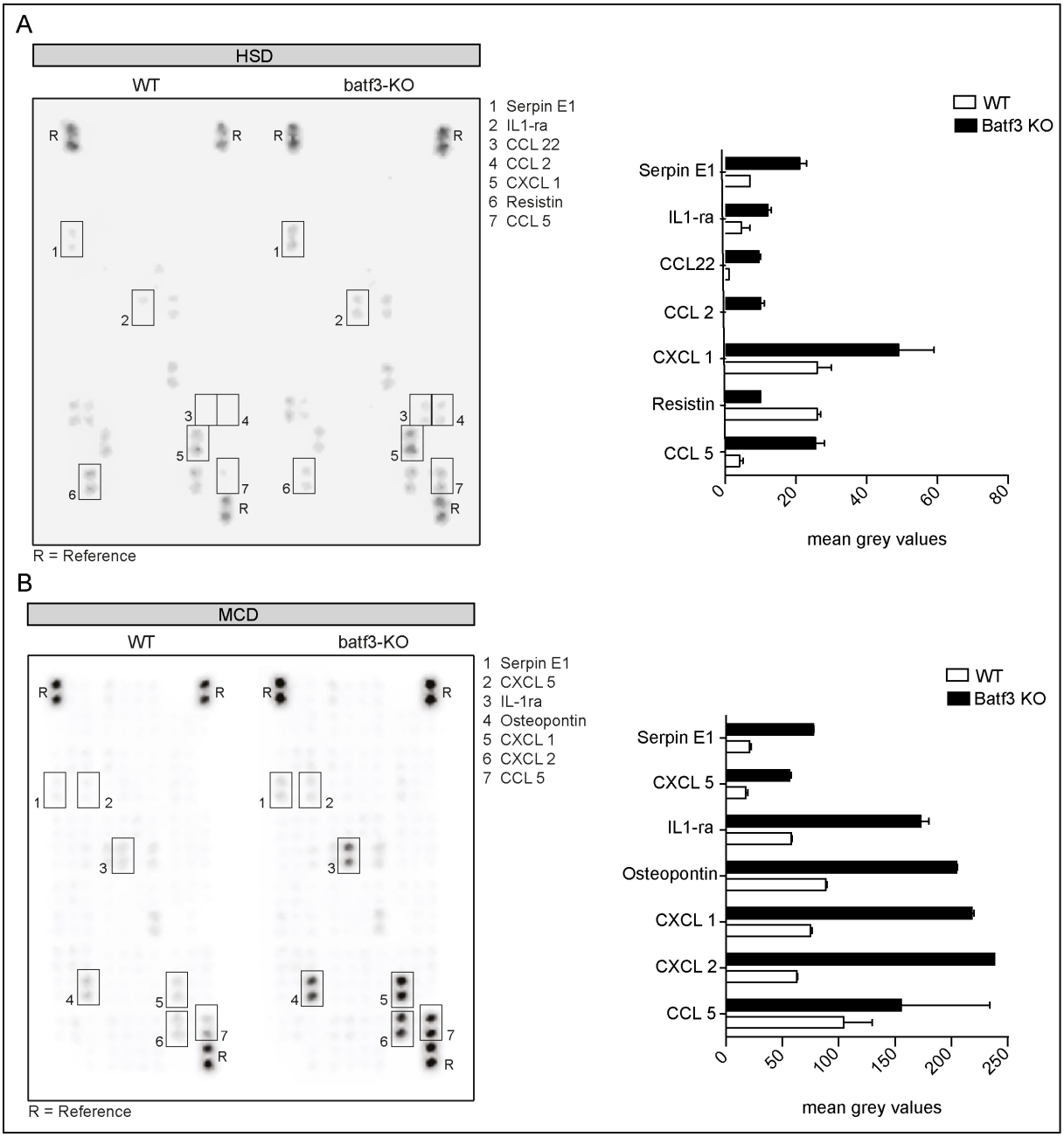

Figure 23 cytokine production of liver cell suspension after 18 hours of stimulation with 250 ng/ml LPS **A)** cytokine array of cell culture supernatant from liver single cells of 5 weeks HSD treated animals. Bar-graph shows mean grey values of the signals of boxed signals. **B)** cytokine array of cell culture supernatant from liver single cells of 5 weeks MCD treated animals. Bar-graph shows mean grey values of boxed signals.

3.5.4.2 *TNFα production*

Chapter 3.3.4 characterizes TNFα-production of DC subtypes and ultimately shows that CD11c$^+$ and F4-80$^+$ cells are the major populations that increase TNFα-production in the inflamed liver after 5 weeks MCD treatment. To see whether the lack of cDCs 1 influences

TNFα-production of these cells an intracellular staining was performed. Figure 24.A shows the gating strategy to select CD11c$^+$ and F4-80$^+$ cells as described in chapter 3.3.4. Cells are then plotted accordingly to their TNFα-signal and the positive events are selected (Figure 24.B and D). As depicted in Figure 24.C, TNFα-production in CD11c$^+$ cells does not show a significant difference one a baseline level (*means NC: WT 5.0%, batff3-KO 6.7%*). Equally to WT animals, in batf3-KO animals TNFα-production increases significantly after MCD diet (*means MCD: WT 12.6%, batf3-KO 15.1%*). Interestingly HSD treated batf3-KO animals show a significant increase in TNFα-production compared to the NC control, contrary to the WT animals which have values similar to their respective control NC group (*means HSD: WT 5.6%, batf3-KO 10.5%*). This effect can also be observed in the F4-80$^+$ cell population. On baseline WT and batf3-KO animals do not differ significantly in their TNFα production and it increases in equal proportions after MCD treatment (*means NC: WT 4.3%, batf3-KO 6.0%; means MCD: WT 21.5%, batf3-KO 23.0%*). In the HSD group, however, TNFα production increases significantly batf3-KO animals, while WTs show no significant change compared to the respective NC control (*means HSD: WT 3.6%, KO 11.5%*). In conclusion, the lack of cDCs 1 does not influence TNFα-production of CD11c$^+$ and F4-80$^+$ cells during steady state or MCD treatment, but causes an increase of TNFα-production during HSD diet.

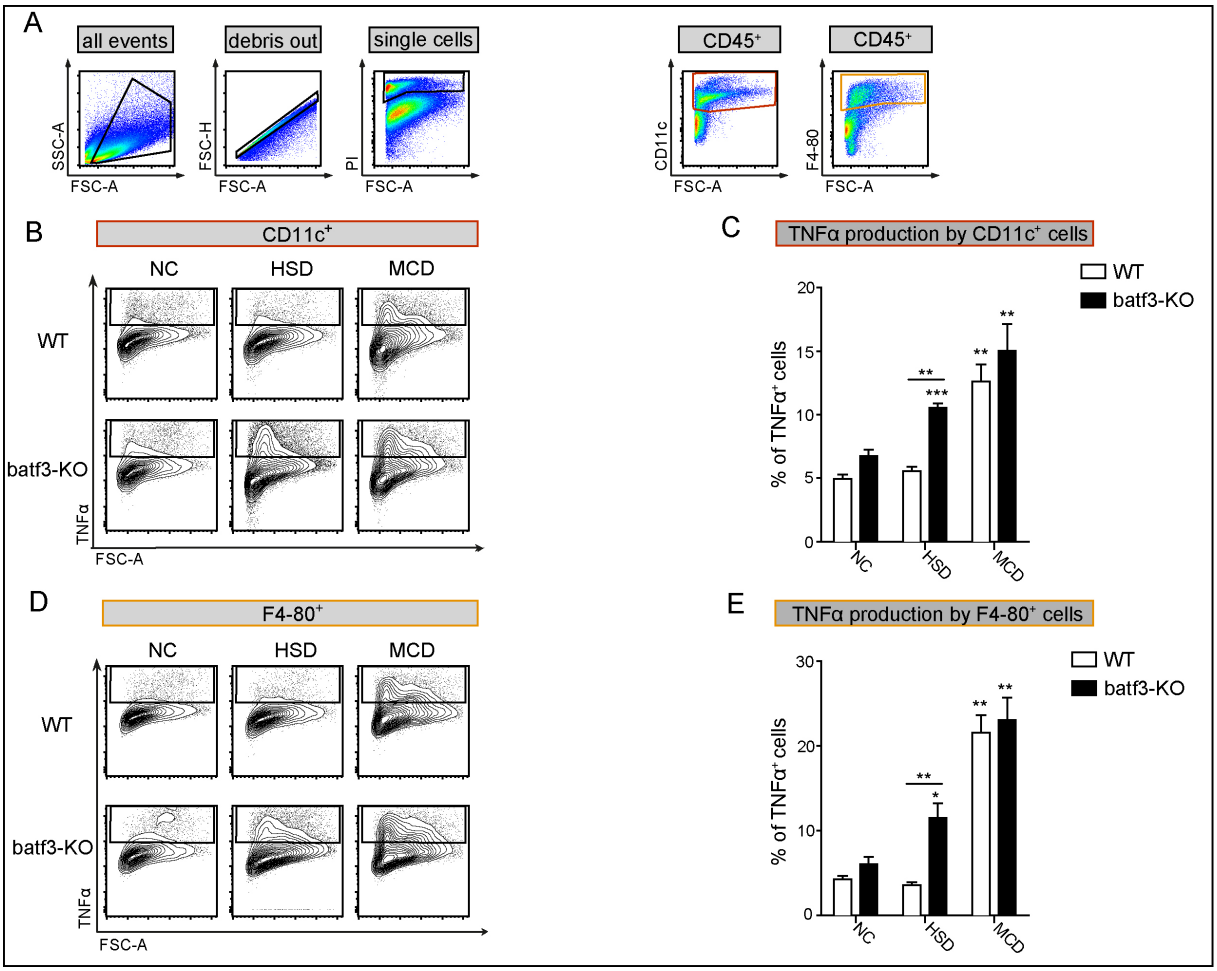

Figure 24 TNFα production of different cell populations stimulated with 250ng/ml LPS for 5 hours in WT C57Bl/6 mice compared to batf3-KO mice after 5 weeks of HSD, MCD or NC feeding **A)** basic gating strategy with debris and doublet cell exclusion. Gating on leukocytes by selecting all CD45$^+$cells, then gating on either CD11c$^+$ cells (red gate) or F4-80$^+$ cells (orange gate) **B)** representative contour-blots of the TNFα signal (*APC 1:200*) plotted against forwards scatter within CD11c$^+$ cells. Gated on TNFα$^+$ cells **C)** bar-graph shows comparison of percentage ratio of TNFα$^+$ cells within CD11c$^+$ cells. n_{NC}=4/group, n_{HSD}=4/group, n_{MCD}=4/group **D)** representative contour-blots of the TNFα signal (*APC 1:200*) plotted against forwards scatter within F4-80$^+$ cells. Gated on TNFα$^+$ cells **C)** bar-graph shows comparison of percentage ratio of TNFα$^+$ cells within F4-80$^+$ cells. n_{NC}=4/group, n_{HSD}=4/group, n_{MCD} =4/group
Data (A-E) shown for CD11c$^+$ cells is representative of multiple independent experiments for HSD and MCD: $repetitions_{HSD}$= 4 (n=4/group), $repetitions_{MCD}$ = 3 (n=4/group). Experiment for NC was performed one time. Data (A-E) shown for F4-80$^+$ cells is representative multiple independent experiments of HSD: $repetitions_{HSD}$ = 3 (n=4/group). Experiments for MCD and NC were performed one time. Bar-graphs depict mean + SEM. Significance is indicated through *p<0.05, ** p<0.005, ***p<0.0001. Asterisks on top of the bar show statistical significance compared to the respective NC group of WT or batf3-KO, underlined asterisks show statistical significance of WT compared to batf3-KO

3.5.4.3 *Production of chemokines*

As the cytokine arrays of both HSD and MCD treated animals show differences in cytokine production an intracellular staining was performed to investigate the production on a cellular level. Three cytokines were selected, namely CXCL-1, CXCL-2 and CCL-5, and the results are depicted in Figure 25. The basic gating strategy on CD11c$^+$ cells is performed as

described in chapter 3.3.4. Cells are then plotted accordingly to their APC signal (FMO control is depicted in Figure 25.B) and the positive signals are selected.

The production of CXCL-1, as depicted in Figure 25.D, shows a baseline difference in the healthy control, where the percentage of CXCL-1 producing $CD11c^+$ cells is significantly higher in batf3-KO animals than in the WT (*means NC: WT 1.3%, batf3-KO 3.1%*). The production then increases significantly in HSD treated batf3-KO animals, whereas HSD treated WT animals show no significant difference with respects to the healthy control (*means HSD: WT 2.2%, batf3-KO 5.2%).* Only after MCD treatment do also WT animals show an increase in CXCL-1 production of $CD11c^+$ cells and batf3-KO animals shows an even further increase to an average (*means MCD: WT 5.4%, batf3-KO 8.1%).*

Figure 25.F shows the percentage ratio of CCL-5 producing cells within the $CD11c^+$ population. The baseline production of CCL-5 in $CD11c^+$ cells shows no significant difference between WT and batf3-KO (*means NC: WT 2.5, batf3-KO 2.5%*). Parallel to observations made for TNFα and CXCL-1, the production of CCL-5 increases significantly in HSD treated batf3-KO mice, while the values of WT animals remain similar as the baseline level (*means HSD: WT 1.5%, batf3-KO 12.2%*). MCD treatment causes an increase in cytokine production in WT animals and a further increase in the batf3-KOs (*means MCD: WT 16.7%, batf3-KO 42.9%*).

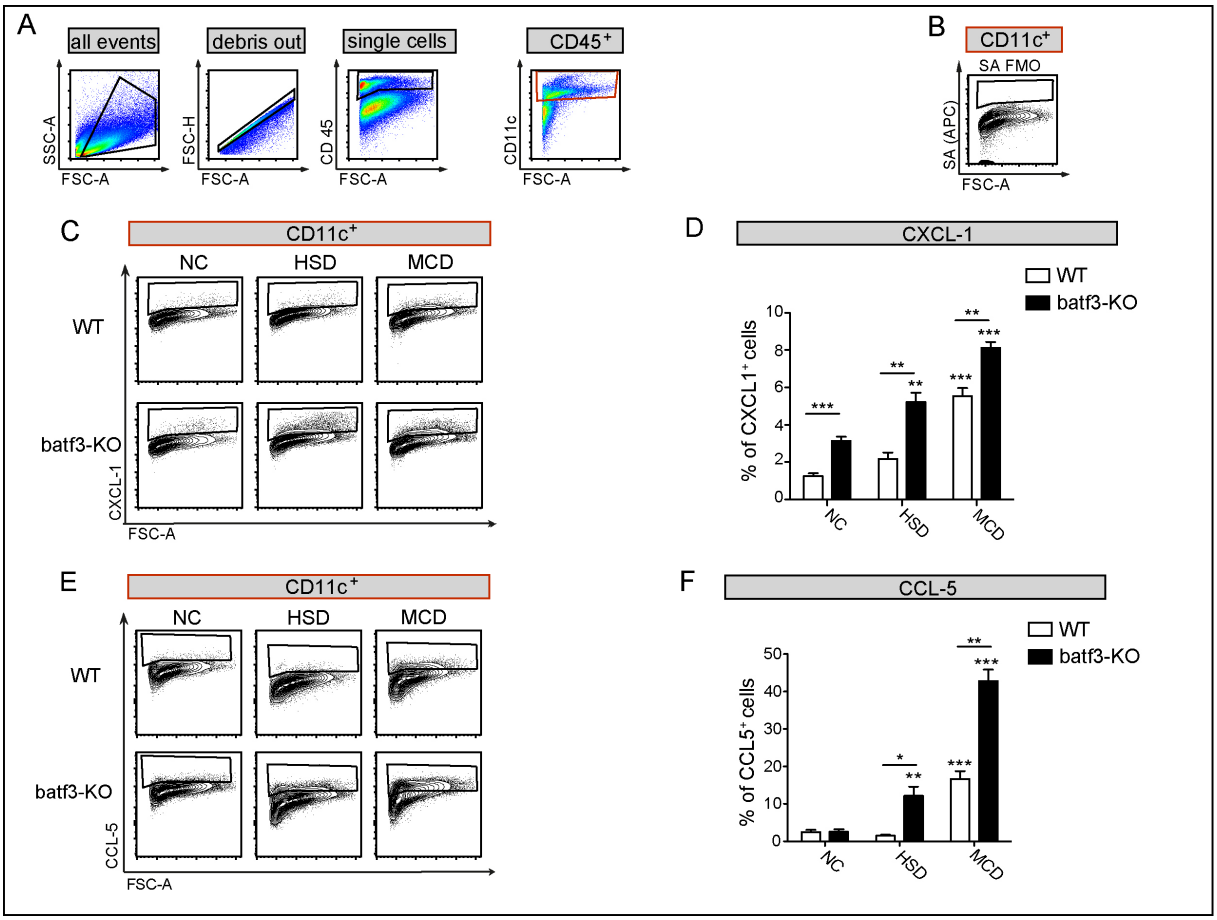

Figure 25 Cytokine production of different cell populations stimulated with 250ng/ml LPS for 5 hours in WT C57Bl/6 mice compared to batf3-KO mice after 5 weeks of HSD, MCD or NC feeding. **A)** basic gating strategy with debris and doublet cell exclusion. Gating on leukocytes by selecting all CD45$^+$cells, then gating on CD11c$^+$ cells (red gate) **B)** FMO control of an intracellular staining without the primary antibody (*SA A647 1:800)* **C)** representative contour-blots of the CXCL-1 signal (*primary AB unlabeled goat 1:500, secondary AB A647 1:800*) plotted against forward scatter within CD11c$^+$ cells. Gated on CXCL-1$^+$ cells **D)** bar-graph shows comparison of percentage ratio of CXCL-1$^+$ cells within CD11c$^+$ cells. n_{NC}=4/group, n_{HSD}=4/group, n_{MCD}=4/group. Data (C, B) is representative of two independent experiments for HSD and MCD (n=4/group). NC experiment was performed one time. **E)** representative contour-blots of CCL-5 signal (*primary AB unlabeled goat 1:500, secondary AB A647 1:800*) plotted against forward scatter within CD11c$^+$ cells. Gated on CCL-5$^+$ cells **F)** bar-graph shows comparison of percentage ratio of CCL-5$^+$ cells within CD11c+ cells. n_{NC}=4/group, n_{HSD}=3/group, n_{MCD}=3/group. Experiment for data (E, F) was performed one time per group. Data was created using the digest protocol I.
Significance is indicated through *p<0.05, ** p<0.005, ***p<0.0001. Asterisks on top of the bar show statistical significance compared to the respective NC group of WT or batf3-KO, underlined asterisks show statistical significance of WT compared to batf3-KO

Summary chapter 3.5.4:

- The lack of cDCs 1 increases the pro-inflammatory cytokine production within a liver homogenate cell culture in both during HSD and MCD treatment
- The lack of cDCs 1 increases TNFα production by CD11c$^+$ and F4-80$^+$ cells during HSD
- The lack of cDCs 1 increases CXCL-1 production by CD11c$^+$ cells on a baseline level as well as during HSD and MCD treatment
- The lack of cDCs 1 increases CCL-5 production by CD11c$^+$ cells during HSD and MCD, but not on a baseline level.

3.6 The influence of batf3-dependent cDCs 1 on incipient NASH

The most striking effects of batf3-dependent cDCs 1 can be observed in the HSD steatosis model: after 5 weeks of HSD batf3-KO mice experience worse liver damage and exhibit clear tendencies towards a higher inflammatory milieu than the WT control. In the 5 weeks MCD induced NASH model the lack of cDCs 1 has a lower impact and shows only little differences between WT and batf3-KO animals. To see whether cDCs 1 influence incipient NASH, a pilot experiment was conducted in which animals were treated with MCD for two weeks instead of five. The hematopoietic infiltrate during the onset of steatohepatitis was then investigated using the same multicolored flow cytometric analysis as in previous experiments.

3.6.1 Dendritic cell subtypes

To investigate changes of individual DC subpopulations the cells were gated as described in chapter 3.3. Figure 26.A and B depicts changes in the cDC 1 population after 2 weeks of MCD diet: in WT animals this treatment causes an increase in percentage ratio of 1.7-fold to an average *3.8%* within all $CD45^+$ cells and a 3.0-fold increase in total cell count to an average *$110x10^3$ cells/g liver*. In comparison after 5 weeks of diet they increase an average 2.4-fold and 8.2-fold respectively.

The $CD11b^+$ DC population of WT animals, as depicted in Figure 26. C and D, also increases significantly in the 2 weeks MCD group compared to respective control animals. Percental ratio increases an average 3.5-fold to *7.7%* and total cell count an average 5.1-fold to *$227x10^3$ cells/g liver*. Here the 5 weeks MCD diet leads to an increase of 3.6-fold in percentage ratio and 13-fold in total cell count. When separating the $CD11b^+$ DCs accordingly to their origin both the cDCs 2 and moDC subtype increase after 2 weeks of MCD feeding (Figure 26.E, F, G). $CD64^-$ cDCs 2 show an average 4.6-fold increase in percentage ratio (*means WT: NC 1.4%, 2 wks MCD 6.0%*) and 6.2-fold increase in total cell count (*means WT: NC $28x10^3$ cells/g liver, 2 wks MCD $178x10^3$ cells/g liver*). moDCs on the other hand show an average 6.4-fold increase in percentage ratio (*means WT: NC 0.3%, 2 wks MCD 1.68%*) and 8.9-fold increase in total cell count (*means WT: NC $5x10^3$ cells/ g liver, 2 wks MCD $49x10^3$ cells/g liver*). In batf3-KO animals $CD11b^+$ DCs increase significantly in percentage ratio (*means batf3-KO: NC 3.9%, 2 wks MCD 11.5%*) as well as in total cell count (*means batf3-KO: NC $59x10^3$ cells/g liver, 2 wks MCD $354x10^3$ cells/g liver*). The significantly higher percentage ratio compared to the WT, which would suggest a higher increase of $CD11b^+$ in the batf3-KO, turns out to be not significant in absolute numbers, although a tendency towards higher numbers can be observed. Separated accordingly to their origin, both subtypes increase

significantly in percentage ratio (*means batf3-KO* cDCs 2*: NC 3.0%, 2wks MCD 7.4%; means batf3-KO* moDCs*: NC 0.3%, 2 wks MCD 3.9%*) as well as total cell count *(means batf3-KO* cDCs 2*: NC 46x10^3 cells/g liver, 2 wks MCD 225x10^3 cells/g liver; means batf3-KO* moDC*s: NC 5x10^3 cells/g liver, 2 wks MCD 123x10^3 cells/g liver*). Importantly in moDCs a significant difference in percentage ratio towards the WT can be observed in batf3-KO animals and although this is not significant in numbers a clear tendency towards higher values in the batf3-KO is detectable.

The pDC population of WT animals shows no significant change in percentage ratio (*means WT: NC 3.0%, 2 weeks MCD 3.0%*), but a slight increase in total cell count (*means WT: NC 9x10^3 cells/10^6 living cells, 2 wks MCD 16x10^3 cells/10^6 living cells*). Showing no significant difference towards the WT, pDCs in batf3-KO animals equally are not changed in percentage ratio (*means batf3-KO: NC 3.0%, 2 wks MCD 2.7%*), but are slightly increased in total cell count (*means batf3-KO: NC 9x10^3 cells/10^6 living cells, 2 wks MCD 15x10^3 cells/10^6 living cells*).

Concluding individual DC subpopulations of WT animals show similar tendencies to increase after 2 weeks of MCD diet as they do after 5 weeks, however in a lower augmentation. Importantly pDC changes can only be detected in total cell count, but not in percentage ratio. The recruitment of CD11b$^+$ DCs includes both cDCs 2 and moDCs, with cDCs 2 forming the larger fraction of cells, but moDCs showing an overall higher increase. In batf3-KO animals DC subtypes change similarly as they do in the WT, although a significant difference can be detected in percentage ratio of CD11b$^+$ DCs, in particular CD64$^+$ moDCs. Importantly, unlike in the HSD treated animals, this difference, although slightly reflected through a tendency towards higher values, remains not significant in total cell count per gram liver.

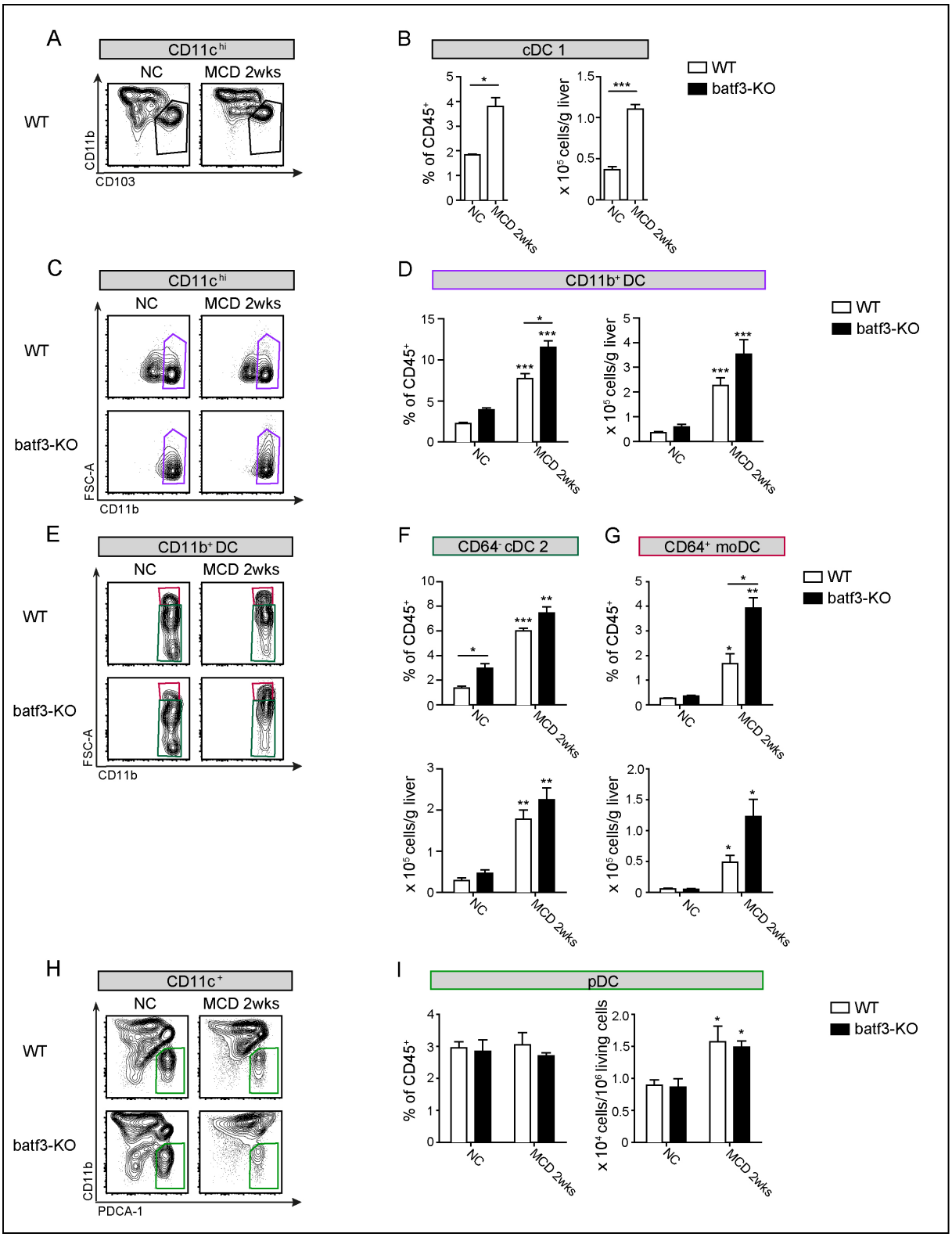

Figure 26 changes of DC subtypes in WT C57Bl/6 mice compared to batf3-KO mice after 2 weeks of MCD and NC feeding **A)** representative contour blots of CD11c^{hi} cells showing CD11b signal (*PE-Cy7 1:2000)* plotted against CD103 signal (*PE 1:200*) to gate on CD103^{+} cells (black gate) **B)** bar-graphs show comparison of percentage ratio within CD45^{+} cells (left graph) and total cell amount per gram digested liver (right graph) of CD11c^{hi}CD11b^{-}CD103^{+} cells (violet gate) **C)** representative contour blots of CD11c^{hi}MHC-II^{hi} cells showing CD11b signal (*PE-Cy7 1:2000)* plotted against forward scatter to gate on CD11b^{+} cells. **D)** bar-graphs show comparison of percentage ratio within CD45^{+} cells (left graph) and total cell amount per gram digested liver (right graph) of CD11c^{hi}MHCII^{hi}CD11b^{+} cells **E)** representative contour blots of CD11c^{hi}MHC-II^{hi}CD11b^{+} cells showing CD64 signal (*Brilliant Violet 421 1:200)*

plotted against CD11b (*PE-Cy7 1:2000)* to gate on $CD64^+$ cells (dark red gate) and $CD64^-$ cells (dark green gate). **F)** bar-graphs show comparison of percentage ratio within $CD45^+$ cells (upper graph) and total cell amount per gram digested liver (lower graph) of $CD11c^{hi}MHCII^{hi}CD11b^+CD64^-$ cells **G)** bar-graphs show comparison of percentage ratio within $CD45^+$ cells (upper graph) and total cell amount per gram digested liver (lower graph) of $CD11c^{hi}MHCII^{hi}CD11b^+CD64^+$ cells **H)** representative contour blots of $CD11c^+$ cells showing CD11b signal (*PE-Cy7 1:2000)* plotted against PDCA-1 signal (*PE 1:200*) to gate on $CD11b^-PDCA\text{-}1^+$ cells (light green gate) **I)** bar-graphs show comparison of percentage ratio within $CD45^+$ cells (left graph) and total cell amount per 10^6 living cells (right graph) of $CD11c^+CD11b^-PDCA\text{-}1^+$ cells. n_{NC}= 5/group, $n_{2wks\ MCD}$= 3/group
Data (A-I) for NC is representative of multiple independent experiments: $repetitions_{NC}$= 2 (n=3-5/group). 2wks MCD experiment was performed one time. Bar-graphs depict mean + SEM. Significance is indicated through *p<0.05, ** p<0.005, ***p<0.0001. Asterisks on top of the bar show statistical significance compared to the respective NC group of WT or batf3-KO, underlined asterisks show statistical significance of WT compared to batf3-KO

Summary chapter 3.6.1:

- Similar as after 5 weeks, 2 weeks feeding of MCD causes an influx of all DC subtypes into the liver, however with lower fold changes than observed in the 5 weeks treatment.
- The influx of $CD11b^+$ DCs consists of both cDCs 2 as well as moDCs with cDCs 2 making up the majority of cells, but moDCs showing an overall higher increase
- The lack of cDCs 1 results in a significant increase in percentage ratio of $CD11b^+$ DCs, particularly moDCs

3.6.2 Myeloid cells

Figure 27 depicts changes within the myeloid cell populations after 2 weeks of MCD treatment in WT and batf3-KO animals compared to the NC control. Surface staining and cell gating was performed as described in chapter 3.5.2.

Figure 27.B shows that the percentage ratio of KCs in both WT and batf3-KO animals decreases similarly as after 5 weeks of MCD diet (*means NC: WT 18,2%, batf3-KO 16.7%; means 2 wks MCD: WT 11,3%, batf3-KO 13,1%*). Contrary to 5 weeks treated animals, however, total cell count does not change significantly compared to the NC control (*means NC: WT 517x10^3 cells/g liver, batf3-KO 482x10^3 cells/g liver. Means 2 wks MCD: WT 436x10^3 cells/g liver, batf3-KO 509x10^3 cells/g liver*). This indicates that the decrease in percentage ratio is due to an increase of other $CD45^+$ cells rather than an actual decrease of KCs. Considering the increased cell count after 5 weeks of MCD treatment, it also suggests that the observed increase of KCs in steatohepatitis happens during later stages of disease development.

Looking at $Ly6C^{hi/int}F4\text{-}80^-$ cells in Figure 27.C they show an increase of percentage ratio both in WT and batf3-KO after 2 weeks of MCD diet, with batf3-KO showing significantly higher values *(means NC: WT 16,9%, batf3-KO 17,2%. Means 2 wks MCD: WT 24,7%, batf3-KO 32,6%*). Total cell counts also show an increase in $Ly6C^{hi/int}F4\text{-}80^-$ cells in 2 weeks MCD treated animals (*means NC: WT 385x10^3 cells/g liver, batf3-KO 356x10^3 cells/g liver. Means 2*

wks MCD: WT 953x10^3 cells/g liver, batf3-KO 129x10^4 cells/g liver). Importantly the total cell count after 2 weeks of MCD treatment ends up being lower than after 5 weeks MCD diet, but higher than after the HSD treatment. Similar as in HSD treated animals the absolute cell count is higher in batf3-KO than in WT animals, albeit this remains not significant.

Lastly Figure 27.D shows changes of the Ly6C$^{hi/int}$F4-80^{low} population. These cells also show an increase of percentage ratio after 2 weeks of MCD diet in both groups, but with significantly higher values in batf3-KO animals compared to the WT (*means NC: WT 0.8%, batf3-KO 0.8%. means 2 wks MCD: WT 4.9%, batf3-KO 11.8%*). Such tendency towards higher values in batf3-KO animals can also be observed in absolute numbers, where batf3-KO animals exhibit a significant increase compared to the NC control, and numbers in the WT are merely slightly increased compared to their respective NC control *(means NC: WT 27x10^3 cells/g liver, batf3-KO 33x10^3 cells/g liver. Means 2wks MCD: WT 191x10^3 cells/g liver, batf3-KO 472x10^3 cells/g liver*).

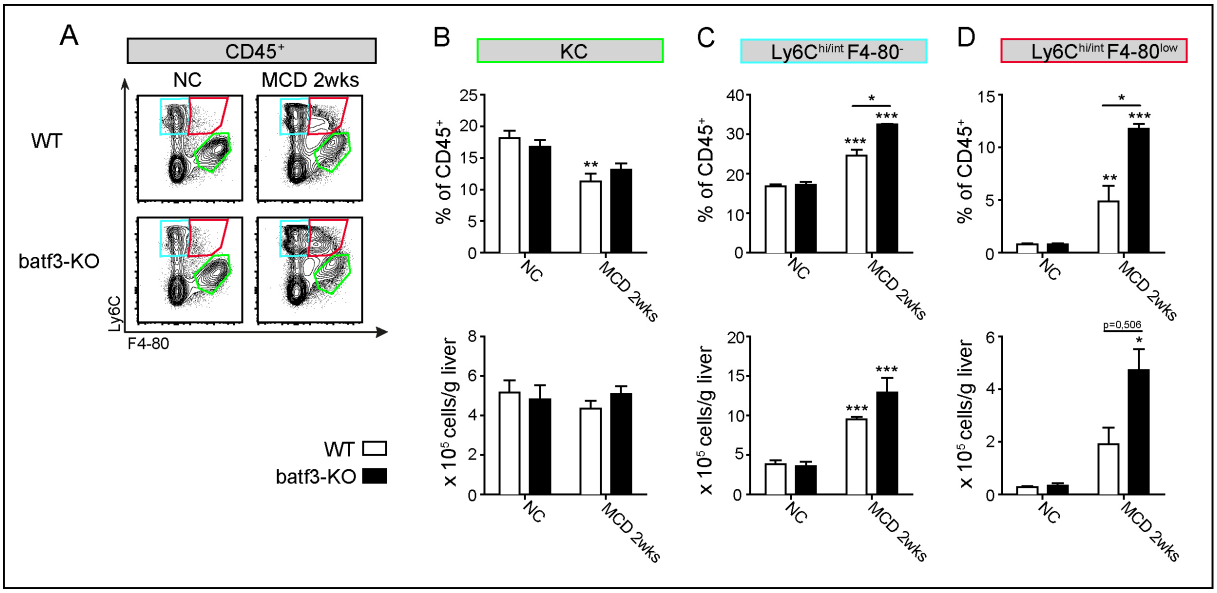

Figure 27 changes of monocyte and macrophage populations in WT C57Bl/6 mice compared to batf3-KO mice after 2 weeks of MCD compared to NC feeding **A)** representative contour blots of CD45$^+$ cells showing Ly6C signal (*APC 1:1000*) plotted against F4-80 signal *(A488 1:200)* to gate on Ly6C$^{hi/int}$ F4-80$^-$ cells (blue gate), Ly6C$^{hi/int}$ F4-80^{low} cells (red gate) and Ly6C$^{low/neg}$ F4-80$^+$ KCs (green gate) **B)** bar-graphs show comparison of percentage ratio within CD45$^+$ cells (upper graph) and total cell amount per gram digested liver (lower graph) of Ly6C$^{low/neg}$ F4-80$^+$ KCs **C)** bar-graphs show comparison of percentage ratio within CD45$^+$ cells (upper graph) and total cell amount per gram digested liver (lower graph) Ly6C$^{hi/int}$F4-80^{neg} cells **D)** bar-graphs show comparison of percentage ratio within CD45$^+$ cells (upper graph) and total cell amount per gram digested liver (lower graph) Ly6C$^{hi/int}$ F4-80^{low} cells. n_{NC}= 5/group, $n_{2wks\ MCD}$= 3/group.
Data (A-D) for NC is representative of multiple independent experiments: repetitions$_{NC}$= 2 (n=3-5/group). 2wks MCD experiment was performed one time. Bar-graphs depict mean + SEM. Significance is indicated through *p<0.05, ** p<0.005, ***p<0.0001. Asterisks on top of the bar show statistical significance compared to the respective NC group of WT or batf3-KO, underlined asterisks show statistical significance of WT compared to batf3-KO

Summary chapter 3.6.2:

- The KC population is not increased during incipient NASH after 2 weeks treatment with MCD
- Both Ly6C$^{hi/int}$F4-80^{-} and Ly6C$^{hi/int}$F4-80^{low} cells increase after 2 weeks of MCD and, similar as in the HSD experiments, the lack of cDCs 1 results in a higher increase of these cell populations after 2 weeks of MCD.
- Differences between WT and batf3-KO after 2 weeks of MCD diet are not as explicit as after HSD diet.

3.6.3 Lymphoid cells

The analysis of lymphoid cell infiltrate was performed as described in chapter 3.5.3. Figure 28.A and B show percentage ratio and absolute cell count of B cells. Similar as the 5 weeks MCD treated group a decrease in percentage ratio can be observed *(means NC: WT 33%, batf3-KO 26%; means 2 wks MCD: WT 24%, batf3-KO 15%*). Again, this decrease is not paralleled by a decrease of absolute numbers, which indicates that it is due to increase of other CD45^{+} cells rather than an actual diminution of the B cell population (*means NC: WT 670x10^3 cells/g liver, batf3-KO 651x10^3 cells/g liver; means 2 wks MCD: WT 766x10^3 cells/g liver, batf3-KO 411x10^3 cells/g liver*). The decrease in percentage ratio of B cells is significantly higher in batf3-KO animals than in the WT control. In absolute cell count this difference cannot be objectified.

Figure 28.C and D depicts changes within the NK cell population after 2 weeks of MCD diet: NK cells show no significant increase in percentage ratio after the treatment (*means NC: WT 4.4%, batf3-KO 4.6%; means 2 wks MCD: WT 5.5%, batf3-KO 5.0%*). In both WT and batf3-KO animals the absolute cell count increases compared to the NC control (*means NC: WT 93x10^3 cells/g liver, batf3-KO 94x10^3 cells/g liver; means 2wks MCD: WT 172x10^3 cells/g liver, batf3-KO 158x10^3 cells/g liver*). Compared to 5 weeks treatment the cell count of NK cells is markedly lower after 2 weeks of MCD, suggesting that they continuously increase with progression of the disease. The lack of batf3-dependent cDCs 1 does not alter NK cell infiltrate.

Changes of the NKT cells are depicted in Figure 28.E and F: NKT cells do not increase significantly after 2 weeks of MCD treatment compared to the NC control neither in percentage ratio (*means NC: WT 0.8%, batf3-KO 0.6%. means 2 wks MCD: WT 1.0%, batf3-KO 0.7%*) nor in absolute cell count (*means NC: WT 18x10^3 cells/g liver, batf3-KO 13x10^3 cells/g liver. means 2 wks MCD: WT 33x10^3 cells/g liver, batf3-KO 18x10^3 cells/g liver*). Interestingly,

however, the percentage ratio as well as the absolute cell count of batf3-KO animals is significantly lower in the 2 weeks MCD treatment group than the WT control.

Figure 28.E and G show changes of all T cells after 2 weeks of MCD feeding. While this treatment does not affect the T cell population in WT animals, it results in significant decrease of the percentage ratio in batf3-KO animals (*means NC: WT 12.6%, batf3-KO 10.5%. means 2 wks MCD: WT 11.1%, batf3-KO 6.2%*). Again, the absolute cell count does not change, therefore this can be accounted by an increase of other $CD45^+$ cells (*means NC: WT 212x10^3 cells/g liver, batf3-KO 149x10^3 cells/g liver. Means 2 wks MCD: WT 354x10^3 cells/g liver, batf3-KO 164x10^3 cells/g liver*). Interestingly, albeit not significant, absolute cell count of T cells seems to slightly increase in WT animals after 2 weeks of MCD. This tendency cannot be observed in the batf3-KO animals. This fits to the observations made in HSD and 5 weeks MCD treatment, where batf3-KO animals show a relative decrease of T cells during NC and HSD, while the absolute cell count does not change. 5 weeks MCD treatment causes an increase in T cells in both groups, however numbers in WT animals are significantly higher. In Figure 28. H and I $CD4^+$ T cells are specifically investigated. As observed after HSD, batf3-KO animals show a significantly lower percentage ratio of $CD4^+$ T cells (*means 2 wks MCD: WT 5.1%, batf3-KO 2.6%*) and also exhibit lower absolute numbers *(means 2wks MCD: WT 163x10^3 cells/g liver, batf3-KO 69x10^3 cells/g liver*).

Summary chapter 3.6.3:

- After 2 weeks of MCD diet B cells show a relative reduction within the $CD45^+$ liver cells, which is higher in WT animals than in batf3-KO animals, but show no significant changes in absolute cell count.
- NK cells increase after 2 weeks of MCD diet and cDCs 1 have no effect on the dynamics of this population
- NKT cells do not increase after 2 weeks of MCD diet. In the absence of cDCs 1 this population is diminished.
- The number of T cells slightly increases after 2 weeks of MCD feeding. Batf3-KO animals consistently show lower T cell numbers than the WT, which includes particularly $CD4^+$ T cells, and do not show an increase in T cells after 2 weeks of MCD.

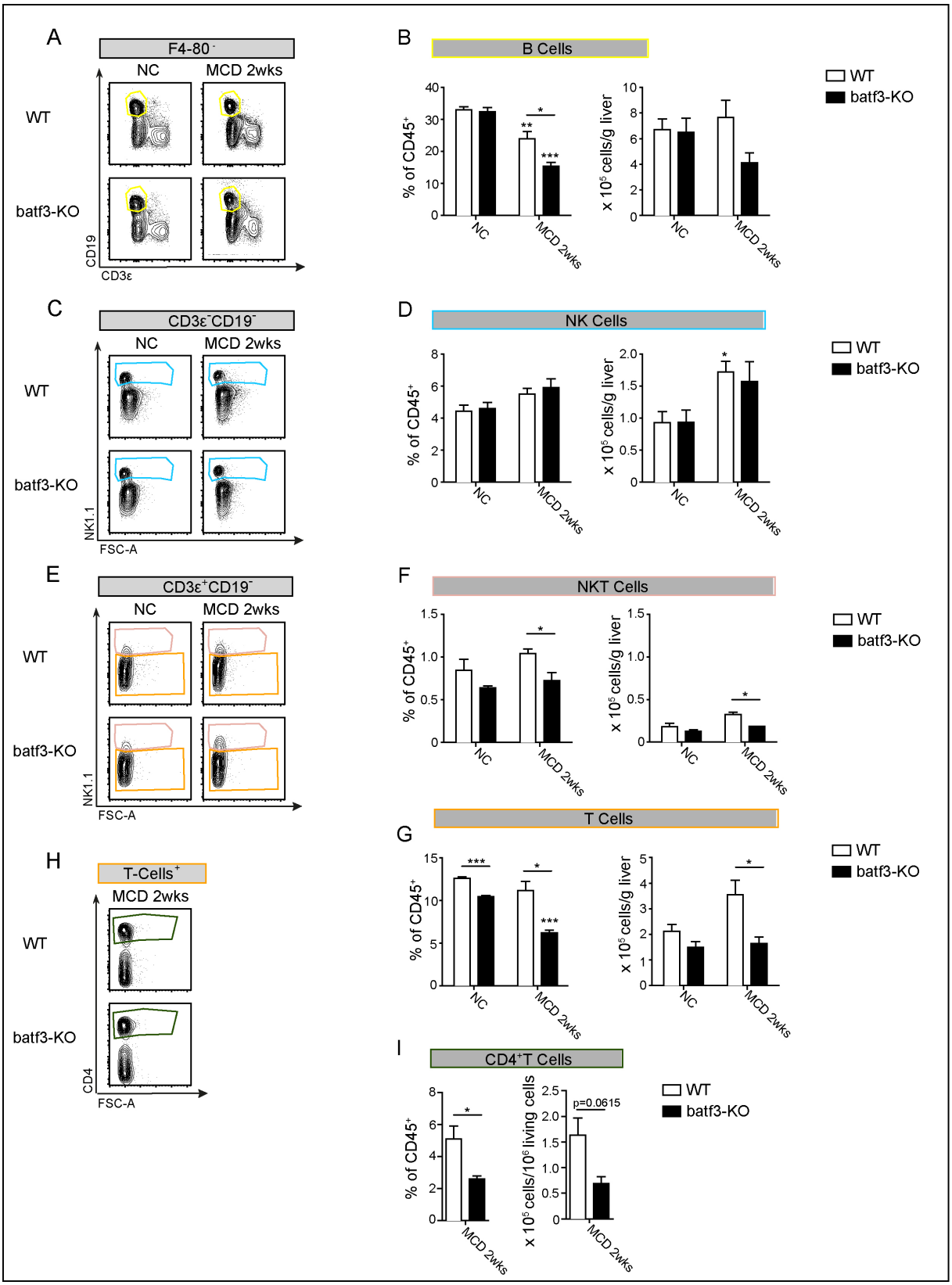

Figure 28 changes of lymphocyte cell populations in WT C57Bl/6 mice compared to batf3-KO mice after 2 weeks of MCD compared to NC feeding **A)** representative contour blots of $CD45^+F4\text{-}80^-$ cells showing CD19 signal (*PE-Cy7 1:100)* plotted against CD3ε (*A488 1:100)* to gate on $CD19^+$ $CD3\varepsilon^-$ cells (yellow gate) **B)** bar-graphs show comparison of percentage ratio within $CD45^+$ cells (left graph) and total cell amount per gram digested liver (right graph) of $CD19^+$ $CD3\varepsilon^-$ cells **C)** representative contour blots of $CD45^+F4\text{-}80^-CD19^-$ $CD3\varepsilon^-$ cells showing NK1.1 signal

(*primary AB: biotin 1:100, secondary AB: A405 1:400)* plotted against forwards scatter to gate on NK1.1$^+$ cells (light blue gate) **D)** bar-graphs show comparison of percentage ratio within CD45$^+$ cells (left graph) and total cell amount per gram digested liver (right graph) of CD19$^-$ CD3ε$^-$ NK1.1$^+$ cells. **E)** representative contour blots of CD45$^+$F4-80$^-$ CD19$^-$ CD3ε$^+$ cells showing NK1.1 signal (*primary AB: biotin 1:100, secondary AB: A405 1:400)* plotted against forwards scatter to gate on NK1.1$^+$ T cells (rosé gate) and NK1.1$^-$ T Cells (orange gate) **F)** bar-graphs show comparison of percentage ratio within CD45$^+$ cells (right graph) and total cell amount per gram digested liver (left graph) of CD19$^-$ CD3ε$^+$ NK1.1$^+$ cells. **G)** bar-graphs show comparison of percentage ratio within CD45$^+$ cells (right graph) and total cell amount per gram digested liver (left graph) of CD19$^-$ CD3ε$^+$ NK1.1$^-$ cells **H)** representative contour blots showing CD4 signal (*APC 1:100*) plotted against forwards scatter of CD19$^-$CD3ε$^+$NK1.1$^-$ cells to gate on CD4$^+$ cells (forest green gate) **I)** bar-graphs show comparison of percentage ratio within CD45$^+$ cells (left graph) and total cell count per gram digested liver (right graph) of CD19$^-$ CD3ε$^+$ NK1.1$^-$ CD4$^+$ cells. n_{NC}= 5/group, $n_{2wks\ MCD}$= 3/group
Data (A-I) for NC is representative of multiple independent experiments: repetitions$_{NC}$= 2 (n=3-5/group). 2 wks MCD experiment was performed one time. Bar-graphs depict mean + SEM. Significance is indicated through *p<0.05, ** p<0.005, ***p<0.0001. Asterisks on top of the bar show statistical significance compared to the respective NC group of WT or batf3-KO, underlined asterisks show statistical significance of WT compared to batf3-KO

3.7 The influence of batf3-dependent cDCs 1 on the systemic metabolism

Previous results primarily concern the effects the lack of batf3-dependent cDCs 1 has on the liver. NAFLD/NASH is closely connected to the metabolic syndrome, which is accompanied by augmented systemic inflammatory response, insulin resistance and modified lipid metabolism. To see whether the increased inflammation observed in the liver was a local effect or part of increased systemic inflammation as an effect of the batf3-KO genotype, analyses were performed to investigate the impact of batf3-dependent cDCs 1 on the systemic fat and glucose metabolism.

3.7.1 Fat metabolism

What first intrigued during the experiments and thus led to further investigations of fat metabolism are the significant differences in weight gain during NC and HSD treatment between WT and batf3-KO animals as depicted in Figure 29.A: During NC treatment, the weight gain in relation to the animals starting weight is significantly higher in batf3-KO animals than in the WT animals (*means NC: WT 11%, batf3-KO 22%*). HSD feeding causes significantly higher weight gain compared to the NC group and here, too, batf3-KO animals gain more weight than the WT controls (*means HSD: WT 26%, batf3-KO 33%*). As expected during MCD treatment the animals lose weight, importantly there is no difference between WT and batf3-KOs (*means MCD: WT -20%, batf3-KO -23%*). Following these observations, the serum leptin was measured as well as the amount of retroperitoneal fat in relation to total body weight. As depicted in Figure 29.B the amount of retroperitoneal fat is significantly higher in NC-fed batf3-KO animals compared to the WT control (*means NC: WT 0,13%, batf3-KO 0,34%*). Although in both groups the retroperitoneal fat increases with HSD feeding, in batf3-KO animals the increase is relatively lower than in the WT, as the baseline difference vanishes in the HSD group (*means HSD: WT 0,42%, batf3-KO 0,55%*). Since MCD animals experience

such a significant weight loss there is no retroperitoneal fat to be measured. Interestingly, as depicted in Figure 29.C, serum leptin levels mirror the dynamics of the retroperitoneal fat. On baseline batf3-KO animals exhibit significantly higher serum leptin values than the WT control *(means NC: WT 4,0 ng/ml, batf3-KO 9,6 ng/ml*). During the HSD treatment, the serum values increase in both groups, but do not show a significant difference between them (*means HSD: WT 14,8 ng/ml, batf3-KO 19,0 ng/ml*). MCD treatment causes a significant decrease of leptin levels, in some cases below the detection limit, in both WT and batf3-KO (*means MCD: WT 0,6 ng/ml, batf3-KO 1,0 ng/ml*).

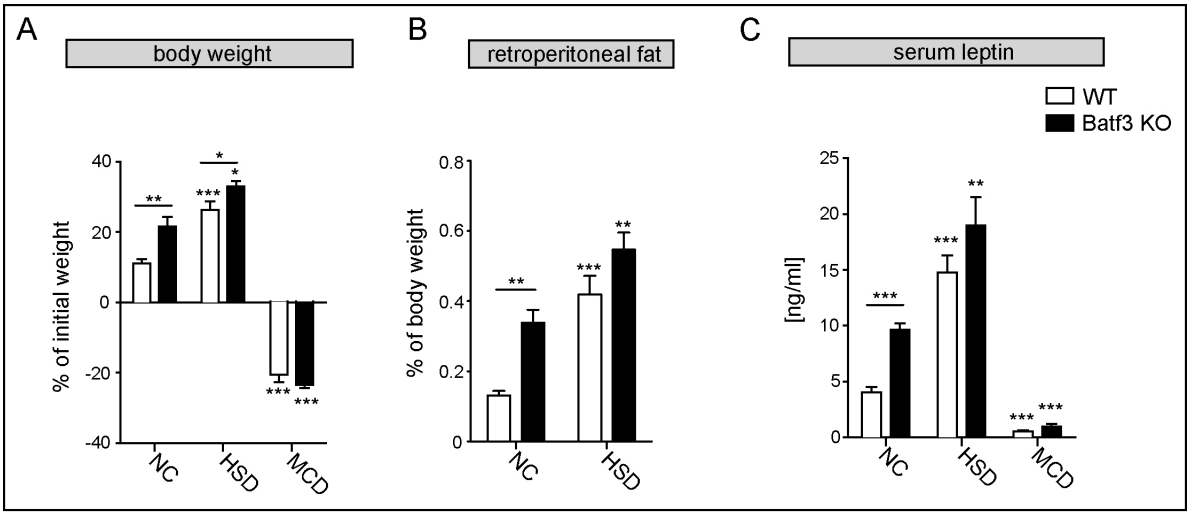

Figure 29 clinical parameters of the fat metabolism in WT C57Bl/6 mice compared to batf3-KO mice after 5 weeks of NC, HSD or MCD treatment **A)** bar-graphs show weight gain or loss in percentage of body weight at the beginning of the treatment n_{NC}=5/group, n_{HSD}=5/group, n_{MCD}=5/group. Graphs are representative for four independent experiments n=3-5/group **B)** bar-graphs show serum leptin levels n_{NC}=5/group, n_{HSD}=5/group, $n_{MCD\ WT}$=4, $n_{MCD\ KO}$=6. Data was created using samples of two independent experiments per group **C)** bar-graphs show the retroperitoneal fat in percentage of total body weight n_{NC}=12/group, n_{HSD}=13/group. Bar-graphs depict mean +SEM. Significance is indicated through *p<0.05, ** p<0.005, ***p<0.0001. Asterisks on top of the bar show statistical significance compared to the respective NC group of WT or batf3-KO, underlined asterisks show statistical significance of WT compared to batf3-KO

In batf3-KO mice HSD treatment leads to a significant increase of inflammatory responses within the liver compared to the WT animals. Keeping this in mind and with the above described differences in fat metabolism the next step was to see whether the lack of batf3-dependent cDCs 1 also affects inflammatory and immune mechanisms in the fat tissue. Figure 30. shows the flow cytometric analysis of fat tissue in NC and HSD treated batf3-KO and WT mice as well as qPCR analysis of retroperitoneal fat tissues of HSD treated mice. As depicted in Figure 30.A the basic gating strategy on leukocytes by selecting only single, living, $CD45^+$ cells is kept for retroperitoneal fat tissue. Figure 30.B and C shows the analysis of F4-80^+ cells, this includes macrophages and inflammatory monocytes, in retroperitoneal fat tissue. Interestingly WT animals show a significant increase of F4-80^+ cells after HSD treatment, whereas batf3-KO animals show no change after HSD treatment compared to their NC control,

but have an increased baseline frequency that corresponds to the WT HSD values (*means NC: WT 45.0%, batf3-KO 77.4%. means HSD: WT 72.0%, batf3-KO 76.0%*). CD11b$^+$ DCs are investigated by gating on F4-80$^-$ cells (magenta gate) and then gating on all CD11c$^+$ MHC-II$^+$ cells (green gate) as depicted in Figure 30.A. The pre-gating on F4-80$^-$ cells excludes all macrophages and inflammatory monocytes, which might otherwise shift into the CD11c and MHC-II expressing population. Following this the CD11b signal is plotted against CD103 signal and only the CD11b expressing cells are selected (blue gate, Figure 30.D). Importantly, changes of the CD11b$^+$ population as observed in the liver do not pertain in retroperitoneal fat tissue. There is no increase of CD11b$^+$ DCs as observed in the liver after HSD treatment, nor does the frequency of CD11b$^+$ DCs show a significant difference between WT and batf3-KO neither in NC (*means NC: WT 4.7%, batf3-KO 4.8%*) nor in HSD treated animals (*means HSD: WT 6.8%, batf3-KO 6.5%*) (Figure 30.E). Ultimately it was investigated whether the lack of batf3-dependet cDCs 1 influences the expression of inflammatory cytokines in retroperitoneal fat tissue during HSD. Figure 30.G shows the fold change for TNFα, CXCL-10, CCL2 and IL-6, none of which is significantly altered in batf3-KO animals.

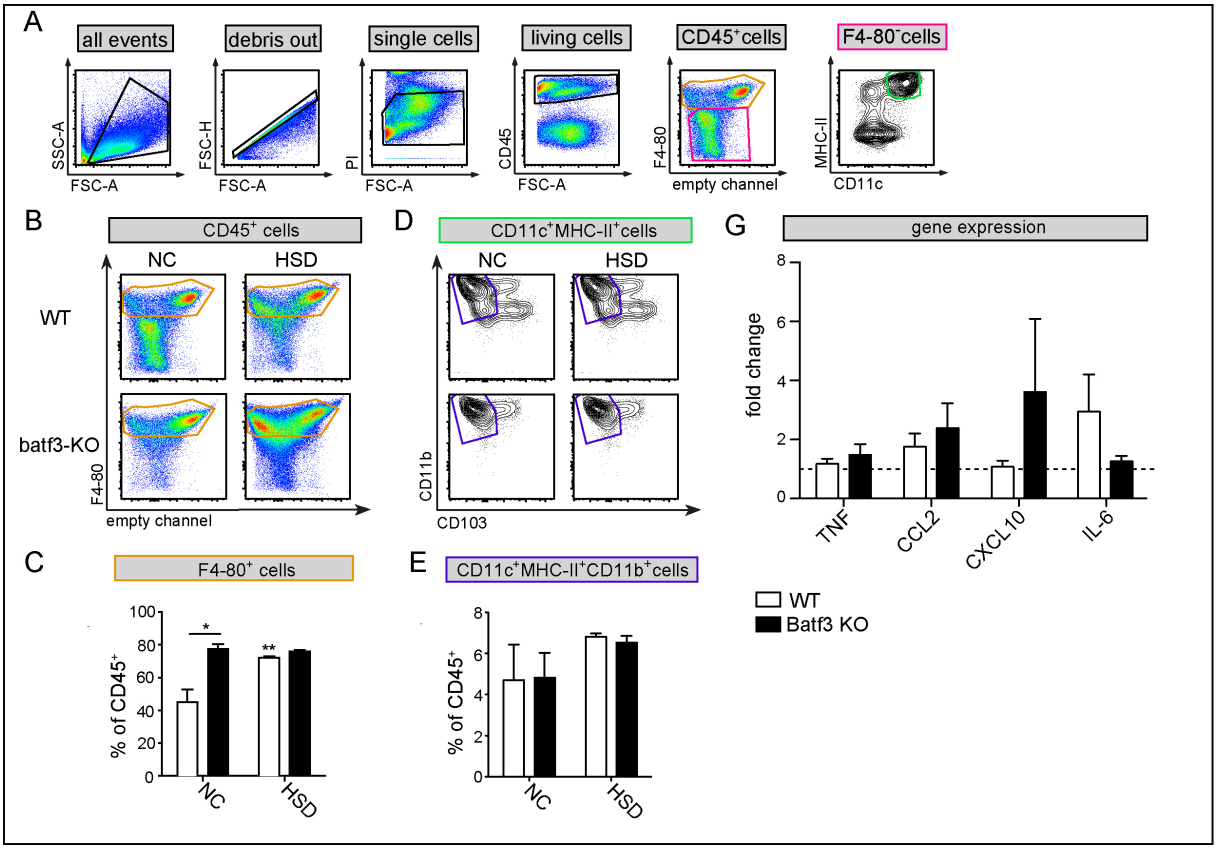

Figure 30 Flow cytometric and qPCR analysis of retroperitoneal fat tissue in WT C57Bl/6 mice compared to batf3-KO mice after 5 weeks of HSD or NC feeding. **A)** basic gating strategy with debris and doublet cell exclusion. Gating on leukocytes by selecting all CD45$^+$cells, plotting the F4-80 (*primary AB biotin 1:20, secondary AB VioBlue 1:400)* against an empty channel to gate on F4-80$^-$ (magenta gate) cells, then plotting MHC-II (*FITC 1:4000*) against CD11c (*APC 1:400*) to gate on CD11c$^+$MHC-II$^+$ cells. **B)** representative dot blots of the F4-80 signal (*primary AB biotin 1:20, secondary AB VioBlue 1:400*) plotted against an empty channel within CD45$^+$ cells. Gated on F4-80$^+$ cells

(orange gate) **C)** bar-graphs shows comparison of percentage ratio of F4-80$^+$ cells within CD45$^+$ cells **D)** representative dot blots of the CD11b signal (*PE-Cy7 1:2000*) plotted against CD103 signal (*PE 1:200*) within F4-80$^-$CD11c$^+$MHC-II$^+$ cells to gate on CD11b$^+$CD103$^-$ cells (blue gate). **E)** bar-graphs show comparison of percentage ratio of CD11c$^+$MHC-II$^+$CD11b$^+$ cells within CD45$^+$ cells. Experiment for Data (A-E) was performed one time with n_{NC}=3/group, n_{HSD}=5/group **G)** bar-graphs show fold changes in gene expression of retroperitoneal fat tissue between HSD treated WT and batf3-KO animal. Beta-actin was used as a housekeeping gene. n=4/group. Bar-graphs depict mean +SEM. Significance is indicated through *p<0.05, ** p<0.005, ***p<0.0001. Asterisks on top of the bar show statistical significance compared to the respective NC group of WT or KO, underlined asterisks show statistical significance of WT compared to KO

Summary chapter 3.7.1:

- The lack of cDCs 1 results in higher weight gain, higher amounts of retroperitoneal fat with a higher frequency of F4-80$^+$ cells and higher serum leptin levels in liver-healthy, NC fed animals.
- The lack of cDCs 1 results in higher weight gain in HSD fed animals, but a relatively lower increase of retroperitoneal fat, F4-80$^+$ cells and serum leptin compared to the respective WT control. It does not influence the expression of inflammatory cytokines in the retroperitoneal fat tissue.
- Unlike in the liver the lack of cDCs 1 does not affect the frequency of CD11b$^+$ DCs in retroperitoneal fat tissue, neither does HSD treatment increase their frequency.

3.7.2 Glucose metabolism

To see whether HSD treatment alters the glucose metabolism an intraperitoneal glucose tolerance test was performed with WT and batf3-KO animals prior to and after HSD diet (Figure 31.B). When fed with NC both WT and batf3-KO show an increase in blood sugar levels that peaks at 30 minutes post injection and then decreases in the following two hours. HSD treatment causes in both WT and batf3-KO animals elevated fasting glucose levels over *200 mg/dl* and with peaks over *450mg/dl* 30 minutes post injection, suggesting impaired glucose tolerance. Interestingly, the decrease of blood glucose in the three hours following the injection is shallower in HSD treated WT animals than in batf3-KO animals. Moreover, WT control animals consistently show higher glucose values than the batf3-KO animals. The analysis of glycated hemoglobin is not significantly altered between WT and batf3-KO (*means HSD: WT 12.5 mmol/mol, batf3-KO 14.3 mmol/mol)*, nor are the serum insulin levels (compare Figure 31.E) (*means HSD: WT 41,3 U/l, batf3-KO 35,6 U/l*) (Figure 31.D).

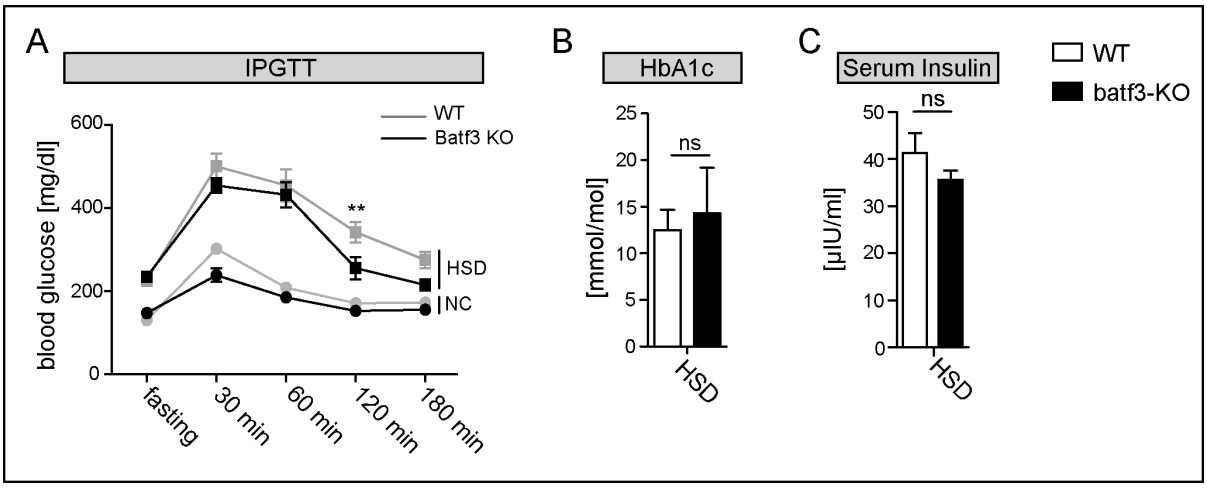

Figure 31 clinical parameters of glucose metabolism in WT C57Bl/6 mice compared to batf3-KO mice after 5 weeks of NC or HSD treatment **A)** Graph curves depict blood glucose values of WT and KO animals during the intraperitoneal glucose tolerance test (IPGTT) before (lower curves) and after (upper curves) 5 weeks HSD treatment. n_{WT}=4, n_{KO}=3. **B)** bar-graphs depict the concentrations of glycated hemoglobin (HbA1c) in 5 wks HSD treated WT and KO animals n_{WT}=4, n_{KO}=3 **C)** bar graphs depict concentration of fasting serum insulin in 5 wks HSD treated WT and KO animals. n_{WT}=4, n_{KO}=3. Significance is indicated through *p<0.05, ** p<0.005, ***p<0.0001

Summary chapter 3.7.2:

- After HSD feeding both WT and batf3-KO animals show elevated glucose levels during the IGPTT compared to the NC control, but batf3-KO animals showed no significant difference in glucose metabolism compared to the respective WT control
- The lack cDCs 1 does not affect serum insulin levels, nor does it affect HbA1c ratio, the parameter for long-term hyperglycemia

4 Discussion

The incidence of the metabolic syndrome and its associated conditions has increased considerably worldwide. NASH is considered as the hepatic consequence of the metabolic syndrome and is suggested to become the first cause for liver transplant over the next years (2). Although it has been in the focus of intense research over the past decades the complex mechanisms involved in the pathophysiology of NASH are still incompletely understood. DCs are powerful mediators of adaptive and innate immune responses and have been suggested to play an important role in the development of NASH. In 2012 Henning et al. showed that the depletion of $CD11c^+$ cells in the MCD model of NASH exacerbates hepatic inflammation, apoptosis and fibrosis (109). Importantly the depletion of $CD11c^+$ cells is not limited to DCs, but can also include macrophages, monocytes or NK cells, therefore the observed effects cannot be accredited solely to DCs (101). Further the DC population consists of different subtypes which hold different functions within the liver and each subtype needs to be individually addressed when trying to figure out their role in the complex pathogenesis of NASH (43). In this study, we mapped different DC subtypes in the liver using dietary models of steatosis and NASH to gather more information on the dynamics of each subset during disease progression. Then we used the batf3 knockout model, which constitutively lacks $CD8^+$ DCs in lymphoid tissue and $CD103^+$ DCs in non-lymphoid tissue, to specify the role these cells play in the prevention or progression of NASH (77).

4.1 A 5-week HSD in WT C57Bl/6 mice results in steatosis, a 5-week MCD results in NASH

NAFLD includes a wide spectrum of liver pathologies that reaches from mild, uncomplicated steatosis to steatohepatitis with inflammation and hepatocyte damage. The histological assessment of mice liver after 5 weeks of MCD reveals micro- and macrovesicular steatosis as well as inflammatory infiltrate and hepatocellular damage. These results concur with the elevated values of liver triglyceride content, $CD45^+$ cell infiltrate and ALT serum levels. Taken together and considering the lack of any other cause for secondary steatosis these findings comply with the diagnosis of NASH (128). MCD is an established dietary model to induce NASH in mice and this confirms the method used to investigate the NASH phenotype (35).

The HSD used in this study was originally provided by the manufacturer as a control diet for MCD treatment and consist of equal amounts of fat and sucrose but contains all amino

acids. In HSD and MCD 20% of calorie intake is provided by fat and 40% by sucrose. Importantly, animals treated with HSD develop increased liver triglyceride content within the liver and show histological signs of mild hepatic steatosis without major inflammatory reaction. This fits to data published by Tetri et al. in 2008 in which animals were treated with “Western diet”, a diet developed to mimic the human dietary situation leading to NAFLD, which, too, contains high amounts of fat and sucrose. Treatment with western diet causes macrovesicular steatosis after 4 weeks and hepatic steatosis with necroinflammatory changes similar to human NASH after 16 weeks of treatment (129). Taking this into account it becomes evident that HSD for 5 weeks should not be used as a healthy control group for MCD treatment in this study, since the high amounts of fat and sucrose by themselves affect the liver. Nevertheless, the HSD for 5 weeks shows to be a suitable model to investigate liver steatosis without developing necroinflammation.

In conclusion, a 5-weeks treatment of WT C57Bl/6 mice with HSD can be used as a model to investigate bland liver steatosis, while the 5-weeks treatment with MCD is useful to investigate NASH.

4.2 NASH is associated with increased abundance of all DC subtypes

Liver DCs consists of CD11c^{hi}MHC-II^{hi}CD103^{+} cDCs 1, CD11c^{hi}MHC-II^{hi}CD11b^{+} cDCs 2 (CD64^{-}) and moDCs (CD64^{+}) as well as CD11c^{int}PDCA-1^{+} pDCs (62,87–89,101). Previous studies to clarify the role of DCs in liver injury have shown that CD11c^{+} cells increase in number and exhibit a pro-inflammatory phenotype in various models of liver damage (105,107,108). However, said studies did not take into account the promiscuity of the CD11c surface marker nor the heterogeneity of the DC population, therefore remains the need to clarify the role of individual DC subtypes in liver disease (101).

This study shows an increase of CD11b^{+} DCs as well as cDCs 1 and pDCs after 5 weeks of MCD treatment. Previously published results describe an increase of CD11c^{+} cells in murine models of both acute and chronic liver injury, e.g. acute acetaminophen hepatotoxicity or MCD induced NASH (105,107). In the NASH model, Henning et al. observed an influx of CD11c^{+}MHC-II^{+} cells after 6 weeks of diet, of which the CD11b^{+} DC subtype shows the highest increase(109). This is in line with our results where CD11b^{+} DCs exhibit the overall highest fold change of all DC subtypes. Henning’s study also details the dynamics of other fractional DC subsets, particularly B220^{+} cells, which the authors identified as pDCs, and CD8^{+} cells, which they identified as cDCs 1(109). In these two DC populations, the authors noticed a decrease after 6 weeks of MCD treatment, which would be contradictory to our results. However when looking at this data two important factors need to be considered: First, using

CD8 as a marker to identify cDCs 1 is valid when investigating this subtype in lymphoid organs, but CD8 is not a suitable marker in non-lymphoid organs, where CD103 should be used instead (60,62). Thus, the observations made for $CD8^+$ cells might not truly represent changes of the cDC 1 subtype. Second, the observed decrease of pDCs and CD8 “cDCs 1” is based on the percentage ratio within all DCs and does not consider changes in absolute numbers. Considering that the $CD11b^+$ subtype shows the highest overall fold change the fractional decrease of the other two populations is a mathematical consequence, but does not necessarily reflect the overall expansion of the DC compartment in the liver. Our study shows an increase of all three DC subtypes as a fraction of all hematopoietic cells as well as in absolute cell count within the liver. Importantly other research groups report similar dynamics, e.g. in the TAA fibrosis models the percentage ratio of the pDC population decreases amongst all liver DCs, while the absolute number is actually augmented compared to the healthy control (107). Therefore, observations made in the 6 weeks MCD study by Henning et al. do not contradict our results, rather they represent a different aspects of DC dynamics during NASH, which would be the relation of DC subtypes amongst each other. Taken together all three DC subsets increase during NASH suggesting they are all involved in the pathomechanism of the disease.

During steady state liver DCs have been described to exhibit mostly tolerogenic properties, while, as presented by Henning et al., during MCD-induced NASH they switch towards a pro-inflammatory phenotype manifesting in increased production of pro-inflammatory cytokines and increased ability to induce $CD4^+$ T-Cell stimulation (100,109). Importantly, until now no studies have been conducted to investigate if and how simple steatosis without inflammatory aspects affects the different liver DC subtypes. In the HSD steatosis model DC subpopulations are not altered compared to the healthy control and the influx of DCs to the liver does not occur until inflammation is present. Liver injury has been associated with DCs evolving towards an immunogenic phenotype, which is associated with increased intracellular lipid content and upregulation of co-stimulatory surface markers(105,107). It remains to be determined whether DCs during simple steatosis retain their tolerogenic function or whether they are altered towards an immunogenic phenotype. Future studies might include more detailed analysis of DCs from steatotic livers on a functional level, such as in vitro experiments to determine cytokine production or their capacity to induce immune cell responses.

4.3 cDCs are not the major TNFα producing CD11c$^+$ cell population in the liver

TNFα is a potent pro-inflammatory cytokine and has been identified as an essential molecule in the pathophysiology of NASH (130). Functional analyzes of liver immune cells have shown that CD11c$^+$ cells increase their TNFα production during liver injury (105,107,109). This led to the assumption that liver DCs modulate the inflammatory environment through increased TNFα production (105,107). To identify the exact source of increased TNFα levels within the CD11c$^+$ population during NASH, CD11b, CD103 and F4-80 are added as additional surface markers in flow cytometric analyses. Similar as in previously published data, CD11c$^+$ cells show a significant increase of TNFα production after 5 weeks of MCD. Importantly neither the cDC 1 subtype nor CD11b$^+$ DCs exhibit a significant change in TNFα production compared to the healthy control. This suggests that other CD11c expressing cells must be the major source of TNFα during inflammation. Importantly when analyzing TNFα-production by F4-80$^+$ cells they display a similar increase as observed in CD11c$^+$ cells. F4-80$^+$ is a surface marker of KCs and some monocyte populations (101,131). KCs and inflammatory monocytes have previously been identified as a major source of TNFα as part of the innate immune response during NASH (132,133). Considering that KCs and monocytes also express CD11c this suggests that the increase of TNFα production Henning et al. observed in CD11c$^+$ cells from NASH liver most likely stems from KCs and DCs are not the major TNFα producing populations during NASH (101).

Nevertheless CD11b$^+$ DCs show some positive signals for TNFα, which suggests that, although not upregulated during inflammation, these cells have a baseline production of TNFα. The cDC 1 gate shows only few TNFα positive signals compared, suggesting that this cell type is no important source of TNFα in the liver.

4.4 cDCs 1 protect from progression of steatosis towards steatohepatitis

Liver steatosis affects around 20 to 30% of the western population (2). While in most cases this does not affect long term prognosis, 10-20% develop the more severe NASH which is accompanied to increased risk for end stage liver disease (13,14). Especially for developing prevention measures and treatment strategies for NASH understanding the exact mechanisms behind this progression is of major importance. As elaborated in the introduction the role of DCs in hepatic injury has been described as of a dichotomous character: on the one hand they hold a protective role as they help to maintain allograft survival after liver transplantation, protect from liver injury through elevated IL-10 production in the ischemia-reperfusion model and protect from acute liver injury, such as in the acetaminophen model where depletion of

$CD11c^+$ cells exacerbates liver pathology (100,101,110,134). On the other hand liver DCs exhibit pro-inflammatory characteristics including increased TNFα-production, high lipid content and T-Cell stimulation as described in models of chronic liver injury such as MCD-induced NASH or TAA-induced fibrosis (101,135). Importantly most of this research is based on the study of CD11c-DTR mice and therefore little is known about the role of individual DC subtypes. The first part of this study shows that NASH is associated with increased abundance of all DC subtypes in the liver, which suggests that all of them are included in the pathogenesis of NASH. To gain more profound insight on how the cDC 1 subtype influences disease development batf3-KO mice were subjected to either NC, HSD or MCD treatment.

Henning et al. showed that in the MCD model of NASH ablation of $CD11c^+$ cells significantly aggravates the disease. CD11c-DTR mice exhibit a larger $CD45^+$ cell infiltrate, increased prevalence of apoptosis and accelerated hepatic fibrosis (109). As opposite to this the isolated absence of cDCs 1 has only little effect on the severity of the disease in MCD induced NASH, as evident in the histopathological scoring which indicates an advanced NASH phenotype, but with no difference to that of WT animals. In contrast to the MCD model the absence of cDC 1 has quite striking effects in the HSD model. While in WT animals 5 weeks of HSD feeding results in elevated liver triglyceride content without overt inflammation, batf3-KO animals undergoing this treatment exhibit clear signs of an exacerbated disease. They develop profound macrovesicular steatosis with markedly elevated liver triglyceride content and histopathological scoring of liver sections indicates severe necroinflammation, which is also reflected in the significant influx of $CD45^+$ hematopoietic cells in the liver. These are typical features of NASH indicating a progression of steatosis towards steatohepatitis in HSD treated mice lacking the cDCs 1 subtype.

Thus, the lack of cDCs 1 has tremendous consequence during liver steatosis, whilst having only little effect on the NASH model. Having said this, both during HSD and MCD treatment batf3-KO animals develop higher liver triglyceride contents than the WT controls. Accumulation of lipotoxic metabolites of free fatty acids and the resulting oxidative stress on hepatocytes has in recent years been identified as a key mechanism in liver injury and inflammation (29). The increase of liver triglycerides indicates that animals lacking cDCs 1 respond differently to the high amounts of sucrose and fat in HSD and MCD. A detailed analysis of the genes involved in lipid metabolism is presented by Anna Meier in her master thesis, where she shows that batf3-KO animals show a different expression profile of genes for fatty acid beta-oxygenation and transport (136). This suggests altered lipid metabolism as a possible cause for the accelerated steatosis progression and inflammation.

Henning et al. postulated that DCs protect from hepatic damage through different mechanisms that limit inflammation, such as being involved in clearance of apoptotic cells and necrotic debris (109). MCD diet causes a significant increase of serum ALT-values in batf3-KO mice, indicating hepatocellular damage, whereas animals treated with HSD show no significant difference to the healthy control. Importantly, compared to WT animals the absence of cDCs 1 does not result in significantly elevated ALT serum values during either diet. Further the expression of apoptotic genes in batf3-KO animals, as presented in detail by Anna Meier in her master thesis, is also not different to the WT animals' (136). This suggests that cDCs 1 have no effect on hepatocellular damage during NASH and that the increased cellular death observed by Henning et al. in CD11c depleted animals under MCD treatment is not due to the lack of cDCs 1, but other CD11c expressing cells. This might include macrophages, which are potent phagocytic cells and thus are more likely to be the population responsible for clearance of dead cells and debris (43). Apart from that, the lack of a significant increase in serum-ALT levels in HSD treated batf3-KO mice does not stand in contrast to the histopathological scoring. In fact this is consistent with observations made in human disease, which indicate that ALT levels do not necessarily correlate with histological findings and NASH can be present also in subjects with normal ALT values (7–9).

Lastly, connective tissue staining shows no significant fibrosis development after HSD or MCD treatment neither in WT nor in batf3-KO animals. This indicates that the lack of cDCs 1 does not result in accelerated fibrogenesis. Nevertheless, one should keep in mind that HSD usually does not cause fibrosis development and that under MCD treatment fibrosis does not occurs only until 8 to 10 weeks of treatment (34,35,129,137). Therefore, a longer MCD treatment might be necessary to determine the exact role of cDCs 1 in fibrosis progression.

4.5 The lack of cDCs 1 increases the inflammatory infiltrate during the development of NASH

Increased inflammatory infiltrate is one of the hallmarks of NASH. At some point during disease progression the delicate homeostasis between immunity and tolerance in the liver is skewed towards an inflammatory response. During HSD, the lack of cDCs 1 results in an influx of $CD45^+$ cells to the liver. DCs are powerful regulators of immune response and communicate closely with cells of the innate and adaptive immune system. To understand how cDCs 1 shape the hematopoietic infiltrate during the progression of NASH the $CD45^+$ cell compartment needs to be analyzed in detail.

Ly6C^{+}F4-80^{low} cells are inflammatory monocytes circulating the blood stream and are rapidly recruited to inflammatory sites where they act as “first responders” to inflammatory signals or differentiate into monocyte-derived macrophages or moDCs (138). Importantly, several studies have shown that inflammatory monocytes contribute to liver inflammation and fibrosis, as for example impaired monocyte recruitment in CCR-2-KO mice results in reduced HSC activation and diminished liver fibrosis (138). In WT animals, HSD treatment does not cause increase of the inflammatory monocyte infiltrate compared to the healthy control. In the absence of cDCs 1 on the other hand inflammatory monocytes significantly expand, which is a clear indicator of an ongoing inflammatory response. Not only inflammatory monocytes, but also other cells of the innate immune system are recruited when feeding HSD to bat3-KO animals. This is evident in the increase of Ly6C$^{hi/int}$F4-80^{-} cells, which are a mixture of myeloid cells including neutrophils, eosinophils and myeloid-derived suppressor cells (117). Importantly during MCD treatment numbers of inflammatory monocytes as well as Ly6C$^{hi/int}$F4-80^{-} myeloid cells are significantly higher in both WT and batf3-KO animals than in the batf3-KO HSD group, thus indicating even more advanced inflammation and further progressed steatohepatitis. Since neutrophil accumulation is a prominent feature of inflammation in NASH, we specifically analyzed Ly6G^{+i} cells, to see whether the lack of cDCs 1 induces neutrophil recruitment (139). As can be expected MCD treated animals exhibit hepatic neutrophil recruitment as part of the inflammatory response. Interestingly HSD treated mice also show a slight tendency towards higher neutrophil numbers indicating a mild immune response even during steatosis. However, despite the elevated recruitment of Ly6C^{hi}F4-80^{-} cells, Ly6G^{+} neutrophils are not significantly increased in batf3-KO animals during HSD diet. This is even more surprising as functional analyzes of chemokine production within the liver reveal differences in cytokine production involved in neutrophil recruitment (compare chapter 4.6.2). It remains to be elucidated whether histological analyses would underline similar presence of Ly6G^{+} cells within the parenchyma of WT and batf3-KO HSD- and MCD-treated animals. It is still a likely possibility that batf3-KO animals have higher tissue neutrophil counts and these cells display increased susceptibility to apoptosis upon isolation.

Hepatic macrophages play a key role during liver injury and fibrogenesis in perpetuating inflammation through the release of proinflammatory cytokines and activation of HSCs (138,140). During steady state KCs, the liver resident macrophages, are self-renewing, while during inflammation the liver macrophage population is greatly augmented by monocyte-derived macrophages (138). This explains why the F4-80^{+}Ly6C^{low} population, which represents KCs, increases relatively little during MCD treatment compared to other myeloid cells. Importantly, although the lack of cDCs 1 promotes inflammation during HSD, there is no

elevated abundance of KCs indicating that cDCs 1 have no direct effect on KC expansion. Nevertheless, their absence might still augment the intrahepatic macrophage population through the observed recruitment of inflammatory monocytes. Importantly, previously published results show, that the frequency of KCs does not change during early stages of NASH, but they acquire an proinflammatory phenotype (133). Our results show that the lack of cDCs 1 causes increased production of inflammatory cytokines of F4-80$^+$ and CD11c$^+$ cells, indicating that cDCs 1 may limit the inflammatory response of KCs. These results are discussed in detail in chapter 4.6.1.

Another cell population that expands in mice lacking cDCs 1 during HSD are CD11b$^+$ DCs. In lymphoid organs CD11b$^+$ DCs are capable of inducing CD4$^+$ T-cell immunity, but in the liver the specific role of CD11b$^+$ DCs remains unclear (117,141). A big challenge in assigning specific functions to these cells remains the heterogeneity of this population as it comprises cells from both the classical DC lineage as well as monocyte derived DCs (61,117). Studies of moDCs, which were formed in the presence of pathogens in various tissues, have shown that they participate in the activation of the innate and adaptive immune system (142). With the abundance of inflammatory monocytes in batf3-KO animals we hypothesized that the increase of CD11b$^+$ DCs results from an increase of moDCs. Indeed, preliminary results indicate that the increase of CD11b$^+$ DCs in batf3-KO animals during HSD stems primarily from an increase of CD64$^+$ moDCs, thus representing another potentially pro-inflammatory cell population that expands in the absence of cDCs 1. During MCD diet, the lack of cDCs 1 has no effect on the total CD11b$^+$ DC population. Regrettably CD64 expression was not analyzed. These are promising results and further studies might be useful to determine the individual dynamics of moDCs and cDCs 2 during NASH and whether this is influenced by cDCs 1. Moreover, experiments to clarify the role of CD11b$^+$ DCs in NASH could also involve IRF4$^{-/-}$ mice, which lack a transcription factor that controls cDC 2 development (61,117,143). Since moDCs develop independently from IRF4 this could help to differentiate functions of moDCs from cDCs 2 (43). Importantly the pDC population remained unchanged in batf3-KO animals, suggesting that their recruitment occurs independently from cDCs 1.

T cells are important effector cells of the adaptive immune response. In WT animals, the T cell population remains stable during HSD induced bland steatosis and expands during MCD indicating involvement of the adaptive immune system. This is consistent with previously published results, where animals treated with high fat diet (HFD) to induce steatosis exhibit no increase in intrahepatic T cells, but animals with NASH under choline deficient HFD do (144). Interestingly, the absence of cDCs 1 does not lead to an expansion of the T cell population during HSD, despite the progression of the disease, and limits T cell expansion during MCD.

Increased $CD4^+$ T cell death has been described in MCD treated animals (145). Importantly this was accredited to their increased sensitivity towards certain metabolic intermediates, namely linoleic acid, a FFA which accumulates during MCD treatment (145). Considering the changes of lipid metabolism observed in the absence of cDCs 1 (compare chapter 4.4), a selective loss of $CD4^+$ T cells due to metabolic disturbances could possibly explain the limited expansion of T cells in batf3-KO mice. Regrettably $CD4^+$ T cells were not investigated in the 5 weeks MCD model, but the fact that in both the HSD model and 2 weeks MCD model $CD4^+$ T cells are significantly lower in batf3-KO animals strongly supports this assumption. Moreover, cDCs 1 are important for the induction of $CD4^+CD25^+FoxP3^+$ T_{regs} (60,84). Another possible explanation for the lack of $CD4^+$ T cells in batf3-KO animals could be impaired induction of regulatory T cells. Importantly, T_{regs} help control inflammation during steatosis, as they reduce inflammatory signaling and protect from LPS-induced hepatotoxicity (146). Impaired induction of T_{regs} in the absence of cDCs 1 could therefore contribute to disease progression. To clarify this, future experiments should include a detailed functional analysis of individual T cell subsets, particularly $CD4^+$ T cells, during steatosis and NASH and to determine the influence of cDCs 1 on constitution and dynamics of individual T cell subtypes. Characterizing the composition of hepatic FFAs in WT and batf3-KO animals during HSD and MCD could also help to assess whether the influence of cDCs 1 on the hepatic lipid metabolism is connected to the lack of hepatic $CD4^+$ T cells.

Besides T cells, B cells represent the second large lymphocyte population of the adaptive immune system. Their prototypical feature is the production of antibodies which contribute to the humoral immune response, but other functions include T cell modulation, cytokine production and antigen presentation (147). Studies show that B cells are involved in the pathogenesis of NASH through the production of antibodies: in MCD treated mice the development of liver injury and inflammation is paralleled by the occurrence of antibodies against lipid peroxidation products (148). Importantly, neither HSD- nor MCD treatment alters the amount of intrahepatic B cells, which is consistent with previously published results of a murine NASH model treated with choline-deficient HFD (144). Correspondingly, the lack of cDCs 1 and the associated progression of disease during HSD treatment also does not affect this cell population. Importantly, as discussed in chapter 4.4, the lack of cDCs 1 alters hepatic lipid metabolism, which might trigger the formation of antibodies against lipid peroxidation products (136,148). Therefore, an interesting aspect might be investigating B cells in the hepatic draining lymph nodes, since their differentiation and clonal expansion typically occurs in the germinal centers of secondary lymphoid organs with the help of $CD4^+$ T_H2 Cells (96). Considering the increase observed in $CD11b^+$ DCs this is even more intriguing as this subtype

is involved in the induction of $CD4^+$ T cell immunity (61). Besides antibody production, B cells have also been indirectly linked to the pathogenesis of NASH through their contribution to insulin resistance and adipose tissue inflammation (147,149). Importantly neither glucose metabolism nor adipose tissue inflammation is significantly worsened in batf3-KO animals during HSD (compare chapter 4.8), suggesting that this, too, is a mechanism independent from cDCs 1.

NK cells are important innate effector cells that arrive very early at the site of inflammation, where they lyse their target cells and mediate inflammation through production of cytokines (97). Their role in liver injury has been studied extensively during viral hepatitis and in fibrosis models. Here NK cells play a critical role in controlling liver fibrogenesis through lysis of HSCs and also hold important anti-viral and anti-tumor functions by killing stressed hepatocytes and tumor cells (150–152). Their contribution in development and progression of NAFLD is less defined (150). Analysis of human liver biopsies reveal that, compared to healthy controls, the number of intrahepatic NK cells in NASH patients is markedly elevated as is the expression of NK cell associated cytotoxic mediators indicating an activated phenotype of these cells (153). Consistent with this, NK cell numbers also increase in MCD treated mice, pointing towards the involvement of NK cells in the pathogenesis of NASH. Interestingly, although several studies have demonstrated intense crosstalk between NK cells and DCs, the progression of disease in batf3-KO animals under HSD treatment is not associated with alterations of the intrahepatic NK cell population, suggesting that here cDCs 1 are not directly involved in the recruitment of NK cells (41,70,74). Likewise, the lack of cDCs 1 also has no effect on NK cells during MCD treatment. Although the lack of cDCs 1 does not affect the intrahepatic NK cells, analyzing the NK cell population in the hepatic draining lymph nodes might reveal more details on dynamics and the relationship between cDCs 1 and NK cells during NAFLD.

NKT cells express surface markers of both T cells and NK cells (97). Current research indicates that they play an important role in the regulation of metabolic disorders mainly through their interaction with CD1d, a MHC-I-like glycolipid antigen presenting molecule (54,154). Their role during NAFLD has been widely analyzed in both murine models as well as human disease (155). Several studies suggest a protective role of NKT cells during mild liver steatosis: CD1d deficient mice, which lack NKT cells, exhibit increased susceptibility to fatty liver during high fat diet (156). Further, reduced numbers of hepatic NKT cells are associated with increased T_H1 cytokine production in WT mice during high fat diet and the adoptive transfer of NKT cells has been shown to reduce steatosis in ob/ob mice (154,157,158). In advanced stages of NAFLD NKT cells seem to harbor an opposite function: in mice NKT cells

increase during choline deficient HFD induced NASH, promote NASH development and contribute to the transition towards hepatocellular carcinoma (144). Another study demonstrated that NKT cells accumulate in livers with NASH induced fibrosis and drive fibrosis progression through simulating myofibroblastic activities of HSCs, while CD1d deficient mice are protected from fibrosis development (159). Tajiri et al. reported that in human NAFLD the number of intrahepatic NKT cells increases as the disease progresses and the expression of CD1d is upregulated (160). This fits to our results, where the number of intrahepatic NKT cells increases during NASH, but is not altered in the steatosis model. Tajiri et. al postulated that during steatohepatitis disease progression is promoted by increased presentation of lipid antigens through elevated expression of CD1d on liver APCs, which then results in activation of NKT cells (160). Although DCs are potent APCs the lack of cDCs 1 has no effect on the intrahepatic NKT cell population, suggesting that the mechanisms by which NKT cells influence hepatic disease progression is independently from cDCs 1.

4.6 The lack of cDCs 1 shifts the balance towards a pro-inflammatory milieu

During inflammatory reactions a variety of cytokines, which are specialized messenger molecules, are involved in mediating inflammation. To obtain information regarding the influence of cDCs 1 on intrahepatic cytokine production in the liver a cytokine array was used. This provides a general overview of the current immunologic milieu within the liver. The lack of cDCs 1 results in differences in the production of several cytokines associated with NASH pathogenesis or liver injury, indicating an augmented inflammatory response in batf3-KO animals. Importantly the proinflammatory shift in the hepatic milieu is not only evident in HSD treated animals, but also in MCD treated animals, suggesting that to some extend cDCs 1 obtain their anti-inflammatory function even during advanced stages of the disease.

Batf3-KO animals exhibit in increased levels of Serpin E1, a molecule that has been associated with hepatic injury. Serpin E1, also known as plasminogen activator inhibitor-1, is a key regulator of fibrinolysis by plasmin (161). It belongs to acute phase proteins and is induced in models of hepatic fibrosis (162–164). Mice lacking serpin E1 develop less injury in response to acetaminophen application and are protected from cholestatic-induced liver damage and fibrosis after bile duct ligation (163,165). Osteopontin (OPN) is synthesized by both immune and non-immune cells and is associated with a variety of pathological processes including cell-adhesion, chemoattraction and immunomodulation (166,167). OPN has been linked to the pathogenesis in MCD induced NASH, where it is upregulated from the early stages of the disease, and OPN-deficient mice develop significantly less liver injury and fibrosis during MCD treatment (34). Interestingly, OPN levels are merely elevated in batf3-KO animals

of the MCD group, not during HSD, which indicates that cDCs 1 are also involved during later stages of disease development. IL-1 is a potent pro-inflammatory cytokine, which is released by activated KCs during liver inflammation (117). IL-1ra is a natural occurring antagonist for IL-1-type cytokines and plays a protective role during liver injury as shown in IL-1ra deficient mice, which develop severe inflammatory infiltrate and portal fibrosis under high fat diet (168). During HSD batf3-KO animals produce higher amounts of IL-1ra than the WT control and this difference increases during MCD diet. The upregulation of IL-1ra might represent a compensatory reaction to counterbalance the increased inflammatory response in batf3-KO animals. This fits to data of human disease, where researchers have linked elevated serum levels of IL-1ra and increased hepatic mRNA expression to the degree of inflammation and presence of NASH (169). Interestingly, during HSD WT animals exhibit higher values of resistin, a pro-inflammatory molecule that promotes inflammation and insulin resistance (170,171). In rodents, resistin is primarily produced by adipocytes and serum levels increase during obesity (170). A previously published study shows that injection of mice with resistin exacerbates inflammatory cell recruitment and necrosis caused by LPS in the liver (172). In mice an intrahepatic production of resistin has not yet been described, but in humans hepatic resistin expression increases during NASH and other chronic inflammatory liver diseases (170,173,174). Importantly, TNFα downregulates resistin expression of adipocytes *in vitro* (175). If this is also true for resistin expression in other tissues, the observed increase of TNFα production observed in batf3-KO animals (compare chapter 4.7) would explain the lowered resistin levels. Future studies should include hepatic qPCR analysis to investigate the expression of resistin in mice during NAFLD and *in vitro* experiments to specify the production of resistin dependent on the presence of TNFα.

Chemokines are a specialized group of cytokines which are involved in recruitment and regulation of immune cells. Changes of chemokine production in the liver is of special interest, as it can provide more insight on how the lack of cDCs 1 alters the immune cell recruitment. The array shows increases in the production of CXCL-1 in batf3-KO animals**.** Analysis of hepatic gene expression patterns have shown that CXCL-1 is upregulated in both humans and mice with NASH (176,177). In the context of hepatic inflammation CXCL-1 has been primarily connected to the recruitment of neutrophils, e.g. forced expression of CXCL-1 in rat liver causes liver injury and neutrophil infiltration (177,178). CXCL-2 and CXCL-5 production is also increased in batf3-KO animals. An upregulation of CXCL-2 expression has been described in the liver of NASH patients, whereas increased CXCL-5 expression has been associated with alcoholic steatohepatitis (176,179). CXCL-2 and CXCL-5 belong to the same chemokine

superfamily as CXCL-1 and are, too, involved in neutrophil recruitment (180,181). Despite the differences in chemokine production the neutrophil infiltrate is not altered during neither steatosis nor steatohepatitis compared to the WT control (compare chapter 1.6). As discussed above, using alternative methods to determine neutrophil infiltration, such as histological staining, could help to gain better understanding of the dynamics of the neutrophil population in batf3-KO animals. Importantly, CXCL-1, -2 and -5 execute their function through CXCR-2, which is also expressed on other immune cells, including immature DCs and monocytes (181). Whether the increased recruitment of monocytes and $CD11b^+$ DCs in batf3-KO animals is linked to increased CXC-chemokine production needs to be further investigated.

Besides CXC-chemokines, the lack of cDCs 1 also increases the production of CCL-2 and CCL-5. These two chemokines hold an important function during hepatic inflammation and the pathogenesis of NASH. CCL-2 is released by activated KCs as well as damaged hepatocytes and activated HSC and is critically involved in the recruitment of inflammatory monocytes during liver injury (182,183). Pharmacologic inhibition of CCL-2 during MCD treatment reduces macrophage infiltration und ameliorates steatohepatitis (184). The upregulation of CCL-2 in batf3-KO mice could thus point to the mechanism involved in the influx of inflammatory monocytes during HSD. CCL-5 promotes hepatic inflammation and fibrosis development by activating macrophages and HSCs through the receptors CCR-1 and CCR-5 (180,183,185). Treatment with CCR-5 antagonists or CCL-5 antagonists significantly lowers inflammation and histological scoring of dietary induced NASH and limits fibrosis development in murine fibrosis models (186,187). Moreover, CCL-5 is also involved in DC T cell crosstalk as well as the recruitment of T cells, eosinophils and basophils (188). Hence, all measured chemokines are involved in the recruitment of inflammatory cells and could therefore contribute to the exacerbation of inflammation observed in batf3-KO animals. Interestingly, batf3-KO animals also exhibit higher values of CCL-22, a chemokine responsible for T_H2 and T_{reg} cell migration (181). In viral hepatitis CCL-22 is involved in the recruitment of regulatory T cells (183,189). Whether the increase of CCL-22 is linked to the decrease of CD4 T-Cells, for example as a compensatory mechanism, will need further investigation.

The shift towards a proinflammatory milieu evident in the cytokine array can also be measured on a cellular level in mice that lack cDCs 1. Henning et al. showed that the lack of $CD11c^+$ cells during MCD diet leads to increased TNFα production by $F4\text{-}80^+$ cells (109). As opposite to this, the isolated absence of cDCs 1 does not lead to significantly changed TNFα production of neither $CD11c^+$ nor $F4\text{-}80^+$ cells in the 5 weeks MCD NASH model. During HSD feeding, however, the lack of cDCs 1 results in elevated TNFα production by said cells. KCs and inflammatory monocytes have been identified as important producers of TNFα during the

onset of steatohepatitis (133). As discussed in chapter 4.3., the TNFα producing CD11c$^+$ cells observed during NASH are most likely CD11c$^+$ expressing F4-80$^+$ cells, such as KCs and monocytes. This suggests that cDCs 1 protect from progression of steatosis towards steatohepatitis by regulating the inflammatory response of KCs and inflammatory monocytes.

Besides TNFα, CD11c$^+$ cells also show elevated production of CXCL-1 and CCL-5 in the absence of cDCs 1. As discussed above both CXCL-1 and CCL-5 are involved in NASH pathogenesis. This indicates an activated phenotype of CD11c$^+$ cells, but as mentioned this is a heterogeneous population and therefore it is not possible to pinpoint the increased chemokine production to one specific cell type. Having said this, as the production of TNFα is elevated in KCs and monocytes, it is likely that they also contribute to the increased chemokine production. Moreover, activated KCs are known to produce CXCL-1 and CCL-5 during liver injury (183). Regrettably, whether KCs are responsible for increased CXCL-1 and CCL-5 production cannot be confirmed, as F4-80$^+$ expression was not analyzed in this experiment and a more detailed characterization of the CD11c$^+$ cells is necessary. Nevertheless, these results hint that cDCs 1 modulate KC activation. *In vitro* experiments on isolated KCs from WT and batf3-KO animals under HSD and MCD diet could be useful to determine how cDCs 1 influence inflammatory response of KCs. This could include characterizing the cytokines produced by KCs or starting a KC cDC 1 co-culture to identify molecules involved in the communication of cDCs 1 and KCs.

4.7 The impact of cDCs 1 on disease progression lessens in advanced stages of disease

In this study, the 5 weeks HSD model and the 5 weeks MCD model have been studied extensively to evaluate the effects of the cDC 1 subtype on liver steatosis and NASH. Importantly, results indicate that cDCs 1 inhibit progression of inflammation during hepatic steatosis, but have only limited effect on the ultimate severity of the disease. Regarding their effects in the NASH model, it is possible that after 5 weeks MCD treatment steatohepatitis is already too advanced to reveal the influence cDCs 1 have on the inflammatory response. Therefore, to confirm the effects cDCs 1 have on disease progression, their impact was also investigated after 2 weeks of MCD treatment. Studies have shown that during this timepoint of the diet hepatic steatosis is already significant and the inflammation is starting to occur (34). Therefore, 2 weeks MCD treatment is a fine model to investigate the effects of cDCs 1 on the onset of steatohepatitis and to see whether they concur with the observations made in the steatosis model. Accordingly, after 2 weeks of MCD treatment, the composition of hepatic

immune cells in WT animals is changed in a manner that corresponds with a state of early inflammation. All DC subtypes increase in the liver after 2 weeks of MCD treatment, although in a lower fold change than after 5 weeks treatment, suggesting that they are all involved in the inflammatory reaction from an early stage on. Inflammatory monocytes ($Ly6C^{hi/int}F4\text{-}80^{low}$) and $Ly6C^{hi/int}F4\text{-}80^{-}$ myeloid cells are, too, infiltrating the liver, but again in a lower fold change than after 5 weeks treatment. Concerning lymphoid cell populations, NK cells start to accumulate in the liver after 2 weeks MCD diet, whereas the NKT cells and T cells seem to be recruited during later phases of the inflammatory reaction. B cells as during steatosis or established steatohepatitis are not affected at all.

Like in the HSD model the inflammatory infiltrate changes in batf3-KO animals. Here, too, the lack of cDCs 1 does not affect the pDC population, but causes tendentially higher recruitment of $CD11b^{+}$ DCs, especially moDCs. Likewise, inflammatory monocytes ($Ly6C^{hi/int}F4\text{-}80^{low}$) and $Ly6C^{hi/int}F4\text{-}80^{-}$ myeloid cells are tendentially higher in batf3-KO animals. Further, the number of intrahepatic T cells, especially $CD4^{+}$ T cells is decreased, consistent with the observations made in the HSD and 5 weeks MCD model. Notably, batf3-KO animals have lower NKT cells than the WT animals after 2 weeks of MCD diet, which has not been observed in any of the other experiments. Further experiments are necessary to analyze the observations in the 2 weeks treated animals. The remaining cell types, including pDCs, KCs, B cells and NK cells are not altered by the lack of cDCs 1 just as in the HSD experiment.

This data suggests that cDCs 1 do not only protect from the progression of steatosis towards steatohepatitis, but also moderate the inflammatory reaction during the onset and early phases of steatohepatitis itself. Indeed, such anti-inflammatory function of $CD103^{+}$ DCs have also been described in other organs, such as the gut, where $CD103^{+}$ DCs protect against experimentally induced colitis, or the lung, where depletion of $CD103^{+}$ cDCs 1 in batf3-KO mice exacerbates airway inflammation (84,190). The regulatory and tolerogenic properties of cDCs 1 are most potent during earlier timepoints in the pathogenesis of NASH and prevent that an inflammatory response occurs in the first place. On this aspect, it would also be interesting to see whether cDCs 1 have a protective effect in other chronic inflammatory liver conditions, such as alcoholic steatohepatitis or viral hepatitis.

4.8 Progression of NASH in the absence of cDCs 1 is not associated with increased adipose tissue inflammation

Excess energy uptake results in augmented fat accumulation and obesity, which is linked to increased risk of IR/ DM-II, NAFLD, hypertension, dyslipidemia and atherosclerosis (191). Importantly development of obesity is multifactorial and depends on life style, appetite control as well as genetic and environmental factors (191). Batf3-KO animals exhibit significantly higher weight gain during both control diet and HSD, suggesting that this strain is more susceptible for developing obesity. One important factor that drives obesity is the organism's sensitivity towards leptin. Under physiologic circumstances leptin is secreted by adipocytes and serves as a negative feedback mechanism to reduce food intake and moderate glucose and fat metabolism (192,193). Obesity in both humans and rodents is associated with hyperleptinemia and the development of a leptin resistant state despite the relative abundance of the hormone (194). Correlating with the increased weight gain batf3-KO animals have significantly higher leptin levels at baseline compared to the WT and exhibit an equal tendency during HSD feeding. Thus, the excessive weight gain could be due to leptin resistance in batf3-KO animals.

Importantly, research suggests that leptin holds an important function in prevention of lipotoxicity through limiting lipid accumulation in non-adipose tissue (195). Furthermore, leptin resistance has been associated with the development of hepatic steatosis (193). In fact both leptin-deficient and leptin-resistant mice are established research models for NAFLD as they develop hepatic steatosis during both normal and high-calorie diets (196). In humans, serum leptin levels correlate directly with the degree of steatosis during NASH (193). Importantly, leptin-deficient and leptin-resistant animals do not spontaneously progress to steatohepatitis, but need a "second hit" to develop steatohepatitis (197). Hence, a predisposition to leptin resistance in batf3-KO mice could account for the elevated liver triglyceride content during HSD, but does not explain the progression towards steatohepatitis.

Not only the total weight gain differs from the WT control, but batf3-KO animals also put on relatively higher amounts of retroperitoneal fat tissue. Interestingly, this is especially significant in animals treated with normal chow, but mice in the HSD group also tend to have relatively higher amounts of retroperitoneal fat. A chronic, low-grade inflammatory state due to adipose tissue dysfunction during obesity has been identified as one of the key factors that drive the metabolic syndrome and its associated conditions (191,198). Such dysfunctional state of the adipose tissue is associated with the infiltration of F4-80^{+} macrophages as well as a shift in the cytokine production towards a pro-inflammatory pattern, including the secretion

of TNFα, IL-6 or chemoattractant molecules like CCL-2 (191,199). This is especially relevant for ectopic fat tissue, which includes visceral, retroperitoneal, omental and organ fat deposits, while subcutaneous fat is comparatively inert and has little influence on metabolic and inflammatory parameters (191,200). Considering the increased retroperitoneal fat and increased hepatic triglyceride content, fat distribution in batf3-KO animals seems to be favored towards ectopic fat accumulation. Therefore, it is reasonable to ask whether the lack of cDCs 1 not only changes distribution of fat tissue, but also drives adipose tissue inflammation, which could accelerate the progression of steatohepatitis. Importantly, the characterization of inflammatory cells in adipose tissue shows that HSD treatment in batf3-KO animals is not associated with an increased abundance of F4-80$^+$ macrophages. Likewise, CD11b$^+$ DCs, which are markedly elevated in the liver of batf3-KO animals on HSD, show no significant difference to WT animals. Fittingly qPCR analysis of retroperitoneal fat tissue also shows no change in the expression of the chemokines CCL-2 or CXCL-10 nor of the cytokines TNFα or IL-6. Hence there is no aggravated adipose tissue inflammation in batf3-KO animals on HSD, suggesting that adipose tissue dysfunction is not involved in the progression towards steatohepatitis in the absence of cDCs 1. Notably, analysis of retroperitoneal fat tissue in batf3-KO animals on normal chow shows an increased frequency of F4-80$^+$ macrophages, which is possibly due to the excess weight gain in these animals. Nevertheless, the role of DCs in adipose tissue inflammation is still poorly understood and will need further clarification (201).

4.9 Progression of NASH in the absence of cDCs 1 is not associated with altered glucose metabolism

IR is the common feature of the metabolic syndrome and its associated conditions and strongly correlates with the development of NAFLD/NASH (202). In adipose tissue it leads to increased lipolysis with increased release of FFA, while hepatic IR promotes hepatic lipogenesis and contributes to hyperglycemia through impaired glycogenesis and increased glycogenolysis and gluconeogenesis (29).

As HSD is known to cause IR in mice, it is important to clarify, whether IR is more severe in batf3-KO mice, which could then contribute to the development of steatohepatitis (38). In the IPGTT mice treated with HSD show markedly higher blood glucose levels than the healthy control, but no difference between WT and batf3-KO mice. This indicates that the HSD causes pathologic glucose tolerance in treated animals, but the lack of cDCs 1 does not further pejorate the insulin response. Concurring with the IPGTT, there are also no significant differences in neither serum insulin levels nor HbA1c levels between WT and batf3-KO. All in

all, this shows that impaired glucose metabolism and worsened IR does not contribute to the progression of steatohepatitis in batf3-KO animals.

4.10 Conclusion and perspective

This study shows that during NASH all hepatic DC subtypes are recruited to the liver, suggesting that they are all involved in the pathogenesis of the disease. It highlights the role of cDCs 1 during steatosis and shows that they hold an important protective function in preventing progression towards steatohepatitis by regulating the composition of hepatic immune cells, the influx of inflammatory cells and the production of cytokines. Through the MCD model this study also demonstrates that the protective influence of cDCs 1 on disease progression is lessened during more advanced stages of the disease. Importantly, this study also demonstrates, that the progression of the disease during HSD in the absence of cDCs 1 is a local effect and is not due to aggravated adipose tissue inflammation or insulin resistance.

cDCs 1 hold a powerful protective function in the development of NASH. This is especially relevant, as further studies have shown that adoptive transfer of cDCs 1 can reverse the changes observed in the steatosis model of batf3-KO mice and even mitigate the outcome of MCD diet in WT animals, which indicates a potential therapeutic relevance of the cDC 1 subset (136,203). Additionally, studies of human transplant liver have shown that the number of hepatic $CD141^+$ DCs, which have been identified as the human equivalent of the murine $CD8/CD103^+$ cDCs 1 subtype, decreases in liver pathologies associated with inflammation, suggesting that, in human disease too, cDCs 1 hold a protective role in liver injury (204,205). A next step could be to investigate the role of cDCs 1 in human NASH and to clarify the molecular mechanisms through which cDCs 1 exert their protective actions. A better understanding of this could help to identify possible therapeutic targets for NASH. It will also be interesting to see, whether cDCs 1 can also protect from other chronic liver diseases with an inflammatory component, such as alcoholic steatohepatitis or chronic viral hepatitis. Moreover, it is an exciting question what role the other liver DC subtypes play during NAFLD. This could be done by using knock out strains, such as the $IRF4^{-/-}$ or $IRF2^{-/-}$ mouse, which specifically lacks $CD11b^+$ DCs, or the $E2\text{-}2^{-/-}$ mouse, which lacks pDCs (117,206).

5 Bibliography

1. Ludwig J, Viggiano TR, McGill DB, Oh BJ. Nonalcoholic steatohepatitis: Mayo Clinic experiences with a hitherto unnamed disease. Mayo Clin Proc. 1980;55(7):434–8.

2. Bellentani S, Scaglioni F, Marino M, Bedogni G. Epidemiology of non-alcoholic fatty liver disease. Dig Dis. 2010;28(1):155–61.

3. Angulo P, Lindor KD. Non-alcoholic fatty liver disease. J Gastroenterol Hepatol. 2002;17 Suppl:S186–90.

4. Neuschwander-Tetri BA, Caldwell SH. Nonalcoholic steatohepatitis: Summary of an AASLD Single Topic Conference. Hepatology. 2003;37(5):1202–19.

5. Roeb E, Steffen HM, Bantel H, Baumann U, Canbay A, Demir M, et al. S2k-Leitlinie nicht alkoholische Fettlebererkrankungen AWMF Register Nr . 021-025 Version Januar 2015 , Erstauflage. Z Gastroenterol. 2015;53(21):668–723.

6. Yeh MM, Brunt EM. Pathological Features of Fatty Liver Disease. Gastroenterology. 2014;147(4):754–64.

7. Pearce SG, Thosani NC, Pan J-J. Noninvasive biomarkers for the diagnosis of steatohepatitis and advanced fibrosis in NAFLD. Biomark Res. 2013;1(1):1–11.

8. Sorrentino P, Tarantino G, Conca P, Perrella A, Terracciano ML, Vecchione R, et al. Silent non-alcoholic fatty liver disease-a clinical-histological study. J Hepatol. 2004;41:751–7.

9. Mofrad P, Contos MJ, Haque M, Sargeant C, Fisher RA, Luketic VA, et al. Clinical and histologic spectrum of nonalcoholic fatty liver disease associated with normal ALT values. Hepatology. 2003;37(6):1286–92.

10. Sass DA, Chang P, Chopra KB. Nonalcoholic fatty liver disease: A clinical review. Dig Dis Sci. 2005;50(1):171–80.

11. Silverman JF, O'Brien KF, Long S, Leggett N, Khazanie PG, Pories WJ, et al. Liver pathology in morbidly obese patients with and without diabetes. Am J Gastroenterol. 1990 Oct;85(10):1349–55.

12. Krawczyk M, Bonfrate L, Portincasa P. Nonalcoholic fatty liver disease. Best Pract Res Clin Gastroenterol. 2010;24(5):695–708.

13. Dam-Larsen S, Franzmann M, Andersen IB, Christoffersen P, Jensen LB, Sorensen TIA, et al.

Long term prognosis of fatty liver: risk of chronic liver disease and death. Gut. England; 2004 May;53(5):750–5.

14. Adams LA, Sanderson S, Lindor KD, Angulo P. The histological course of nonalcoholic fatty liver disease: A longitudinal study of 103 patients with sequential liver biopsies. J Hepatol. 2005;42(1):132–8.

15. Caldwell SH, Oelsner DH, Iezzoni JC, Hespenheide EE, Battle EH, Driscoll CJ. Cryptogenic cirrhosis: clinical characterization and risk factors for underlying disease. Hepatology. 1999;29(3):664–9.

16. Ong J, Younossi ZM, Reddy V, Price LL, Gramlich T, Mayes J, et al. Cryptogenic cirrhosis and posttransplantation nonalcoholic fatty liver disease. Liver Transplant. 2001;7(9):797–801.

17. Marchesini G, Bugianesi E, Forlani G, Cerrelli F, Lenzi M, Manini R, et al. Nonalcoholic fatty liver, steatohepatitis, and the metabolic syndrome. Hepatology. 2003;37(4):917–23.

18. Marchesini G, Brizi M, Morselli-Labate AM, Bianchi G, Bugianesi E, McCullough AJ, et al. Association of nonalcoholic fatty liver disease with insulin resistance. Am J Med. 1999 Nov;107(5):450–5.

19. Powell EE, Cooksley WGE, Hanson R, Searle J, Halliday JW, Powell W. The natural history of nonalcoholic steatohepatitis: A follow-up study of forty-two patients for up to 21 years. Hepatology. 1990;11(1):74–80.

20. Haque M, Sanyal AJ. The metabolic abnormalities associated with non-alcoholic fatty liver disease. Best Pract Res Clin Gastroenterol. England; 2002 Oct;16(5):709–31.

21. Day CP, James OF. Steatohepatitis: A Tale of Two “Hits”? Gastroenterology. 1998;114(4):842–5.

22. Neuschwander-Tetri BA. Hepatic lipotoxicity and the pathogenesis of nonalcoholic steatohepatitis: The central role of nontriglyceride fatty acid metabolites. Hepatology. 2010;52(2):774–88.

23. Tilg H, Moschen AR. Evolution of inflammation in nonalcoholic fatty liver disease: The multiple parallel hits hypothesis. Hepatology. 2010;52(5):1836–46.

24. Tiniakos DG, Vos MB, Brunt EM. Nonalcoholic fatty liver disease: pathology and pathogenesis. Annu Rev Pathol. 2010;5:145–71.

25. Yamaguchi K, Yang L, McCall S, Huang J, Yu XX, Pandey SK, et al. Inhibiting triglyceride synthesis improves hepatic steatosis but exacerbates liver damage and fibrosis in obese mice

with nonalcoholic steatohepatitis. Hepatology. 2007 Jun;45(6):1366–74.

26. Wei Y, Wang D, Topczewski F, Pagliassotti M. Saturated fatty acids induce endoplasmic reticulum stress and apoptosis independently of ceramide in liver cells. Am J Physiol Endocrinol Metab. 2006;291:E275-281.

27. Nolan C, Larter C. Lipotoxicity: why do saturated fatty acids cause and monounsaturates protect against it? J Gastroenterol Hepatol. 2009;24:703–6.

28. Malhi H, Gores G. Molecular Mechanisms of Lipotoxicity in Nonaloholic Fatty Liver Disease. Semin Liver Dis. 2008;28(4):360–9.

29. Patel V, Sanyal AJ. Nonalcoholic Fatty Liver Disease. In: Gershwin M, Vierling J, Manns M, editors. Liver Immunology. 2nd ed. New York: Springer Science+Buisness Media; 2014. p. 345–59.

30. Brun P, Castagliuolo I, Di Leo V, Buda A, Pinzani M, Palu G, et al. Increased intestinal permeability in obese mice: new evidence in the pathogenesis of nonalcoholic steatohepatitis. J Physiol Gasrointestinal Liver Physiol. 2007;292(G518-525).

31. Wigg A, Roberst-Thomson I, Dymock R, McCarthy P, Grose R, Cummins A. The role of small intestinal bacterial overgrowth, intestinal permeability, endotoxaemia, and tumour necrosis factor alpha in the pathogenesis of non-alcoholic steatohepatitis. Gut. 2001;48(206–211).

32. Romeo S, Kozlitina J, Xing C, Pertsemlidis A, Cox D, Pennacchio L, et al. Genetic variation in PNPLA3 confers susceptibility to nonalcoholic fatty liver disease. Nat Genet. 2008;40:1461–5.

33. Anstee QM, Goldin RD. Mouse models in non-alcoholic fatty liver disease and steatohepatitis research. Int J Exp Pathol. 2006;87(1):1–16.

34. Sahai A, Malladi P, Melin-Aldana H, Green RM, Whitington PF. Upregulation of osteopontin expression is involved in the development of nonalcoholic steatohepatitis in a dietary murine model. Am J Physiol Gastrointest Liver Physiol. 2004 Jul 11;287(1):G264-73.

35. Itagaki H, Shimizu K, Morikawa S, Ogawa K, Ezaki T. Morphological and functional characterization of non-alcoholic fatty liver disease induced by a methionine-choline-deficient diet in C57BL / 6 mice. Int J Clin Exp Pathol. 2013;6(12):2683–96.

36. Ouyang X, Cirillo P, Sautin Y, McCall S, Bruchette JL, Diehl AM, et al. Fructose consumption as a risk factor for non-alcoholic fatty liver disease. J Hepatol. 2008;48(6):993–9.

37. Feldstein AE, Canbay A, Guicciardi ME, Higuchi H, Bronk SF, Gores GJ. Diet associated hepatic steatosis sensitizes to Fas mediated liver injury in mice. J Hepatol. 2003 Dec;39(6):978–83.

38. Fernandes-Lima F, Monte TLRG, Amorim De Morais Nascimento F, Gregorio BM. Short exposure to a high-sucrose diet and the first “hit” of nonalcoholic fatty liver disease in mice. Cells Tissues Organs. 2016;201(6):464–72.

39. O’Farrelly C, Doherty D. Core Concepts in Immunology. In: Gershwin M, Vierling J, Manns M, editors. Liver Immunology. 2nd ed. New York: Springer Science+Buisness Media; 2014. p. 11–26.

40. Coico R, Sunshine G. Elements of innate and acquired immunity. In: Immunology - A short course. 6th ed. Hoboken, NJ, USA: John Wiley & Sons; 2009. p. 11–26.

41. Cooper MA, Fehniger TA, Fuchs A, Colonna M, Caligiuri MA. NK cell and DC interactions. Trends Immunol. 2004;25(1):47–52.

42. Cooper M, Fehninger T, Caligiuri M. The biology of human natural killer-cell subsets. Trends Immunol. 2001;22(11):633–40.

43. Guilliams M, Ginhoux F, Jakubzick C, Naik SH, Onai N, Schraml BU, et al. Dendritic cells, monocytes and macrophages: a unified nomenclature based on ontogeny. Nat Rev Immunol. Nature Publishing Group; 2014;14(8):571–8.

44. Yona S, Jung S. Monocytes: subsets, origins, fates and functions. Curr Opin Hematol. 2010;17(April):53–9.

45. Geissmann F, Jung S, Littman DR. Blood monocytes consist of two principal subsets with distinct migratory properties. Immunity. 2003;19(1):71–82.

46. Yona S, Kim K-W, Wolf Y, Mildner A, Varol D, Breker M, et al. Fate mapping reveals origins and dynamics of monocytes and tissue macrophages under homeostasis. Immunity. 2013;38(1):79–91.

47. Naik SH, Sathe P, Park H-Y, Metcalf D, Proietto AI, Dakic A, et al. Development of plasmacytoid and conventional dendritic cell subtypes from single precursor cells derived in vitro and in vivo. Nat Immunol. 2007;8(11):1217–26.

48. Coico R, Sunshine G. Activation and Function of T and B Cells. In: Immunology - A short course. 6th ed. Hoboken, NJ, USA: John Wiley & Sons; 2009. p. 141–62.

49. Carambia A, Herkel J. CD4 T cells in hepatic immune tolerance. J Autoimmun. Elsevier Ltd; 2010;34(1):23–8.

50. Bettelli E, Oukka M, Kuchroo VK. T H -17 cells in the circle of immunity and autoimmunity. Nat Immunol. 2007;8(4):345–50.

51. Jensen PE. Recent advances in antigen processing and presentation. Nat Immunol. 2007;8(10):1041–8.

52. Smith-Garvin J, Koretzky G, Jordan MS. T cell activation. Annu Rev Immunol. 2009;27:591–619.

53. Godfrey DI, MacDonald HR, Kronenberg M, Smyth MJ, Van Kaer L. NKT cells: what's in a name? Nat Rev Immunol. 2004;4(3):231–7.

54. Porcelli SA, Modlin RL. THE CD1 SYSTEM: Antigen-Presenting Molecules for T Cell Recognition of Lipids and Glycolipids. Annu Rev Immunol. 1999;17(1):297–329.

55. Godfrey DI, Kronenberg M. Going both ways: Immune regulation via CD1d-dependent NKT cells. J Clin Invest. 2004;114(10):1379–88.

56. Tian Z, Zhang C, Lian Z-X. The Liver and Immune Tolerance. In: Gershwin ME, Vierling JM, Manns MP, editors. Liver Immunology. 2nd ed. New York: Springer Science+Buisness Media; 2014. p. 79–94.

57. Steinman RM, Cohn ZA. Identification of a Novel Cell Type in Peripheral Lymphoid Organs of Mice. J Exp Med. 1973;137:1142–62.

58. Banchereau J, Steinman RM. Dendritic cells and the control of immunity. Nature. 1998;392:245–52.

59. Steinman RM, Banchereau J. Taking dendritic cells into medicine. Nature. 2007;449(7161):419–26.

60. Hopp AK, Rupp A, Lukacs-Kornek V. Self-antigen presentation by dendritic cells in autoimmunity. Front Immunol. 2014;5:1–14.

61. Mildner A, Jung S. Immunity Review Development and Function of Dendritic Cell Subsets. Immunity. 2014;40:642–56.

62. Rahman AH, Aloman C. Dendritic cells and liver fibrosis. Biochim Biophys Acta [Internet]. 2013 Jul [cited 2016 Apr 23];1832(7):998–1004. Available from: http://www.sciencedirect.com/science/article/pii/S0925443913000082

63. Mellman I, Steinman RM. Dendritic cells: Specialized and regulated antigen processing machines. Cell. 2001;106(3):255–8.

64. Benson R a, Patakas A, Conigliaro P, Rush CM, Garside P, McInnes IB, et al. Identifying the cells breaching self-tolerance in autoimmunity. J Immunol. 2010;184(11):6378–85.

65. Steinman R, Idoyaga J. Features of the dendritic cell lineage. Immunol Rev. 2010;234(1):5–17.

66. Sousa CR e. Dendritic cells in a mature age. Nat Rev Immunol. 2006;6(6):476–83.

67. Coico R, Sunshine G. Role of the major histocompatibility comples in the immune response. In: Immunology - A short course. 6th ed. Hoboken, NJ, USA: John Wiley & Sons; 2009. p. 107–22.

68. Albert ML, Sauter B, Bhardwaj N. Dendritic cells acquire antigen from apoptotic cells and induce class I-restricted CTLs. Nature. 1998;392(6671):86–9.

69. Heath WR, Belz GT, Behrens GMN, Smith CM, Forehan SP, Parish IA, et al. Cross-presentation, dendritic cell subsets, and the generation of immunity to cellular antigens. Immunol Rev. 2004;199:9–26.

70. Fernandez N, Lozier A, Flament C, Ricciardi-Castgnoli P, Bellet D, Suter M, et al. Dendritic cells directly trigger NK cell functions : Cross-talk relevant in innate anti-tumor immune responses in vivo. Nat Med. 1999;5(4):405–11.

71. Andrews DM, Scalzo AA, Yokoyama WM, Smyth MJ, Degli-Esposti MA. Functional interactions between dendritic cells and NK cells during viral infection. Nat Immunol. 2003;4(2):175–81.

72. Gerosa F, Baldani-guerra B, Nisii C, Marchesini V, Carra G, Trinchieri G. Reciprocal Activating Interaction between Natural Killer Cells and Dendritic Cells. J Exp Med. 2002;195(3).

73. Durai V, Murphy KM. Functions of Murine Dendritic Cells. Immunity. 2016;45(4):719–36.

74. Piccioli D, Sbrana S, Melandri E, Valiante NM. Contact-dependent Stimulation and Inhibition of Dendritic Cells by Natural Killer Cells. J Exp Med. 2002;195(3):335–41.

75. Liu K, Victora G, Schwickert T, Guermonprez P, Meredith MM, Yao K, et al. In vivo analysis of dendritic cell development and homeostasis. Science (80-). 2009;324:392–7.

76. Ginhoux F, Liu K, Helft J, Bogunovic M, Greter M, Hashimoto D, et al. The origin and development of nonlymphoid tissue CD103+ DCs. J Exp Med. 2009;206:3115–30.

77. Hildner K, Edelson BT, Purtha WE, Diamond M, Matsushita H, Kohyama M, et al. Batf3 deficiency reveals a critical role for CD8α+ dendritic cells in cytotoxic T cell immunity. Science (80-). 2008;322(5904):1097–100.

78. Hacker C, Kirsch RD, Ju X-S, Hieronymus T, Gust TC, Kuhl C, et al. Transcriptional profiling identifies Id2 function in dendritic cell development. Nat Immunol. 2003;4(4):380–6.

79. Schiavoni G, Mattei F, Sestili P, Borghi P, Venditti M, Morse HC 3rd, et al. ICSBP is essential for

the development of mouse type I interferon-producing cells and for the generation and activation of CD8alpha(+) dendritic cells. J Exp Med. 2002 Dec;196(11):1415–25.

80. Kashiwada M, Pham N-LL, Pewe LL, Harty JT, Rothman PB. NFIL3/E4BP4 is a key transcription factor for CD8alpha(+) dendritic cell development. Blood. 2011 Jun;117(23):6193–7.

81. Miller J, Brown D, Shay T, Gautier E, Jojic V, Cohain A, et al. Deciphering the transcriptional network of the DC lineage. Nat Immunol. 2012;13(9):888–99.

82. Coombes JL, Siddiqui KRR, Arancibia-Cárcamo C V, Hall J, Sun C-M, Belkaid Y, et al. A functionally specialized population of mucosal CD103+ DCs induces Foxp3+ regulatory T cells via a TGF-beta and retinoic acid-dependent mechanism. J Exp Med. 2007;204(8):1757–64.

83. Matteoli G, Mazzini E, Iliev ID, Mileti E, Fallarino F, Puccetti P, et al. Gut CD103 + dendritic cells express indoleamine 2 , 3-dioxygenase which influences T regulatory / T effector cell balance and oral tolerance induction. Gut. 2010;59:595–604.

84. Khare A, Krishnamoorthy N, Timothy B, Fei M, Ray P, Ray A. Cutting edge: Inhaled Antigen Upregulates Retinaldehyde Dehydrogenase in Lung CD103+ but Not Plasmacytoid Dendritic Cells To Induce Foxp3 De Novo in CD4+ T Cells and Promote Airway Tolerance. J Immunol. 2013;191:25–9.

85. Shortman K, Liu Y. Mouse and Human Dendritic Cell Subtypes. Nat Rev Immunol. 2002;2(3):151–61.

86. Mildner A, Yona S, Jung S. A close encounter of the third kind: monocyte-derived cells. Adv Immunol. 2013;120:69–103.

87. Langlet C, Tamoutounour S, Henri S, Luche H, Ardouin L, Gregoire C, et al. CD64 Expression Distinguishes Monocyte-Derived and Conventional Dendritic Cells and Reveals Their Distinct Role during Intramuscular Immunization. J Immunol. 2012;188(4):1751–60.

88. Tamoutounour S, Henri S, Lelouard H, de Bovis B, de Haar C, van der Woude CJ, et al. CD64 distinguishes macrophages from dendritic cells in the gut and reveals the Th1-inducing role of mesenteric lymph node macrophages during colitis. Eur J Immunol. 2012;42(12):3150–66.

89. Tamoutounour S, Guilliams M, Montanana Sanchis F, Liu H, Terhorst D, Malosse C, et al. Origins and functional specialization of macrophages and of conventional and monocyte-derived dendritic cells in mouse skin. Immunity. 2013;39(5):925–38.

90. Trautwein-Weidner K, Gladiator A, Kirchner FR, Becattini S, Rülicke T, Sallusto F, et al. Antigen-Specific Th17 Cells Are Primed by Distinct and Complementary Dendritic Cell Subsets in

Oropharyngeal Candidiasis. PLOS Pathog. 2015;11:1–23.

91. Satpathy AT, Briseño CG, Lee JS, Ng D, Manieri NA, Kc W, et al. Notch2-dependent classical dendritic cells orchestrate intestinal immunity to attaching- and-effacing bacterial pathogens. Nat Immunol. 2013;14(9).

92. Merad M, Sathe P, Helft J, Miller J, Mortha A. The Dendritic Cell Lineage: Ontogeny and Function of Dendritic Cells and Their Subsets in the Steady State and the Inflamed Setting. Annu Rev Imunnology. 2013;31(9):563–604.

93. Cisse B, Caton ML, Lehner M, Maeda T, Scheu S, Locksley R, et al. Transcription factor E2-2 is an essential and specific regulator of plasmacytoid dendritic cell development. Cell. 2008;135(1):37–48.

94. Rogers NM, Isenberg JS, Thomson AW. Plasmacytoid dendritic cells: No longer an enigma and now key to transplant tolerance? Am J Transplant. 2013;13(5):1125–33.

95. Asselin-Paturel C, Boonstra A, Dalod M, Durand I, Yessaad N, Dezutter-Dambuyant C, et al. Mouse type I IFN-producing cells are immature APCs with plasmacytoid morphology. Nat Immunol. 2001 Dec;2(12):1144–50.

96. Knolle P. The Liver as a Lymphoid Organ. In: Gershwin M, Vierling J, Manns M, editors. Liver Immunology. 2nd ed. New York: Springer Science+Buisness Media; 2014. p. 55–64.

97. Heikenwalder M, Knolle P, Protzer U. Innate Immunity and Disorders of the Liver. In: Gershwin M, Vierling J, Mann M, editors. Liver Immunology. New York: Springer Science+Buisness Media; 2014. p. 65–77.

98. Holz L, Benseler V, Bowen D, Bouillet P, Strasser A, O'Reilly L, et al. Intrahepatic murine CD8 T-Cells activation associates with a distinct phenotype leading to Bim-dependent death. Gastroenterology. 2008;135:989–97.

99. Klugewitz K, Blumenthal-Barby F, Knolle PA, Hamann A, Crispe IN. Immunomodulatory Effects of the Liver: Deletion of Activated CD4 + Effector Cells and Suppression of IFN- γ -Producing Cells After Intravenous Protein Immunization. J Immunol. 2002;169:2407–13.

100. Thomson AW, Knolle P a. Antigen-presenting cell function in the tolerogenic liver environment. Nat Rev Immunol. Nature Publishing Group; 2010;10(11):753–66.

101. Lukacs-Kornek V, Schuppan D. Dendritic cells in liver injury and fibrosis: Shortcomings and promises. J Hepatol. 2013;59(5):1124–6.

102. Duffield JS. Dendritic cells take on more tasks in the liver? Hepatology. 2012;55(1):16–9.

103. Pillarisetty VG, Shah AB, Miller G, Bleier JI, DeMatteo RP. Liver dendritic cells are less immunogenic than spleen dendritic cells because of differences in subtype composition. J Immunol. 2004;172(2):1009–17.

104. De Creus A, Abe M, Lau AH, Hackstein H, Raimondi G, Thomson AW. Low TLR4 expression by liver dendritic cells correlates with reduced capacity to activate allogeneic T cells in response to endotoxin. J Immunol. 2005;174(4):2037–45.

105. Ibrahim J, Nguyen AH, Rehman A, Ochi A, Jamal M, Graffeo CS, et al. Dendritic cell populations with different concentrations of lipid regulate tolerance and immunity in mouse and human liver. Gastroenterology. 2012;143(4):1061–72.

106. Chen Y, Jiang G, Yang HR, Gu X, Wang L, Hsieh CC, et al. Distinct response of liver myeloid dendritic cells to endotoxin is mediated by IL-27. J Hepatol. 2009;51(3):510–9.

107. Connolly MK, Bedrosian AS, Mallen-St Clair J, Mitchell AP, Ibrahim J, Stroud A, et al. In liver fibrosis, dendritic cells govern hepatic inflammation in mice via TNF-alpha. J Clin Invest. 2009;119(11):3213–25.

108. Bleier JI, Katz SC, Chaudhry UI, Pillarisetty VG, Kingham TP, Shah AB, et al. Biliary Obstruction Selectively Expands and Activates Liver Myeloid Dendritic Cells. J Immunol. 2006;176(12):7189–95.

109. Henning JR, Graffeo CS, Rehman A, Fallon NC, Zambirinis CP, Ochi A, et al. Dendritic Cells Limit Fibro-Inflammatory Injury in NASH. Hepatology. 2013;58(2):589–602.

110. Connolly MK, Ayo D, Malhotra A, Hackman M, Bedrosian AS, Ibrahim J, et al. Dendritic cell depletion exacerbates acetaminophen hepatotoxicity. Hepatology. 2011;54(3):959–68.

111. Jiao J, Sastre D, Fiel MI, Lee UE, Ghiassi-Nejad Z, Ginhoux F, et al. Dendritic cell regulation of carbon tetrachloride-induced murine liver fibrosis regression. Hepatology. 2012;55(1):244–55.

112. Guo J, Friedman SL. Toll-like receptor 4 signaling in liver injury and hepatic fibrogenesis. Fibrogenesis Tissue Repair. 2010;3:1–19.

113. Seki E, Brenner DA. Toll-like receptors and adaptor molecules in liver disease: update. Hepatology. 2008;48(1):322–35.

114. Li L, Chen L, Hu L, Liu Y, Sun H-Y, Tang J, et al. Nuclear factor high-mobility group box1 mediating the activation of Toll-like receptor 4 signaling in hepatocytes in the early stage of nonalcoholic fatty liver disease in mice. Hepatology. 2011 Nov;54(5):1620–30.

115. Vyas JM, Van der Veen A, Ploegh HL. The known unknowns of antigen processing and

presentation. Nat Rev Immunol. 2008;8(8):607–18.

116. Bar-On L, Jung S. Defining In Vivo Dendritic Cell Functions Using CD11c-DTR Transgenic Mice. In: Dendritic Cell Protocols [Internet]. Totowa, NJ: Humana Press; 2010. p. 429–42. Available from: https://doi.org/10.1007/978-1-60761-421-0_28

117. Eckert C, Klein N, Kornek M, Lukacs-Kornek V. The complex myeloid network of the liver with diverse functional capacity at steady state and in inflammation. Front Immunol. 2015;6:1–11.

118. Trowbridge IS, Ostergaard HL, Johnson P. CD45: a leukocyte-specific member of the protein tyrosine phosphatase family. BBA - Mol Cell Res. 1991;1095(1):46–56.

119. Solovjov DA, Pluskota E, Plow EF. Distinct roles for the α and β subunits in the functions of integrin αMβ2. J Biol Chem. 2005;280(2):1336–45.

120. Austyn JM, Gordon S. F4/80, a monoclonal antibody directed specifically against the mouse macrophage. Eur J Immunol. 1981;11(10):805–15.

121. Rose S, Misharin A, Perlman H. A novel Ly6C/Ly6G-based strategy to analyze the mouse splenic myeloid compartment. Cytometry. 2012;81(4):343–50.

122. Rickert RC, Rajewsky K, Roes J. Impairment of T-cell-dependent B-cell responses and B-1 cell development in CD19-deficient mice. Vol. 376, Nature. 1995. p. 352–5.

123. Guy CS, Vignali DA. Organization of proximal signal initiation at the TCR:CD3 complex. Immunol Rev. 2009;232(1):7–21.

124. Hedrich HJ, Nicklas W. Housing and Maintenance. In: Hedrich HJ, editor. The Laboratory Mouse [Internet]. 2nd ed. Amsterdam: Elsevier, Academic Press; 2012. p. 521–45. Available from: http://dx.doi.org/10.1016/B978-0-12-382008-2.00022-2

125. Darzynkiewicz Z, Bruno S, Del Bino G, Gorczyca W, Hotz MA, Lassota P, et al. Features of apoptotic cells measured by flow cytometry. Cytometry. 1992;13(8):795–808.

126. Ormerod MG. Flow Cytometry- A basic introduction [Internet]. 2008 [cited 2017 Dec 8]. Available from: http://flowbook.denovosoftware.com/

127. Hulspas R, O'Gorman MRG, Wood BL, Gratama JW, Robert Sutherland D. Considerations for the control of background fluorescence in clinical flow cytometry. Cytom Part B - Clin Cytom. 2009;76(6):355–64.

128. Björnsson E, Angulo P. Non-alcoholic fatty liver disease. Scand J Gastroenterol. 2007;42:1023–30.

129. Tetri LH, Basaranoglu M, Brunt EM, Yerian LM, Neuschwander-Tetri BA. Severe NAFLD with hepatic necroinflammatory changes in mice fed trans fats and a high-fructose corn syrup equivalent. Am J Physiol Gastrointest Liver Physiol. 2008;295(5):G987-95.

130. Tomita K, Tamiya G, Ando S, Ohsumi K, Chiyo T, Mizutani A, et al. Tumour necrosis factor alpha signalling through activation of Kupffer cells plays an essential role in liver fibrosis of non-alcoholic steatohepatitis in mice. Gut. 2006;55(3):415–24.

131. Lloyd CM, Phillips ARJ, Cooper GJS, Dunbar PR. Three-colour fluorescence immunohistochemistry reveals the diversity of cells staining for macrophage markers in murine spleen and liver. J Immunol Methods. 2008;334(1–2):70–81.

132. Luster MI, Germolec DR, Yoshida T, Kayama F, Thompson M. Endotoxin-induced Cytokine Gene Expression and Excretion in the Liver. Hepatology. 1994;19(2):480–8.

133. Tosello-Trampont AC, Landes SG, Nguyen V, Novobrantseva TI, Hahn YS. Kupffer cells trigger nonalcoholic steatohepatitis development in diet-induced mouse model through tumor necrosis factor-alpha production. J Biol Chem. 2012;287(48):40161–72.

134. Zhang M, Ueki S, Kimura S, Yoshida O, Castellaneta A, Ozaki KS, et al. Roles of dendritic cells in murine hepatic warm and liver transplantation-induced cold ischemia/reperfusion injury. Hepatology. 2013;57(4):1585–96.

135. Ibrahim J, Nguyen AH, Rehman A, Ochi A, Jamal M, Graffeo CS, et al. Dendritic cell populations with different concentrations of lipid regulate tolerance and immunity in mouse and human liver. Gastroenterology. 2012 Oct;143(4):1061–72.

136. Meier A. Influence of Batf3-dependent dendritic cells on the progression of nonalcoholic steatohepatitis and the regulation of lipid metabolism. Saarland University; 2016.

137. Hebbard L, George J. Animal models of nonalcoholic fatty liver disease. Nat Rev Gastroenterol Hepatol. 2011;8(1):35–44.

138. Tacke F. Functional role of intrahepatic monocyte subsets for the progression of liver inflammation and liver fibrosis in vivo. Fibrogenesis Tissue Repair. 2012;5(Suppl 1):1–8.

139. Xu R, Huang H, Zhang Z, Wang F-S. The role of neutrophils in the development of liver diseases. Cell Mol Immunol. 2014;11(3):224–31.

140. Peverill W, Powell LW, Skoien R. Evolving concepts in the pathogenesis of NASH: Beyond steatosis and inflammation. Int J Mol Sci. 2014;15(5):8591–638.

141. Lewis KL, Caton ML, Bogunovic M, Greter M, Grajkowska LT, Ng D, et al. Notch2 receptor

signaling controls functional differentiation of dendritic cells in the spleen and intestine. Immunity. 2011;35(5):780–91.

142. Domínguez PM, Ardavín C. Differentiation and function of mouse monocyte-derived dendritic cells in steady state and inflammation. Immunol Rev. 2010;234(1):90–104.

143. Suzuki S, Honma K, Matsuyama T, Suzuki K, Toriyama K, Akitoyo I, et al. Critical roles of interferon regulatory factor 4 in CD11b high CD8 alpha- dendritic cell development. Proc Natl Acad Sci U S A. 2004;101(24):8981–6.

144. Wolf MJ, Adili A, Piotrowitz K, Abdullah Z, Boege Y, Stemmer K, et al. Article Metabolic Activation of Intrahepatic CD8 + T Cells and NKT Cells Causes Nonalcoholic Steatohepatitis and Liver Cancer via Cross-Talk with Hepatocytes. Cancer Cell. 2014;26:549–64.

145. Ma C, Kesarwala AH, Eggert T, Medina-echeverz J, Kleiner DE, Jin P, et al. NAFLD causes selective CD4+ T lymphocye loss and promotes hepatocarcinogenesis. Nature. 2016;531(7593):253–7.

146. Hua J, Mohamood AR, Hamad ARA, Ravi R, Li Z. A High-Fat Diet and Regulatory T Cells Influence Susceptibility to Endotoxin-Induced Liver Injury. Hepatology. 2007;46(5):1519–29.

147. Winer D a, Winer S, Chng MHY, Shen L, Engleman EG. B Lymphocytes in obesity-related adipose tissue inflammation and insulin resistance. Cell Mol life Sci. 2014;71:1033–43.

148. Sutti S, Jindal A, Locatelli I, Vacchiano M, Gigliotti L, Bozzola C, et al. Adaptive immune responses triggered by oxidative stress contribute to hepatic inflammation in NASH. Hepatology. 2014;59(3):886–97.

149. Magee N, Zou A, Zhang Y. Pathogenesis of Nonalcoholic Steatohepatitis: Interactions between Liver Parenchymal and Nonparenchymal Cells. Biomed Res Int. 2016;2016:1–11.

150. Tian Z, Chen Y, Gao B. Natural killer cells in liver disease. Hepatology. 2013;57(4):1654–62.

151. Muhanna N, Tair LA, Doron S, Amer J, Azzeh M, Mahamid M, et al. Amelioration of hepatic fibrosis by NK cell activation. Gut. 2011;60:90–8.

152. Cheent K, Khakoo SI. Natural killer cells and hepatitis C : action and reaction. Gut. 2011;60:268–78.

153. Kahraman A, Schlattjan M, Kocabayoglu P, Yildiz-Meziletoglu S, Schlensak M, Fingas CD, et al. Major histocompatibility complex class I-related chains A and B (MIC A/B): A novel role in nonalcoholic steatohepatitis. Hepatology. 2010;51(1):92–102.

154. Tajiri K. CD1d-restricted Natural Killer T Cells in Metabolic Disorders. J Immune Res. 2014;1(2):4–7.

155. Tajiri K, Shimizu Y. Role of NKT Cells in the Pathogenesis of NAFLD. Int J Hepatol. 2012;2012:1–6.

156. Martin-Murphy B V., You Q, Wang H, De La Houssaye BA, Reilly TP, Friedman JE, et al. Mice lacking natural killer T cells are more susceptible to metabolic alterations following high fat diet feeding. PLoS One. 2014;9(1):1–11.

157. Elinav E, Pappo O, Sklair-Levy M, Margalit M, Shibolet O, Gomori M, et al. Adoptive transfer of regulatory NKT lymphocytes ameliorates non-alcoholic steatohepatitis and glucose intolerance in ob/ob mice and is associated with intrahepatic CD8 trapping. J Pathol. 2006;209(1):121–8.

158. Li Z, Soloski MJ, Diehl AM. Dietary factors alter hepatic innate immune system in mice with nonalcoholic fatty liver disease. Hepatology. 2005;42(4):880–5.

159. Syn W-K, Htun Oo Y, Pereira TA, Karaca GF, Jung Y, Omenetti A, et al. Accumulation of natural killer T cells in progressive nonalcoholic fatty liver disease. Hepatology. 2010;51(6):1998–2007.

160. Tajiri K, Shimizu Y, Tsuneyama K, Sugiyama T. Role of liver-infiltrating CD3+CD56+ natural killer T cells in the pathogenesis of nonalcoholic fatty liver disease. Eur J Gastroenterol Hepatol. 2009;21(6):673–80.

161. Kozlova N, Jensen JK, Chi TF, Samoylenko A, Kietzmann T. PAI-1 modulates cell migration in a LRP1-dependent manner via beta-catenin and ERK1/2. Thromb Haemost. 2015;113(5):988–98.

162. Dimova EY, Kietzmann T. Metabolic, hormonal and environmental regulation of plasminogen activator inhibitor-1 (PAI-1) expression: Lessons from the liver. Thromb Haemost. 2008;100(6):992–1006.

163. Ganey PE, Luyendyk JP, Newport SW, Eagle TM, Maddox JF, Mackman N, et al. Role of the coagulation system in acetaminophen-induced hepatotoxicity in mice. Hepatology. 2007;46(4):1177–86.

164. Zhang LP, Takahara T, Yata Y, Furui K, Jin B, Kawada N, et al. Increased expression of plasminogen activator and plasminogen activator inhibitor during liver fibrogenesis of rats: Role of stellate cells. J Hepatol. 1999;31(4):703–11.

165. Bergheim I, Guo L, Davis MA, Duveau I, Arteel GE. Critical Role of Plasminogen Activator Inhibitor-1 in Cholestatic Liver Injury and Fibrosis. J Pharmacol Exp Ther. 2006;316(2):592–600.

166. O'Regan A, Berman JS. Osteopontin: A key cytokine in cell-mediated and granulomatous inflammation. Int J Exp Pathol. 2000;81(6):373–90.

167. Denhardt DT, Giachelli CM, Rittling SR. Role of Osteopontin in Cellular Signaling and Toxicant Injury. Annu Rev Pharmacol Toxicol. 2001;41:723–49.

168. Isoda K, Sawada S, Ayaori M, Matsuki T, Horai R, Kagata Y, et al. Deficiency of interleukin-1 receptor antagonist deteriorates fatty liver and cholesterol metabolism in hypercholesterolemic mice. J Biol Chem. 2005;280(8):7002–9.

169. Pihlajamäki J, Kuulasmaa T, Kaminska D, Simonen M, Kärjä V, Grönlund S, et al. Serum interleukin 1 receptor antagonist as an independent marker of non-alcoholic steatohepatitis in humans. J Hepatol. 2012;56(3):663–70.

170. Steppan CM, Bailey ST, Bhat S, Brown EJ, Banerjee RR, Wright CM, et al. The hormone resistin links obesity to diabetes. Nature. 2001;409:307–12.

171. Polyzos SA, Kountouras J, Mantzoros CS. Adipokines in nonalcoholic fatty liver disease. Metabolism. 2016;65(8):1062–79.

172. Beier JI, Guo L, von Montfort C, Kaiser JP, Joshi-Barve S, Arteel GE. New role of resistin in lipopolysaccharide-induced liver damage in mice. J Pharmacol Exp Ther. 2008;325(3):801–8.

173. Bertolani C, Sancho-bru P, Failli P, Bataller R, Aleffi S, Defranco R, et al. Resistin as an Intrahepatic Cytokine: Overexpression during Chronic Injury and Induction of proinflammatory actions in Hepatic Stellate Cells. Am J Pathol. 2006;169(6):2042–53.

174. Park HK, Ahima RS. Resistin in Rodents and Humans. Diabetes Metab J. 2013;37:404–14.

175. Fasshauer M, Klein J, Neumann S, Eszlinger M, Paschke R. Tumor Necrosis Factor alpha Is a Negative Regulator of Resistin Gene Expression and Secretion in 3T3-L1 Adipocytes. Biochem Biophys Res Commun. 2001;288(4):1027–31.

176. Bertola A, Bonnafous S, Anty R, Patouraux S, Saint-Paul MC, Iannelli A, et al. Hepatic expression patterns of inflammatory and immune response genes associated with obesity and nash in morbidly obese patients. PLoS One. 2010;5(10):1–11.

177. Semba T, Nishimura M, Nishimura S, Ohara O, Ishige T, Ohno S, et al. The FLS (Fatty liver Shionogi) mouse reveals local expressions of lipocalin-2 , CXCL1 and CXCL9 in the liver with non-alcoholic steatohepatitis. BMC Gastroenterol. 2013;13:1–11.

178. Maher JJ, Scott MK, Saito JM, Burton MC. Adenovirus-Mediated Expression of Cytokine-Induced Neutrophil Chemoattractant in Rat Liver Induces a Neutrophilic Hepatitis. Hepatology.

1997;25(3):624–30.

179. Dominguez M, Miquel R, Colmenero J, Moreno M, Pagán JCG, Bosch J, et al. Hepatic Expression of CXC Chemokines Predicts Portal Hypertension and Survival in Patients with Alcoholic Hepatitis. Gastroenterology. 2009;136(5):1639–50.

180. Musso G, Cassader M, Gambino R. Non-alcoholic steatohepatitis: emerging molecular targets and therapeutic strategies. Nat Rev Drug Discov. 2016;15(4):249–74.

181. Griffith JW, Sokol CL, Luster AD. Chemokines and chemokine receptors: positioning cells for host defense and immunity. Annu Rev Immunol. 2014;32:659–702.

182. Dambach DM, Watson LM, Gray KR, Durham SK, Laskin DL. Role of CCR2 in Macrophage Migration Into the Liver During Acetaminophen-Induced Hepatotoxicity in the Mouse. Hepatology. 2002;35:1093–103.

183. Marra F, Tacke F. Roles for Chemokines in Liver Disease. Gastroenterology. 2014;147(3):577–94.

184. Baeck C, Wehr A, Karlmark KR, Heymann F, Vucur M, Gassler N, et al. Pharmacological inhibition of the chemokine CCL2 (MCP-1) diminishes liver macrophage infiltration and steatohepatitis in chronic hepatic injury. Gut. 2012;61:416–26.

185. Seki E, Minicis S De, Gwak G, Kluwe J, Inokuchi S, Bursill CA, et al. CCR1 and CCR5 promote hepatic fibrosis in mice. J Clin Invest. 2009;119(7):1858–70.

186. Lefebvre E, Moyle G, Reshef R, Richman LP, Thompson M, Hong F, et al. Antifibrotic Effects of the Dual CCR2 / CCR5 Antagonist Cenicriviroc in Animal Models of Liver and Kidney Fibrosis. PLoS One. 2016;11:1–19.

187. Berres M, Koenen RR, Rueland A, Zaldivar MM, Heinrichs D, Sahin H, et al. Antagonism of the chemokine Ccl5 ameliorates experimental liver fibrosis in mice. J Clin Invest. 2010;120(11):4129–40.

188. Charo IF, Ransohoff M. The Many Roles of Chemokines and Chemokine Receptors in Inflammation. N Engl J Med. 2006;354:610–21.

189. Larrea E, Aldabe R, Guembe L, Casares N, Galeano E, Echeverria I, et al. Hepatitis C virus induces the expression of CCL17 and CCL22 chemokines that attract regulatory T cells to the site of infection. J Hepatol. 2011;54:422–31.

190. Annacker O, Coombes JL, Malmstrom V, Uhlig HH, Bourne T, Johansson-lindbom B, et al. Essential role for CD103 in the T cell – mediated regulation of experimental colitis. J Exp Med.

2005;202(8):1051–61.

191. Blüher M. Adipose tissue dysfunction in obesity. Exp Clin Endocrinol Diabetes. 2009;117(6):241–50.

192. Friedman JM, Halaas JL. Leptin and the regulation of body weight in mammals. Nature. 1998;395(6704):763–70.

193. Chitturi S, Farrell G, Frost L, Kriketos A, Lin R, Liddle C, et al. Serum leptin in NASH correlates with hepatic steatosis but not fibrosis: A manifestation of lipotoxicity? Hepatology. 2002;36(2):403–9.

194. Mantzoros CS. The role of leptin and hypothalamicneuropeptides in energy homeostasis: Update on leptin in obesity. Growth Horm IGF Res. 2001;11:S85–9.

195. Lee Y, Wang MY, Kakuma T, Wang ZW, Babcock E, McCorkle K, et al. Liporegulation in Diet-induced Obesity: The antisteatotic role of hyperleptinemia. J Biol Chem. 2001;276(8):5629–35.

196. Trak-Smayra V, Paradis V, Massart J, Nasser S, Jebara V, Fromenty B. Pathology of the liver in obese and diabetic ob/ob and db/db mice fed a standard or high-calorie diet. Int J Exp Pathol. 2011;92(6):413–21.

197. Anstee Q, Goldin R. Mouse models in non-alcoholic fatty liver disease and steatohepatitis research. Int J Exp Pathol. 2006;87:1–16.

198. Shoelson SE, Herrero L, Naaz A. Obesity, Inflammation, and Insulin Resistance. Gastroenterology. 2007;132(6):2169–80.

199. Weisberg SP, McCann D, Desai M, Rosenbaum M, Leibel RL, Ferrante AW. Obesity is associated with macrophage accumulation in adipose tissue. J Clin Invest. 2003;112(12):1796–808.

200. Klein S, Fontana L, Young VL, Andrew RC, Kilo C, Patterson BW, et al. Absence of an Effect of Liposuction on Insulin Action and Risk Factors for Coronary Heart Disease. N Engl J Med. 2004;350(25):2549–57.

201. Lee B, Lee J. Biochimica et Biophysica Acta Cellular and molecular players in adipose tissue in fl ammation in the development of obesity-induced insulin resistance. BBA - Mol Basis Dis. 2014;1842(3):446–62.

202. Bugianesi E, McCullough AJ, Marchesini G. Insulin resistance: A metabolic pathway to chronic liver disease. Hepatology. 2005;42(5):987–1000.

203. Heier E-C, Meier A, Julich-Haertel H, Djudjaj S, Rau M, Tschernig T, et al. Murine CD103+ dendritic cells protect against steatosis progression towards steatohepatitis. J Hepatol. 2017;66:1241–50.

204. Kelly A, Fahey R, Fletcher JM, Keogh C, Carroll AG, Siddachari R, et al. CD141 + myeloid dendritic cells are enriched in healthy human liver. J Hepatol. 2014;60(1):135–42.

205. Villadangos JA, Shortman K. Found in translation : the human equivalent of mouse CD8+ dendritic cells. J Exp Med. 2010;207:1131–4.

206. Cervantes-barragan L, Lewis KL, Firner S, Thiel V, Hugues S, Reith W. Plasmacytoid dendritic cells control T-cell response to chronic viral infection. Proc Natl Acad Sci U S A. 2012;109:3012–7.

6 Publications

Journal Articles

Heier E-C, Meier A, Julich-Haertel H, Djudjaj S, Rau M, Tschernig T, et al. Murine CD103+ dendritic cells protect against steatosis progression towards steatohepatitis. J Hepatol. 2017;66:1241–50. https://doi.org/10.1016/j.jhep.2017.01.008

See Appendix

Abstracts

EC. Heier, A. Meier, T. Tschernig, F. Lammert, V. Lukacs-Kornek
CD103+ DCs are a key population in the progression of non-alcoholic steatohepatitis: could DCs represent a novel therapeutic application in NASH?
21.04.2017: The international liver congress of the European Association for the study of the liver

EC. Heier, H.Borchardt, H. Julich, C. Eckert, N. Klein, T. Tschernig, V. Lukacs-Kornek
Alterations in liver dendritic cell subtypes during non-alcoholic steatohepatitis.
16.11.2015: The liver meeting ® 2015 of the American Association for the study of liver diseases

7 Acknowledgement

First, I would like to express my deepest gratitude to jun. Prof. Dr. Dr. Veronika Lukacs-Kornek for the opportunity to work with her and the trust and confidence she showed in me. Thank you for your support and guidance, for accepting me in your lab, teaching me and providing me with amazing opportunities. You showed me the hard, but also rewarding life of a scientist and I truly miss working with you.

Further I would like thank Dr. Miroslav Kornek for his support, motivation and advice during all this time. Thank you for your stories that have often shortened the experiments.

I would also like to thank Prof. Dr. Frank Lammert at the Klinikum für Innere Medizin II, University of Saarland for his support and insight into this project.

I also thank Prof. Dr. Thomas Tschernig at the institute of Anatomy and Cell Biology, University of Saarland for his support and allowing me to use his research facilities. I am also very grateful to Marion Schwarz and Ingrid Lang for the technical assistance with the tissue samples.

Special thanks to Anna Meier, who worked on this project with me and provided the data for liver triglyceride content

I also would like to thank Henrike Julich-Haertel for supporting me during my experiments and offering good advice.

Thank you also to the rest of the lab crew for offering help, friendship and laughter at any time.

My deepest gratitude goes to my family. Especially to my parents, who have always supported me and encouraged me to follow my path, to my sisters, Hanna and Sophie, who always listen to my complaints, make me laugh and keep me grounded and to my grandfather, who has injected me with the love for science since my early childhood. Thank you.

Ultimately, I would like to thank Leonie, Anna and Katharina, who turned Homburg into a home.

8 Appendix

Research Article

JOURNAL OF HEPATOLOGY

Murine CD103$^+$ dendritic cells protect against steatosis progression towards steatohepatitis

Eva-Carina Heier[1,†], Anna Meier[1,†], Henrike Julich-Haertel[1], Sonja Djudjaj[3], Monica Rau[4], Thomas Tschernig[2], Andreas Geier[4], Peter Boor[3], Frank Lammert[1], Veronika Lukacs-Kornek[1,*]

[1]*Department of Medicine II, Saarland University Medical Center, Homburg, Germany;* [2]*Insitute of Anatomy and Cell Biology, University of Saarland, Germany;* [3]*Institute of Pathology and Department of Medicine II, University Hospital, RWTH Aachen, Germany;* [4]*Department of Internal Medicine II, University Hospital Würzburg, Germany*

See Editorial, pages 1120–1122

Background & Aims: Non-alcoholic fatty liver (NAFL) is the hepatic consequence of metabolic syndrome and can progress to non-alcoholic steatohepatitis (NASH). The identification of molecular and cellular factors that determine the progression of NASH and lead to irreversible hepatocellular damage are crucial. Dendritic cells (DCs) represent a heterogeneous cell population among which CD103$^+$ DCs play a significant role in immunity and tolerance. We aimed to clarify the role of this DC subset in the pathomechanism of NASH.

Methods: Steatosis progression towards steatohepatitis was analysed using multicolor FACS analyses, cytokine and qPCR array in high sucrose diet (HSD) and methionine and choline deficient diet (MCD) fed wild-type and basic leucine zipper transcription factor, ATF-Like-3 (*Batf3*) deficient animals, which lack CD103$^+$ DCs (classical type-1 DC, cDC1s).

Results: Metabolic challenge of *Batf3*$^{-/-}$ animals resulted in the progression of steatosis towards steatohepatitis, manifesting by an increased influx of inflammatory cells into the liver and elevated inflammatory cytokine production of myeloid cells upon innate stimuli. However, the lack of cDC1s did not affect cellular apoptosis and fibrosis progression but altered genes involved in lipid metabolism. The adoptive transfer of CD103$^+$ cDC1s to *Batf3* deficient animals reversed these observed changes and more importantly could attenuate cellular damage and inflammation in established murine steatohepatitis.

Conclusion: Here, we have identified the murine CD103$^+$ cDC1s as a protective DC subtype that influences the pro–anti-inflammatory balance and protects the liver from metabolic damage. As guardians of liver integrity, they play a key role in the inflammatory process during the development of steatohepatitis in mice.

Lay summary: Non-alcoholic fatty liver (NAFL) is the hepatic consequence of metabolic syndrome and can lead to non-alcoholic steatohepatitis (NASH). The current study demonstrated that a specific murine dendritic cell subtype possesses a potent regulatory role to influence the inflammatory milieu of the liver in this process.

Keywords: Dendritic cells; Inflammation; NASH; Steatosis.
Received 18 July 2016; received in revised form 3 January 2017; accepted 4 January 2017; available online 18 January 2017

* Corresponding author. Address: Department of Medicine II, Saarland University Medical Center, Homburg, Germany. Tel.: +49 (0)6841 16 23299; fax: +49 (0)6841 16 23267.
E-mail address: lukacsver@aol.com (V. Lukacs-Kornek).
† These authors contributed equally to this work.

Introduction

The prevalence of metabolic syndrome and non-alcoholic fatty liver disease (NAFLD) in the last decade has increased dramatically worldwide and affects both adults and children [1–3]. Non-alcoholic fatty liver (NAFL) is characterized by fat accumulation that can progress towards non-alcoholic steatohepatitis (NASH) distinguished by intrahepatic inflammation, increased steatosis with hepatocellular ballooning and cellular damage [4]. The chronic inflammatory response in NASH often results in progressive fibrosis and cirrhosis, which predisposes individuals to hepatocellular carcinoma [5,6]. The exact pathomechanisms of NASH are not fully understood. Nevertheless, it has been suggested that the disease develops in two-steps ('two-hit hypotheses') where increased lipid accumulation and hepatic steatosis ('first hit') sensitizes the liver to a 'second hit' that leads to inflammation and to further disease progression [7]. Oxidative stress and gut-derived endotoxin were implicated as potential components in this process [7,8]. In contrast, recent evidence suggest that the sequence of events between steatosis and inflammation might not be as strict and independent from each other as previously thought, and perhaps multiple factors in parallel play a role in disease development [9]. According to this, the various elements such as dysregulation of lipid metabolism, gut microbiota and local inflammatory response act side by side to promote NASH [9–12]. Since approximately only one fifth of the cases of non-alcoholic liver steatosis progresses towards NASH [8], the factors that mediate the switch and lead to disease progression are especially important. It remains to be elucidated which crucial cellular and molecular components and which circumstances protect or predispose to disease progression.

Dendritic cells (DCs) provide a link between innate and adaptive immunity and represent a tolerogenic cell population within

the steady state liver [13,14]. DCs are heterogeneous consisting of various subsets: plasmacytoid DCs, classical type-1 DCs (cDC1; $CD103^+CD11c^+CD11b^-$) and classical type-2 DCs (cDC2; $CD103^-$-$CD11c^+CD11b^+$) [13,14]. While DCs seem to be protective in acute liver damage they are suggested to promote inflammation in chronic liver injury and fibrosis [13,15–18]. Most studies however utilize animal models where these cells could be depleted using surface proteins expressed by DCs but not exclusively restricted to this cell population such as the CD11c-DTR system [15,19]. Specifically in NASH, $CD11c^+$ cells (involving DCs, some neutrophils, inflammatory monocytes and natural killer [NK] cells) limited liver necroinflammation via reducing the destructive effects of innate cells and promoting the clearance of cellular debris [19,20]. Given the importance of cDC1s in tolerance, apoptotic cell clearance and immune priming [14], we aimed to clarify the role of this DC subset in the pathomechanism of NASH.

Using a mouse model that specifically lacks the cDC1 subpopulation, we determined that this DC subset attenuated liver inflammation, balanced the pro–anti-inflammatory cytokine milieu and affected lipid metabolism. Importantly, animals lacking $CD103^+$ cDC1s exhibited progression of liver steatosis towards steatohepatitis, whereas wild-type mice remained steatotic without manifesting inflammation. Additionally, $CD103^+$ DCs could be utilized to reduce liver inflammation in established murine NASH. Thus, cDC1s play a key role in protecting the liver from inflammatory and metabolic damage, suggesting a hitherto unrecognized role of this DC subset in the switch from steatosis towards steatohepatitis.

Materials and methods

Mice

Mice were obtained from Charles River (Sulzfeld, Germany) or Jackson Laboratories (Bar Harbor, USA). Basic leucine zipper transcription factor, ATF-Like 3 (*Batf3*) KO animals (JAX stock number: 013755) were maintained under specific pathogen free conditions at the Helmholtz Centre for Infection Research (Braunschweig, Germany). Animals were housed in an assigned mouse cabinet (Bioscape, Castrop-Rauxel, Germany) in the Institute of Internal Medicine II (Saarland University, Homburg, Germany). All experimental procedures were conducted with the approval of the ethics and animal care committees of Saarland University Medical Center, Homburg, Germany. Seven to ten week old C57Bl/6 or $Batf3^{-/-}$ male mice were fed methionine and choline deficient diet (MCD) (Research Diets, New Brunswick, NJ, USA), standard normal chow (NC) (cereal based without addition of sucrose; 1324, Altromin) or high sucrose diet (HSD, 20% of calories are derived from fat and 40% from sucrose) (Research Diets) for 5 weeks.

Statistics

For statistical analyses Prism5 (Graphpad Software) was used. Data were compared using an unpaired two-tailed *t* test, Mann-Whitney two-tailed *t* test or one-way ANOVA using Bonferoni *post hoc* test. $^*p$ <0.05, $^{**}p$ <0.005, $^{***}p$ <0.0001

Further detailed protocols can be found in the Supplementary material and methods.

Results

$CD103^+$ cDC1s are protective during the progression of steatosis towards steatohepatitis

To identify the role of the $CD103^+$ cDC1 subtype in the progression of steatohepatitis, we utilized animals that lack *Batf3*. Batf3 is required for the differentiation of cDC1s, but it is dispensable for the development of cDC2s or pDCs [21]. Accordingly, $Batf3^{-/-}$ mice lack $CD8\alpha^+$ DCs in lymphoid organs and $CD103^+$ DCs in non-lymphoid organs involving the liver [21,22]. *Batf3* deficient (*Batf3* KO) and wild-type (WT) mice were subjected to standard NC diet containing elevated sucrose (HSD) and MCD. In accordance with previous reports, MCD diet caused steatohepatitis with marked steatosis, increased liver triglyceride contents (Fig. 1A, B) and at least a 2-fold increase in the hematopoietic cellular infiltrate indicated by the percentage of $CD45^+$ cells (Fig. 1C). Additionally, the necroinflammation observed during MCD diet was paralleled by increased serum alanine transaminase (ALT) activities (Fig. 1D, E). The lack of cDC1s did not change the frequency of $CD45^+$ cells present during MCD-induced steatohepatitis but further elevated liver triglyceride contents (Fig. 1A–C). In contrast, HSD significantly increased the quantity of triglycerides present in WT liver without resulting in overt inflammatory cellular infiltration (Fig. 1A–C). More importantly, HSD in *Batf3* deficient animals resulted in significantly elevated inflammatory infiltrates and profound liver steatosis (Fig. 1A–C). Histological analyses of $Batf3^{-/-}$ livers revealed the presence of lipid droplets, hepatocyte ballooning, inflammatory infiltrates and mild cellular necrosis indicating the progression of steatosis towards steatohepatitis (Fig. 1A–E). Despite the marked changes in histology under HSD feeding, these alterations were not paralleled by significantly increased serum ALT level (Fig. 1D). Notably, the increased liver steatosis in *Batf3* deficient animals was accompanied by a slightly elevated weight gain during HSD feeding (Fig. S1).

According to the increased necroinflammation scores in MCD and HSD fed animals (Fig. 1E), livers of *Batf3* deficient mice displayed elevated expression of apoptosis related genes such as *Bcl2* and *Fas* (Fig. 2A, B). Nevertheless, the changes did not differ significantly between WT and $Batf3^{-/-}$ animals indicating that cellular apoptosis is not affected by cDC1s.

Next, we evaluated whether the cDC1s could affect the progression of fibrosis observed in NASH. According to previous reports [19,23], *Col1a1* expression showed a significant increase in MCD treated animals, suggesting the presence of fibrosis associated with steatohepatitis. *Col1a1* expression demonstrated an increased tendency in gene deficient animals in both HSD and MCD treatment, however differences remained statistically non-significant (Fig. 2C). Moreover, under HSD feeding *Col1a1* remained unaltered as compared to NC fed animals, indicating that fibrosis is a later consequence of the progressive inflammatory liver injury observed in steatohepatitis.

Thus, $CD103^+$ cDC1s seem to influence the degree of steatosis in the liver and the progression of steatosis towards steatohepatitis without apparent effect on cellular apoptosis and fibrosis during the 5 week treatment.

$CD103^+$ cDC1s influence the inflammatory infiltrate during the development of steatohepatitis

One of the major hallmarks of steatohepatitis is the increased abundance of inflammatory cells within the liver [4,9]. Metabolic challenge with MCD increased the abundance of DC subtypes including cDC1, cDC2, and pDCs (Fig. S2A–C), whereas HSD did not result in any alterations of DC subtypes in WT animals (Fig. S2A–C). Moreover, the presence of the cDC2 subtype was slightly increased in KO compared to WT animals on HSD without differences in the abundance of pDCs (Fig. S2C). Importantly, KO animals on NC diet did not display alterations in the remaining

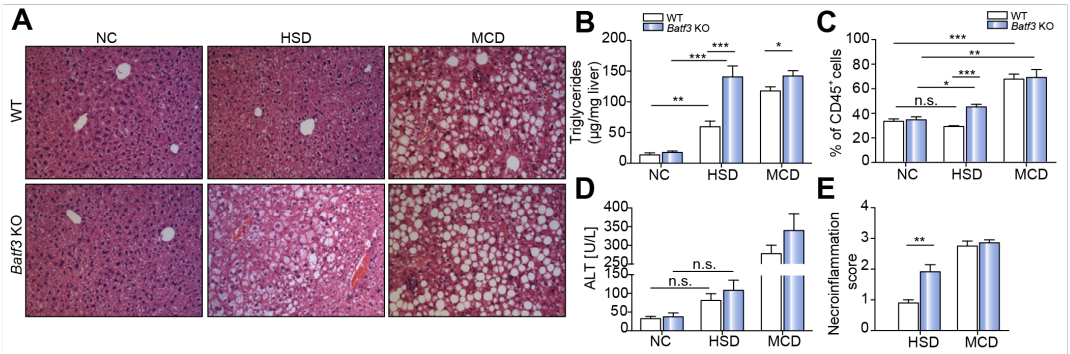

Fig. 1. CD103⁺ cDC1s protect the progression of steatosis towards steatohepatitis. (A) C57Bl/6 and *Batf3*$^{-/-}$ animals were fed with NC, HSD or MCD diet for 5 weeks. Liver paraffin sections were stained with hematoxylin eosin (HE) and imaged at 20x objectives. (B) The liver triglyceride contents are depicted. (C) Shown are the percentages of CD45⁺ cells among the living cells. (D) Serum ALT values are depicted. (E) Liver samples were scored based on the presence of necrosis, ballooning and inflammation. Data (A–E) are representative of three-four independent experiments, n = 4–5 mice per group. One-way ANOVA using Bonferoni *post hoc* test. Mean ± SEM. **p* <0.05, ***p* <0.005, ****p* <0.0001.

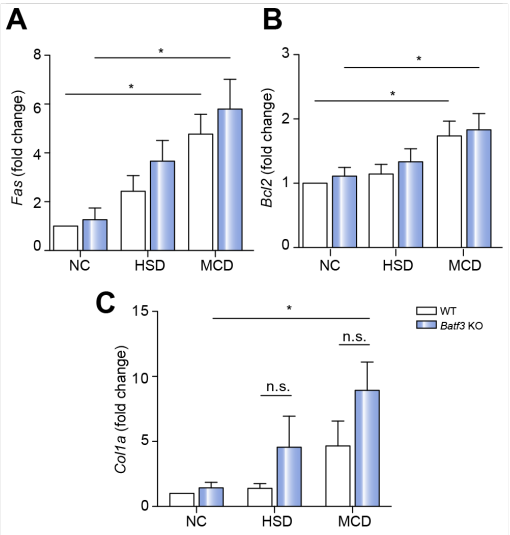

Fig. 2. CD103⁺ cDC1s do not affect apoptosis and liver fibrosis progression. C57Bl/6 and *Batf3*$^{-/-}$ animals were fed with NC, HSD or MCD diet for 5 weeks. Livers were evaluated for the expression of (A) *Fas* (B) *Bcl2* (C) *Col1a* using qPCR analyses. Data (A–C) are representative of three to four independent experiments, n = 4 mice per group. One-way ANOVA using Bonferoni *post hoc* test. Mean ± SEM. **p* <0.05, ***p* <0.005, ****p* <0.0001.

DC subtypes (cDC2 and pDCs) (Fig. S2C). Additionally, previous animal studies indicated that a specific cell population among CD11c⁺ cells (involving DCs) may guard the presence of the inflammatory infiltrate in NASH [19]. In order to determine whether cDC1s would represent such protective cell type in the liver, we analysed further myeloid and lymphoid cell populations in treated WT and KO animals. Indeed, the lack of CD103⁺ cDC1s in HSD increased the frequency of CD11c⁺ cells (data not shown). More detailed analyses revealed a rearrangement in CD11b and CD11c expression patterns within the myeloid cell compartment (Fig. 3A, B). Specifically the frequency of cells expressing both CD11c and CD11b among myeloid cells increased in *Batf3* deficient animals during HSD feeding. In MCD treatment, these changes were non-significant between WT and KO animals, suggesting a role of lymphoid DCs in influencing myeloid cells during rather the early progression of steatohepatitis (Fig. 3A, B).

Since inflammatory monocyte recruitment plays a significant role in liver injury promoting inflammation also in steatohepatitis [24], we explored the elevated abundance of Ly6C^{hi}F4/80^{low} inflammatory monocytes, resident Kupffer cells (Ly6C$^{low/-}$F4/80^{hi}) and Ly6C$^{hi/int}$F4/80^{-} cells representing a mixture of myeloid cells involving e.g. neutrophils, eosinophils and myeloid derived suppressor cells [18]. Indeed, HSD feeding of *Batf3* deficient animals resulted in a significant influx of inflammatory monocytes (already after 2 weeks in MCD) (Fig. S3F) and in the increase of the Ly6C$^{hi/int}$F4/80^{-} myeloid cell population (Fig. 3C, D; Fig. S3A). Despite the increase in Ly6C$^{hi/int}$F4/80^{-} cells, the frequency of Ly6G^{hi} neutrophils were unaltered between WT and KO animals and showed a minor but significant elevation during HSD feeding in both settings (Fig. S3D). Greater neutrophil recruitment was rather associated with established steatohepatitis of the MCD model (Fig. S3D). Moreover, Kupffer cells (Fig. S3B) and pDCs (data not shown) as well as lymphoid cells did not differ during HSD between WT and *Batf3*$^{-/-}$ deficient animals (Fig. S3A, D, E). Notably, slightly elevated NK and reduced T cell contents could be observed in MCD treated KO animals (Fig. S3D, E, F).

In summary, during HSD feeding of *Batf3* deficient animals, the observed progression of liver pathology towards steatohepatitis was associated with a greater influx of inflammatory myeloid cells and with an enlarged proportion of the CD11c⁺CD11b⁺ cell population.

The absence of CD103⁺ cDC1s shifts the balance towards a pro-inflammatory milieu

To better understand the increased inflammatory response, we compared the cytokine expression patterns of liver single cell suspensions derived from HSD fed WT and KO animals. Based

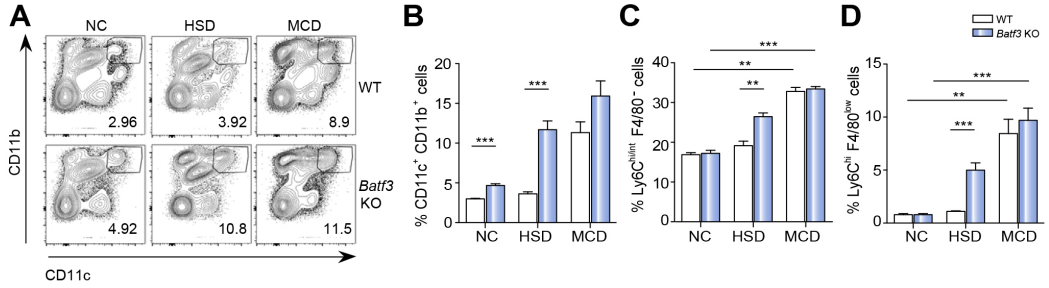

Fig. 3. CD103$^+$ cDC1s influence the inflammatory infiltrate during the development of steatohepatitis. Liver single cell suspension was stained with CD45, CD11b, CD11c, Ly6C, F4/80 and propidium iodide (PI). (A) Representative dot plot and gating strategy for CD11c$^+$CD11b$^+$ is displayed of PI$^-$CD45$^+$ cells. The percentage of CD11b$^+$CD11c$^+$ cells (B), Ly6C^{hi}F4/80$^-$ (C) and Ly6C^{hi}F4/80^{low} cell population is depicted among CD45$^+$ living cells. Data (A–C) are representative of three-four independent experiments, n = 4 mice per group. One-way ANOVA using Bonferoni *post hoc* test. Mean ± SEM. *p <0.05, **p <0.005, ***p <0.0001.

on cytokine protein array, lipopolysaccharide (LPS) treatment induced the production of pro-inflammatory mediators such as IL-1ra, CCL2, CXCL1 and CCL5 (Fig. 4A, B). Importantly these alterations were elevated in HSD-treated *Batf3* KO mice as compared to WT animals suggesting an exacerbated inflammatory response that could influence the progression of steatosis towards steatohepatitis. In line with these observations based on single cell analyses, the frequencies of CD11c$^+$ cells that produced CXCL1 and CCL5 upon LPS challenge were more elevated in KO than in WT animals (Fig. S4A, B). Interestingly, these changes were also significant in MCD treated *Batf3* KO mice, indicating the role of CD103$^+$ cDC1s in balancing inflammation during the development of steatohepatitis (Fig. S4A, B).

Tumor necrosis factor (TNF) plays a central role in inflammatory responses and represent an early inflammatory mediator in various liver damages including NASH [18]. According to the observed injury progression in *Batf3* KO HSD fed animals (Fig. 1A–E), the TNF response of CD11c$^+$ and F4/80$^+$ cells was significantly increased when compared to WT HSD fed mice (Fig. 4C). Importantly, CD11c$^+$ cells derived from WT HSD fed animals did not exhibit increased TNF, CXCL1 or CCL5 response compared with NC fed WT animals (Fig. 4C; Fig. S4A, B), indicating that steatosis in HSD fed WT animals is not associated with an increased inflammatory response. Notably, slightly increased CXCL1 cytokine response upon LPS treatment (but significantly lower than in HSD or MCD) could be observed in *Batf3* KO NC fed animals compared to their WT counterparts (Fig. S4A). Such phenomenon could not be observed for other cytokines (Fig. 4C; Fig. S4B).

Although above data demonstrated a greater cytokine response at the single cell level in the lack of cDC1 cells, we looked for inflammatory cytokine expression in liver homogenates that could underline increased inflammation in the *Batf3* KO animals. Indeed, livers from HSD-treated mice tended to display increased expression of TNF, CCL2 and CXCL10 (Fig. S4C) in line with the changes observed in inflammatory cell infiltrates (Fig. 3; Fig. S3); nevertheless, the differences between KO and WT animals remained non-significant. The same inflammatory cytokines during 5 weeks MCD treatment did not show differences consistent with the abundance of similar cellular infiltrates in KO and WT MCD animals (Fig. 3A–D; Fig. S3A–E, 4C).

Overall, CD103$^+$ cDC1s influenced the cytokine pattern produced by myeloid cells and slightly influenced the expression of pro-inflammatory cytokines and thereby the pro- and anti-inflammatory balance within the liver environment.

The lack of CD103$^+$ cDC1s modifies the lipid metabolic profile

The observed elevation of liver steatosis in *Batf3*$^{-/-}$ animals (Fig. 1) pointed our attention towards lipid metabolism. While steatosis itself is considered protective in the progression of NASH, lipotoxicity and metabolic dysregulation play a defining role in hepatocyte damage [12]. Inflammatory cell-derived cytokines (Fig. 4C; Fig. S4A–C) could influence transcription factors involved in lipid biosynthesis [25], which could ultimately connect the inflammatory changes to lipid metabolism and metabolic dysregulation. To this end, we performed qPCR analyses of key metabolic regulators using liver homogenates. Both the genes involved in lipogenesis (acetyl-CoA carboxylase, *Acac1*; fatty acid synthase, *Fasn*; and stearyl-CoA-desaturase, *Scd1*) and the metabolism regulating transcription factors (peroxisome proliferator-activated receptor alpha [*Ppara*] and sterol regulatory element-binding transcription factor 1 [*Srebf1*]) did not show significant alterations between WT and *Batf3* KO HSD fed animals (Fig. 5A). On the other hand, mitochondrial *Cpt1a* (carnitine acyltransferase-I), a gene involved in β-oxidation of long chain fatty acids, demonstrated significantly reduced upregulation in *Batf3* KO animals during HSD feeding. Moreover, *Acot3* (acyl-CoA thioesterase-3) that catalyzes the hydrolysis of acyl-CoA to free fatty acids (FFA) and Coenzyme A in the peroxisome [26] showed increased upregulation in *Batf3* KO HSD mice (Fig. 5B). Besides, genes involved in fatty acid transport mostly remained unchanged between WT and *Batf3* KO HSD mice, except for *Fabp5* (fatty acid binding protein-5), which was significantly downregulated, and *Slc27a1* that was slightly stronger upregulated in gene deficient animals (Fig. 5A). In contrast, MCD fed *Batf3* KO mice showed no changes as compared to WT (Fig. S5A). Notably, *Batf3* deficient animals under NC feeding (without metabolic challenge) exhibited slightly higher expression of *Acac1* (acetyl-Coenzyme A acyltransferase-1) while other metabolic genes were similar to WT NC fed animals (Fig. S5B).

Since increased lipotoxcity has been linked to increased influx of FFA [8], we determined serum levels in the various fed animals. Indeed, HSD treatment increased FFA serum levels albeit these remained non-significant between WT and *Batf3* KO mice (Fig. S5C). Furthermore, serum triglycerides (Fig. S5C) remained

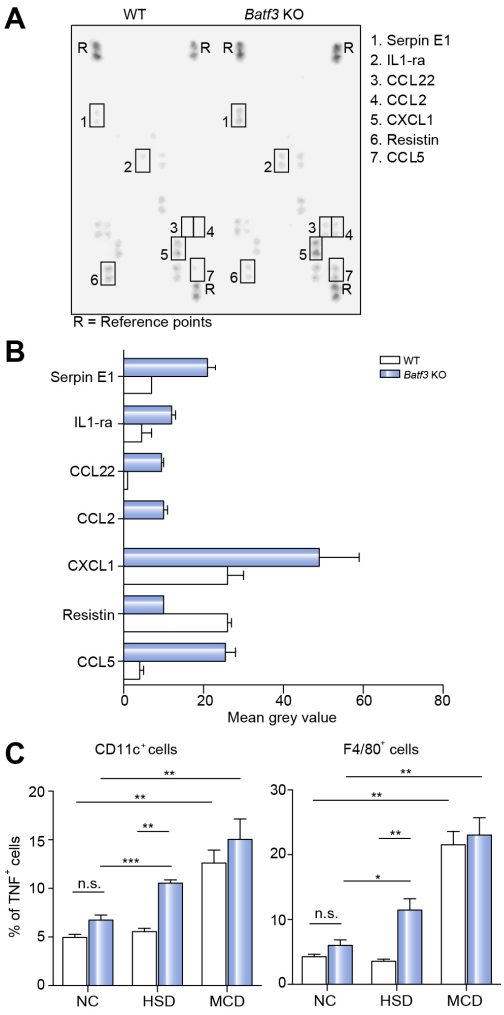

Fig. 4. The absence of cDC1s shift the balance towards pro-inflammatory milieu. C57Bl/6 and *Batf3*$^{-/-}$ animals were fed with HSD for 5 weeks. Liver cells were stimulated with LPS (250 ng/ml) for 18 h, supernatant was used for cytokine array. (A) Representative membrane and (B) the quantification of signal are depicted. (C) C57Bl/6 and *Batf3*$^{-/-}$ animals were fed with NC, HSD or MCD diet for 5 weeks. Liver cells were stimulated with LPS (250 ng/ml) for 5 h. The percentages of TNF producing cells are depicted among CD11c^{+} and F4/80^{+} cells. Data are representative of four independent experiments, n = 4 mice/group. One-way ANOVA using Bonferoni *post hoc* test. Mean ± SEM. *p <0.05, **p <0.005, ****p <0.0001.

similar between the experimental HSD groups. Notably, serum cholesterol was elevated in both HSD WT and *Batf3* KO animals (Fig. S5C). Beyond these metabolic parameters, HSD is known to alter insulin responses, and insulin resistance represents a key parameter that affects the progression of NASH [27,28], therefore we performed intraperitoneal glucose tolerance tests (IPGTT) and adipose tissue analyses. Importantly, IPGTT indicated increased insulin resistance on HSD, but neither IPGTT nor serum levels of fasting insulin or glycated hemoglobin revealed differences between HSD-treated WT and KO animals (Fig. S6A–C). Moreover, the weight of retroperitoneal fat (RP), inflammatory cellular infiltrates (F4/80^{+} macrophages and CD11c^{+}MHCII^{+}-CD11b^{+} cells) and inflammatory cytokine expression did not differ between KO and WT HSD-treated animals (Fig. S6D–G), suggesting that insulin resistance and the response of adipose tissue in HSD animals are indeed similar and changes observed in the liver are specific to its microenvironment. Notably, KO animals on chow diet possessed more RP and showed an increased frequency of F4/80^{+} cells in accordance with previous results [29].

Adoptive transfer of lymphoid DCs attenuates liver pathology in steatosis and steatohepatitis

Since the lack of CD103^{+} cDC1s exacerbated inflammation and steatosis, we aimed to determine whether adoptive transfer of these cells could reverse the disease progression in *Batf3* KO animals. As expected, adoptive transfer of bone marrow derived CD103^{+} DCs (Fig. 6A, B) significantly reduced pro-inflammatory monocyte influx and decreased (albeit non-significantly) the production of TNF by CD11c^{+} cells (Fig. 6C, D). These changes were paralleled by the increased influx of CD3e^{+}NK1.1^{-} T cells (Fig. 6C). More importantly, the transfer of DCs resulted in reduced triglyceride, cholesterol, FFA and leptin levels without altering significantly liver triglyceride contents or ALT activities (Fig. 6E, F; Fig. S7A, B).

In order to evaluate whether CD103^{+} DC could be beneficial in reducing the severity of inflammation in established steatohepatitis, we adoptively transferred these cells to a 2 week MCD fed WT animals where some degree of steatosis and inflammation are already established [30] (Fig. 7A) and similar inflammatory differences could be identified between KO and WT animals as during HSD (Fig. 3D; Fig. S3F). Importantly, CD103^{+} DCs could reduce inflammatory monocyte recruitment, serum ALT activities indicative of cellular liver damage and the expression of CCL2 inflammatory cytokine expression in the liver (Fig. 7B–D). Notably, these changes were also associated with an influx of T cells (Fig. 7C) and changes in serum cholesterol without affecting the weight of animals, serum triglyceride or FFA contents (Fig. S7C, D). Interestingly, despite the reduced ALT levels, liver triglyceride contents were slightly elevated upon DC transfer (Fig. S7B). Thus, the CD103^{+} cDC1s subtype could reduce inflammation both during progression and in established steatohepatitis.

Discussion

Emerging evidence indicates that DCs play a significant role in the progression of various liver injuries and at the same time guide the restitution of tissue integrity [13,31]. DCs consist of heterogeneous subpopulations that significantly differ in their cellular functions and their abilities in the induction of immunity and tolerance [14,20]. Importantly, it has been suggested that CD11c^{+} cells play a central role in the fibro-inflammatory response during the development of steatohepatitis [19]. The lack of CD11c^{+} cells increased the inflammatory response, fibrosis and

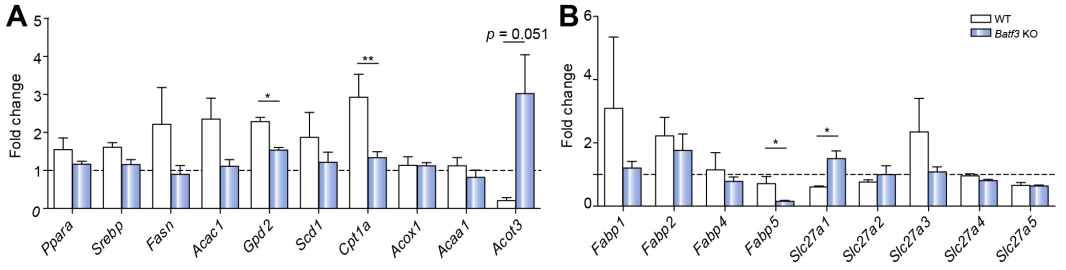

Fig. 5. The absence of cDC1s is associated with slightly altered lipid metabolism. RNA and cDNA were prepared from livers of HSD fed animals and qPCR was performed. Graphs depict the fold changes between WT and *Batf3*$^{-/-}$ HSD-treated animals. Genes of lipid metabolism (A) or lipid transport (B) are depicted. Data (A–B) are representative for three independent experiment n = 3–4/group. Unpaired two-tailed *t* test, Mean ± SEM. $^{*}p$ <0.05, $^{**}p$ <0.005.

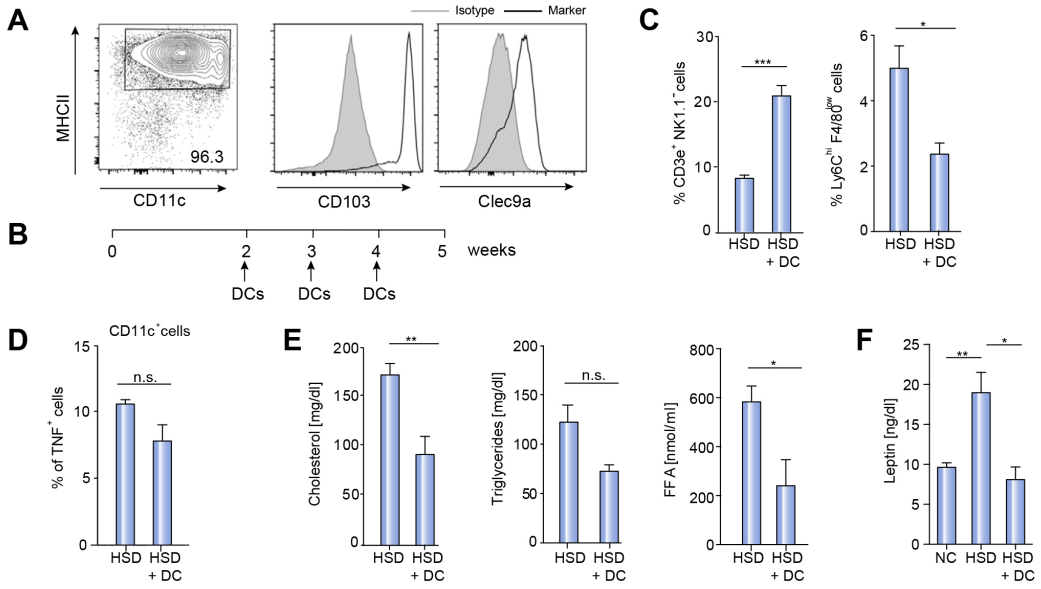

Fig. 6. Adoptive transfer of CD103^{+} cDC1s to *Batf3*$^{-/-}$ animals attenuates inflammation and reduces metabolic disturbances. *Batf3*$^{-/-}$ animals were fed with HSD for 5 weeks. Bone marrow derived CD103^{+}Clec9a^{+} DCs (A) were transferred during continuing diet feeding (B). Liver cells were stained with CD45, Ly6C, F4/80 or CD45, NK1.1, CD3e, CD19 and propidium iodide(PI). (C) The percentages of cell population are depicted among CD45^{+} living cells. (D) The percentages of TNF producing cells are depicted among CD11c^{+} cells after LPS stimuli (5 h, 250 ng/ml). (E) Serum cholesterol, triglyceride, free fatty acid (FFA) and (F) leptin levels are displayed. n = 4/group. One-way ANOVA using Bonferoni *post hoc* test and Mann-Whitney two-tailed *t* test, Mean ± SEM. $^{*}p$ <0.05, $^{**}p$ <0.005, $^{***}p$ <0.0001.

cellular damage in the MCD model of murine NASH [19]. CD11c^{+} cells contain multiple DC subtypes and despite their suggested role in liver injury, the subset contribution to disease progression has not been investigated in the liver. Here, we identified CD103^{+} cDC1s as a protective cell type capable of orchestrating the pro-anti-inflammatory milieu during the progression of murine steatohepatitis. The lack of cDC1 cells increased the frequency of the CD11c^{+}CD11b^{+} myeloid cell compartment and inflammatory monocytes in HSD and early MCD treatment (2 weeks). In contrast to this, the absence of CD103^{+} cDC1s only slightly altered NK and T cell numbers but did not modify significantly the inflammatory influx and TNF response of myeloid cells in the 5 week MCD model. A stronger cellular response of CCL5 and CXCL1 production was observed in the 5 week MCD fed *Batf3* deficient animals, suggesting some involvement of the cDC1 subset in the innate response of myeloid cells during established MCD steatohepatitis. Importantly, HSD feeding increased only liver triglyceride contents in WT animals, whereas *Batf3* deficient mice exhibited profound inflammation, macrovesicular steatosis and myeloid cellular influx, indicating the progression of steatosis towards steatohepatitis. In HSD fed KO animals the remaining cDC2 subtype exhibited increased abundance, suggesting its

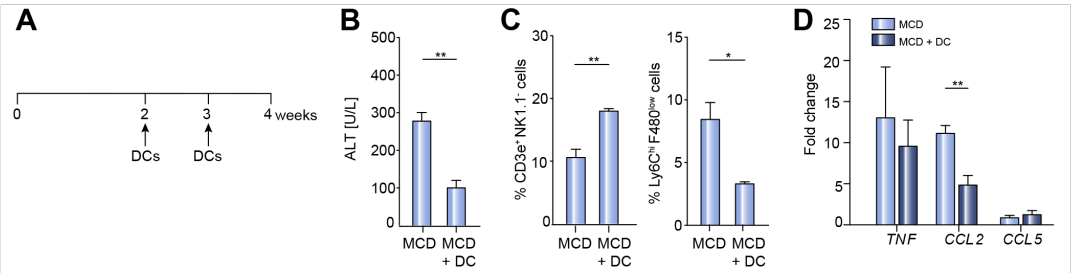

Fig. 7. Adoptive transfer of CD103⁺ cDC1s attenuates inflammation in established steatohepatitis. (A) C57Bl/6 animals were fed with MCD diet for 4 weeks. Bone marrow derived CD103⁺Clec9a⁺ DCs were transferred weekly during continuing diet feeding. (B) Serum ALT values are displayed. (C) Liver cells were stained with CD45, Ly6C, F4/80 or CD45, NK1.1, CD3e, CD19 and propidium iodide (PI). (D) cDNAs were prepared from livers of MCD and MCD + DC treated animals and qPCR was performed. Graph depicts the fold changes. Beta actin was used as a housekeeping gene. n = 3–4/group. The percentages of cell population are depicted among CD45⁺ living cells. n = 4/group. Mann-Whitney two-tailed *t* test, Mean ± SEM. **p* <0.05, ***p* <0.005.

possible involvement in the inflammatory process. Future studies are necessary to clarify the functional connection between cDC1 and cDC2 subtypes in the liver and their roles in murine liver pathology. Additionally, myeloid cells exhibited an increased inflammatory cytokine response, similarly as found in a previous report [19]. We observed increases at the cellular level in the production of TNF, CCL5 and CXCL1 in *Batf3* deficient animals during HSD feeding. Additionally, CCL2, CXCL10 and TNF showed slightly elevated expressions in liver homogenates, indicating that not only the cellular response but the general liver microenvironment is altered in KO animals on HSD. CCL2 is a major chemokine involved in the recruitment of inflammatory monocytes [24], CCL5 is chemotactic for T cells, eosinophils and basophils, CXCL10 is for T, NK cells and myeloid cells, whereas CXCL1 particularly targets neutrophils [32]. Thus, all measured chemokines play active roles in the recruitment of inflammatory cells and could contribute to the escalation of inflammation and cell recruitment changes associated with NASH [9,24].

Multiple hypotheses have addressed the question of which factors trigger the advancement of NAFL to NASH [9]. Steatosis itself is considered as potentially protective mechanism and liver damage is associated with an excess FFA influx rather than simple triglyceride accumulation [8]. Fabp5, a fatty acid binding protein [33], displayed decreased expression in *Batf3* KO animals upon HSD challenge. Fabp5 is mostly active in long chain fatty acid transport, and gene deficient animals are protected from metabolic syndrome [34]. Its downregulation could be a compensatory mechanism for the presence of the elevated FFA observed also in previous animal studies [35]. Additionally, *Batf3* KO animals on HSD feeding exhibited an increased level of *Slc27a1* (FATP1, fatty acid transporter-1). Elevated lipid transport is often associated with increased serum FFA levels in NAFL [36,37], nonetheless serum FFA as well as serum leptin levels increased similarly in both WT and *Batf3* KO HSD animals. It remains to be elucidated whether the overall liver FFA uptake is altered in the absence of cCD1s. Liver lipid content is not only dependent on lipid uptake but also on *de novo* lipogenesis and β-oxidation [8]. Indeed, *Ctp1a* (carnitine palmitoyltransferase I), a key enzyme in mitochondrial β-oxidation, was repressed in KO animals upon HSD feeding. Notably, the expression of this gene is also typically lower in NAFLD [38]. Moreover, *Acot3* (acyl-CoA thioesterase 3), which regulates β-oxidation in the peroxisome [26], showed increased expression in *Batf3* KO HSD mice. The peroxisomal β-oxidation metabolizes long chain saturated and unsaturated fatty acids and provides an alternative mechanism beside the mitochondrial β-oxidation to remove excessive fatty acids [12,26]. Thus, the lack of CD103⁺ cDC1s not only altered the inflammatory milieu but contributed to gene expression alterations related to lipid metabolism in the HSD model. Possibly the imbalance between β-oxidation and alternative clearance mechanisms for FFA could contribute to increased steatosis and progression of NASH observed in these animals. It remains to be elucidated whether hepatocyte metabolic alterations could be related to the altered inflammatory milieu or be a direct consequence of the absence of DC derived molecules. It is intriguing that hepatic lipids can efficiently alter the functional properties of myeloid cells [39] and therefore it is plausible that the altered lipid contents might additionally contribute to the elevated pro-inflammatory response observed during steatohepatitis.

Adoptive transfer of CD103⁺ cDC1s could reduce the inflammatory cellular influx during HSD feeding in *Batf3* KO animals and more importantly decreased the frequency of inflammatory monocytes and the expression of Ccl2 in liver homogenates and attenuated the cellular damage in MCD steatohepatitis of WT mice. Notably, in both the HSD and MCD models the adoptive transfer of DCs was associated with the increased presence of T cells. These cells did not change during HSD challenge neither in WT nor in *Batf3* KO animals but showed reduced abundance in primarily CD4 T cells (data not shown) in established MCD steatohepatitis. The reduction of T cells (specifically CD4 T cells) due to dysregulation of lipid metabolism caused accelerated hepatocarcinogenesis that could be reversed by reactive oxygen species blockade [40]. Thus, DC-T cell interaction *in situ* might play a significant role not only in carcinogenesis but also in the protection of overt inflammation within the liver. Additionally, DCs are antigen-presenting cells and their presentation of viral peptides *in situ* determines CD8 T cell immunity in the liver [41]. It is unknown whether the presentation of lipid or other protein antigens and the consequent T cell responses would play a role in regulating inflammation or NASH progression.

Multiple studies demonstrated that high sugar intake together with lipids exacerbate liver pathology [8]. Moreover, dietary sucrose, a disaccharide built by glucose and fructose, is absolutely required for the development of MCD-induced liver injury [42]. The consumption of fructose (specifically in the form of high fructose corn syrup) markedly increases the incidence of NAFLD

worldwide and directly facilitates *de novo* lipid synthesis, increases fat deposition in visceral adipose tissue and alters mucosal permeability [43–45]. Multiple genes connected to lipogenesis together with the quantity of RP, insulin resistance and adipose tissue inflammation did not differ between WT and *Batf3* KO animals on HSD. It remains to be elucidated whether cDC1s would play a role in mucosal changes and thus participate in additional checkpoints during metabolic damage and NASH. Indeed, adipose tissue function and serum leptin level correlates with liver lipid content in NASH patients [46,47]. Interestingly, elevated serum leptin levels decreased upon $CD103^+$ cDC1 transfer in HSD mice that coincided with reduced serum triglyceride and cholesterol contents, while liver lipids remain unchanged. The role of elevated leptin in NASH is not fully defined, and further studies are necessary to clarify how cDC1s influence leptin levels during NASH progression in mice.

Numerous animal models exist that exhibit hepatic steatosis and/or varying degrees of steatohepatitis [48]. Nevertheless, none of them can completely replicate the entire human phenotype. MCD is one of the most widely used models, and genetic analyses have revealed great resemblance to human NASH despite the lack of obesity [48,49]. HSD feeding over eight weeks containing 65% of sucrose induces macrovesicular steatosis in WT animals [50]. In our model, 40% sucrose quantity elevated liver triglycerides in WT mice but did neither result in macrovesicular steatosis nor profound hepatic inflammation after 5 weeks of treatment. Additionally, our HSD and MCD diets contained the exact same dietary components except methionine and choline. Therefore, these diets provided useful short-term models for the comparative analyses of steatosis and steatohepatitis. Notably, Westernized diet containing trans-fat and fructose could closely recapitulate human NAFLD [51], and it will be important in the future to confirm the role of cDC1s in these models as well.

The lack of $CD103^+$ cDC1s increased inflammation but did not significantly alter fibrosis and apoptosis over the five weeks of treatment. It remains to be elucidated whether long-term HSD feeding would further exacerbate liver pathology, fibrosis and hepatocarcinogenesis.

Importantly, the adoptive transfer of $CD103^+$ cDC1s could reduce inflammation and cellular damage that raises an intriguing question about how the animal data relate to human NASH. This is especially relevant as the human counterpart of cDC1, the $CD141^+$ population, shows distinct abundance within the liver [13,52,53]. DC analyses of human liver samples have been performed in digested fresh or in perfusates from transplanted livers [52,54]. Importantly, the selective disappearance of $CD141^+$ DCs (cDC1s) has been observed in human livers with advanced end-stage disease, including NAFLD [52], suggesting a correlation of reduced cDC1s and advanced liver pathology. These analyses required multicolor flow cytometry techniques on fresh liver tissue to precisely identify DC subtypes [52]. Thus, future studies are necessary to understand whether human NASH severity would align with the specific abundance of cDC1s or whether cDC1s would exhibit significant effects on the inflammatory milieu in human liver as well.

In summary, we demonstrated that the murine $CD103^+$ cDC1s of the liver represent a protective DC subset that regulates inflammatory cellular influx, balances the pro-anti-inflammatory microenvironment and influences lipid metabolism. Importantly, adoptive transfer of DCs attenuated inflammation and cellular damage in murine NASH. The molecular events that determine the progression of steatosis towards steatohepatitis are not fully understood and there are no effective therapeutic interventions to stop the progression of inflammation and fibrosis and to restore liver integrity. Understanding the relation of the various DC subtypes in mice and in humans as well as their interactions with other immune and parenchymal cells are critical to understand not only the underlying pathomechanism during steatohepatitis and liver injury but also to unravel future therapeutic strategies for NASH.

Financial support

This work was supported by SFB/Transregio 57, BO 3755/3-1 and Else-Kröner Fresenius Foundation (EKFS 2012_A216) to PB and by the Alexander von Humboldt Foundation, Sofja Kovalevskaja Award, to VLK.

Conflict of interest

The authors who have taken part in this study declared that they do not have anything to disclose regarding funding or conflict of interest with respect to this manuscript.

Authors' contributions

A.M., E-C.H. performed individual experiments, analysed and interpreted results and prepared figures. H.J. provided technical help in cell preparation. S. D. performed histology analyses, T.T. provided help with histological analyses. P. B. supervised the histological analyses. A. G. and M. R. provided tissue samples. F.L. provided laboratory support and critically read the manuscript. V.L.K designed and directed the study, performed experiments, analysed and interpreted results and wrote the manuscript.

Acknowledgements

The authors thank to Ingrid Lang and Marion Schwarz for technical assistance at the Institute of Anatomy and Cell Biology, Saarland University, Germany. The technical assistance of Simon Wilhelm Otten is gratefully acknowledged.

Supplementary data

Supplementary data associated with this article can be found, in the online version, at http://dx.doi.org/10.1016/j.jhep.2017.01.008.

References

[1] Blachier M, Leleu H, Peck-Radosavljevic M, Valla DC, Roudot-Thoraval F. The burden of liver disease in Europe: a review of available epidemiological data. J Hepatol 2013;58:593–608.
[2] Browning JD, Szczepaniak LS, Dobbins R, Nuremberg P, Horton JD, Cohen JC, et al. Prevalence of hepatic steatosis in an urban population in the United States: impact of ethnicity. Hepatology 2004;40:1387–1395.

[3] Schwimmer JB, Deutsch R, Kahen T, Lavine JE, Stanley C, Behling C. Prevalence of fatty liver in children and adolescents. Pediatrics 2006;118:1388–1393.
[4] Tiniakos DG, Vos MB, Brunt EM. Nonalcoholic fatty liver disease: pathology and pathogenesis. Annu Rev Pathol 2010;5:145–171.
[5] Loomba R, Sanyal AJ. The global NAFLD epidemic. Nat Rev Gastroenterol Hepatol 2013;10:686–690.
[6] Michelotti GA, Machado MV, Diehl AM. NAFLD, NASH and liver cancer. Nat Rev Gastroenterol Hepatol 2013;10:656–665.
[7] Day CP, James OF. Steatohepatitis: a tale of two "hits"? Gastroenterology 1998;114:842–845.
[8] Sharma M, Mitnala S, Vishnubhotla RK, Mukherjee R, Reddy DN, Rao PN. The riddle of nonalcoholic fatty liver disease: progression from nonalcoholic fatty liver to nonalcoholic steatohepatitis. J Clin Exp Hepatol 2015;5:147–158.
[9] Tilg H, Moschen AR. Evolution of inflammation in nonalcoholic fatty liver disease: the multiple parallel hits hypothesis. Hepatology 2010;52:1836–1846.
[10] Federico A, Dallio M, Godos J, Loguercio C, Salomone F. Targeting gut-liver axis for the treatment of nonalcoholic steatohepatitis: translational and clinical evidence. Transl Res 2016;167:116–124.
[11] Lanthier N, Molendi-Coste O, Cani PD, van Rooijen N, Horsmans Y, Leclercq IA. Kupffer cell depletion prevents but has no therapeutic effect on metabolic and inflammatory changes induced by a high-fat diet. FASEB J 2011;25:4301–4311.
[12] Neuschwander-Tetri BA. Hepatic lipotoxicity and the pathogenesis of nonalcoholic steatohepatitis: the central role of nontriglyceride fatty acid metabolites. Hepatology 2010;52:774–788.
[13] Lukacs-Kornek V, Schuppan D. Dendritic cells in liver injury and fibrosis: shortcomings and promises. J Hepatol 2013;59:1124–1126.
[14] Lukacs-Kornek V, Turley SJ. Self-antigen presentation by dendritic cells and lymphoid stroma and its implications for autoimmunity. Curr Opin Immunol 2011;23:138–145.
[15] Connolly MK, Ayo D, Malhotra A, Hackman M, Bedrosian AS, Ibrahim J, et al. Dendritic cell depletion exacerbates acetaminophen hepatotoxicity. Hepatology 2011;54:959–968.
[16] Connolly MK, Bedrosian AS, Mallen-St Clair J, Mitchell AP, Ibrahim J, Stroud A, et al. In liver fibrosis, dendritic cells govern hepatic inflammation in mice via TNF-alpha. J Clin Invest 2009;119:3213–3225.
[17] Bleier JI, Katz SC, Chaudhry UI, Pillarisetty VG, Kingham 3rd TP, Shah AB, et al. Biliary obstruction selectively expands and activates liver myeloid dendritic cells. J Immunol 2006;176:7189–7195.
[18] Eckert C, Klein N, Kornek M, Lukacs-Kornek V. The complex myeloid network of the liver with diverse functional capacity at steady state and in inflammation. Front Immunol 2015;6:179.
[19] Henning JR, Graffeo CS, Rehman A, Fallon NC, Zambirinis CP, Ochi A, et al. Dendritic cells limit fibroinflammatory injury in nonalcoholic steatohepatitis in mice. Hepatology 2013;58:589–602.
[20] Steinman RM, Idoyaga J. Features of the dendritic cell lineage. Immunol Rev 2010;234:5–17.
[21] Hildner K, Edelson BT, Purtha WE, Diamond M, Matsushita H, Kohyama M, et al. Batf3 deficiency reveals a critical role for CD8alpha+ dendritic cells in cytotoxic T cell immunity. Science 2008;322:1097–1100.
[22] Ginhoux F, Liu K, Helft J, Bogunovic M, Greter M, Hashimoto D, et al. The origin and development of nonlymphoid tissue CD103+ DCs. J Exp Med 2009;206:3115–3130.
[23] Teufel A, Itzel T, Erhart W, Brosch M, Wang XY, Kim YO, et al. Comparison of gene expression patterns between mouse models of nonalcoholic fatty liver disease and liver tissues from patients. Gastroenterology 2016;151:513–525 e510.
[24] Baeck C, Wehr A, Karlmark KR, Heymann F, Vucur M, Gassler N, et al. Pharmacological inhibition of the chemokine CCL2 (MCP-1) diminishes liver macrophage infiltration and steatohepatitis in chronic hepatic injury. Gut 2012;61:416–426.
[25] Carter-Kent C, Zein NN, Feldstein AE. Cytokines in the pathogenesis of fatty liver and disease progression to steatohepatitis: implications for treatment. Am J Gastroenterol 2008;103:1036–1042.
[26] Hunt MC, Siponen MI, Alexson SE. The emerging role of acyl-CoA thioesterases and acyltransferases in regulating peroxisomal lipid metabolism. Biochim Biophys Acta 2012;1822:1397–1410.
[27] Torres DM, Williams CD, Harrison SA. Features, diagnosis, and treatment of nonalcoholic fatty liver disease. Clin Gastroenterol Hepatol 2012;10:837–858.
[28] Takahashi Y, Soejima Y, Fukusato T. Animal models of nonalcoholic fatty liver disease/nonalcoholic steatohepatitis. World J Gastroenterol 2012;18:2300–2308.
[29] Stefanovic-Racic M, Yang X, Turner MS, Mantell BS, Stolz DB, Sumpter TL, et al. Dendritic cells promote macrophage infiltration and comprise a substantial proportion of obesity-associated increases in CD11c+ cells in adipose tissue and liver. Diabetes 2012;61:2330–2339.
[30] Sahai A, Malladi P, Melin-Aldana H, Green RM, Whitington PF. Upregulation of osteopontin expression is involved in the development of nonalcoholic steatohepatitis in a dietary murine model. Am J Physiol Gastrointest Liver Physiol 2004;287:G264–G273.
[31] Jiao J, Sastre D, Fiel MI, Lee UE, Ghiassi-Nejad Z, Ginhoux F, et al. Dendritic cell regulation of carbon tetrachloride-induced murine liver fibrosis regression. Hepatology 2012;55:244–255.
[32] Griffith JW, Sokol CL, Luster AD. Chemokines and chemokine receptors: positioning cells for host defense and immunity. Annu Rev Immunol 2014;32:659–702.
[33] Makowski L, Hotamisligil GS. The role of fatty acid binding proteins in metabolic syndrome and atherosclerosis. Curr Opin Lipidol 2005;16:543–548.
[34] Maeda K, Cao H, Kono K, Gorgun CZ, Furuhashi M, Uysal KT, et al. Adipocyte/macrophage fatty acid binding proteins control integrated metabolic responses in obesity and diabetes. Cell Metab 2005;1:107–119.
[35] Renaud HJ, Cui JY, Lu H, Klaassen CD. Effect of diet on expression of genes involved in lipid metabolism, oxidative stress, and inflammation in mouse liver-insights into mechanisms of hepatic steatosis. PLoS One 2014;9 e88584.
[36] Fabbrini E, deHaseth D, Deivanayagam S, Mohammed BS, Vitola BE, Klein S. Alterations in fatty acid kinetics in obese adolescents with increased intrahepatic triglyceride content. Obesity 2009;17:25–29.
[37] Korenblat KM, Fabbrini E, Mohammed BS, Klein S. Liver, muscle, and adipose tissue insulin action is directly related to intrahepatic triglyceride content in obese subjects. Gastroenterology 2008;134:1369–1375.
[38] Kohjima M, Enjoji M, Higuchi N, Kato M, Kotoh K, Yoshimoto T, et al. Re-evaluation of fatty acid metabolism-related gene expression in nonalcoholic fatty liver disease. Int J Mol Med 2007;20:351–358.
[39] Ibrahim J, Nguyen AH, Rehman A, Ochi A, Jamal M, Graffeo CS, et al. Dendritic cell populations with different concentrations of lipid regulate tolerance and immunity in mouse and human liver. Gastroenterology 2012;143:1061–1072.
[40] Ma C, Kesarwala AH, Eggert T, Medina-Echeverz J, Kleiner DE, Jin P, et al. NAFLD causes selective CD4(+) T lymphocyte loss and promotes hepatocarcinogenesis. Nature 2016;531:253–257.
[41] Krueger PD, Kim TS, Sung SS, Braciale TJ, Hahn YS. Liver-resident CD103+ dendritic cells prime antiviral CD8+ T cells in situ. J Immunol 2015;194:3213–3222.
[42] Pickens MK, Yan JS, Ng RK, Ogata H, Grenert JP, Beysen C, et al. Dietary sucrose is essential to the development of liver injury in the methionine-choline-deficient model of steatohepatitis. J Lipid Res 2009;50:2072–2082.
[43] Ouyang X, Cirillo P, Sautin Y, McCall S, Bruchette JL, Diehl AM, et al. Fructose consumption as a risk factor for non-alcoholic fatty liver disease. J Hepatol 2008;48:993–999.
[44] Stanhope KL, Schwarz JM, Keim NL, Griffen SC, Bremer AA, Graham JL, et al. Consuming fructose-sweetened, not glucose-sweetened, beverages increases visceral adiposity and lipids and decreases insulin sensitivity in overweight/obese humans. J Clin Invest 2009;119:1322–1334.
[45] Spruss A, Kanuri G, Wagnerberger S, Haub S, Bischoff SC, Bergheim I. Toll-like receptor 4 is involved in the development of fructose-induced hepatic steatosis in mice. Hepatology 2009;50:1094–1104.
[46] Lee SA, Yuen JJ, Jiang H, Kahn BB, Blaner WS. Adipocyte-specific overexpression of retinol-binding protein 4 causes hepatic steatosis in mice. Hepatology 2016;64:1534–1546.
[47] Chitturi S, Farrell G, Frost L, Kriketos A, Lin R, Fung C, et al. Serum leptin in NASH correlates with hepatic steatosis but not fibrosis: a manifestation of lipotoxicity? Hepatology 2002;36:403–409.
[48] Anstee QM, Goldin RD. Mouse models in non-alcoholic fatty liver disease and steatohepatitis research. Int J Exp Pathol 2006;87:1–16.
[49] Teufel A, Itzel T, Erhart W, Brosch M, Wang XY, Kim YO, et al. Comparison of gene expression patterns between mouse models of nonalcoholic fatty liver disease and liver tissues from patients. Gastroenterology 2016.
[50] Feldstein AE, Canbay A, Guicciardi ME, Higuchi H, Bronk SF, Gores GJ. Diet associated hepatic steatosis sensitizes to Fas mediated liver injury in mice. J Hepatol 2003;39:978–983.
[51] Tetri LH, Basaranoglu M, Brunt EM, Yerian LM, Neuschwander-Tetri BA. Severe NAFLD with hepatic necroinflammatory changes in mice fed trans fats and a high-fructose corn syrup equivalent. Am J Physiol Gastrointest Liver Physiol 2008;295:G987–G995.

Research Article

[52] Kelly A, Fahey R, Fletcher JM, Keogh C, Carroll AG, Siddachari R, et al. CD141 (+) myeloid dendritic cells are enriched in healthy human liver. J Hepatol 2014;60:135–142.
[53] Dutertre CA, Wang LF, Ginhoux F. Aligning bona fide dendritic cell populations across species. Cell Immunol 2014;291:3–10.
[54] Haniffa M, Shin A, Bigley V, McGovern N, Teo P, See P, et al. Human tissues contain CD141hi cross-presenting dendritic cells with functional homology to mouse CD103+ nonlymphoid dendritic cells. Immunity 2012;37:60–73.